

**PETROLOGY, STRUCTURE AND EXHUMATION
OF THE SOUTHERN SAWATCH MOUNTAINS,
SOUTH-CENTRAL COLORADO**

by

REBECCA ROBBINS

B.S., Kansas State University, 1992

A THESIS

Submitted in partial fulfillment
of the requirements for the degree

MASTER OF SCIENCE

Department of Geology

College of Arts and Sciences

KANSAS STATE UNIVERSITY
Manhattan, Kansas
2005

Approved By:

Major Professor
Dr. Mary Hubbard

ABSTRACT

The southern Sawatch Range of the Southern Rocky Mountains of south-central Colorado is composed of Precambrian crystalline igneous and metamorphic rocks that have undergone at least three major mountain building events during the Phanerozoic, the Ancestral Rockies Orogeny, the Laramide Orogeny, and Rio Grande rifting. In order to determine how the ancient basement structures might have influenced later episodes of deformation, a small area of basement terrain was mapped along the western margin of the Poncha Pass transfer zone between the San Luis and Upper Arkansas basins in the northern Rio Grande rift.

The two dominant rock types in the map area, (hornblende) amphibolite gneiss and (felsic) quartzofeldspathic gneiss, may represent interlayered metabasalt/metadiorite and metarhyolite/metagranite, with lenses of exotic lithologies throughout. Metamorphic foliations were found to be oriented predominantly N35°W 47°NE and to have had an influence on younger brittle structures related to the rifting episode. Lineations and fractures in the gneissic fabric also are parallel to brittle deformation structures.

Apatite Fission-Track (AFT) analysis provided a means of determining when this crust was exhumed and cooled by the removal of overburden in response to erosion and/or tectonics. The resultant AFT age distribution revealed that exhumation occurred at the higher elevations during the Laramide orogeny (~29-46 Ma), and at lower elevations during Rio Grande rifting (~29-19 Ma). Although it is commonly thought that these mountains were exhumed during the rifting episode, the results of this study indicate that older events played a significant role in the exhumation.

TABLE OF CONTENTS

Table of Contents	i
List of Figures	ii
List of Tables	viii
Acknowledgements	ix
Dedication	x
Introduction	1
Geological Background	4
Precambrian and Paleoproterozoic Formation	7
Ancestral Rockies Orogeny	16
Laramide Orogeny	19
Rio Grande Rifting Extension	24
Sawatch Range	32
Timing	38
Field Area	39
Petrology	60
Methods	60
Hand Specimens	60
Thin Sections	60
Results	63
Discussion	115
Structure	126
Methods	126
Results	131
Discussion	173
Exhumation	180
Methods	180
Mineral Separation	180
Apatite Fission-Track (AFT) Thermochronology	181
Results	190
Discussion	205
Conclusion	207
References	210
Appendix A: Lithologic Units	223
Appendix B: Ridgeline Equivalencies	234
Appendix C: Hand Specimens	236
Appendix D: Thin Sections	245
Appendix E: Field Measurements	258
Appendix F: Stereonets	278
Appendix G (Maps: Plates I, II, and III enclosed)	284
Plate I (Petrologic Map)	
Plate II (Structural Map)	
Plate III (Geologic Cross-section)	

LIST OF FIGURES

Figure 1. Continental U.S. map	3
Figure 2. Western U.S. and Southern Rocky Mountains	6
Figure 3. Precambrian Paleoproterozoic Events Timeline	7
Figure 4a. Yavapai and Mazatzal Proterozoic Tectonic Provinces	8
Figure 4b. Northern Yavapai and Southern Yavapai Proterozoic Tectonic Provinces.....	9
Figure 5a. Paleoproterozoic Southern Laurentia	12
Figure 5b. Deformational Events of the Area.....	15
Figure 6. Ancestral Rockies Orogeny within Colorado.....	17
Figure 7a. Laramide Uplifts.....	20
Figure 7b. Laramide Orogeny.....	22
Figure 8a. Rocky Mountain Foreland.....	23
Figure 8b. Northern Rio Grande rift	24
Figure 9a. Rio Grande Rift Ranges, Volcanic Fields, Basins and Transfer Zones.....	29
Figure 9b. DEM of Poncha Pass Transfer Zone of northern Rio Grande Rift.....	30
Figure 10. South Central Colorado and Southern Sawatch Range	31
Figure 11. Sawatch Range “Fourteeners”	33
Figure 12a. Sawatch and Sangre de Cristo Ranges of the Rio Grande rift.....	35
Figure 12b. Koutner (1969) findings	36
Figure 12c. Dippold (1999) findings	37
Figure 13. Digital Elevation Model of Field Area.....	40
Figure 14a. Traverse of Ridgelines on Topographic Map	41
Figure 14b. Topographic Map of Field Area.....	42

Figure 14c. Subdivision of Field Area by Elevation.....	43
Figure 15. View of ridgelines from afar with adjacent units, photo	45
Figure 16. Paleozoic Allochthonous Block “Elephant Rock”, photo	46
Figure 17. Field Area ridgelines from “Elephant Rock”, photo	46
Figure 18. View of ridgelines looking south over Tertiary sediments, photo	47
Figure 19. Conforming Ridgelines, photo	48
Figure 20. Conforming Ridgelines, photo	49
Figure 21. North Ridgeline, photo	50
Figure 22. South Ridgeline, photo	51
Figure 23. Interridge Saddle outcrops, photo.....	52
Figure 24. Interridge Saddle view looking down Pass Creek, photo.....	53
Figure 25. Interridge Saddle from South Ridgeline, photo.....	54
Figure 26. Looking at Interridge Saddle, photo.....	55
Figure 27. Major apices of Ridgelines.....	56
Figure 28. Continental Divide, photo	57
Figure 29a. Aerial Photo 139	58
Figure 29b. Aerial Photo 139 Notations	59
Figure 30. Three Broad Mappable units and sub-units.....	62
Figure 31. Simplified Geologic Map of Ridgelines.....	65
Figure 32. Surficial Expression of Lithologic Units, photo.....	66
Figure 33. Surficial Expression of Lithologic Units, photo.....	67
Figure 34a. Black Amphibolite (1a.Xag:Xh) exposure, photo	68
Figure 34b. Black Amphibolite (1a.Xag:Xh) hand specimen, photo	69

Figure 34c. Black Amphibolite (1a.Xag:Xh) thin section photomicrograph.....	71
Figure 35a. Gray comp-banded amphibolite (1b.Xag:Xf) exposure, photo	72
Figure 35b. Gray comp-banded amphibolite (1b.Xag:Xf) hand specimen, photo.....	73
Figure 35c. Gray comp-banded amphibolite (1b.Xag:Xf) thin section photomicrograph.....	74
Figure 36a. Quartzofeldspathic Schist (1c.Xag:Xfs) hand specimen, photo	75
Figure 36b. Quartzofeldspathic Schist (1c.Xag:Xfs) thin section photomicrograph.....	76
Figure 37a. Quartzofeldspathic Gneiss (2.Xqfg) exposure, photo.....	77
Figure 37b. Quartzofeldspathic Gneiss (2.Xqfg) hand specimen, photo.....	78
Figure 37c. Quartzofeldspathic Gneiss (2.Xqfg) thin section photomicrograph	80
Figure 38a. Felsic Hornblendic Gneisses (3.Xfh) exposures, photo.....	82
Figure 38b. Felsic Hornblendic Gneisses (3.Xfh) exposures, photo	83
Figure 38c. Amphibolite Gneiss (3a.Xfh:Xa) hand specimen, photo.....	84
Figure 38d. Amphibolite Gneiss (3a.Xfh:Xa) thin section photomicrograph	85
Figure 38e. Quartzofeldspathic Gneiss (3b.Xfh:Xqf) hand specimen, photo.....	86
Figure 38f. Quartzofeldspathic Gneiss (3b.Xfh:Xqf) thin section photomicrograph	87
Figure 38g. Feather Amphibolite (3c.Xfh:Xfa) hand specimen, photo	88
Figure 38h. Feather Amphibolite (3c.Xfh:Xfa) thin section photomicrograph	89
Figure 39a. Calc Silicate Gneiss (2a.Xqfg:Xcs) exposure, photo.....	91
Figure 39b. Calc Silicate Gneiss (2a.Xqfg:Xcs) hand specimen, photo.....	92
Figure 39c. Calc Silicate Gneiss (2a.Xqfg:Xcs) thin section photomicrograph	93
Figure 40a. Amphibolite Gneiss (5a.Pf) “porphyroblastic rock” hand specimen, photo	95
Figure 40b. Amphibolite Gneiss (5a.Pf) “porphyroblastic rock” thin section photomicrograph.....	96

Figure 41a. Quartzofeldspathic Schist (5b.Pfs) “porphyroblastic rock” hand specimen, photo	97
Figure 41b. Quartzofeldspathic Schist (5b.Pfs) “porphyroblastic rock” thin section photomicrograph	98
Figure 41c. Quartzofeldspathic Schist (5b.Pfs) “porphyroblastic rock” thin section photomicrograph	99
Figure 42a. Quartzofeldspathic Gneiss (2.Xqfg) “porphyroblastic” exposure, photo	100
Figure 42b. Quartzofeldspathic Gneiss (2.Xqfg) “porphyroblastic” hand specimen, photo	101
Figure 42c. Quartzofeldspathic Gneiss (2.Xqfg) “porphyroblastic” thin section photomicrograph	102
Figure 43a. Hornblende pods (3d.Xfh:Xhb) “porphyroblastic rock” hand specimen, photo	104
Figure 43b. Hornblende pods (3d.Xfh:Xhb) “porphyroblastic rock” thin section photomicrograph	105
Figure 43c. Quartz pods “porphyroblastic rock” thin section photomicrograph	106
Figure 44a. Igneous Intrusion exposure, photo.....	108
Figure 44b. Igneous Intrusion hand specimen, photo	109
Figure 44c. Igneous Intrusion thin section, photomicrograph	110
Figure 44d. Igneous Intrusion hand specimen, photo	111
Figure 44e. Igneous Intrusion thin section, photomicrograph	112
Figure 44f. Quartz Mica Schist (3e. Xfh: Xqms) hand specimen, photomicrograph	113
Figure 44g. Quartz Mica Schist (3e. Xfh: Xqms) thin section, photomicrograph	114
Figure 45. Geologic Map of Field Area and Surrounding Region	115
Figure 46. Metamorphic Facies PT Diagram with Al ₂ SiO ₅ Polymorphs	119

Figure 47. South Ridgeline Profile with suspicious features, photos	129
Figure 48. Scree Slope, photo	130
Figure 49. Ridgeline Exposure, photo	131
Figure 50. Foliations Along Ridgelines	133
Figure 51. Foliations by Unit	135
Figure 52. Lineations by Unit	137
Figure 53a. Fractures by Unit	138
Figure 53b. Fractures of Amphibolite Gneiss (1.Xag) Unit	139
Figure 53c. Fractures of Quartzofeldspathic Gneiss (2. Xqfg) Unit.....	141
Figure 53d. Fractures of Felsic Hornblendic Gneiss (3. Xfh) Unit	141
Figure 54. Planar face, photo	142
Figure 55. Planar face, photo	143
Figure 56. Lower Hemisphere Equal Area Projected plots of units for Foliation	149-150
Figure 57. Lower Hemisphere Equal Area Projected plots of units for Lineation	151
Figure 58. Lower Hemisphere Equal Area Projected plots of units for Fracture	152-153
Figure 59. Base Map showing Proposed Faults.....	154
Figure 60. Digital Elevation Model showing Proposed Faults.....	155
Figure 61. Aerial photo 140, photo.....	156
Figure 62. Suspected fault (“hump jut”), photo.....	159
Figure 63. The southernmost basin-bounding fault (WCTF) of the Upper Arkansas Basin, photo	161
Figure 64. A fold in the Quartzofeldspathic Gneiss, photo	165

Figure 65. Photomicrograph of faulted vein, Specimen NR1499.....	167
Figure 66. Photomicrograph of faulted vein, Specimen NR2699.....	168
Figure 67a. Photomicrograph of extended grain, SpecimenNR1099	169
Figure 67b. Close-up photomicrograph of extended grain, Specimen NR1099.....	169
Figure 68. Etched fission tracks in an apatite grain	183
Figure 69. Closure Temperatures.....	184
Figure 70. Track Length Distributions.....	186
Figure 71. Caricature of PAZ Preservation.....	187
Figure 72. Preservation of PAZ	188
Figure 73. Simplified Geologic Map with Apatite Fission-Track (AFT) results	189
Figure 74. Simplified Geologic Cross-section with Apatite Fission-Track (AFT) results	191
Figure 75. AFT results for eastern specimens	192
Figure 76. AFT results for western specimens	193
Figure 77. Age vs. Elevation plot of AFT results	196
Figure 78. Age vs. Distance from basin-bounding Fault plot of AFT results	197
Figure 79. Explanation of Results.....	198
Figure 80. Dippold Sample Results	200
Figure 81. Cooling History Plot.....	203

LIST OF TABLES

Table 1. Evolution of the Southern Rockies	4
Table 2. Average Measurements of Precambrian Bedrock by Ridgeline and Unit	144
Table 3. Average Measurements of Precambrian Bedrock by Unit	147
Table 4. Apatite Fission-Track (AFT) Thermochronology Results.....	204

ACKNOWLEDGEMENTS

I would like to thank my major advisor Dr. Mary Hubbard of Kansas State University for providing me with this project and her guidance throughout the duration. It was through her ideas, knowledge, funding and support that I was able to achieve my goals and complete this thesis. My work was supported by the generous contributions of the NASA Space Grant and the American Chemical Society Grant, without which would have made this unattainable.

I would also like to thank the following individuals: Dr. Jack Oviatt the co-primary investigator at Kansas State University for his confidence and assistance throughout the project, and serving on my committee; Dr. Robert Cullers at Kansas State University for his petrologic upbringing and assistance, and serving on my committee; Cassandra “Cassie” Dippold for allowing me to assist her in the field area and showing me the ropes; Ryan Rutherford for his field assistance and survival despite the odds and the elements; Tony Wedel for his field assistance when I was most in need, and knowledge of the local stratigraphy; Tijanguang Xu for assisting me with mineral separations at KU. Kefa Wang & Doug Walker both of the IGL at KU for allowing me to perform my mineral separation in their facilities; Shari Kelley of New Mexico Tech and the NMGRL for her apatite fission-track dating, analysis of samples and helpful advice; Linda Clough of the KSU Geology Department Secretary for her dealing with all the expenditures and paperwork in making this possible; Richard W. Allmendinger at Cornell (<http://www.geo.cornell.edu/geology/faculty/RWA/RWA.html>) for StereoWin v.1.2.0 stereonet software; Kelly Lui for map figures; Kirsten Nicolaysen for photomicrographs and encouragement; Andrea Auckly for encouragement and buddydom; Camp Dirty Six

off County Road CR 210 by Little Cochetopa Creek for your hospitality; Dud for uplifting mailings and visits; Cecile and Jim Zachary for their friendship and saintdom; and Bob Isaac for his experience, consistent pep talks and unrenowned strength.

I would especially like to thank my family, particularly my mother for all her love and encouragement, and inspiring me to complete my graduate degree. I would like to dedicate this thesis to my father for being a great role model and teaching me to strive, persist and achieve.

Thanks to all others I may have unforeseen and overlooked and whose paths crossed mine to give me perspective and appreciation. Thank you all for your contributions and assistance to me throughout the pursuit of this research and the quest for this degree!



INTRODUCTION

Despite the extensive geologic research efforts in the Rocky Mountains, the uplift and geologic evolution of this mountain range is still not fully understood. It is known, however, that the Rocky Mountains have undergone several orogenic episodes, and the southern Rocky Mountains have specifically undergone three general episodes. The oldest of these three orogenic episodes created mountains known as the Ancestral Rockies approximately 300 million years ago, followed by the middle episode of compression during the Laramide orogeny, from 80 - 40 Ma (Marshak et al., 2000; Keller and Baldrige, 1999). The youngest episode of deformation was the Tertiary to the present extension, resulting in the Rio Grande rift. Questions remain regarding how each of these deformational events has influenced the exhumation and cooling history of the southern Rocky Mountains that we see today (Keller and Baldrige, 1999).

The economic geology of the southern Rockies has been explored within both the basins and crystalline basement (Landon, 1994; Gries, 1983). Due to the wealth of resources (hydrocarbons and economic minerals) within the southern Rockies, it is pertinent to determine the deformational history and the role of the three orogenic events of the range so as to create better predictive models for resource exploration. The occurrence of the resources has been influenced by the structures present including zones of inherent weakness within the basement both in the basins and ranges.

It has been suggested that ancient structures within the basement can influence the geometry of later structures. This process is known as basement reactivation. Holdsworth et al., (1997) define reactivation as “the accommodation of geologically separable displacement events (intervals > 1Ma) along pre-existing structures.” Periodic

reactivation of long-lived lineaments (e.g. shear zones) in the basement can focus further deformation and fluid migration through tectonic inheritance (Butler et al., 1997). By studying the exposed basement rocks in the southern Rockies, the structural fabric and fault orientations can be compared with the younger structures seen in the basins in order to assess the degree of reactivation.

In order to understand the basement structures, a study area in the southern Sawatch Mountains was chosen for geologic mapping and structural characterization. This area of Precambrian basement rocks within the southern Rocky Mountains experienced all three orogenic episodes and exists adjacent to the intracontinental Rio Grande rift (Figure 1). This area is adjacent to a transfer zone between basins of the rift system and should be characteristic of the basement beneath the adjacent basins. Any inherent weaknesses within the basement might be expressed in the orientations of the faults, fabric and joints within the basement and if reactivated will also show in the basins above the basement. By analyzing the basement within the Poncha Pass Transfer Zone between the northernmost basins of the Rio Grande rift, the basement beneath the rift basins can be further understood.

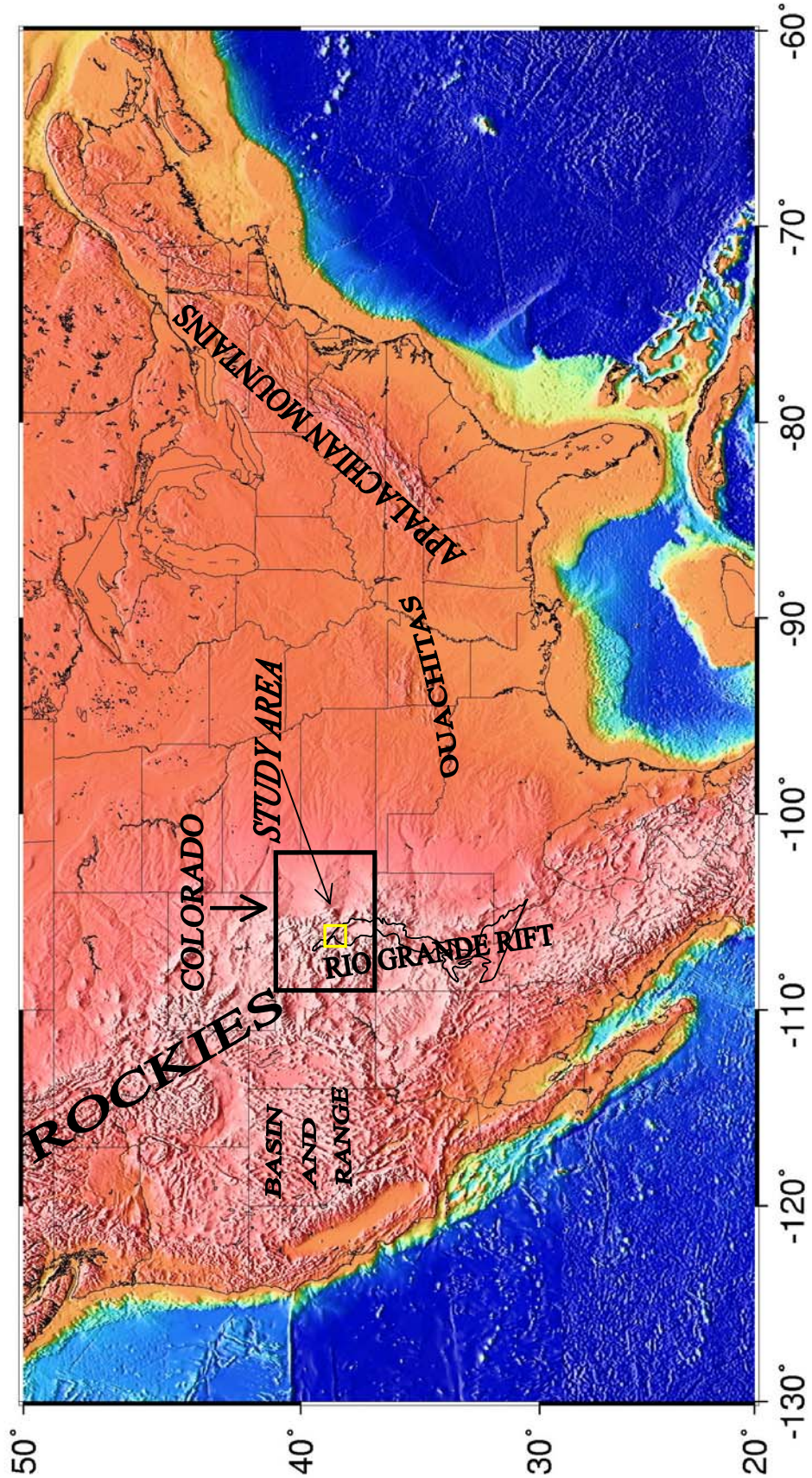


Figure 1. Continental U.S. map showing location of study area within northern Rio Grande rift of southern Colorado. Also shown are the southern Rocky Mountains ("Rockies") relative to the other mountain belts of North America, the Appalachian Mountains and Ouachitas (image courtesy of Dr. Kelly Lui, 2003, Kansas State University).

GEOLOGIC BACKGROUND

REGIONAL TECTONICS OF ROCKY MOUNTAINS

The development of the southern Rocky Mountains thus far has been attributed to three separate orogenic episodes: The Ancestral Rockies orogenic episode in the mid-Pennsylvanian, 300 m.y. ago; the Laramide Orogeny in the late Mesozoic to early Cenozoic, 80-40 m.y. ago; and rifting related to the formation of the Rio Grande rift, 30-0 Ma (Baars and Stevenson, 1984; Bird, 1998; Keller and Baldrige, 1999) (Table 1). The

TIME SPAN	EVENT
21-15 Ma	earliest normal faulting
37-28 Ma	volcanism (Oligocene Tv)
38-34 Ma	onset and initiation of rifting of Rio Grande rift; early Oligocene pre-rift volcanism
38-0 Ma (the present)	Rifting and regional extension event
80-40 Ma	Laramide Orogeny (very late Cretaceous compression)
320-270 Ma	Ancestral Rockies Orogeny (late Paleozoic compression; generation of the Fountain Formation; deformation of Paleozoic sedimentary rocks)
570-500 Ma	intrusion of alkalic rocks & faulting (late Proterozoic; Neoproterozoic)
1.0 Ga (1000 Ma)	intrusion of batholiths @ ~5km depth, e.g. Pikes Peak Batholith
1.2 Ga (1200 Ma)	regional terrane uplift
1.4-1.3 Ga (1400-1300 Ma)	widespread (anorogenic) plutonism, e.g. San Isabel Batholith; NE-trending shear zones reactivation, e.g. Fish Creek-Soda Creek Shear Zone; increased granite fertility
1.75-1.70 Ga (1750-1700 Ma)	Following deposition and intrusion of arc terranes, formation of crystalline basement by regional metamorphism of arc assemblage during Yavapai (1.8-1.7 Ga) and Mazatzal (1.7-1.6 Ga) orogenies to high grades, then intruded by numerous plutons (early Proterozoic; Paleoproterozoic)

Table 1. Summary of the Geologic History of South-central Colorado and the evolution of the southern Rockies (after Van Schmus et al., 1993; Baars and Stevenson, 1984; Bird, 1998; Keller and Baldrige, 1999; Bryant and Naeser, 1980).

southern Rocky Mountains (SRM) of the western U.S. trend NW and follow an arcuate trend with the other main mountain belts of the U.S. to the east, the Phanerozoic orogenic

belts of the Ouachitas (325-310 Ma) and the Appalachian Mountains (480-460 Ma) to the east and farther east, respectively (Figure 1). The southern Rocky Mountains exist between the Colorado Plateau to the west and the Great Plains to the east in southwestern North America, and the Basin and Range province to the west of the Colorado Plateau (Figure 2).

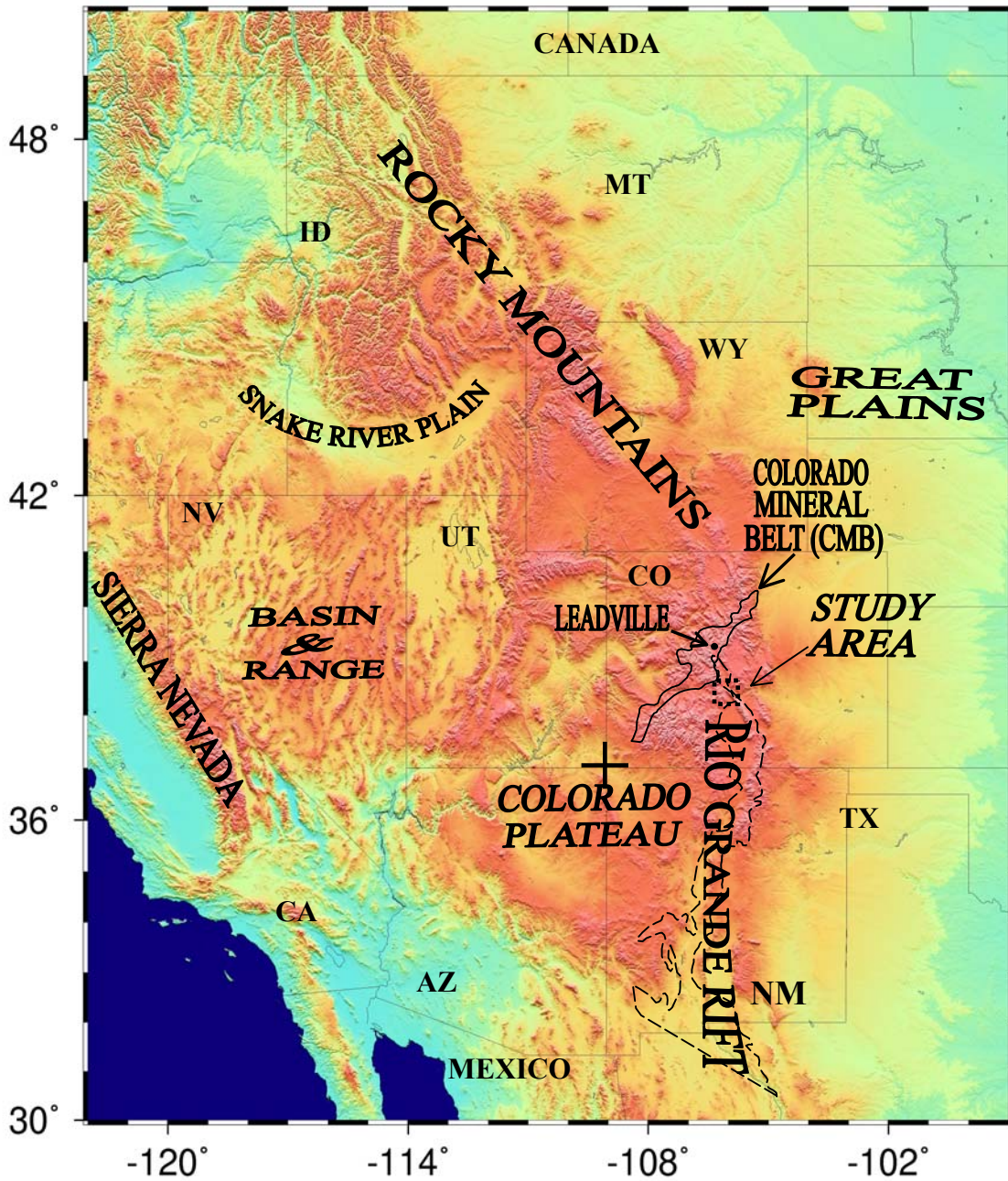


Figure 2. Western U.S., Rocky Mountain Foreland (MT, WY, CO & NM) and the Southern Rocky Mountains. Also shown is the Four Corners Region (UT to NW, CO to NE, NM to SE and AZ to SW) at the crosshatch symbol and the physiographic provinces of Basin & Range, Colorado Plateau and Rio Grande rift, and the general location of the study area in dotted lines (image courtesy of Dr. Kelly Lui, 2003, Kansas State University).

PRECAMBRIAN ASSEMBLY

The Precambrian basement, which comprises the field area, is Paleoproterozoic in age, and ranges from 1.8 – 1.6 Ga (Figure 3) (Bryant and Naeser, 1980).

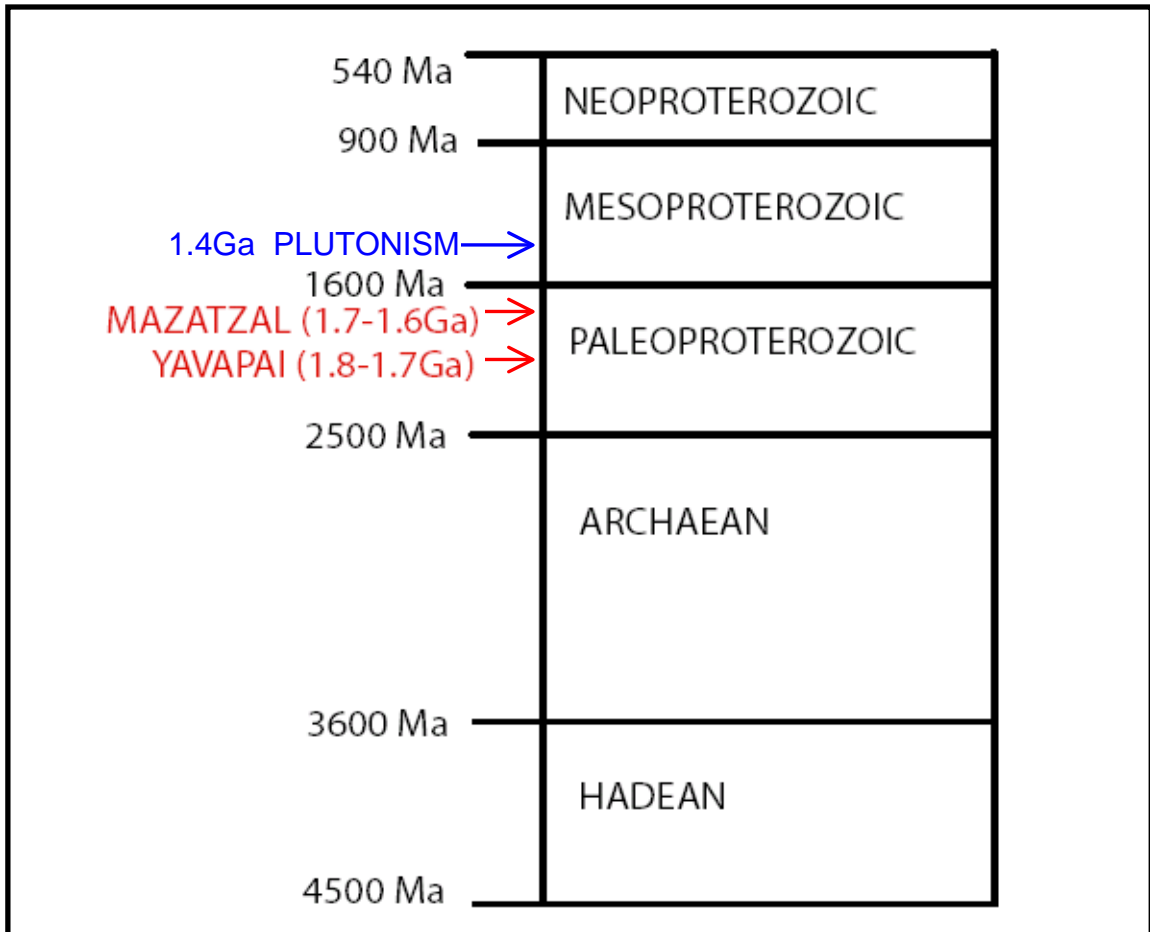


Figure 3. A Precambrian Era timeline of events showing the Statherian (1800 – 1600 Ma), and more specifically the Yavapai and Mazatzal Orogenies, during which the arc terranes were assembled in southern Colorado.

These rocks have experienced and been succumbed to many events and pulses of activity throughout the Precambrian since their initial assembly, including regional high-grade metamorphism, extensive plutonism and regional terrane uplifts. Although the rocks of the study area were initially estimated to be 1.4 - 1.6 Ga in age by Koutner (1969), it has been found by more recent age determination methods, based on Rb-Sr

dating, that they are slightly older than initially thought and range in age from 1.70-1.75 Ga (Peterman and Hedge, 1968). These ancient Statherian (1800 - 1600 Ma) rocks have been subdivided into tectonic provinces, with the older being the Yavapai (1.8-1.7 Ga) and the younger being the Mazatzal (1.7-1.6 Ga) (Bowring and Karlstrom, 1990) (Figures 4a & 4b), and have recently been deemed a product of the Colorado Orogeny (1.78-1.65 Ga) (Sims and Stein, 2001).

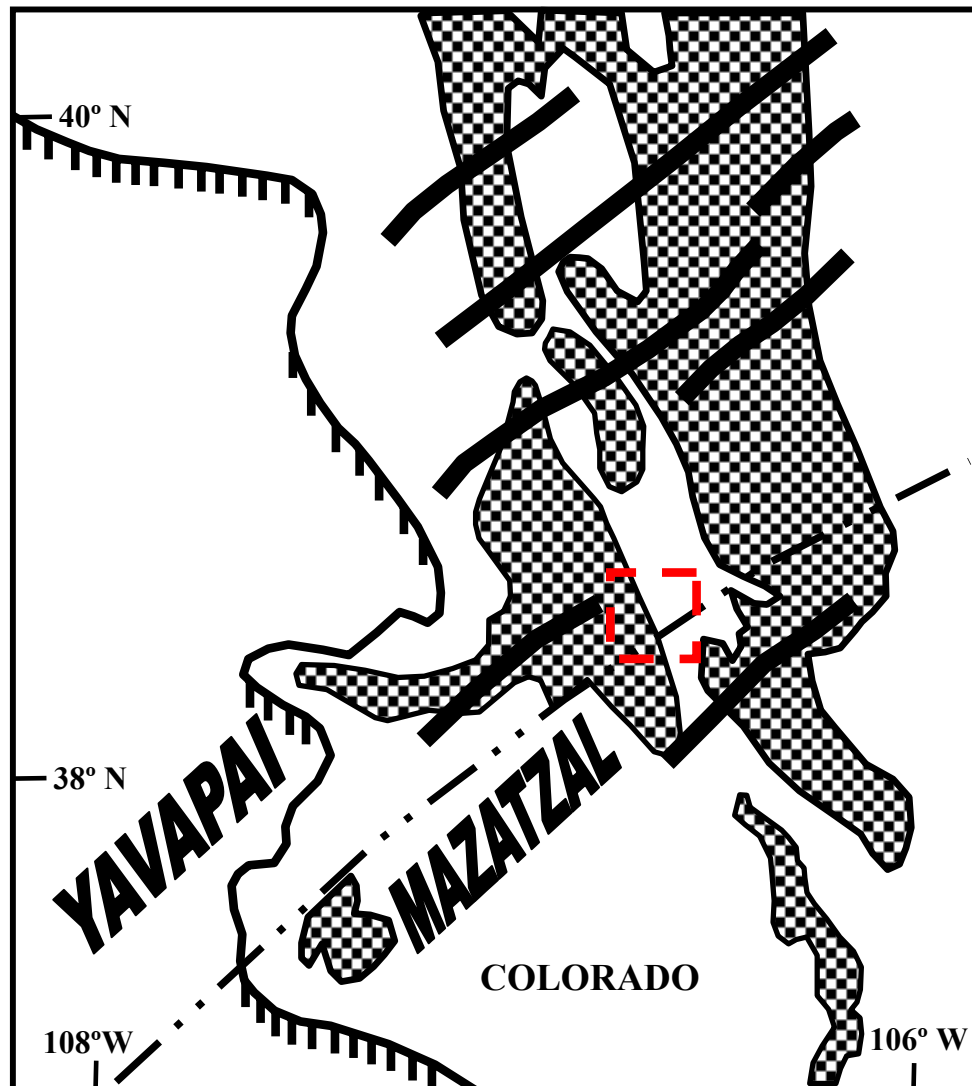


Figure 4a. Boundary of Yavapai and Mazatzal Precambrian Tectonic Provinces (dashed line); Shear Zones (bold northeast-trending lines); and Early Proterozoic Rocks {1.8-1.6 Ga} (stipled areas); Field area containing ~1.75-1.70 Ga Early Proterozoic rocks located along the Yavapai-Mazatzal Tectonic Provinces boundary shown in dashed line box pointed to with arrow (modified after Bowring and Karlstrom, 1990).

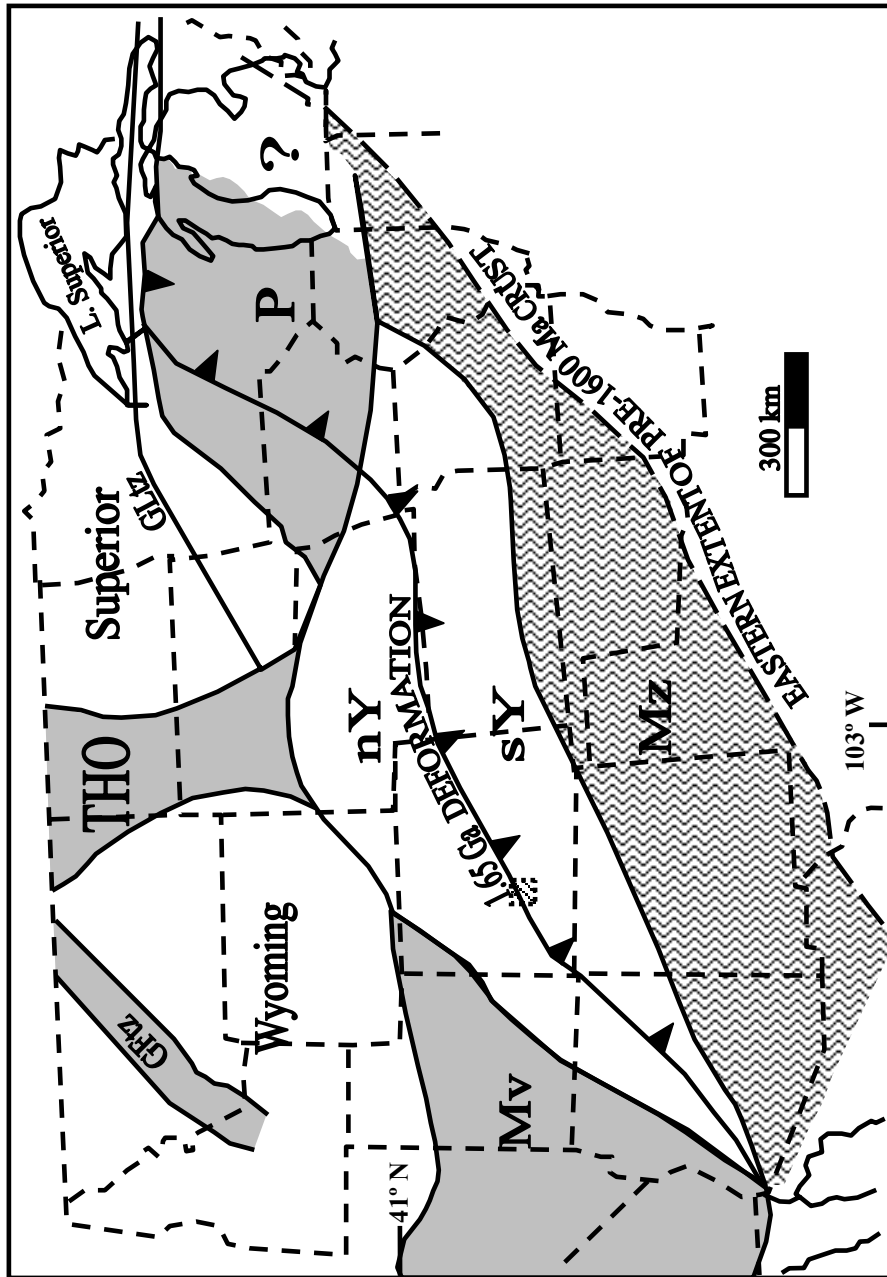


Figure 4b. Yavapai and Mazatzal Proterozoic Provinces, showing northern Yavapai (nY) and southern Yavapai (sY) subdivisions relative to state boundaries and the Study Area shown in dotted rectangle. Also shown are the Mazatzal Province (Mz); Superior Province (Superior); Penokean Orogen (P); Trans-Hudson Orogen (THO); Wyoming Province (Wyoming); Mojave Province (Mv); Great Lakes tectonic zone (GLIZ); and Great Falls tectonic zone (GFIZ) (modified from Schneider et al., 2002).

Based on metamorphic grade, age of deformation and chemical boundaries, such as Pb and Nd isotopic compositions, these Proterozoic tectonic provinces are distinguished not only by their age difference, but geochemical and structural differences as well (Williams and Karlstrom, 1996). It is unknown and still being investigated as to which specific age bracket of these two provinces the Precambrian crystalline basement

rocks of the field area lie within, relative to the boundary (Williams and Karlstrom, 1996). It has been suggested that the two terranes of the Yavapai and Mazatzal have been docked to the Archean rocks of the southern margin of Laurentia during a long-lived convergent orogen (Figure 5a). The Yavapai-Mazatzal boundary in the Southern Rocky Mountains trends northeastward through southern Colorado and is at different locations throughout the ~300 km-wide transitional zone. The exact location of the province boundary has recently been explored due to the potential influence on later thermal and tectonic activity. Shaw and Karlstrom (1999) searched for, but were unable to locate, a discrete northeast-trending Proterozoic shear zone or early accretionary boundary within the juvenile Paleoproterozoic crust (Tyson et al., 2001), in the Arkansas River valley. Tectonic fabrics comply with the initial juxtaposition of the accretionary arc terranes of the Proterozoic crustal provinces, but the fabrics and bounding structures become more shallow in Colorado compared to farther west (Shaw and Karlstrom, 1999). The Yavapai-Mazatzal boundary in the Southern Rocky Mountains that crosses through the field area consists of a low-angle suture along which the Yavapai province was thrust over the Mazatzal province that later folded and deformed with subsequent Proterozoic accretion. The low-angle suture is thought to have formed due to a lack of a rigid cratonic footwall and arc magmatism high heat flow. Its location is extrapolated by connecting Mazatzal-age plutons that suffered substantial syn-emplacement deformation (e.g. Trout Creek pluton aureole north of Salida). Given that proposed boundary, the rocks of the field area lie along the Mazatzal Front, the northern limit of Mazatzal-age (ca. 1.70-1.65 Ga) deformation (Shaw and Karlstrom, 1999), as well as the northern boundary of the Southern Yavapai Province (Karlstrom et al., 2002) (Figure 4b).

These Precambrian Paleoproterozoic rocks of the field area formed juvenile crust that was part of the late Paleozoic supercontinent of Pangaea, consisting of the landmasses of Laurentia in the north and Gondwana in the south (Figure 5a) (Hoffman, 1988; Karlstrom et al., 2001). Laurentia was a central part of the pre-Pangaea early- to mid-Neoproterozoic supercontinent Rodinia, which survived until eastern Gondwana separated from western margin of Laurentia (Hoffman, 1988). Recent paleomagnetism data findings suggest that it survived until 750 Ma (Moores, 1991). Two of the most popular models proposed for the configuration of the continents within Rodinia are the SWEAT (Southwestern US and East Antarctica) and AUSWUS (Australia and western US) (Moores, 1991). The SWEAT configuration was proposed using the orogeny that accreted Mazatzal to Yavapai as a Laurentian continuation of the Wompay orogeny on Antarctica (Moores, 1991) (Figure 5a). The AUSWUS configuration is based on the fitting of Australia with the southwestern United States (Burrett and Berry, 2000) (Figure 5a). Of these two models, the AUSWUS model has been argued to be the better fit based on statistical evidence of paleomagnetic data and geological piercing points (Burrett and Berry, 2001; Karlstrom et al., 2001). Recent work completed by Timmons et al., (2001) supports the AUSWUS model, but additional data is needed before this debate can be resolved.

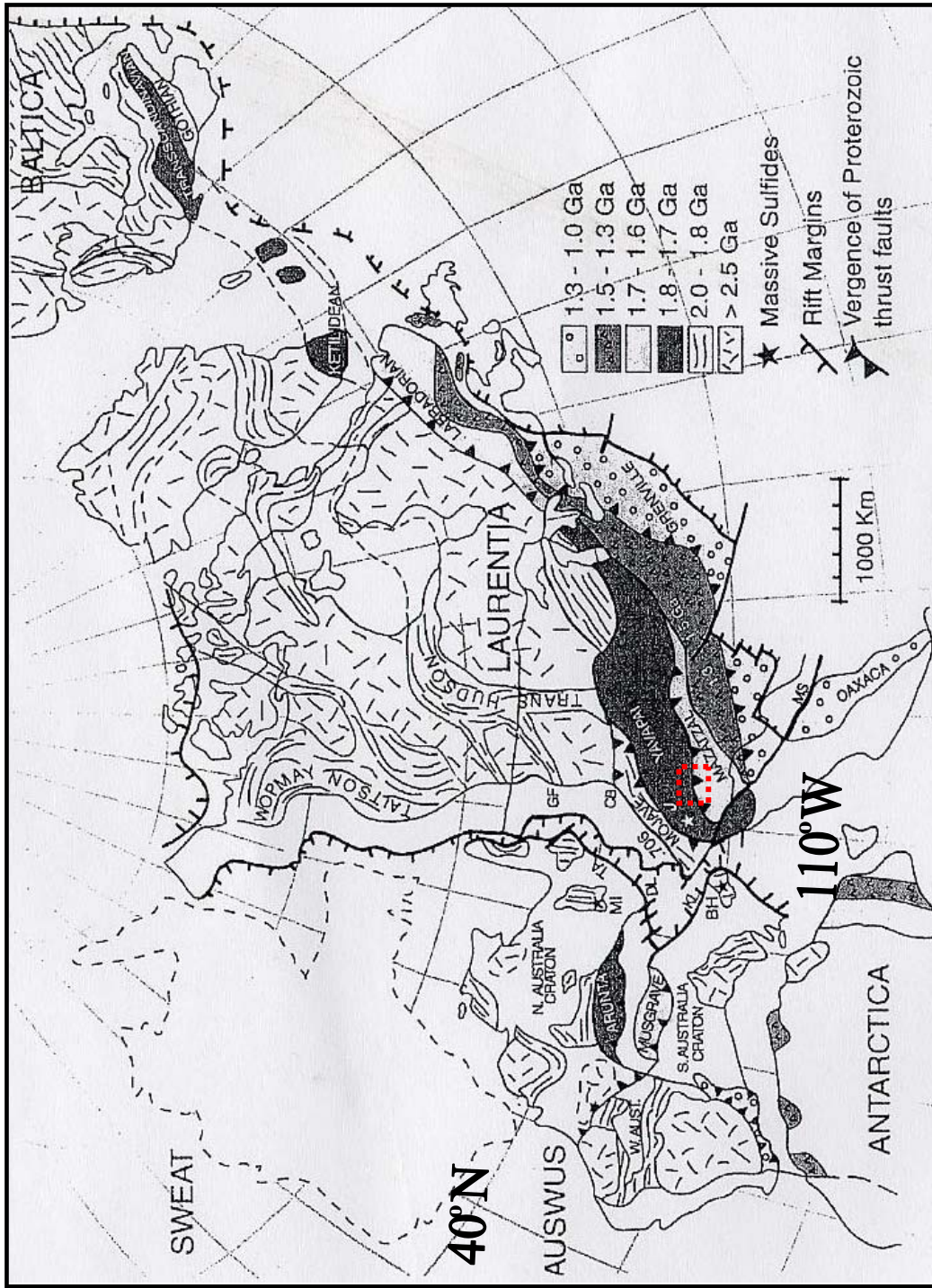


Figure 5a. Paleoproterozoic Tectonic Provinces at 1.8-1.6 Ga showing southwestern margin of Laurentia, Yavapai and Mazatzal crustal provinces, and Study Area within dashed-line rectangle. Also shown are the hypothetical SWEAT and AUSWUS locations forming the later supercontinent of Rodinia (after Karlstrom et al., 2001).

It is thought that this Proterozoic crust has undergone growth through a southward accretion along a northeast-trending continental margin of southern Laurentia. It is thought that the southwestern U.S. Proterozoic lithosphere has been constructed by an

accretionary event and convergent tectonism. There are two hypotheses of how this accretion of metasedimentary and metaigneous (volcanic and calc-alkaline plutons) rocks may have occurred; progressive island arc collisions in an island arc setting (Van Schmus et al., 1993) or diachronous assembly of tectonostratigraphic terranes and orogenic collage (Hill and Bickford, 2001) in an extensional continental setting. The rocks of the field area are interlayered amphibolite gneiss and quartzofeldspathic gneiss. Similar Precambrian assemblages of gneiss that have been recognized elsewhere, have been attributed to attendant bimodal magmatism in an extensional continental rift setting or an island arc backarc setting (Munyanyiwa et al., 1997; Hill and Bickford, 2001). Felsic magmas were produced by the partial melting of preexisting continental crust. The bimodal volcanic suites of mafic and felsic magmas were possibly formed during crustal extension in a continental backarc setting or transpressional rifting following the accretion of arc terranes (Hill and Bickford, 2001).

The age and origin of these ancient crystalline rocks of the Precambrian basement have recently been analyzed by utilizing the geophysical techniques of seismic reflection, seismic refraction, teleseismic and geological data (Dueker et al., 2001; Snyder et al., 2002). It is thought that Paleoproterozoic subduction zones, active during the collision of juvenile terranes, have influenced modern lithospheric structure in that a lower crustal layer formed at the base of the crust is actually younger than the crustal sutures and underplatings. This crust is thought to have grown by underplatings and the addition of multi-age intrusive bodies (Karlstrom et al., 2002).

The Colorado Mineral Belt (CMB) (Figure 2) to the north of these Paleoproterozoic rocks is an ancient long-lived zone of lithospheric weakness defined by

a northeast-trending Proterozoic shear zone system (Karlstrom and Humphreys, 1998; Karlstrom and Bowring, 1988) (Figure 4a) that includes the Homestake Shear Zone (NW of Leadville), Soda Creek-Fish Creek Shear Zone, Independence Pass Shear Zone (SW of Leadville) and the Idaho Springs-Ralston Shear Zone (NE of Leadville) (McCoy, 2001; Shaw et al., 2001; Shaw et al., 2002). This northeast-trending shear zone system is slightly younger than (1.65-1.4 Ga) the rocks of the field area and is thought to be either an ancient tectonic province boundary or a product of intracratonic deformation (McCoy, 2001; Shaw and Karlstrom, 1999).

The Paleoproterozoic experienced major plutonism, including an episode of granitic plutonism at 1.67-1.77 Ga, following the initiation of plutonism at ~1.8 Ga. The earliest intrusions were calc-alkaline in composition and are similar to plutons formed within magmatic arcs at subduction zones, based on the trace-element signatures. Paleoproterozoic plutons that formed later, at 1.7 Ga, increased in volumes of felsic, peraluminous and iron-bearing compositions (Anderson and Cullers, 1999).

These Precambrian rocks have experienced multiple Phanerozoic deformational events and the major directions of forces of extension and compression and the orientation of the axes and resultant structures on pre-existing structures (Figure 5b). Reactivation of the basement, through subsequent episodes of deformation along these ancient dominant structural fabric trends, and reenacting an ancestry of structures can create complex scenarios and be influential in the appearance of the crust in the present. The northeast-trending Precambrian structural grain (Keller and Baldrige, 1999), despite being overprinted in some areas, still bears a significant role as to how the basement

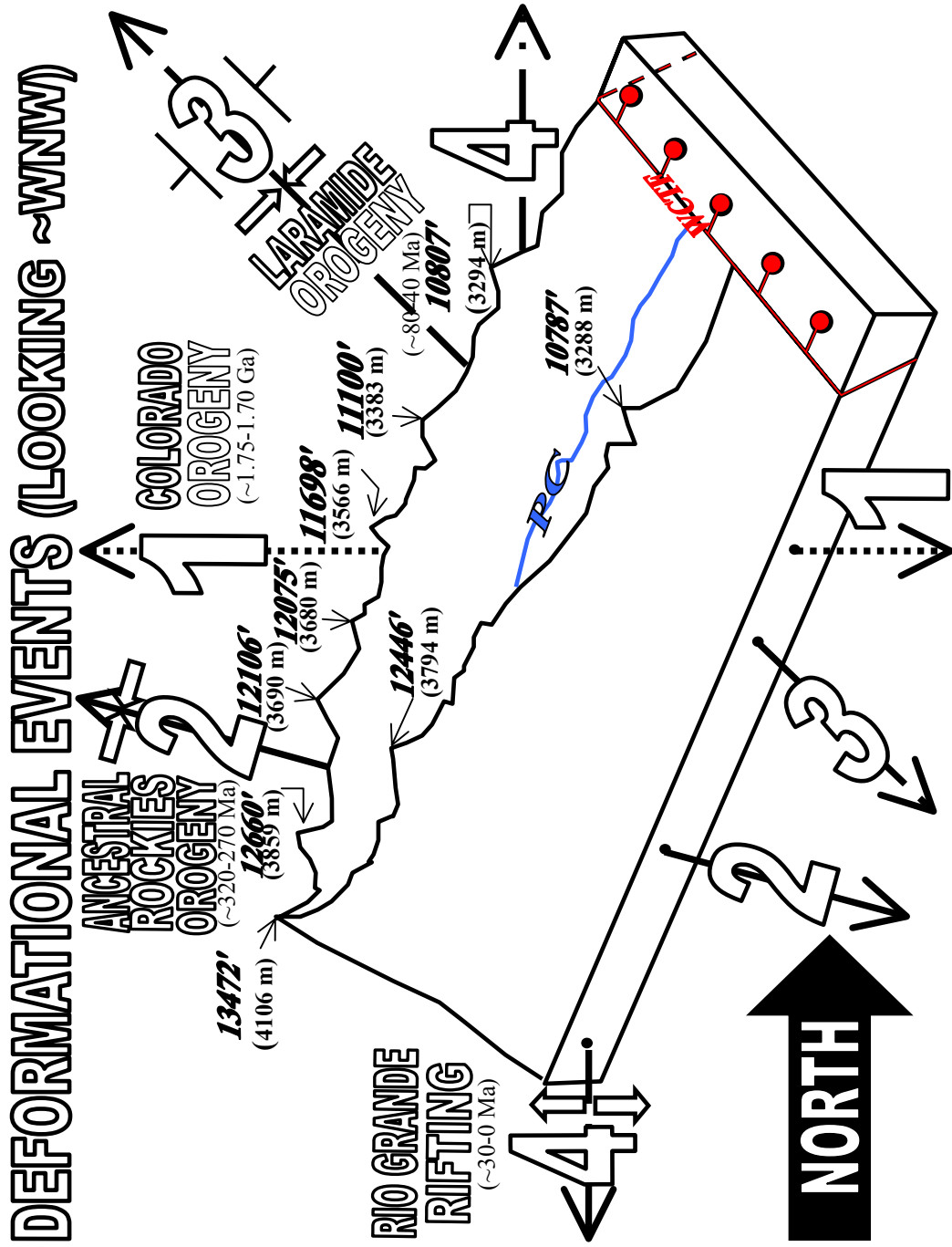


Figure 5b. Orthogonal Block Diagram Cartoon Cross-section showing the general axes of orientation of the major deformational events this area has experienced, the directions of forces, and the dominant structural trends, grains and features which resulted and possibly have been reactivated and/or inverted through subsequent deformations; PC = Pass Creek; WCTF = Willow Creek Transfer Fault.

continues to deform. The influence of the lithology and pre-existing inherited structural geometries of the basement on the spatial patterns of fault development and fracture formation (Beacom et al., 2001) is applicable to the exposed basement of the study area and was the basis for this study. Proterozoic extensional-fault systems, of both the assembly and breakup of the supercontinents, can undergo inversion and become reactivated later (Marshak et al., 2000). This mechanism might have affected the crust of the study area and facilitated younger faulting. These Precambrian rocks have experienced multiple Phanerozoic deformational events. One of the goals of this study was to examine the major directions of extension and compression on pre-existing structures (Figure 5b).

ANCESTRAL ROCKIES

The Ancestral Rockies were formed approximately 300 m.y. ago (320-270 Ma) through the late Paleozoic, more specifically from the late Mississippian through the Pennsylvanian and into the early Permian, reaching greatest extent in middle Pennsylvanian time. The orogeny consisted of basement-cored uplifts, with the Uncompahgre uplift in the west and the Frontrange uplift in the east in central Colorado (Figure 6). Both the Uncompahgre and Frontrange uplifts are part of a single, very strong and rapid uplift event (Baars and Stevenson, 1984; Kluth and Coney, 1981). The field area is located on the northeast margin of the Uncompahgre uplift (Kouther, 1969) and the southwest margin of the Frontrange uplift.

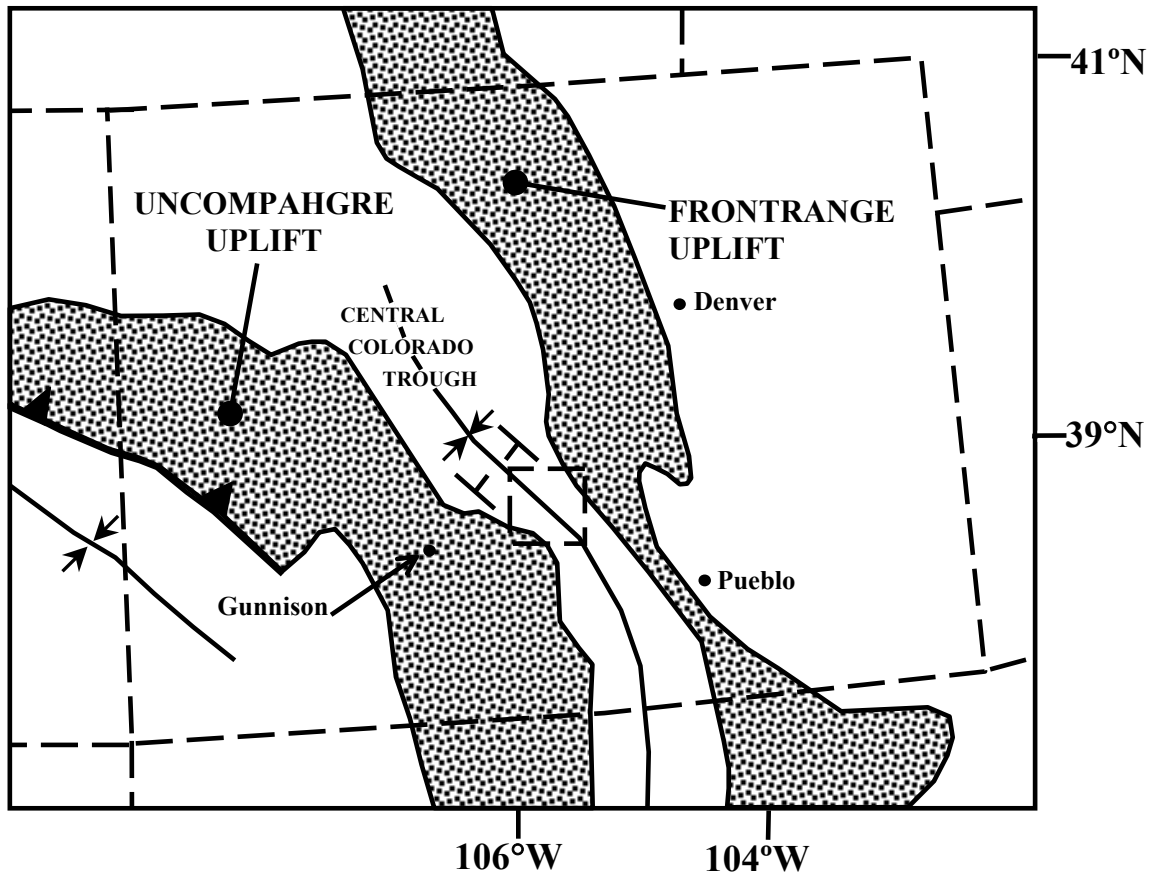


Figure 6. Ancestral Rockies Orogeny uplifts of Colorado, the Uncompahgre and Frontrange Uplifts, and the study area in square relative to these highlands (from Burchfiel et al., 1993; Knepper, 1974).

The Uncompahgre uplift formed the prominent physiographic feature of the Uncompahgre Plateau, the source of coarse arkosic clastics. Evidence for this uplift comes from the sedimentary rocks comprised of the clastics that fled into the adjacent basins, deposited in the area during the uplift. Tectonic activity along the uplift is now mostly obscured and covered by Mesozoic and Tertiary sediments. The area was overlain by kilometers of central Colorado deposits, one of which is called the Fountain Formation (also known as ‘Sangre de Cristo Formation’ to the south). The Pennsylvanian-aged Fountain Formation is a ~1,000-4,000 ft, medium to thick bedded arkosic conglomerate, with angular-subangular grains ranging from clay size to boulders

(Tweto, 1979). This uplift event is recorded in the deposition of this unit, following removal of the unit from the highlands down to the peneplain. This sediment allows the denudation to be studied, with basement reactivation potentially governing both the rate and route of removal. Recent work has utilized alpine glaciation as recorded by proglacial strata to estimate paleoelevations and determine higher elevations than previously thought for this late Paleozoic icehouse (Soreghan et al., 2002).

The Ancestral Rocky Mountains are unique, being as they formed in an intraplate setting in the middle of the North American plate, approximately 1500 km away from any active plate boundary, contrary to the formation of most mountain belts along plate margins. Collision along the northeast-southwest boundary of North America (to the northwest) and South America-Africa (to the southeast) generated northwest-southeast-trending paleoanticlines (the Uncompahgre and Frontrange in Colorado) and the similar trending paleovalley (the Colorado central trough), located between. The Penn-Perm Ancestral Rockies orogeny (ARO) entailed collision along North America's eastern and southern margins and compression along both the northern and eastern borders of the Colorado Plateau. This known pattern, coupled with recent paleomagnetic data, suggest rotation of the Colorado Plateau relative to cratonic North America, due to the existence of an independent microplate present then and even prior (Steiner, 2004).

The tectonic setting that caused the Ancestral Rockies orogenic event is still up for debate. One hypothesis is that the Ancestral Rockies formed from intraplate deformation from a continental collision to the east, along with the Appalachians (Kluth & Coney, 1981). A second hypothesis is that the action of subduction processes farther west directed an intra-plate shortening with basement-cored overthrusts (Ye et al., 1996).

The Ancestral Rockies uplifts reactivated Precambrian structures and zones of weaknesses, and influenced surficial processes up into the Triassic.

LARAMIDE OROGENY

The Laramide Orogeny uplift event across western states, primarily Montana, Wyoming, Colorado and New Mexico, formed a series of roughly north-northeast - trending anticlines and synclines as a result of the northwest-directed Laramide Orogeny. The prominent uplifts that formed during this orogeny are Beartooth, Bighorn, Black Hills, Front Range, Gunnison, Laramie, Medicine Bow, Park Range, Owl Creek, Sangre de Cristo, San Juan, Sawatch, Uinta, Wind River and Wet Mountains (Dickinson et al., 1988; Brown, 1988) (Figure 7a).

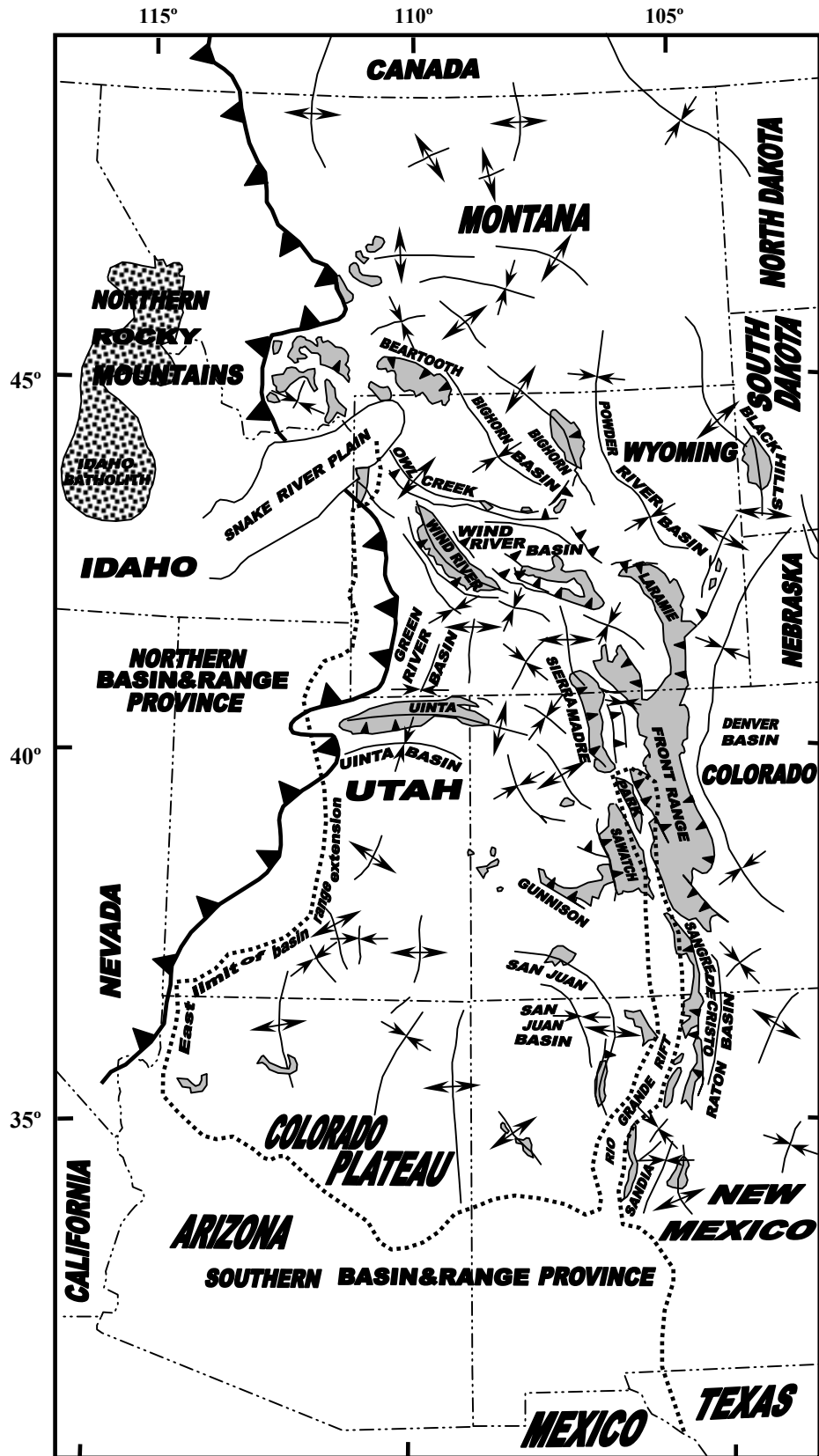


Figure 7a. Laramide uplifts (modified after Brown, 1988).

The Laramide orogeny started approximately 80 Ma and lasted up to about 40 Ma (Tweto, 1975). This (very) late Cretaceous to early Tertiary orogeny consisted of an episode of northward compression and dextral transpression along the western margin of North America and generally involved thrusting of the Precambrian metamorphic basement on faults of 25-30° dip with throws up to 13km over Phanerozoic sediments (Dickinson et al., 1988). The late Mesozoic to early Cenozoic Laramide uplift created the single large major structural feature of the north-plunging ‘Laramide Sawatch Range’ anticline, whose axis trends north-northwest and is defined by the Sawatch Range crest (Boardman, 1971). The overall ‘Laramide Sawatch Range’ anticline consisted of the Sawatch Range on the west flank and the Mosquito Range on the east flank, cut obliquely across the Central Colorado trough and dipping gently on the east side (Bryant and Naeser, 1980).

Laramide structures trend in a variety of orientations which implies multiple stages of development, basement reactivation, transpressive motions, indentation by the Colorado Plateau, and detachment of the crust through roughly 40 Ma (Erslev and Gregson, 1996). Throughout the Laramide foreland, northwest-trending uplifts, folds and arches, high-angle dip-slip faults, and the overall strike of the Laramide features being northwest, all suggest a northeast-southwest directed slip (Erslev, 1993). In addition to a west to northwest orientation there is a north to northeast trend in features resulting in a rhombohedral pattern and not regional parallelism. It has been proposed that these two trends formed by different local kinematics but were active coevally, and formed by inversion of Proterozoic extensional-fault systems (Marshak et al., 2000; Erslev and Wiechelman, 1997). Recently, a component of right-lateral displacement has been

proposed to be part of the tectonic regime within this dextral transpressional (Wawrzyniec et al., 2002).

Due to the fact that the Laramide orogeny occurred within a plate interior where the Phanerozoic section atop was near sea level, the strain and uplift were preservable (Bird, 1998). The Laramide shortening episode of deformation occurred concurrently with the Sevier orogeny farther west (Schmidt and Perry, 1988) (Figure 7b).

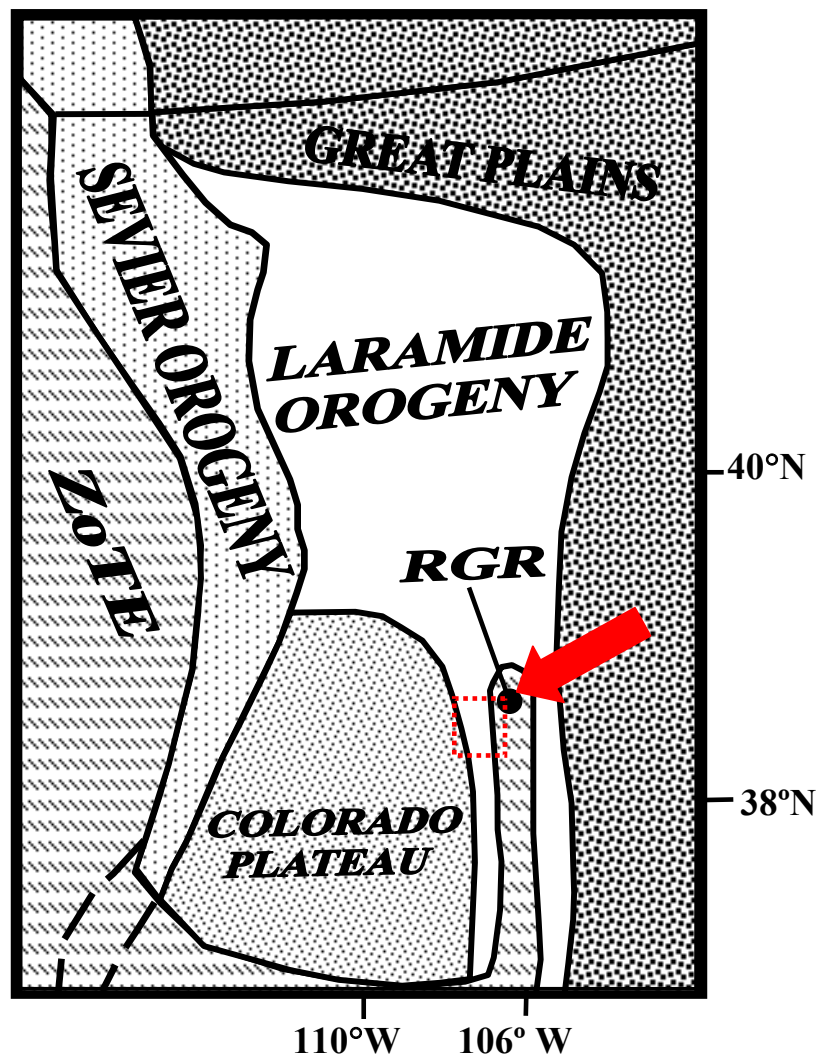


Figure 7b. The Laramide Orogen as a result of the Laramide Orogeny, shown relative to the study area in the dotted rectangle pointed to by gray arrow, the Zone of Tertiary Extension (“ZoTE”; dashed diagonal lines), the Rio Grande rift (RGR), the Colorado Plateau, the Sevier Orogen to the west and the Great Plains to the east (modified from Bird, 1988).

There are a few hypotheses as to how the shortening occurred, with one being a shallow-slab subduction model (Dickinson and Snyder, 1978), and another being a hit-and-run collisional model (Maxson and Tikoff, 1996). One other proposed model for how this shortening occurred is a lateral transmission of horizontal end-load stress, caused by flat subduction (Livaccari and Perry, 1993).

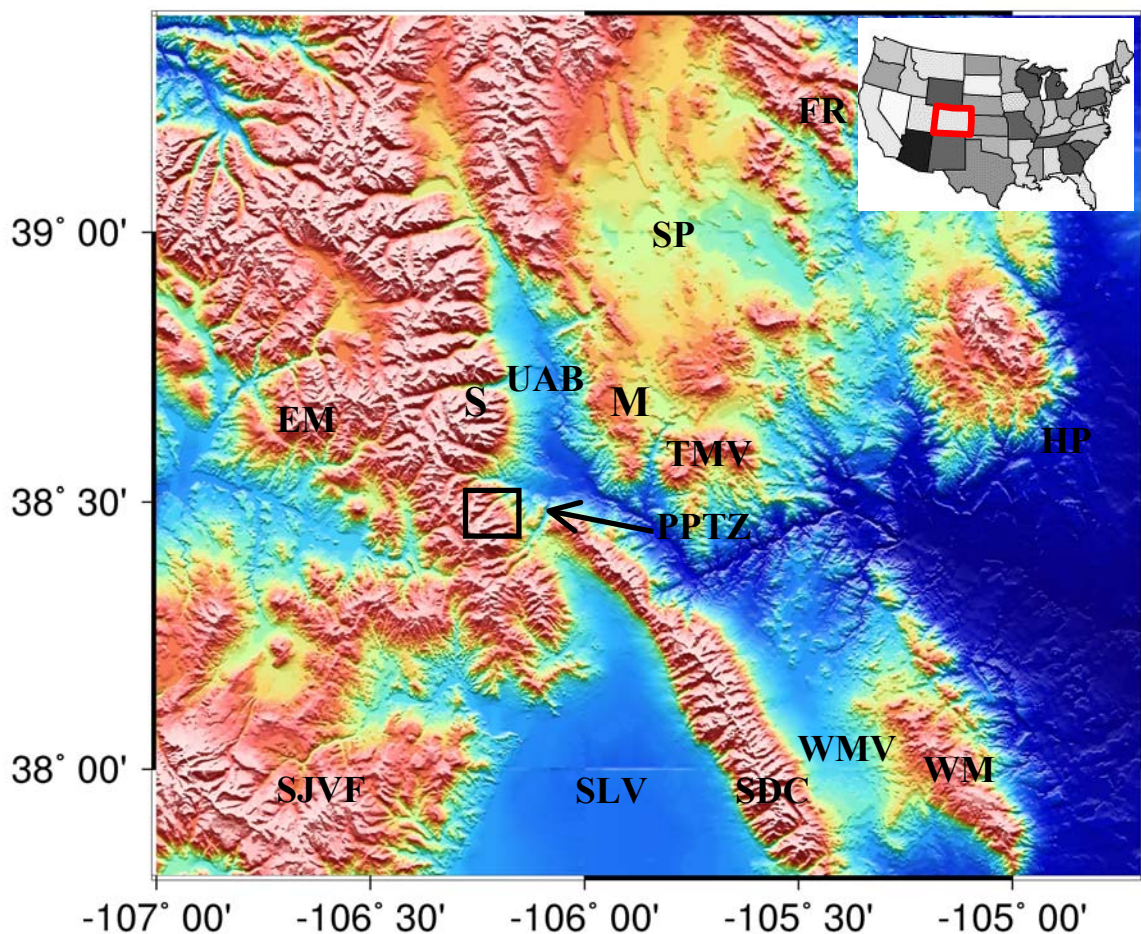


Figure 8a. Rocky Mountain Foreland of South Central Colorado showing the Southern Sawatch Range (S) with the Field Area outlined in a rectangle and the Poncha Pass Transfer Zone (PPTZ). Other regions noted: SLV=San Luis Valley, SJVF=San Juan Volcanic Field, M=Mosquito Mountains, UAB=Upper Arkansas Basin, SDC=Sangre de Cristo Mountains, WM=Wet Mountains, WMV=Wet Mountain Valley, HP=High Plains, TMV=Thirtynine Mile Volcanic Field, SP=South Park, FR=Front Range, & EM=Elk Mountains; Image courtesy of Dr. Kelly Liu, 2003, Kansas State University.

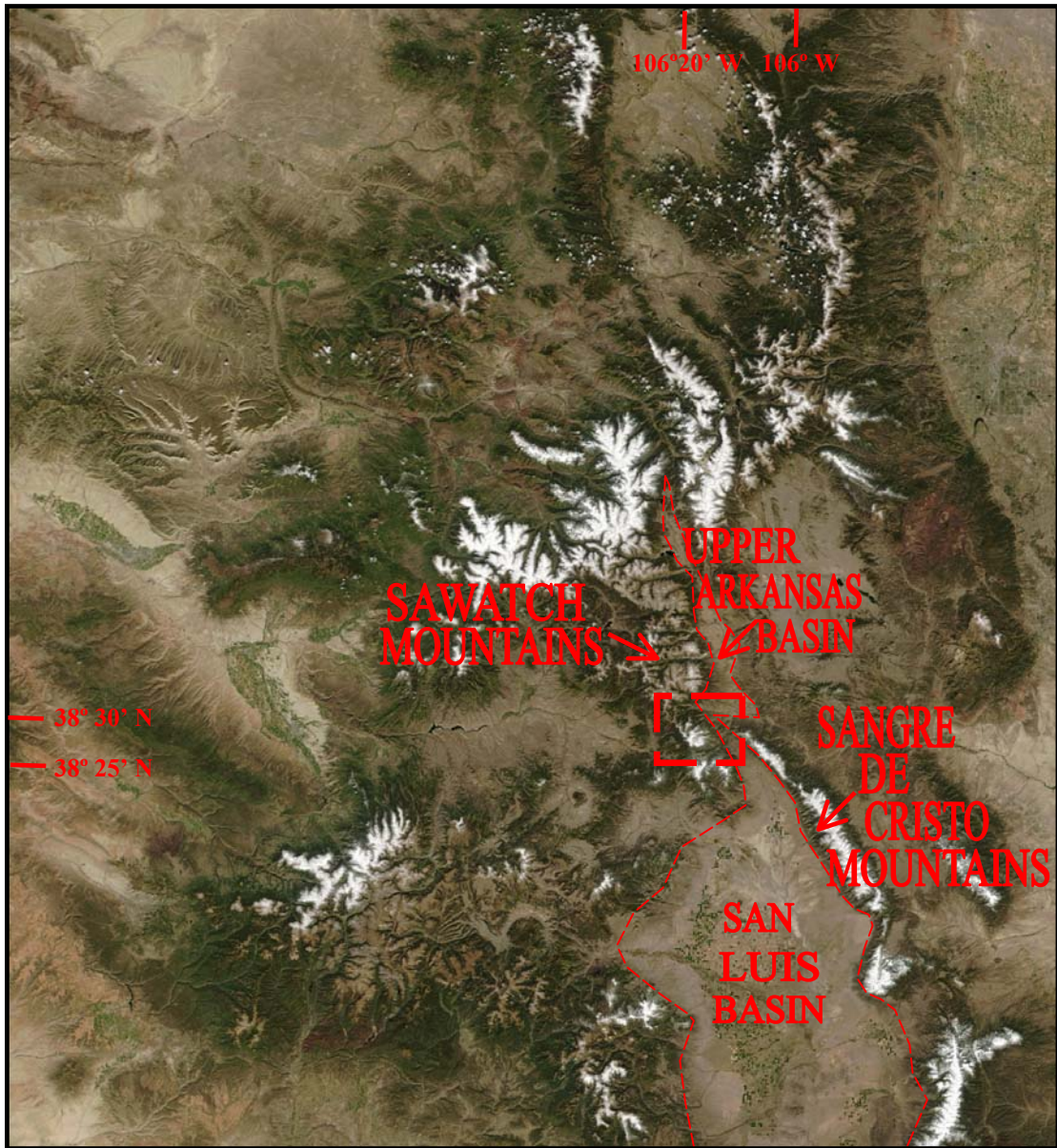


Figure 8b. Northern Rio Grande rift. Field area shown in dashed rectangle (image obtained from NASA's visible earth <http://visibleearth.nasa.gov/>).

EXTENSION ALONG THE RIO GRANDE RIFT

During the (late) Oligocene to early Miocene (22-0 Ma), the southern Rocky Mountains experienced a phase of rifting of the continental lithosphere, forming the Rio Grande rift (RGr) system. The Tertiary extension and basin development began at

approximately 30 Ma and continues into the present (Chapin and Cather, 1994; Kluth and Schaftenaar, 1994). The intracontinental zone of rifting is located in an area of extension between the Great Plains (High Plains of southern Colorado and eastern New Mexico) of the stable North American craton and the Colorado Plateau block to the west (Keller and Baldrige, 1999) (Figures 2, 8a & 9a). The Rio Grande rift is the youngest tectonic feature in the region and represents somewhat of a collapse structure, which bisects and is superimposed on the Southern Rocky Mountains (SRM). The Rio Grande rift is characterized by high heat flow, thin crust and Neogene volcanic centers (Keller et al., 1991).

The initial stages of rifting in Colorado began at ~30-27 Ma (Kluth and Schaftenaar, 1994). The Cenozoic rifting event formed a series of interconnected, asymmetrical en-echelon half-graben basins which alternate in polarity of the dip direction on the basin-bounding fault along their north-south trend (Chapin and Cather, 1994). Throughout this rift, there are four individual axial basins, which from north to south are: the Upper Arkansas Basin, the San Luis Basin, the Española Basin & the Albuquerque Basin (subdivided into the Northern and Southern Albuquerque Basins). The transfer/accommodation zones (between the basins of the Rio Grande rift) from north to south are: the Embudo Transfer Zone (San Luis Basin-Española Basin), Santa Ana Transfer Zone (Española Basin-Northern Albuquerque Basin), Tijeras Transfer Zone (Northern Albuquerque Basin-Southern Albuquerque Basin), and Socorro/Pompatosa Transfer Zone (Southern Albuquerque Basin-Palomas Basin) (Figure 9a).

The upper Arkansas basin/valley (uAb/uAv) is the northern-most half-graben of the Rio Grande rift and is connected and linked to the San Luis Basin, the largest rift

basin in the system, via the Poncha Pass Transfer Zone (aka Poncha Pass Accommodation Zone & Villa Grove Transfer/Accommodation Zone; PPTZ/PPAZ/VGTZ/VGAZ) (Figures 8a, 8b, 9a & 9b). Between the Sangre de Cristo Range and the Sawatch Range, the Poncha Pass Transfer Zone region consists of elevated, late Tertiary Dry Union Formation, along with other Tertiary sediments (gravels (Td/Ts) & Oligocene volcanic rocks (Tv)) resulting from early stages of the Rio Grande rift (Van Alstine, 1968) (Figure 9b). The Dry Union Formation was named and defined by Tweto (1961) as being composed of unconsolidated gravel, sand, silt, clay, volcanic ash, and limestone. Within the trough are some allochthonous Paleozoic breccia blocks, which appear to have slid eastward from the Sawatch Range for several miles (Van Alstine, 1970) (Figure 10). The Poncha Pass Transfer Zone is a feature of interest due to the fact that the normal fault, which bounds the eastern margin of the San Luis Basin to the immediate south of the zone, transfers over to bound the western margin of the upper Arkansas basin/valley, just north of the zone (Figures 8b, 9a & 9b). It has been proposed that the Poncha Pass Transfer Zone represents a transition between a west-dipping, basin-bounding fault of the San Luis basin and an east-dipping basin-bounding fault of the upper Arkansas basin/valley (Chapin and Cather, 1994). Understanding the exhumation history and the fault geometry of adjacent ranges will ultimately help to verify or dispose this suggestion.

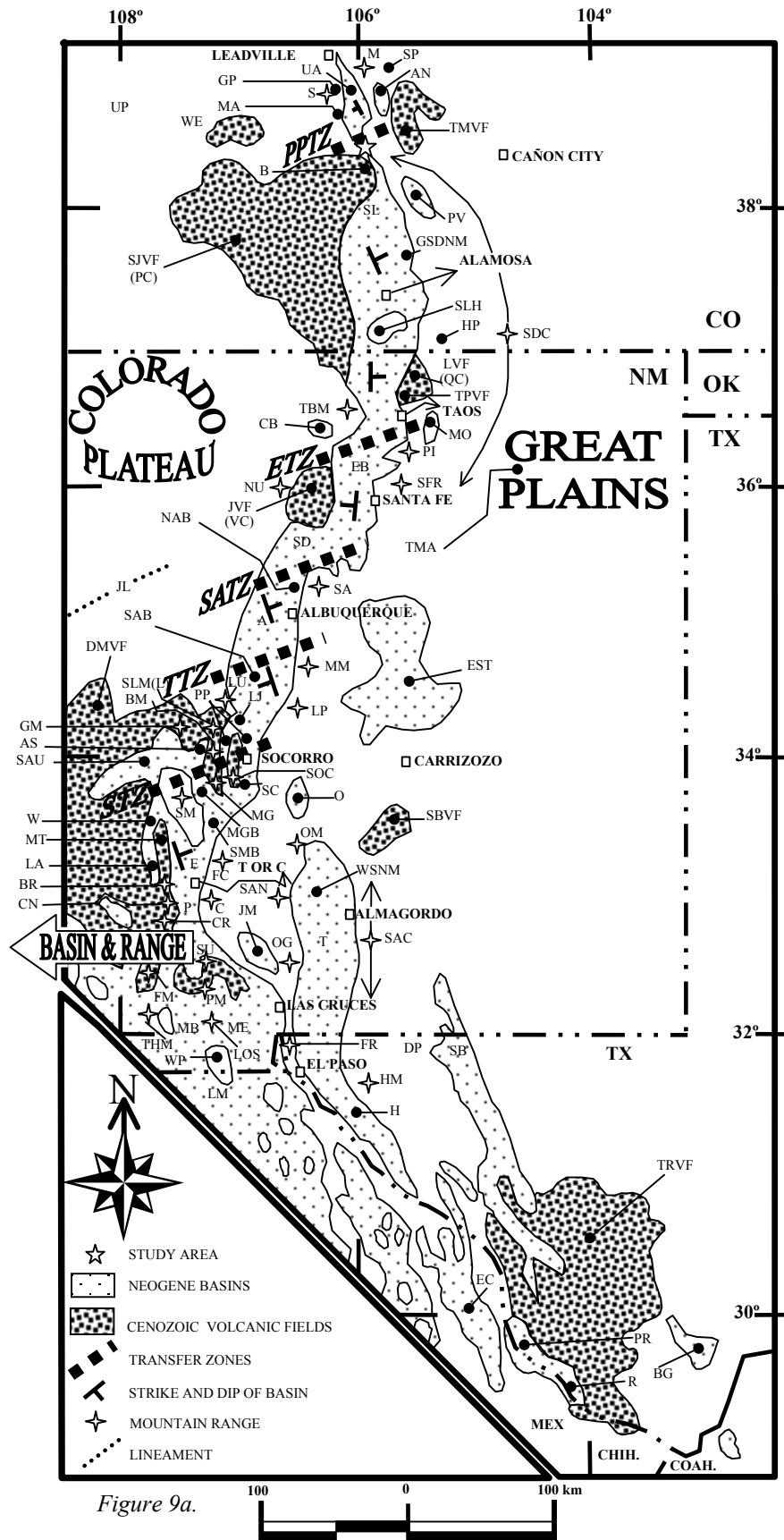
The influence of former deformational events and delineation of limits, relative to adjacent provinces of different ages, has been extensively studied to better define the Rio Grande rift. The Rio Grande rift is thought to coincide with and be influenced by an underlying potential pre-existing set of northeast-trending Precambrian lineaments,

parallel and sub-parallel to the rotational directions between the stable craton and the Colorado Plateau during the Miocene extension (Chapin and Cather, 1994). The north-south axis of the rift cuts across the northeast-trending Precambrian structural grain (Keller and Baldrige, 1999). The Rio Grande rift is also thought to represent a north-trending extension of the southern Basin and Range province into the southern Rocky Mountains (Russell and Snelson, 1994) (Figures 1, 8a & 9a). The northern termination of the rift is still uncertain but may be expressed as a narrow, north-tapering, sharply defined trough that extends for at least 60 miles (~100 km) to the Continental Divide, north of Leadville, Colorado (Chapin, 1971; Keller and Baldrige, 1999) (Figure 8b). The rift bifurcates and widens into parallel basins and ranges south of the Albuquerque basin (Chapin, 1971). The southern termination of the rift is thought to be near the border of United States and Mexico, by Chihuahua, Mexico (Figure 9a).

The upper Arkansas basin/valley (uAb/uAv) has many characteristics despite being the northernmost basin of the Rio Grande rift. To the east of the uAb/uAv it has been shown that there is a progressive steepening of the fault planes towards the eastern margin of the upper Arkansas graben, which culminates in upthrusting of the crest of the Mosquito Range along reverse faults (Chapin, 1971). In the Miocene (30 to 16 Ma), directly along the eastern margin of the Laramide Sawatch anticline/anticlinorium, the upper Arkansas graben developed as a result of the rifting episode (Bryant and Naeser, 1980). The major fault in the San Luis basin which bounds the rift just south of the upper Arkansas valley/basin, dips to the west on the eastern side of the basin along the Sangre de Cristo Mountains on the eastern flank. In the upper Arkansas basin/valley, the northernmost basin, the major basin-bounding fault is located along the western margin,

dipping to the east (Figure 8b), south of Salida and Poncha Springs (Miller, 1999). The upper Arkansas valley/basin can be subdivided into a northern elongate, rhomb-shaped, pull-apart sub-basin, with a flat valley floor and a southern triangular-shaped sub-basin, where the western half is elevated and the Tertiary sediments are uplifted with respect to the northern part (more deeply incised and better exposed than in the north) (Hubbard and Wawrzyniec, 2000; Denesha, 2003; Leonard et al., 2002). The post-Laramide elevations of the Southern Rocky Mountains have been consistent over the majority of the Cenozoic (Leonard et al., 2002) and any rock uplift has been an isostatic response to erosion.

Figure 9a (next page). The Rio Grande rift with basins and transfer/accommodation zones. The Cenozoic Volcanic Fields, Transfer Zones and Basins with Basin Fill of the Rio Grande rift shown; Abbreviations: SP = South Park; M = Mosquito Range; GP = Grizzly Peak Caldera; S = Sawatch Range; MA = Mount Aetna Caldera; UP = Uncompahgre Plateau; WE = West Elk Mountains; SDC = Sangre De Cristo Range; B = Bonanza Caldera; SLH = San Luis Hills; HP = Huerfano Park; GSDNM = Great Sand Dunes National Monument; NU = Nacimiento Uplift; PI = Picuris Mountains; SFR = Santa Fe Range; TBM = Tusas-Brazos Mountains; CB = Chama Basin/Platform; TMA = Turkey Mountain Anticline; SA = Sandia Mountains; MM = Manzano Mountains; LU = Lucero Uplift; LP = Los Piños Mountains; SLM = Sierra Ladrones (L=Ladron Peak/Uplift); GM = Gallinas Mountains; BM = Bear Mountains; SOC = Socorro-Lemitar (Soc-Lem) Mountains (with Socorro Peak); MG = Magdalena Mountains; JL = Jemez Lineament; SM = San Mateo Range; OM = Oscura Mountains; FC = Fra Cristobal Mountains; WSNM = White Sands National Monument; BR = Black Range; SAN = San Andres Mountains; C = Caballo Mountains; CN = Cuchillo Negra Uplift; CR = Cooks Range; SAC = Sacramento Mountains; OG = Organ Mountains; SU = Sierra De Las Uvas; FM = Florida Mountains; PM = Potrillo Mountains; LOS = Los Medanos; THM = Tres Hermanos Mountains; FR = Franklin Mountains; DP = Diablo Plateau; HM = Hueco Mountains; CENOZOIC VOLCANIC FIELDS: TMVF = Thirtynine Mile Volcanic Field; SJVF = San Juan Volcanic Field (with PC = Platoro Caldera); TPVF = Taos Plateau Volcanic Field; LVF = Latir Volcanic Field (with QC=Questa Caldera); JVF = Jemez Volcanic Field (with VC = Valles Caldera); DMVF = Datil-Mogollon (aka Mogollon-Datil) Volcanic Field; SBVF = Sierra Blanca Volcanic Field; WPVF = West Potrillo Volcanic Field; and TRVF = Trans-Pecos Volcanic Field; TRANSFER ZONES: PPTZ = Poncha Pass Transfer Zone (TZ1/5); ETZ = Embudo Transfer Zone (TZ2/5); SATZ = Santa Ana Transfer Zone (TZ3/5); TTZ = Tijeras Transfer Zone (TZ4/5); STZ = Socorro/Pompatosa Transfer Zone (TZ5/5); BASINS (WITH BASIN FILL DEPOSITS) from north to south: UA = Upper Arkansas Basin (BASIN1/5) {west-dipping/tilting}; AN = Antero Basin; PV = Pleasant Valley Graben; SL = San Luis Basin (BASIN2/5) {east-dipping/tilting}; MO = Moreno Basin; CB = Chama Basin; EB = Española Basin (BASIN3/5) {west-dipping/tilting}; SD = Santo Domingo Basin; EST = Estancia Basin; NAB = Northern Albuquerque Basin (BASIN4/5); A = Albuquerque-Belen Basin; SAB = Southern Albuquerque Basin (BASIN5/5) {west-dipping/tilting}; LJ = La Jencia Basin; SC = Socorro Basin /Constriction (the SC & LJ and interveining Soc-Lem Mountains comprise the early rift basin Popotosa (PP)); PP = Popotosa Basin; AS = Abbe Springs Basin (aka northern Milligan Gulch Basin (MGB)); SAU = San Augustin Basin; O = Oscura Basin; MGB = Milligan Gulch Basin; SMB = San Marcial Basin; MT = Monticello Basin; W = Winston Basin; LA = Las Animas Basin; E = Engle Basin; P = Palomas Basin; T = Tularosa Basin; JM = Jornada del Muerto Basin; MB = Mimbres Basin; ME = Mesilla Basin; LM = Los Muertos Basin; H = Hueco Basin; SB = Salt Basin; EC = El Cuervo Basin; PR = Presidio Basin; BG = Black Gap Basin; and R = Redford Basin (modified from Keller and Cather, 1994; Russell and Snelson, 1994; Chapin and Cather, 1994; Keller and Baldrige, 1999 and Chapin, 1971).



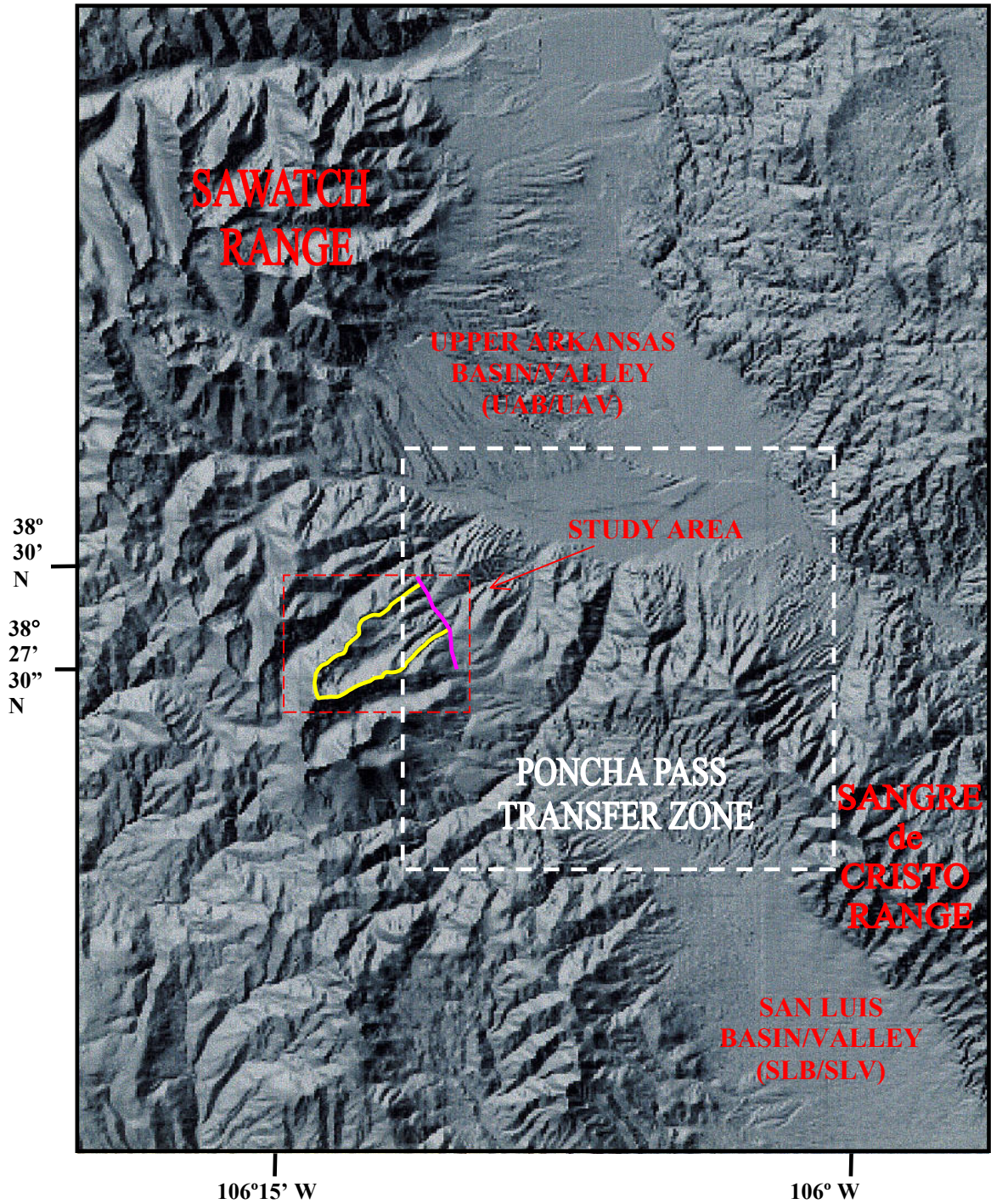


Figure 9b. Digital Elevation Model showing the Poncha Pass Transfer Zone (PPTZ), located between the San Luis basin/valley/half-graben (SLb/SLv) to the south and the upper Arkansas basin/valley/half-graben (uAb/uAv) to the north. Also shown is the traverse of the ridgelines within the study area that is truncated to the northeast by the WCTF (Willow Creek Transfer Fault), shown with purple line.

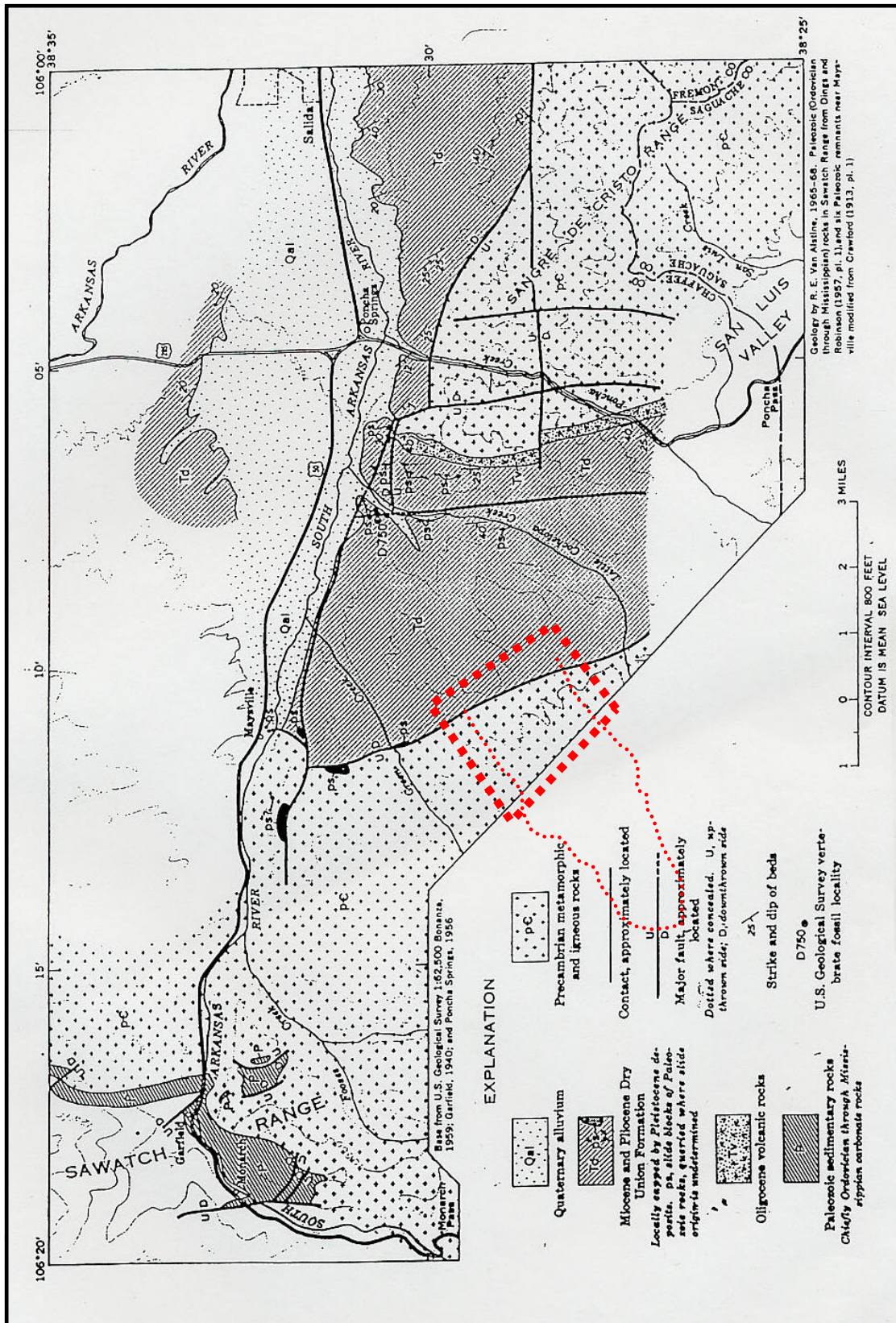


Figure 10. Sawatch and Sangre de Cristo Ranges of the Rio Grande Rift with the ridgelines (dotted) of the field area (dashed) (modified after Van Alstine, 1970).

SAWATCH RANGE

The Sawatch Range of south-central Colorado is part of the Southern Rockies province, in addition to the mountain ranges between southern Idaho and Montana, and northern Mexico (Leonard et al., 2002). The Sawatch Range bounds the west side of the upper Arkansas basin/valley of the Rio Grande rift, just northwest of the Poncha Pass Transfer Zone (Figures 8a & 8b). The Mosquito Range bounds the eastern margin of the upper Arkansas basin/valley. The Sawatch and Mosquito ranges were part of the overall Laramide Sawatch Anticline uplift that was dissected by the gash or collapse structure referred to as the Rio Grande rift. These two ranges were separated as a result of the extension in the rift. The Arkansas River flows along this downfaulted valley, which maintains the separation (Figure 10).

The Sawatch Range trends roughly north-northwest and consists of 15 peaks that have an elevation of $\geq 14,000'$ (4267 m) (“Fourteeners”) out of the total 54 peaks that have an elevation of $\geq 14,000'$ (4267 m) within the state of Colorado. These peaks have been referred to as the “Collegiate Peaks”, with the prominent peaks of Mt. Oxford (14,153' [4314m]), Mt. Harvard (14,420' [4395 m]), Mt. Yale (14,196' [4327 m]), Mt. Princeton (14,197' [4327 m]), and Mt. Columbia (14,073' [4289 m]) (Figure 11).

Elevations of the region range from 7,800 feet (2377 m) in the Upper Arkansas Basin, up to the surrounding peaks of approximately 12,000 to 14,000 feet (3658 to 4267 m). Poncha Pass, which divides the watershed into the Rio Grande River to the south and the Arkansas River to the north, is 9,010 feet (2746 m) in elevation. In the surrounding region, to the east of the Sawatch Range and east of the Mosquito Range, is the Thirtynine Mile Volcanic Field. To the south and southwest is the San Juan Volcanic

Field. Due south is the San Luis Basin and to the southeast, are the Sangre de Cristo Mountains (Figures 8a, 9a & 9b).

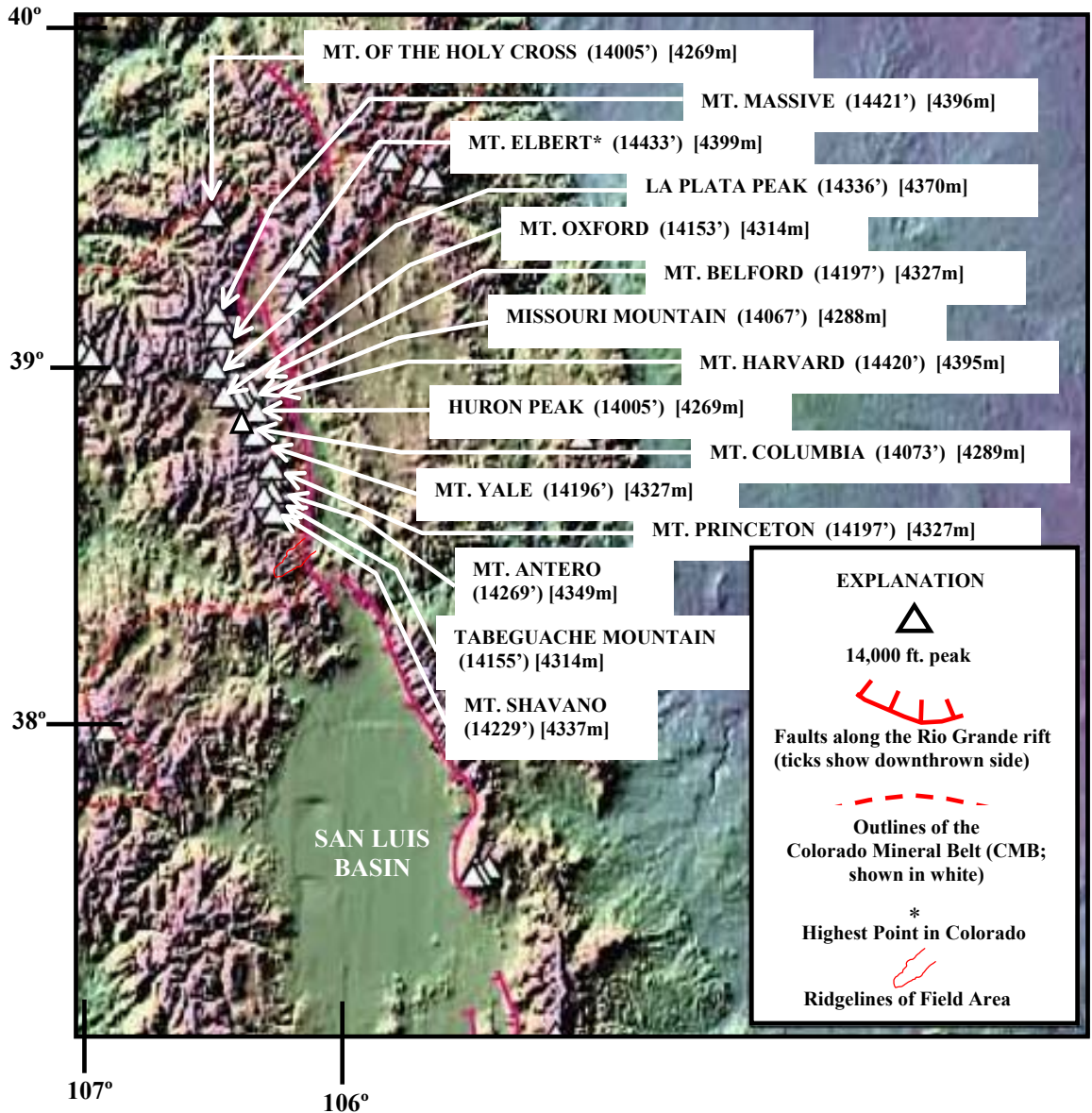


Figure 11. The 15 “Fourteeners” within the Sawatch Range of the southern Rocky Mountains in south-central Colorado of the 54 within the state of Colorado (modified from Reed, 2000).

The geology of the Sawatch consists of the Precambrian igneous and metamorphic rocks (Barnes, 1935; Barnes and Butler, 1935; Stark and Barnes, 1935; Stark, 1935), the Tertiary/Upper Cretaceous intrusive rocks, the overall Tertiary,

Mesozoic, and Paleozoic sedimentary rocks and Tertiary volcanic rocks (Figure 12a).

The Precambrian rocks in Colorado underwent regional high-grade metamorphism, about 1,700 to 1,750 Ma (Bryant and Naeser, 1980). Immediately after the assembly, the Precambrian rocks were intruded by numerous plutons (Peterman and Hedge, 1968). The broad north-trending structural arch (anticlinal uplift) of the Sawatch Range is said to have been eroded, resulting in an exposure of the Precambrian crystalline rock core (Pearson et al., 1962). This region was initially mapped and originally classified as the “Sawatch schists” (Stark and Barnes, 1935) and migmatites (Stark, 1935). The Precambrian crystalline rocks are marked by the presence of trace amounts of sillimanite and are predominantly amphibolites (Dippold, 1999). The Precambrian bedrock displays two structural trends (primarily older northwest-trending faults and younger northeast-trending faults) within the field area (Kouther, 1969) (Figure 12b). To the immediate east of the field area, the metamorphic foliation displays a transition from one structural trend (northwest) to another (north-northeast) from the north to south (Dippold, 1999) (Figure 12c). Following the Precambrian formation and throughout both the Paleozoic and Mesozoic, numerous depositional events occurred to form the overlying strata. The Paleozoic sediments, namely the Mississippian-Ordovician Formations of Carbonates (being the Mississippian Leadville Formation and the Ordovician Manitou Dolomite, Harding Sandstone, and Fremont Dolomite Formations (MDO)), crop out to the south and southwest of the study area (Figure 10). The Mesozoic sediments include the Dakota and Morrison Formations (KJdm), which crop out to the northwest of the study area (Tweto, 1979).

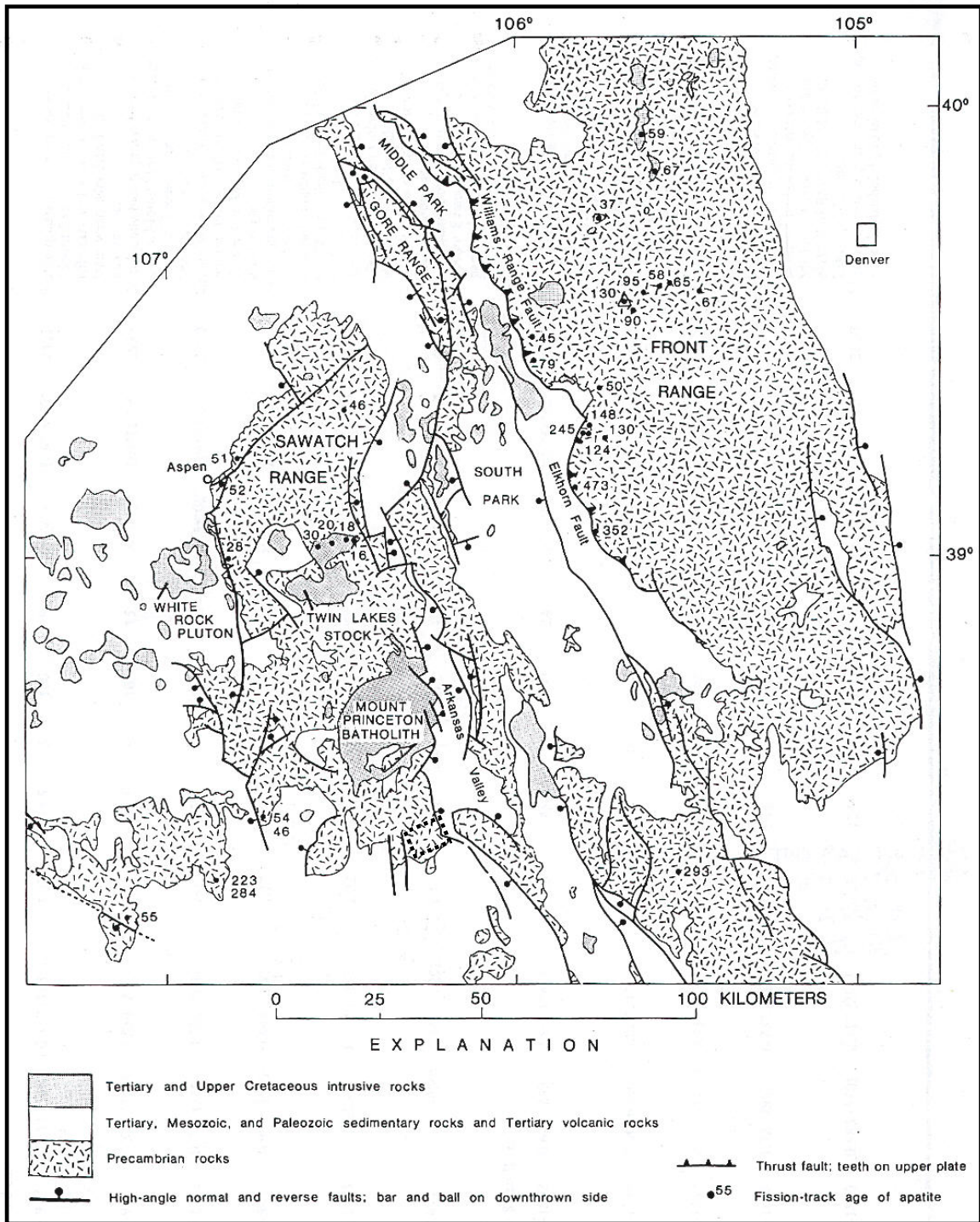


Figure 12a. Simplified Geologic Map of southern Sawatch Range showing Field Area in dashed-line rectangle (modified from Bryant and Naeser, 1980).

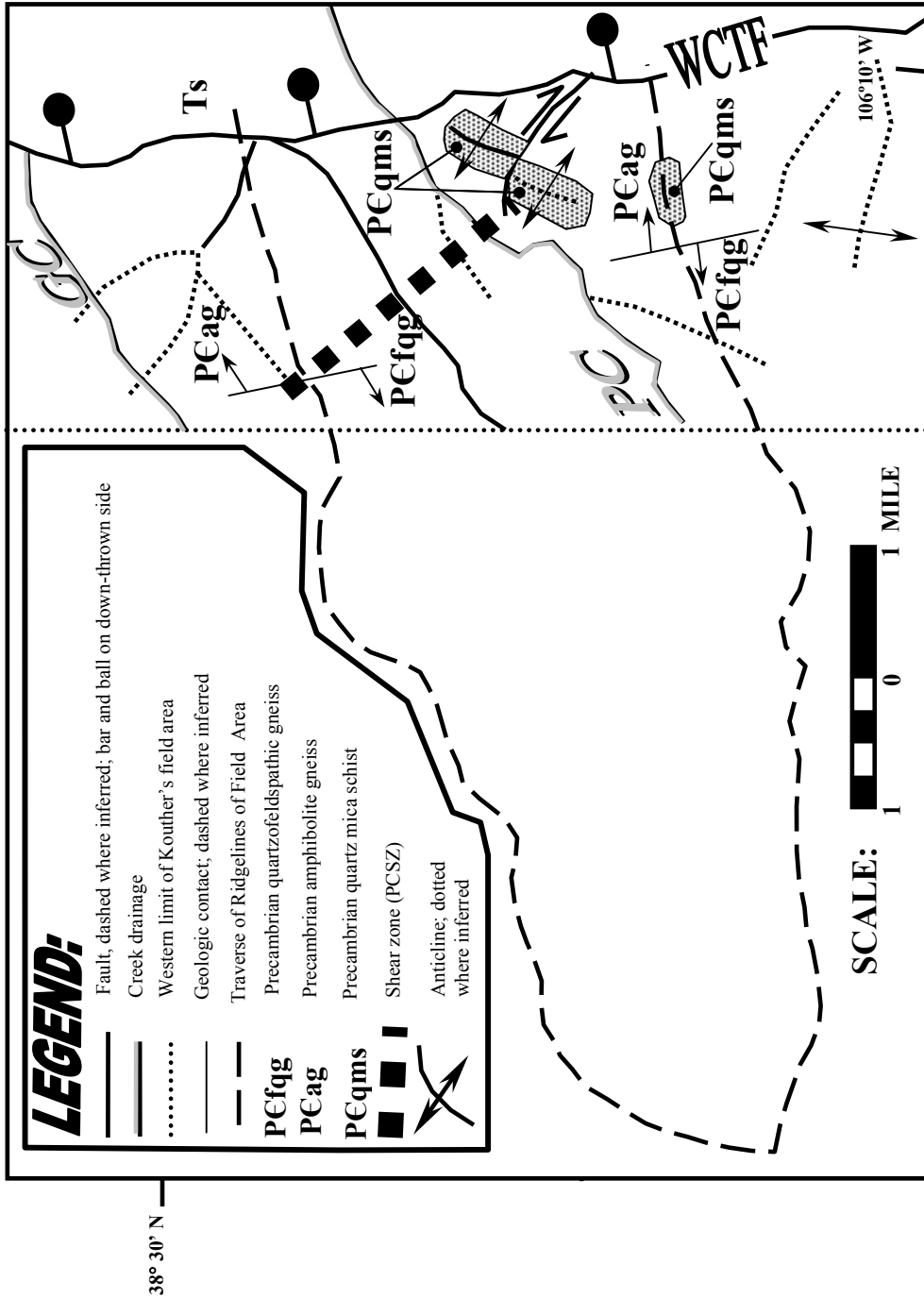


Figure 12b. Kauther's (1969) findings in the eastern extent of field area, showing the proposed 3 anticlines and 1 syncline down by Little Cochetopa Creek, within the proximity of the traverse of the ridgelines. PC = Pass Creek, GC = Green Creek, WCTF = Willow Creek Transfer Fault; Ts = Tertiary sediments.

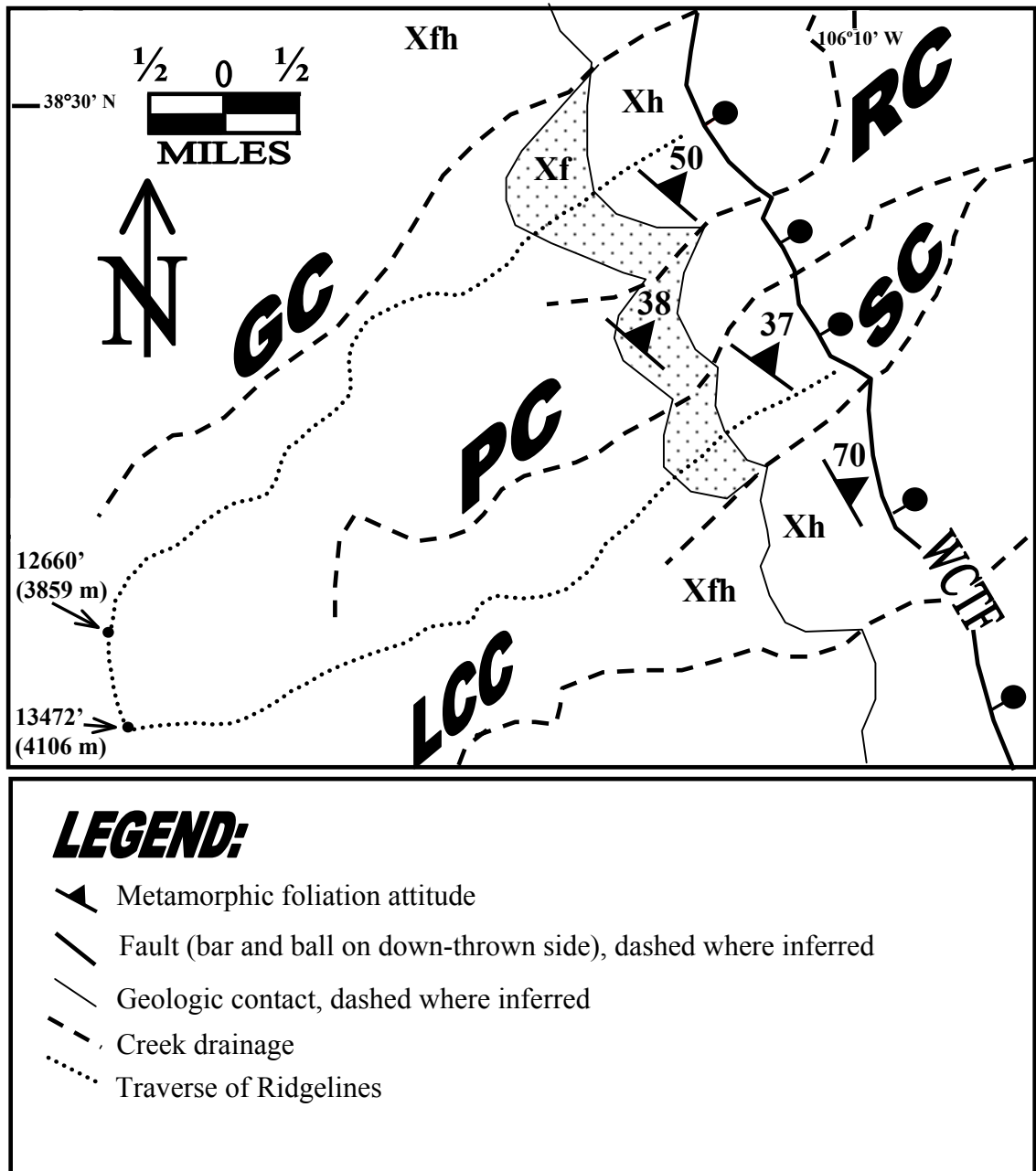


Figure 12c. Dippold (1999) findings. WCTF = Willow Creek Transfer Fault; GC=Green Creek, RC=Redmans Creek, PC=Pass Creek, SC=Stumpy Creek, LCC=Little Cochetopa Creek; Xfh =Precambrian hornblende-feldspathic gneisses; Xh =Precambrian Gneissic Amphibolite; Xf = Precambrian Quartzo-feldspathic Gneiss.

TIMING

Previous work done in the Sawatch by Bryant and Naeser (1980) documented that, based on apatite fission-track ages, significant uplift of the Sawatch must have occurred during or after the Eocene (45 to 30 Ma) along the western flank of the Upper Arkansas Basin, with additional uplift occurring in the Miocene (30 to 16 Ma). Kelley et al. (1992), found that in the Sawatch Range from the west to the east, the apparent apatite fission-track ages decrease, which has been interpreted as a westward rotation of the block during the rift formation. The eastern margin samples dated to be 9 to 15 Ma and the western interior samples were older, about 15 to 20 Ma, which coincides with the rifting episode of 22-0 m.y. ago. My work builds upon this by presenting new fission track ages, coupled with structural analysis from an area south of the Kelley et al. (1992) study area, in order to address the nature of mountain uplift, exhumation and the role of basement reactivation adjacent to a transfer zone.

In order to understand the basement structures and the influence the basement had on later deformation, possible emplacement of hydrocarbons, and mineralization related to structures associated with inherent weaknesses (both within the basins and in the range), a study area in the southern Sawatch Mountains was chosen for geologic mapping and structural characterization of the structural fabric and fault orientations. This area of Precambrian basement rocks within the southern Rocky Mountains underwent all three orogenic episodes and exists adjacent to the intracontinental Rio Grande rift (Figure 2). By studying the exposed basement rocks in the southern Rockies, the structures can be characterized in order to make comparisons with the younger structures seen in the basins. By obtaining apatite fission-track (AFT) ages and coupling them with the

$^{40}\text{Ar}/^{39}\text{Ar}$ ages of the higher closure-temperature minerals, a specification as to which southern Rocky Mountain orogenic event coincided with the exhumation of the Sawatch Range can be made. This study area is adjacent to a transfer zone between basins of the rift system and should be characteristic of the basement beneath the adjacent basins. Any pre-existent structures and inherent weaknesses within the basement that may have formed during reactivation might be expressed in the orientations of the faults, fabric and joints within the basement and the basins above the basement. By analyzing the basement within the transfer zone between the northernmost basins of the Rio Grande rift, the basement beneath the rift basins can be further understood.

There has been an extensive history of igneous activity in the vicinity of the northern upper Arkansas valley. Isolated exposures of the Sawatch Range have been studied by others, specifically the Mesoproterozoic 1396 ± 40 Ma St. Kevin Granite (Pearson et al., 1966; Doe and Pearson, 1969), the 66 Ma Twin Lakes Stock granodiorite batholith (Fridrich et al., 1991), the 29.0 ± 3.0 Ma Mt. Antero Granite (Thompson and Pulfrey, 1973; Shannon, 1986) and California Intrusions (Shannon, 1986), 34 Ma Grizzly Peak Caldera (Fridrich et al., 1991, 1998), the late Eocene 36.6 Ma Mount Princeton quartz monzonite Batholith (Kelley, 1991; Kelley et al., 1992), the middle Tertiary Oligocene (26-38Ma) intrusive White Rock Pluton (Wawrzyniec et al., 2002; Gaskill et al., 1991), and the Mount Aetna Cauldron (Shannon, 1988) (Figures 9a & 12a).

FIELD AREA

My field area is located to the west of the study areas of Koucher (1969) (Figure 12b) and Dippold (1999) (Figure 12c). My field area is located within the following

U.S.G.S. 7.5 minute quadrangles at elevations ranging from 9,500 feet (2896 m) to 13,472 feet (4106 m): 1.) Mt. Ouray; 2.) the southern edge of Maysville; and 3.) the eastern half of Pahlone Peak. The longitude of the field area ranges between 106°10'00"W - 106°15'00"W and the latitude between 38°25'00"N -38°32'30"N, and the field area lies mostly within T49N and R7E (Figures 11, 12 & 13; Plate I).

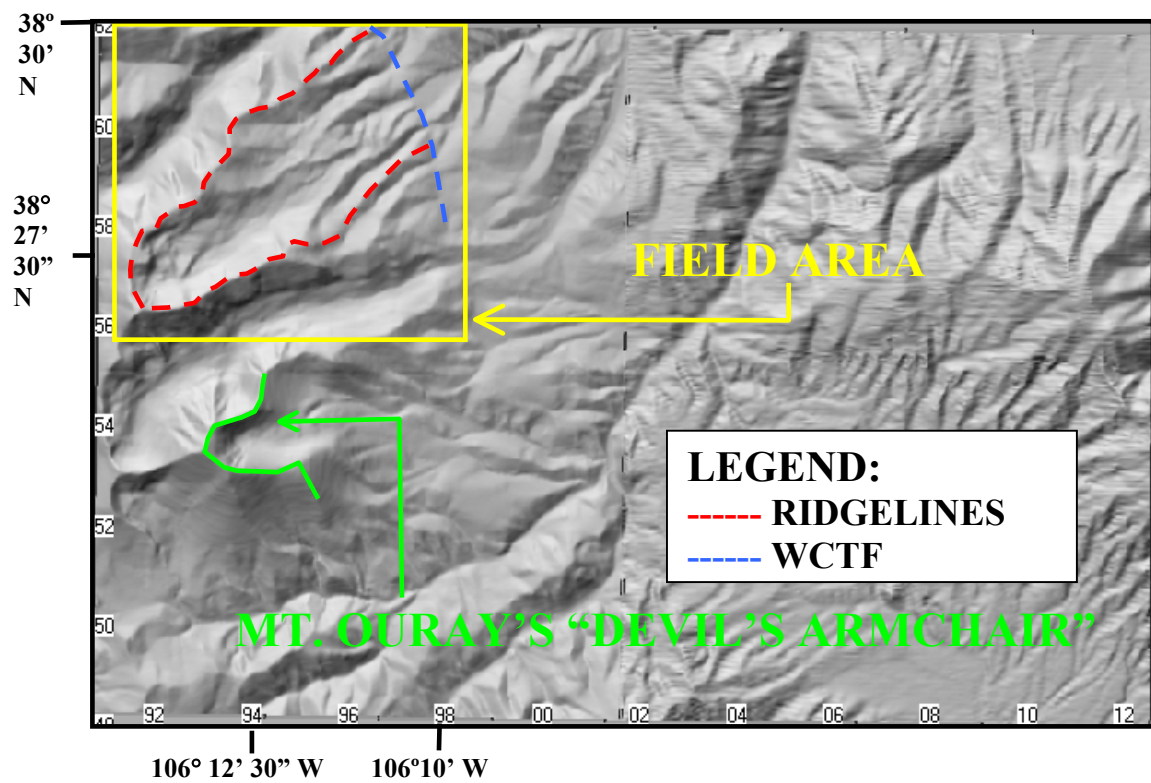


Figure 13. Digital Elevation Model of Field Area.

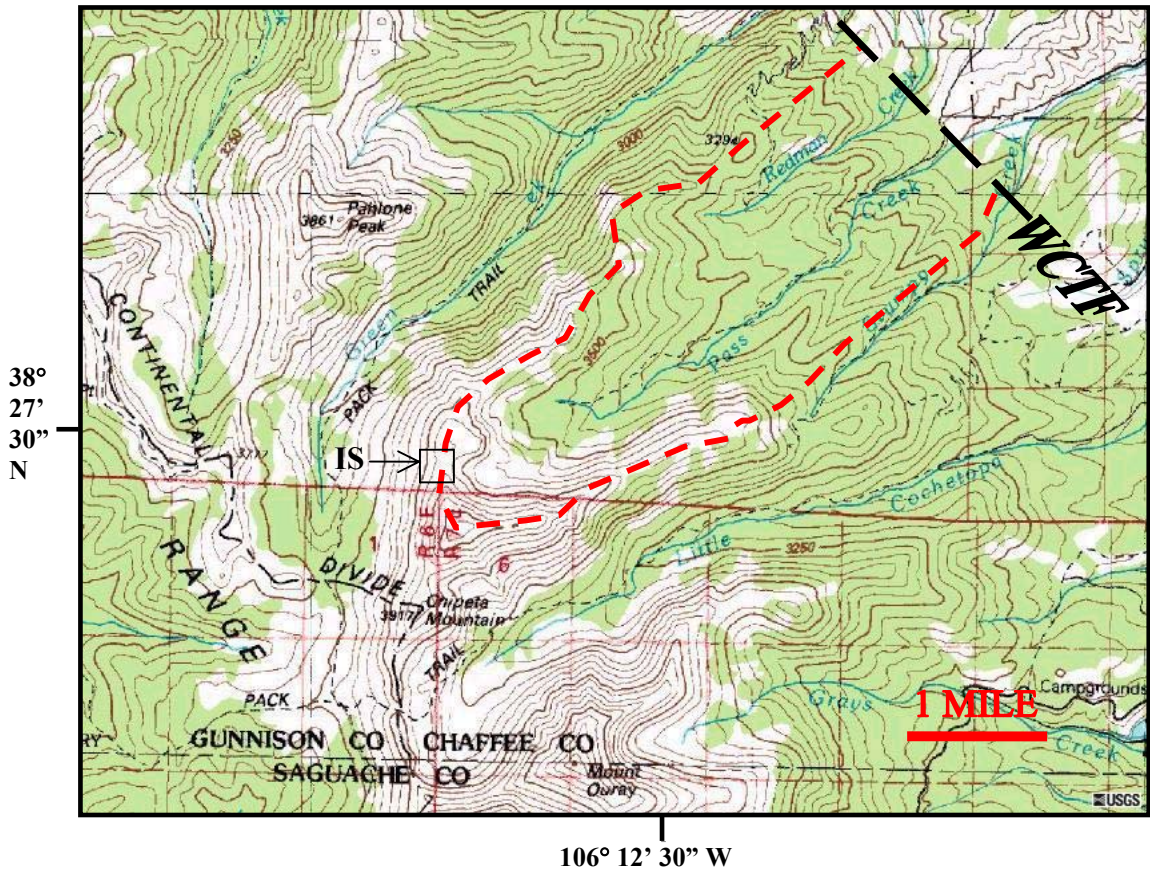


Figure 14a. Topographic map showing the traverse of the ridgelines (red dashed line) relative to the basin-bounding fault WCTF (black dashed line) and the interridge saddle (IS) shown in square.

The field area consists of two ridgelines trending roughly northeast/southwest (North Ridgeline “NR” trends northeast & South Ridgeline “SR” trends east-northeast), with an Interridge saddle (“IS”) located between, and truncated to the east by the major basin-bounding fault, the Willow Creek Transfer Fault (WCTF) (Figures 14a & 14b). The WCTF is the southernmost basin-bounding fault of the Poncha Pass Transfer Zone (PPTZ), located at the southern limit of the upper Arkansas valley/basin (uAv/uAb) of the Rio Grande rift (RGr) (Figures 13 & 14a) (Dippold, 1999). The two ridgelines are located between Mt. Ouray (13,971')(4258 m) to the southeast and Pahlone Peak (12,667')(3861 m) to the northwest (Figure 14a). The field area is located within the San

Isabel National Forest (Figure 14b) and the ridgelines are within close proximity to and situated northeast of the northwest-trending continental divide (Figure 14a).

Pass Creek, Green Creek, Little Cochetopa Creek, Stumpy Creek, Redman Creek and Browns Creek drain from the field area down into the Arkansas River. Pass Creek drains from the land between the two ridgelines at the higher elevations, while Redman

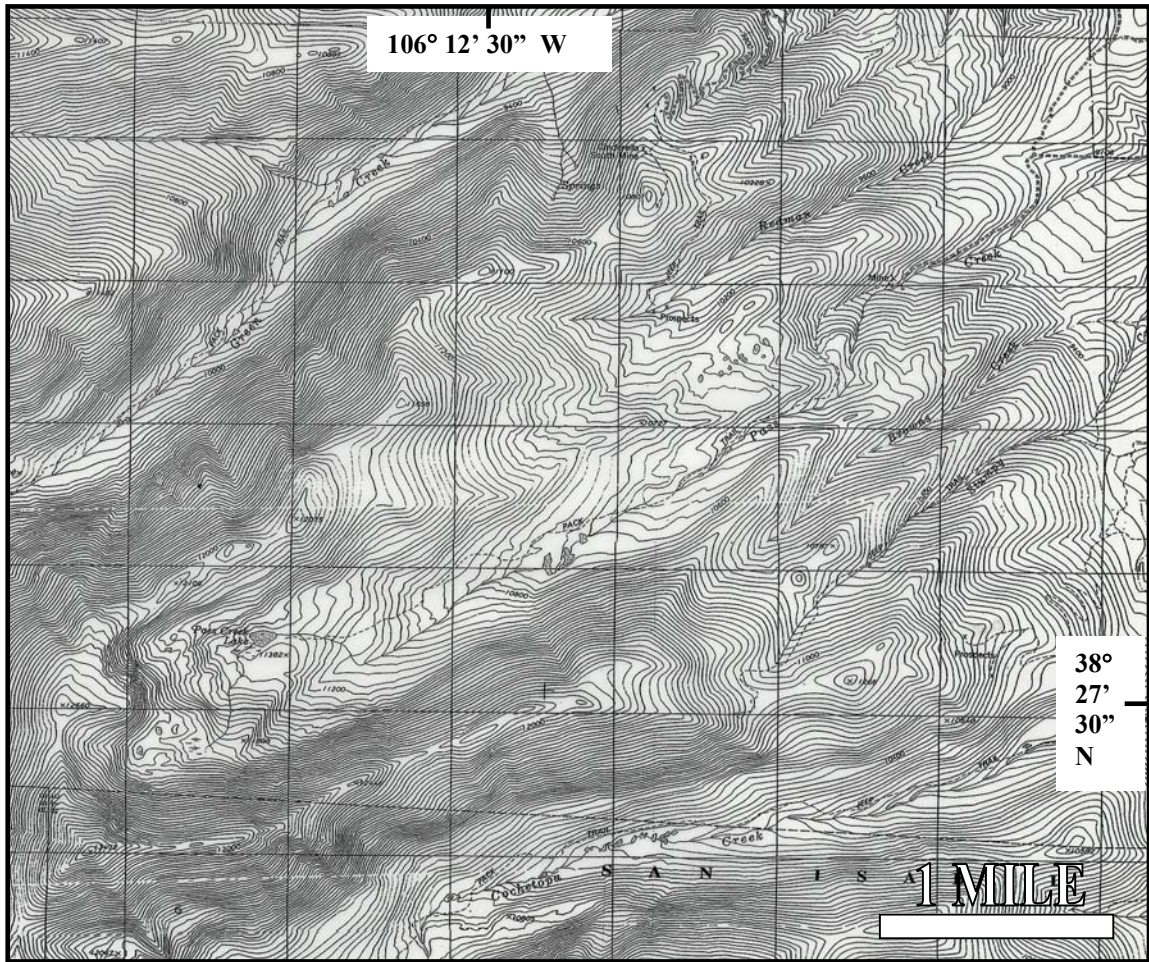


Figure 14b. Topographic map of the field area

and Browns Creek drain the area north and south of Pass Creek, respectively, at the lower elevations. The two ridgelines are both encompassed by Stumpy Creek at lower elevations. At higher elevations, the ridgelines are encompassed by Little Cochetopa

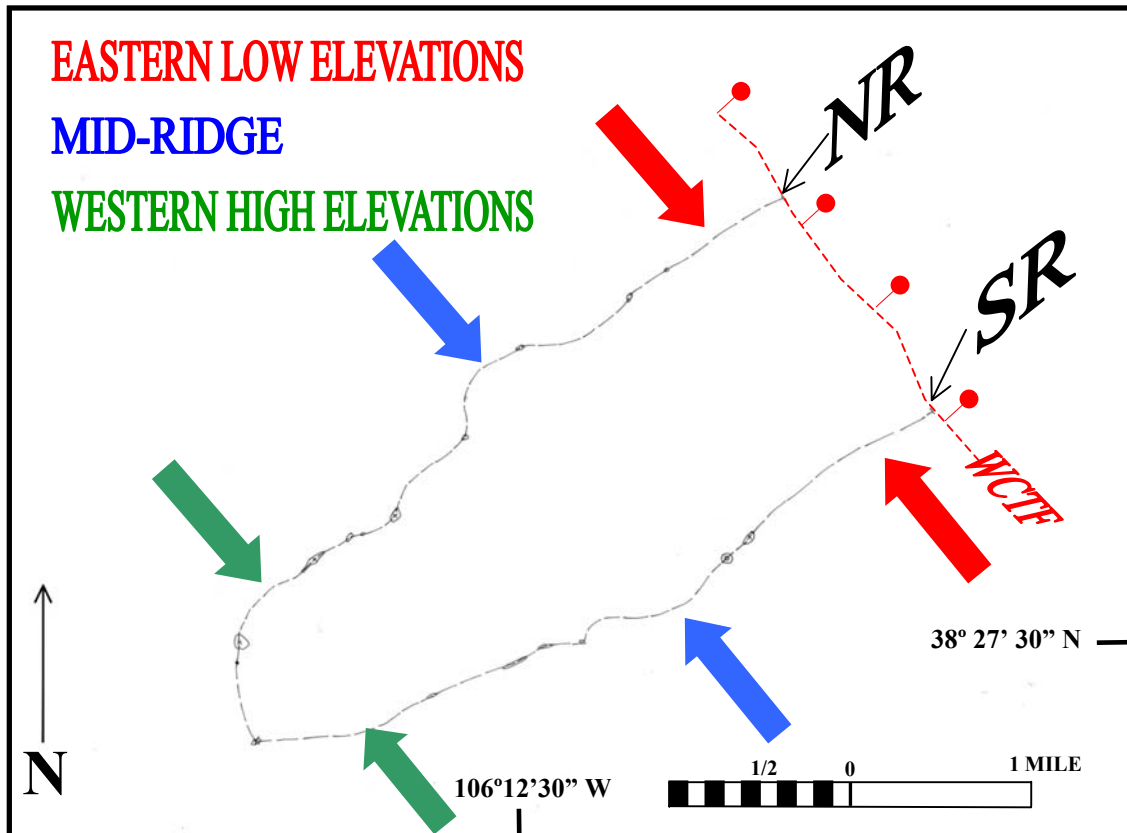


Figure 14c. Subdivision of Field Area into Eastern Low Elevations, Central Mid-Ridge Elevations and Western High Elevation for comparisons both along and across ridgelines and a final assessment of the cooling history or exhumation of the area.

Creek to the south (SR) and Green Creek to the north (NR). Pass Creek Lake forms a prominent recognizable feature of interest down in the drainage and was useful for taking bearings off of and orienting relative to in the western high elevations and interridge area (Figures 14a & 14b).

The field area was subdivided into three general elevation ranges for comparison, both along and across ridgelines, the Eastern Low Elevations, the central Mid-Ridge Elevations and the Western High Elevations. Comparison of high and low present-day elevations of the field area was necessary for assessing the cooling history and exhumation of these ridgelines relative to the rift to the east of the field area (Figure 14c).

Both the northridge (NR) and the southridge (SR) are roughly composed of the same

petrologic units, though there are some differences based on the abundance and location of igneous intrusions, the texture of “porphyroblasticity/podicity” exposed and the thickness of the “fingers/layers” within the undifferentiated interfingered/interlayered area.

Other surrounding adjacent units not present along the ridgelines in the field area are the younger Quaternary Gravels (Qd/ Quaternary alluvium), the Tertiary units (Tv/Td), and the Paleozoic carbonates (MO_r). The ridgelines stand out from the surrounding landscape as snow-capped peaks located behind the Paleozoic carbonates (Mississippian-Ordovician {MO_r} Mississippian Leadville Formation and the Ordovician Manitou Dolomite-Harding Sandstone-Fremont Dolomite Formations) allochthonous landslide block “Elephant Rock” (Van Alstine, 1970) (Figure 15, 16, & 17). The elongate Tertiary gravel hills (Tertiary Gravels (Tertiary Hills/Tertiary Sediments/Td/Ts/T) and Tertiary “Volcanics” (Tv; Oligocene volcanic rocks)), with sparse vegetation, stand out from adjacent land and have been described by other authors and locals as “Tiger stripes” (Figure 18).

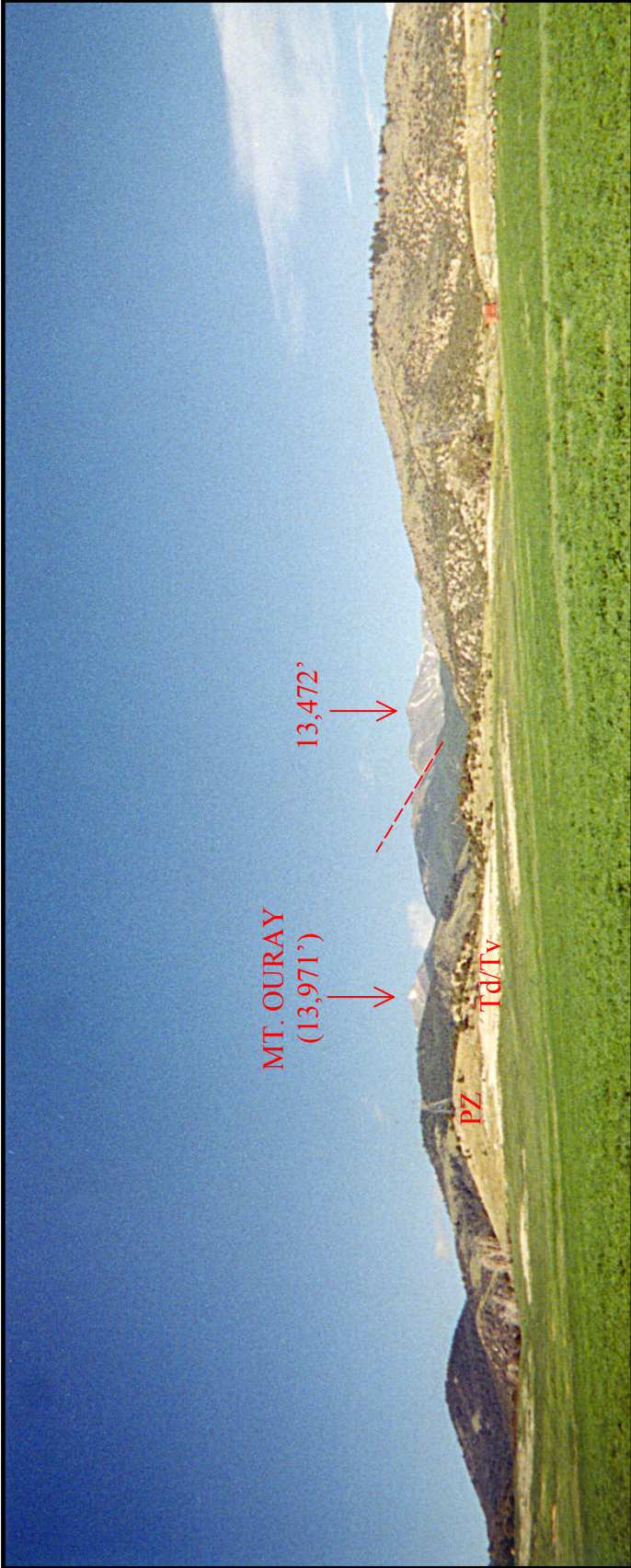


Figure 15. Looking southwest from afar to the ridgelines on the far right background, the summit of Mt. Ouray in the left background, the allochthonous Paleozoic MO_r (Fremont, Harding & Manitou Formations) landslide block "Elephant Rock" (PZ) on Bill Friend's property, and Tertiary sediments (units Tv & Td) in the foreground. A gully thought to be fault-derived (Drainage Divide Fault (5)) coincides with prominent change in both elevation and profile is specified by dashed line. Field of view \approx 0.5 miles [860 m].



Figure 16. Paleozoic allochthonous block "Elephant Rock". Field of view = 18 feet [5.5 m]

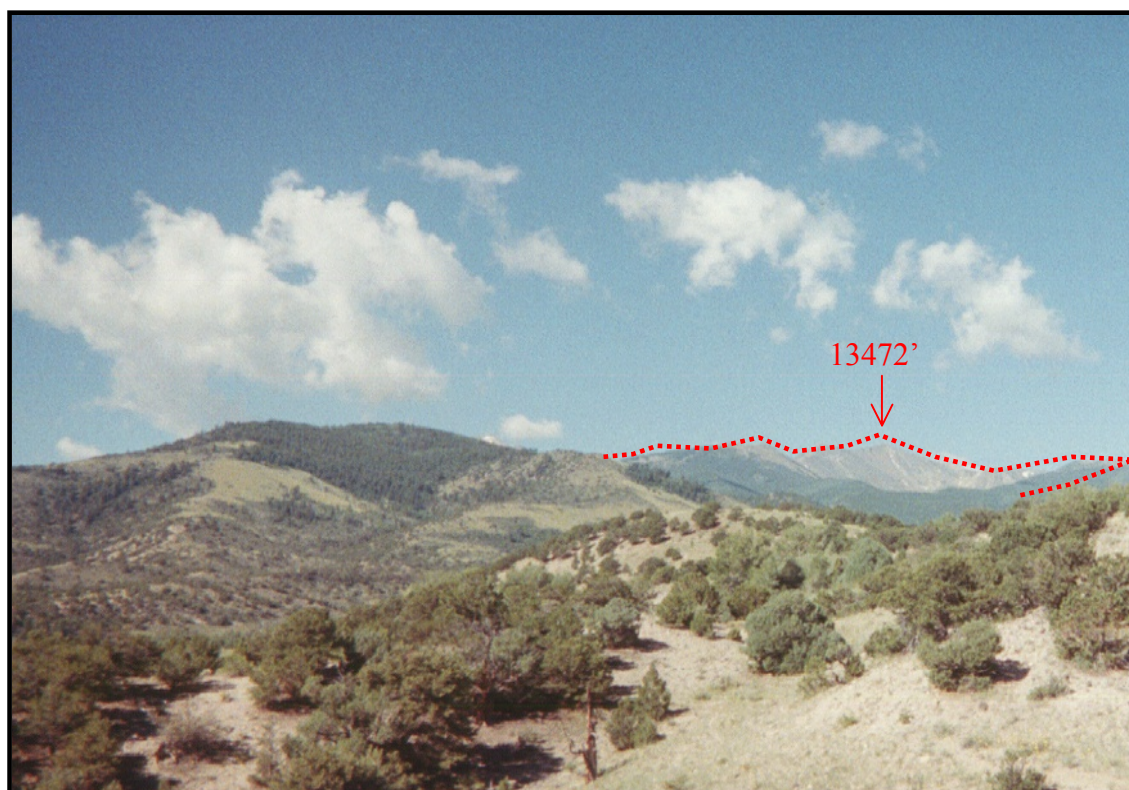


Figure 17. View of ridgelines from Paleozoic allochthonous block "Elephant Rock". Traverse shown in background. Field of view = 80 feet [25m].

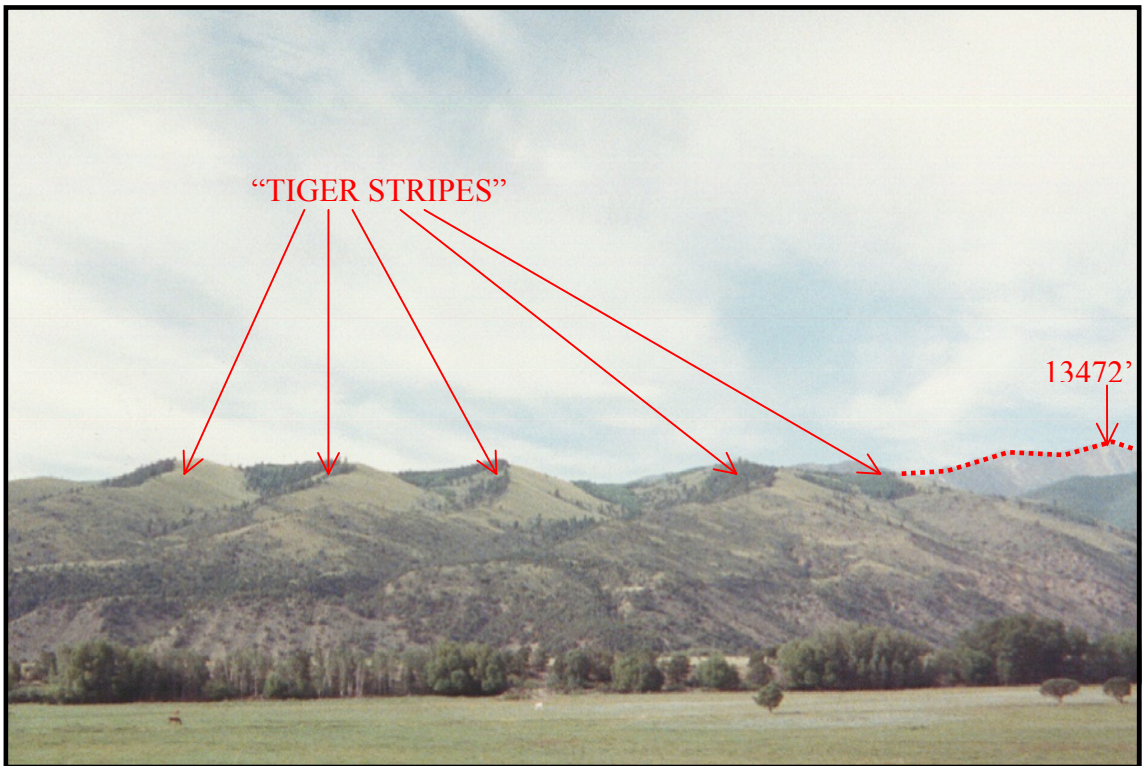


Figure 18. Looking south from Highway 50 at the “tiger stripes” with more vegetation on the east-facing slopes due to soil moisture differences atop the Tertiary sediments, with the extreme elevations of the SR exposed in the far right of the photo. Field of view = 2000 feet [612 m].

When the ridgelines are viewed from the north, while looking south-southeast, they both conform in shape and have a similar profile (Figure 19). This similarity in appearance could be due to the weathering patterns of the interlayered/interfingered units/exposures/stripes, underlying antiformal/anticlinorial controls, and/or faulting obscured by vegetation. Despite the proximity of the two ridgelines, they vary in elevation and land cover, with the north ridgeline being generally lower in elevation along the traverse and densely vegetated, whereas the south ridgeline is generally higher in elevation along the traverse and less vegetated (Figure 20).

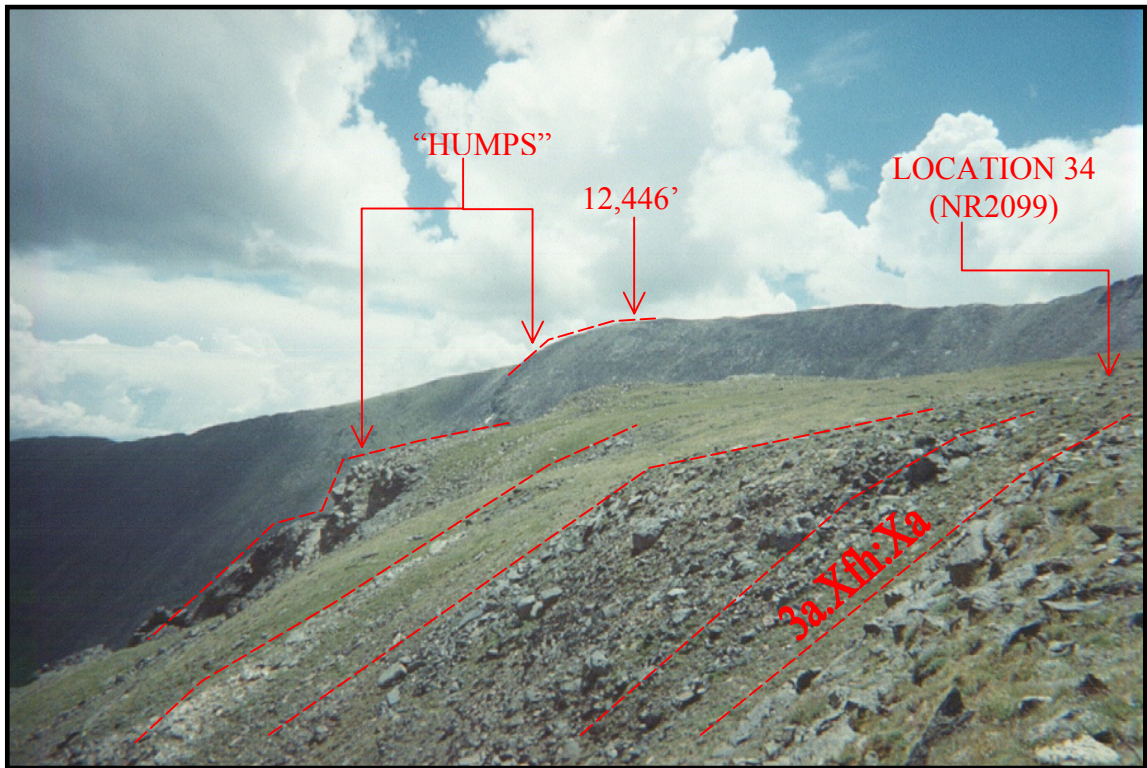


Figure 19. Looking south-southeast over the prominent jutting out (north face to northeast of 12106') of NR in the foreground, to the SR's notable feature at 12446' peak. Note the conforming in shape and similarity in profile across ridgelines and the striping of the interfingered 3a.Xfh.Xa and 3b.Xfh.Xqf units along the ridgeline. Field of view=50 feet[15m].

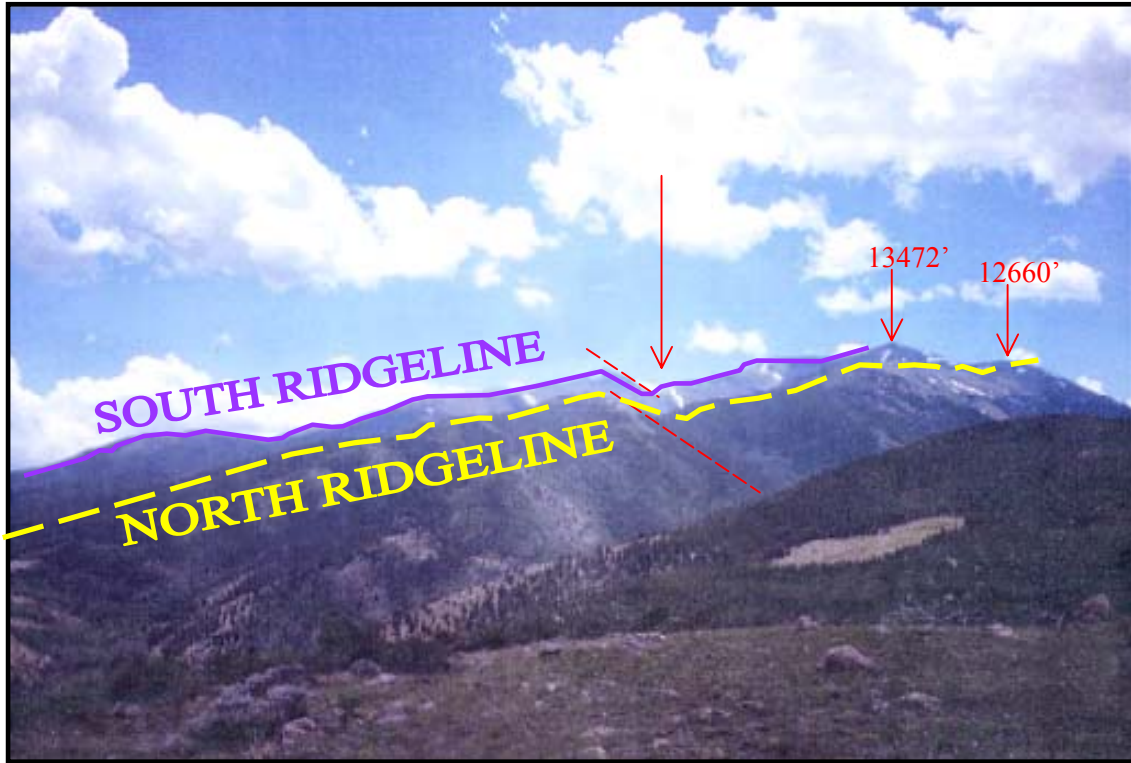


Figure 20. Looking south-southwest from above Willow Creek at the conforming shape and similarity in profile of the SR in background and NR in foreground. The NR, in the foreground, is densely vegetated compared to the barren SR, in the background. Drainage Divide Fault (indicated by red dashed lines and arrow). Field of view = 3 miles [4844 m]. (Image courtesy of Dippold, 1999, KSU)

The overall appearance of the exposures/outcrops along the traverse and the weathering patterns differ amongst the ridgelines as well, with the NR more smooth (Figure 21) and the SR more irregular (Figure 22). The 12,660' (3859 m) summit of the NR has prominent exposures, which jut out towards Pass Creek Lake (Figure 23) and when looking down Pass Creek from the 12,660' (3859 m) peak, the pattern of these prominent exposures are pronounced (Figure 24). The “Interridge Saddle” between 13,472' (4106 m) and 12,660'(3859 m), is roughly the same elevation as the apex of the NR and the difference in elevation between the apices of 13,472' (4106 m) and 12,660'(3859 m), is notable (Figures 23 & 25). The exposures are quite abundant and

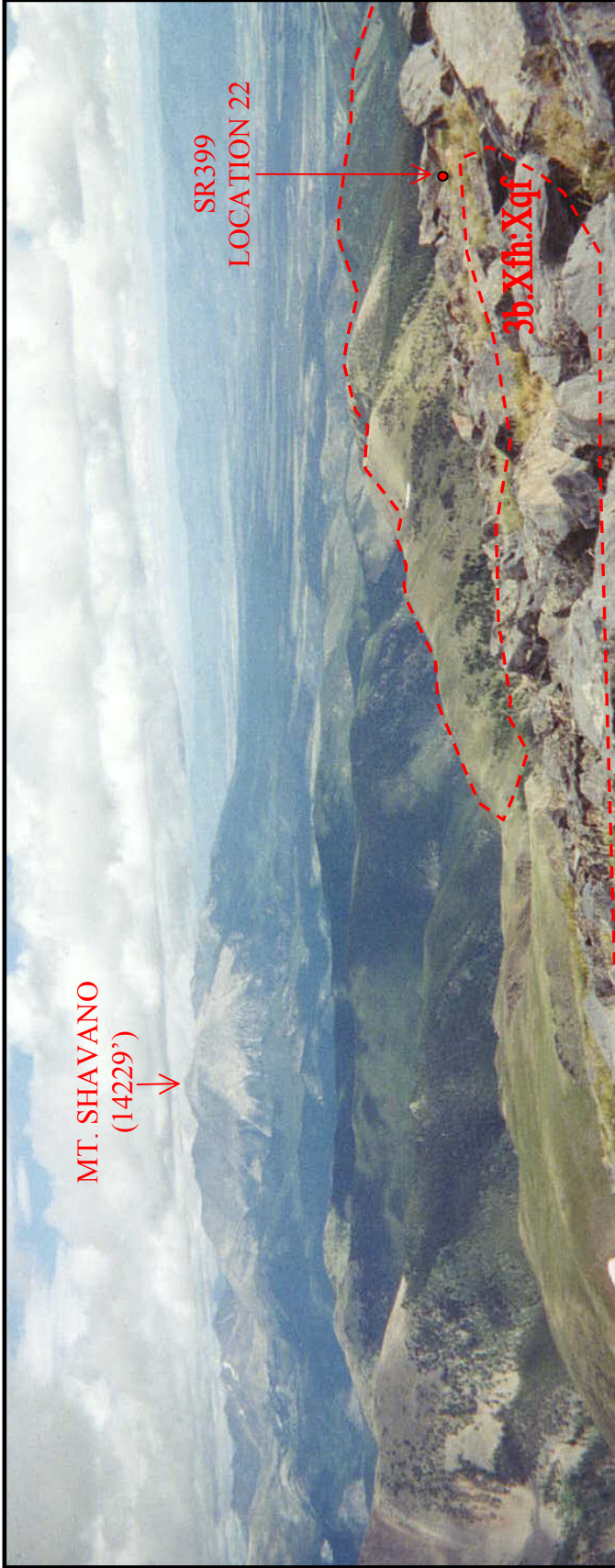


Figure 21. North Ridgeline. Looking north-northeast from location 22 (hand specimen SR399) at 13472' over to 12660' and down the North Ridgeline with Mt. Shavano (14229') in the background.. Field of View = 15 feet [5 m].

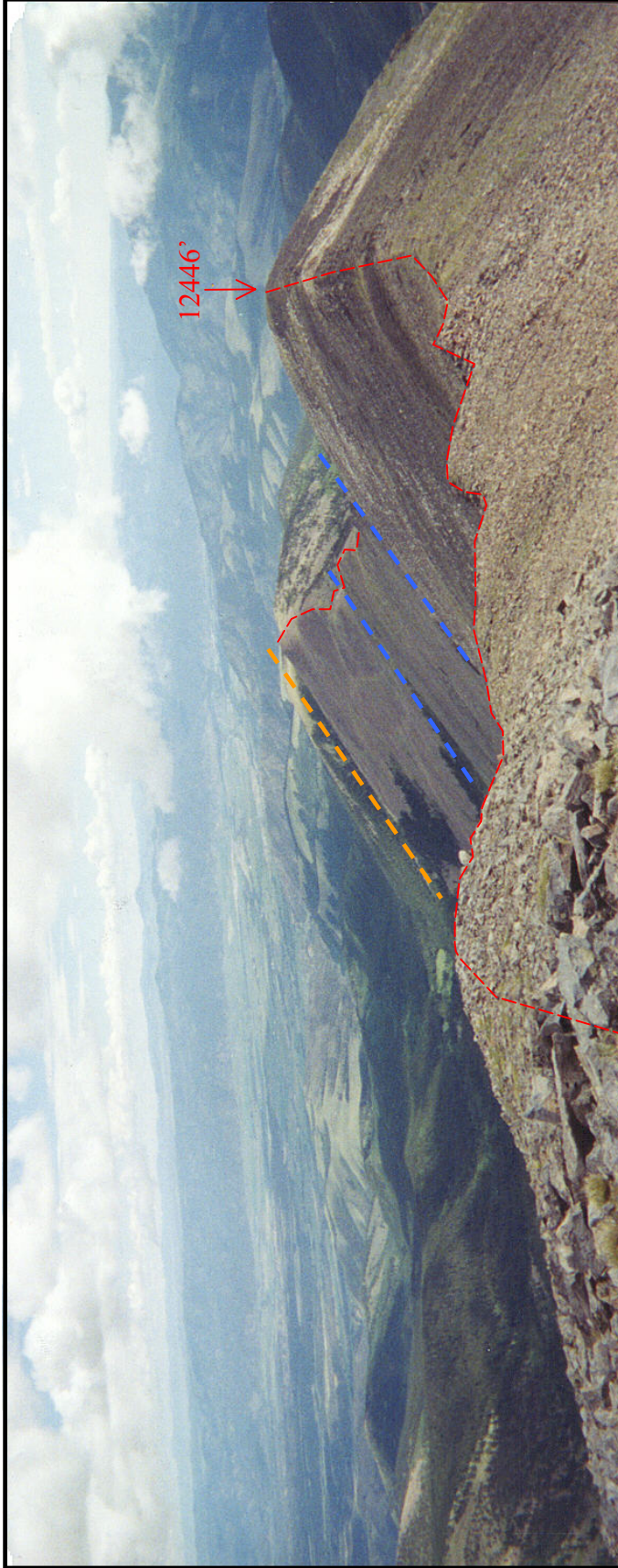


Figure 22. South Ridgeline. Looking northeast from 13472' down the South Ridgeline (SR). Red dashed line shows the traverse of the south ridgeline. Proposed faults are shown in blue dashed lines (Hump Jut Fault) and orange dashed line (Pass Creek Fault). Field of View = 25 feet [7 m].

prominent in particular locations (Figures 19, 23, 24 & 26) compared to the ridgelines themselves (Figures 25 & 28).

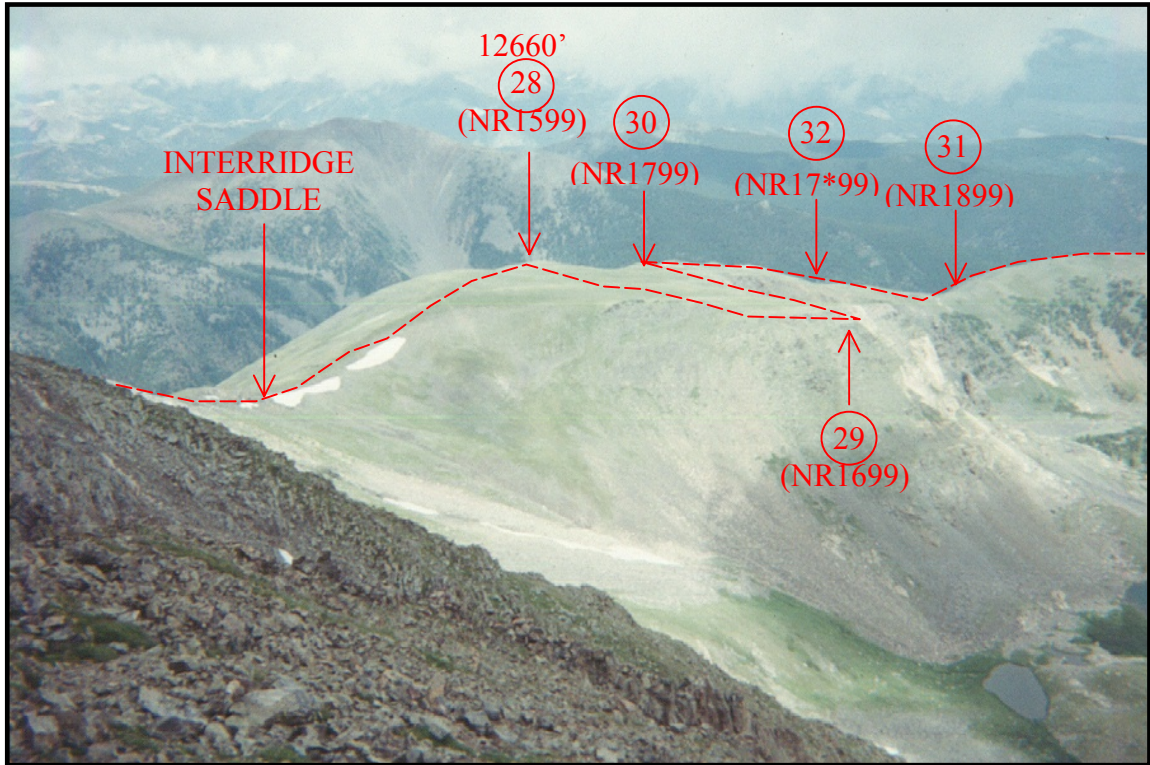


Figure 23. Looking north-northwest over at the exposures at 12,660' on NR, with the Interridge Saddle to the northwest. Some of the prominent exposures, which jut out towards Pass Creek Lake, are light-colored intrusives. Taken from location 37 (hand specimen SR799) viewing locations 28-32. Field of view = 150 feet [46 m].

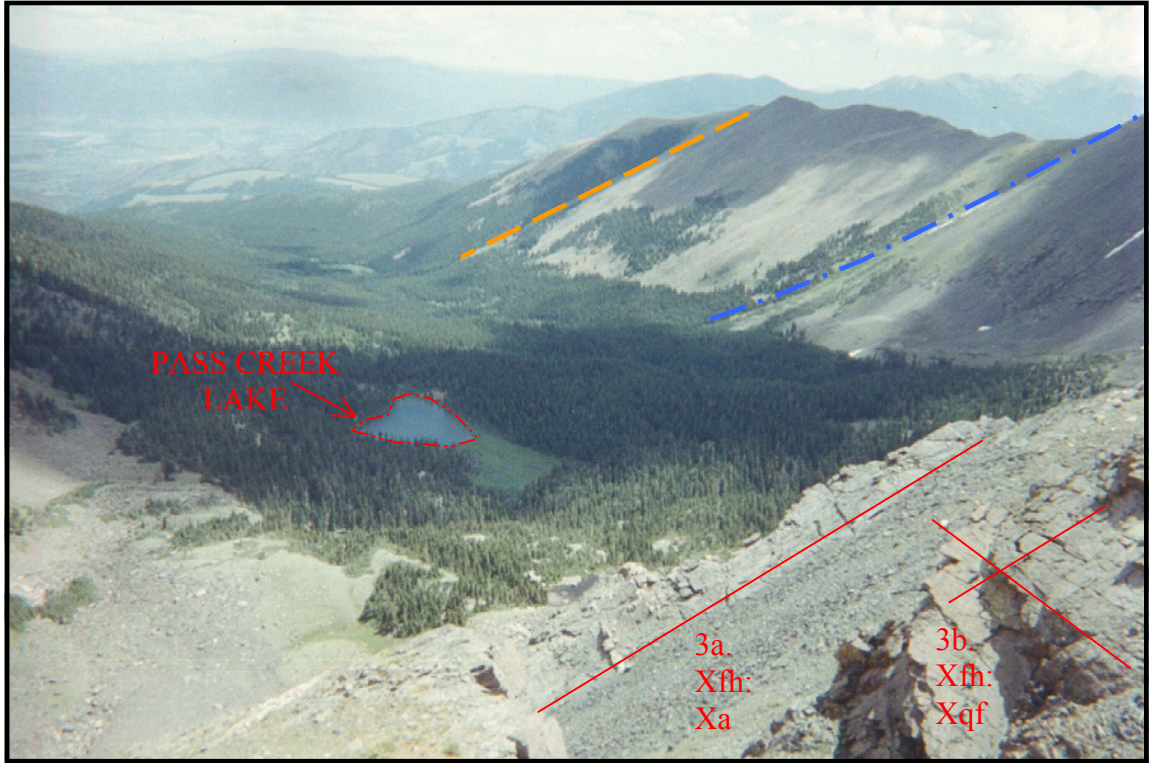


Figure 24. Looking southeast down Pass Creek from location 30 (hand specimen NR1799) at 12,660' showing prominent stripes of quartzofeldspathic (3b.Xfh:Xqf) and amphibolite (3a. Xfh:Xa) northwest-striking and exposures in the foreground. Suspected faults "Hump Jut Fault" (2; blue line) and "Pass Creek Fault" (1; orange line) on SR indicated on right side of photo, and Pass Creek Lake located down in the drainage. Field of view= 20 feet [6 m].

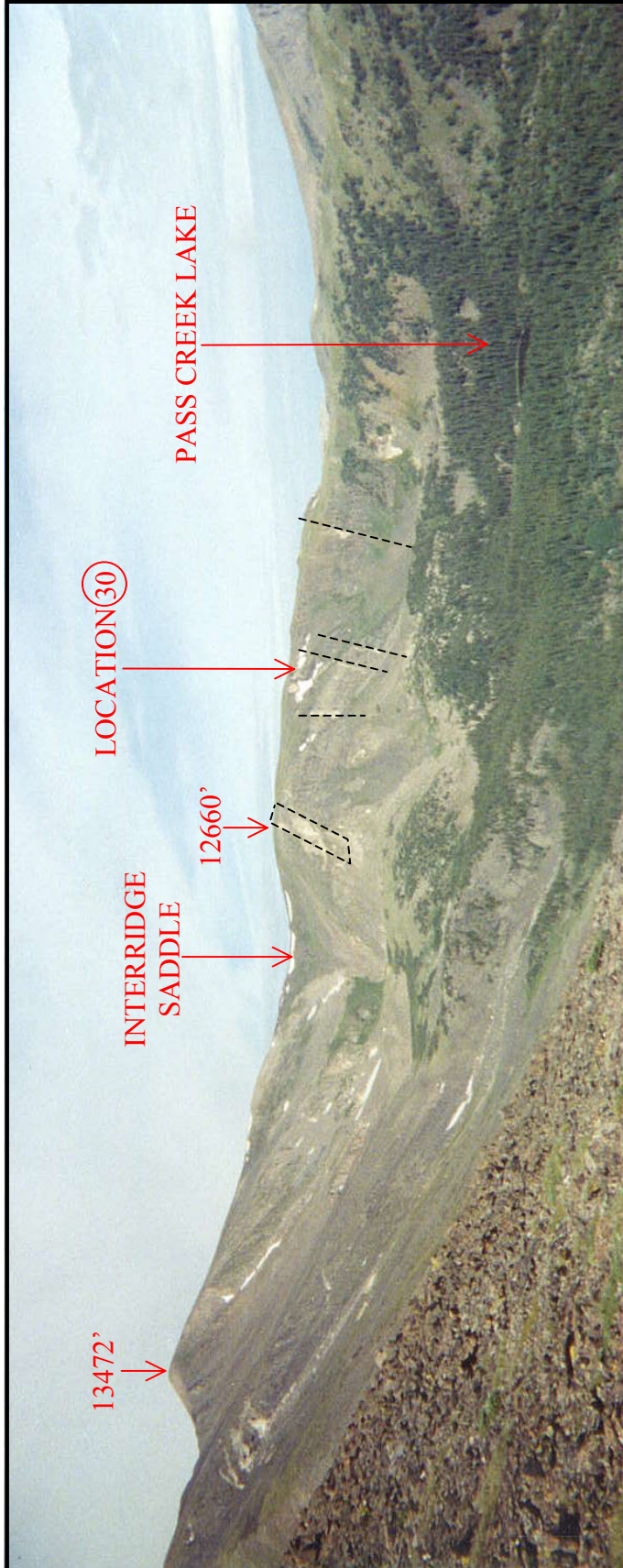


Figure 25. Looking west at the Interridge Saddle and up into the horseshoe bend from the SR above Pass Creek. The difference in elevation of the apices of 13,472' and 12,660' is notable and the prominent vertical light stripes within the dark exposures (specified with dashed lines) are igneous intrusions, which have intruded up through brittle fault planes or fractures. Taken from location 4 (AKA location 64). Field of view = 0.4 miles [640 m].

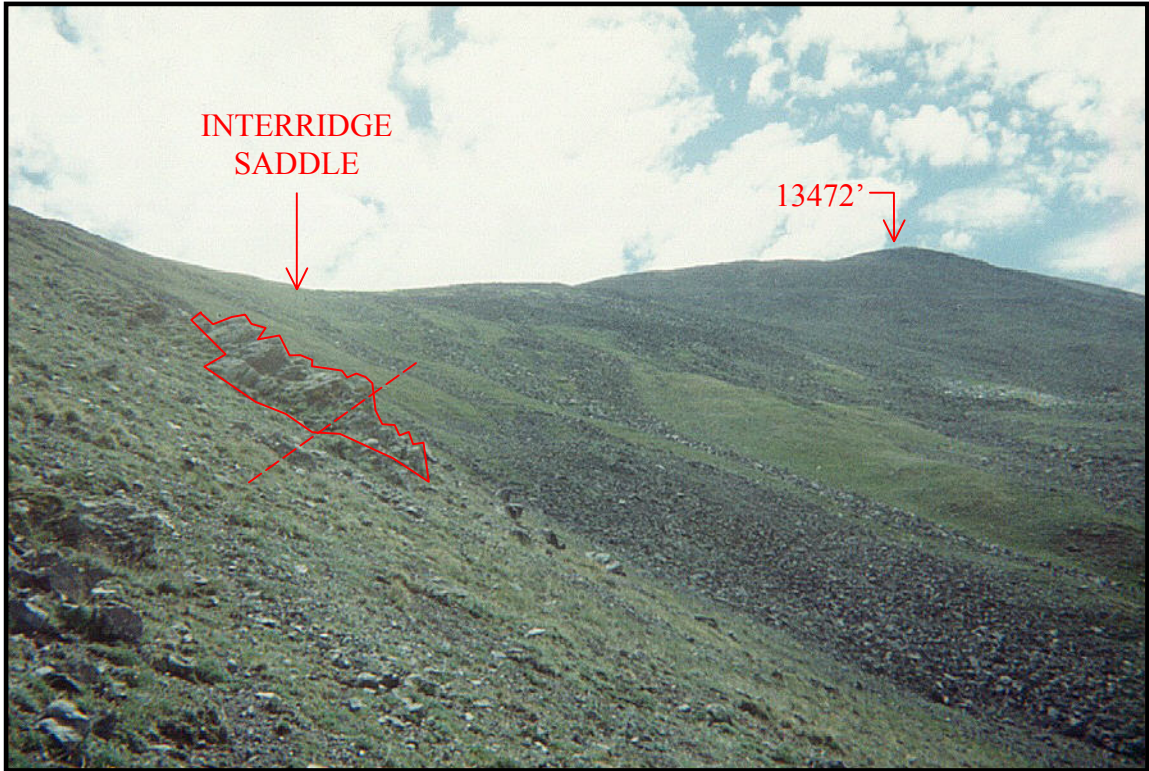


Figure 26. Looking southeast at the interridge saddle and a northwest-striking northeast-dipping exposure jutting out into Green Creek, on the backside of the interridge saddle. Photo taken from northwest of location 80. Field of view = 190 ft [58 m].

The prominent apices along the ridgelines are far fewer in number for the SR as compared to the NR. The NR has six (6) major apices with the elevations of 12,660' [3859 m], 12,106' [3690 m], 12,075' [3680 m], 11,698' [3566 m], 11,100' [3383 m] and 10,807' [3294 m], along the traverse of the ridgeline, whereas the SR only has three (3) major apices of decreasing elevations of 13,472' [4106 m], 12,446' [3794 m], and 10,787' [3288 m] (Figure 27).

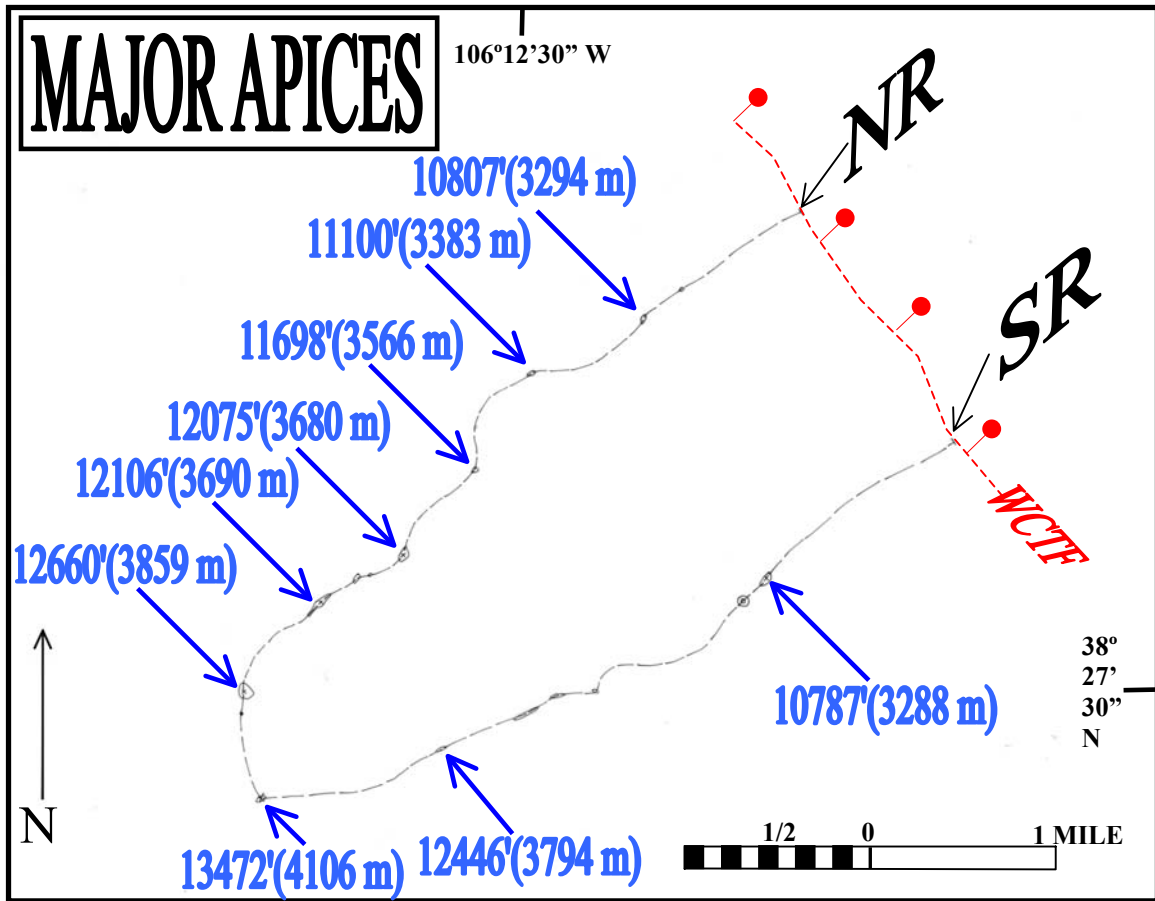


Figure 27. Major apices of both ridgelines.

For this thesis, I mapped the location of structures, the orientation of the basement fabric and sampled the ridgelines for petrologic classification and apatite fission-track (AFT) thermochronology. Aerial photo notations (Figures 29a & 29b) were made prior to the field season and were explored during field reconnaissance. In order to determine if the basement has been reactivated and has influenced the appearance in the present, the structural features of the rock were measured, the undifferentiated area was mapped to identify petrologic units and the exhumation was interpreted from new apatite fission-track (AFT) low-temperature thermochronology (age-dating) data.

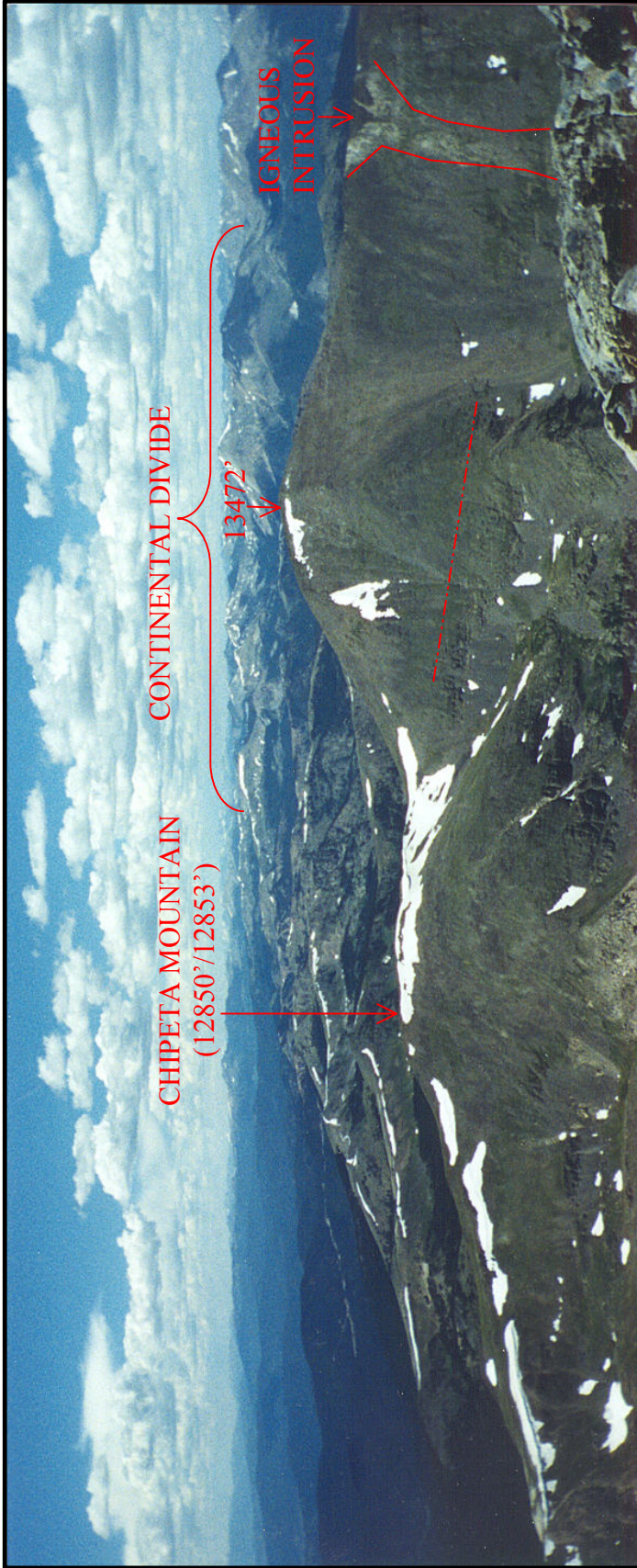


Figure 28. Looking northwest from Mt. Ouray (13,971') over to the continental divide in the background with the 13,472' peak and Chipeta Mountain in the foreground. A major igneous intrusion is outlined in the right of the photo. Field of view = 0.2 miles [351 m].



Figure 29a. Aerial photo 139

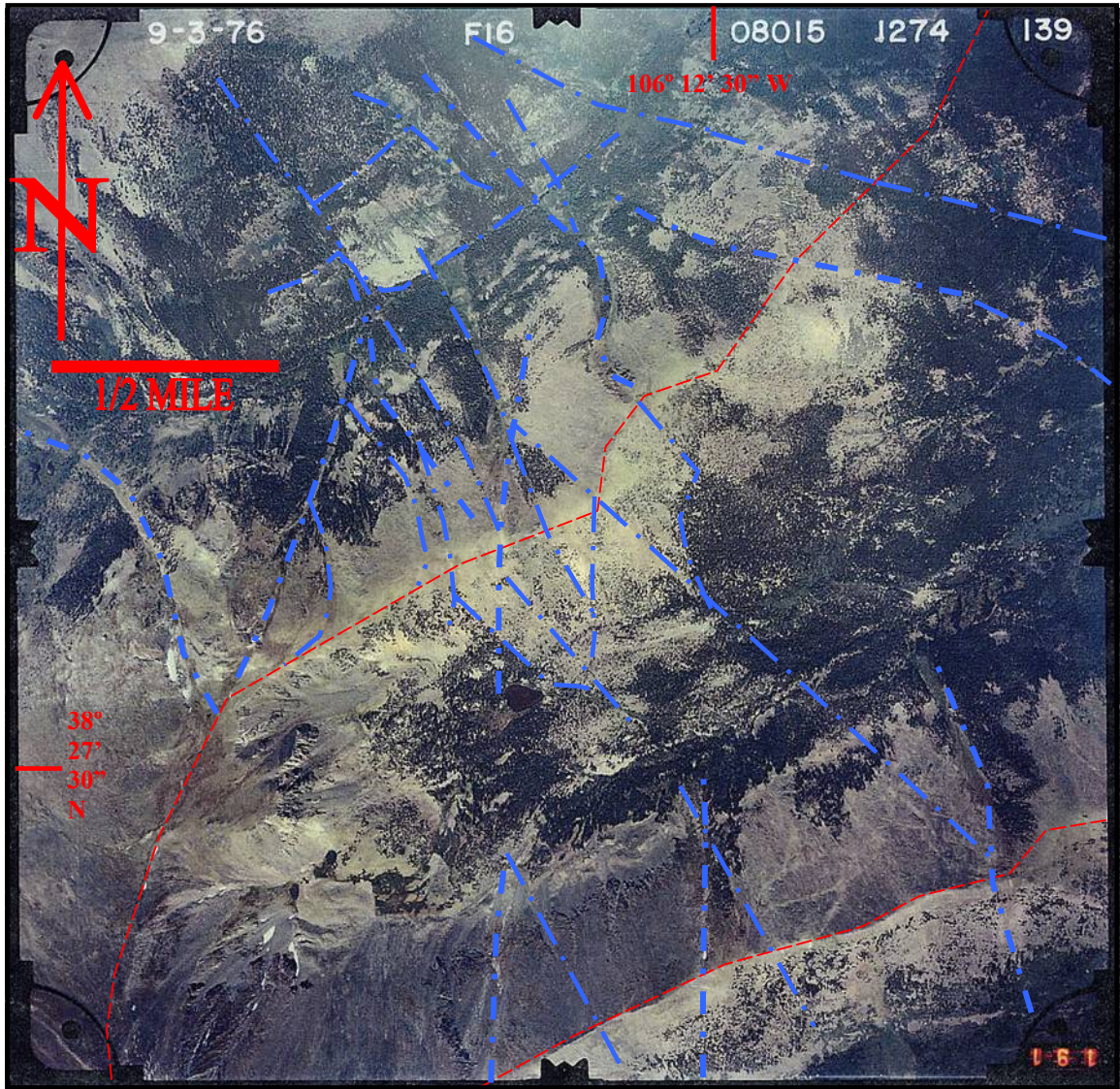


Figure 29b. Aerial photo 139 Notations

PETROLOGY

The undifferentiated interlayered Precambrian unit was petrologically analyzed in order to identify and differentiate the various rock units within, as compared to other Precambrian exposures within the Rockies, and to correlate the rock units across the ridgelines. The petrology was also studied to structurally assess the basement for offset and uplift, compare the basement structure to the regional Precambrian history and determine potential basement reactivation.

METHODS

I collected a total of 69 hand specimens in the field from the ridgelines. This included 30 specimens from the north ridgeline (NR), 38 specimens from the south ridgeline (SR), and one (1) from the Interridge Saddle (Appendix A; Appendix B; Appendix C; Appendix D; Plate I). Twenty-five specimens were selected for thin section analysis based on the distribution along the ridgeline, the lithology of the specimen and the lithology of adjacent coexisting specimens (Appendix C). The abundance of talus (or scree) on the ridgelines, the dense vegetation below the tree line, the surficial covering of lichens masking the weathered color and the differing colors of the weathered surfaces (depending on orientation of the exposures), all made field assessment a challenge and thin section analysis vital.

Oriented samples were collected from shear zones for structural analysis. These oriented specimens were cut parallel to the stretching lineations and perpendicular to the foliation. This orientation of the samples reveals possible sense of shear indicators. Thin

sections of intrusive samples were not oriented as they were cut solely for mineralogical determination.

To further analyze the interstriped unit, mineralogical comparisons were made with ratios of the quartz to both quartz and feldspars [Q/Q+SPAR], as well as plagioclase feldspar to feldspar (both plagioclase feldspar and potassium feldspar) {P/P+K}. The hornblende, quartz, plagioclase feldspar, and microcline potassium feldspar (HQPM) ratios (to each other and adjacent units) were analyzed within the stripes and aided in the classification scheme of the amphibolites. To assist in the approximations of the feldspars, which have been succumbed to sericitic alteration, and to easily decipher the potassium feldspar (microcline & untwinned orthoclase) and plagioclase feldspar (An>20; An~30; andesine & oligoclase) visually, a sodium cobaltinitrite (NaCONO₃) staining of the specimens was performed in the laboratory. By etching with hydrofluoric acid and then allowing the specimen to remain immersed for approximately one minute in NaCONO₃ (sodium cobaltinitrite), the potassium feldspars were stained yellow (Hutchison, 1974).

Throughout the remainder of the text details of the hand specimen identified and mentioned such as additional information regarding hand specimen number, thin section number, unit/subunit classification, location number and additional figure numbers can be found within Plate I and Appendices A-E.

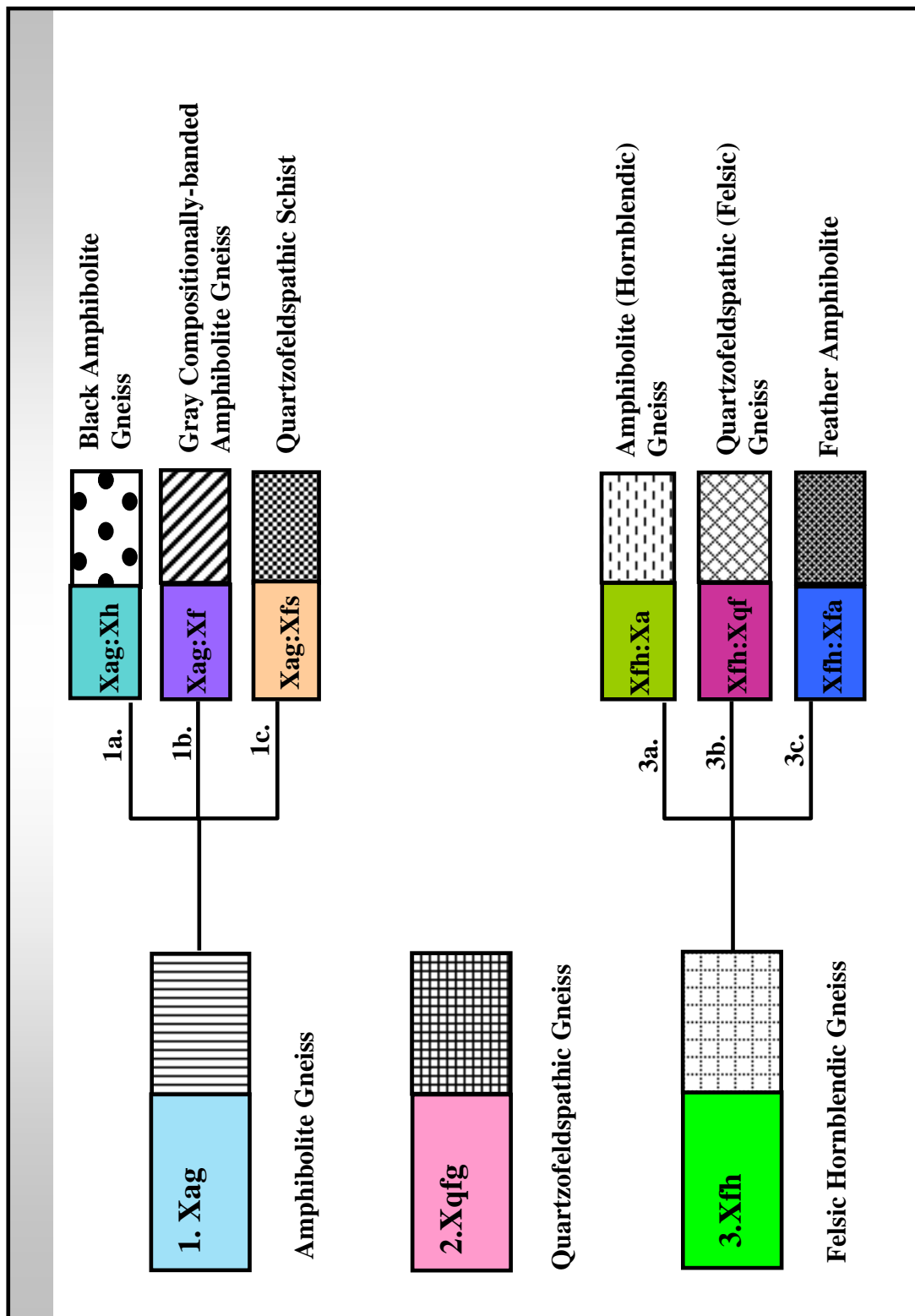


Figure 30. The lithologic units are subdivided into three main broad units and six sub-units.

RESULTS

Based on the metamorphic assemblages of samples along the two ridgelines, the study area can be considered to be of high-grade amphibolite facies. This area has been mapped as Paleoproterozoic gneisses (Tweto, 1979). Various igneous intrusions and pegmatites along the traverse penetrate the amphibolite gneisses and quartzofeldspathic gneisses, along with localized lenses of other lithologies, such as calc-silicate gneiss, whiteschist and porphyroblastic rocks. The majority of the exposures of the field area can be characterized as interlayered amphibolite gneiss and quartzofeldspathic gneiss and grades between felsic (feldspathic/quartzofeldspathic) and hornblendic (amphibolitic) gneisses (Xfh). This arrangement results in a striped appearance (Figures 30, 31, 32, and 33; Plate I). Despite the overall striped appearance, the rocks were divided into three broad, lithologic subdivisions; those being an amphibolite gneiss (Xag), quartzofeldspathic gneiss (Xqfg) and felsic hornblendic gneiss (Xfh). These three subdivisions were based on field observations, hand specimens and thin section analysis, proposed metamorphic protoliths and structural measurements (Figure 31; Plate I).

The hornblende was compared throughout the ridgelines on the basis of grain size, color variety (brown, blue-green and green) and total ratio of rock mass. Within the entire Xfh unit, the hornblendes of the amphibolite gneisses were found to be generally fine-grained in the east and coarse-grained in the west. The coarse-grained amphibolites in the western high elevations are predominantly feather amphibolite and drastically stand out compared to the fine-grained amphibolite at low elevations near the basin-bounding fault along the eastern limit (Appendix C & Appendix D). When traversing through the stripes (Xfh) and transitioning from a felsic (feldspathic/quartzofeldspathic)

gneiss (Xf) into a hornblendic (amphibolitic) gneiss (Xh), there is generally a decrease of microcline and quartz and an increase of hornblende and plagioclase.

Based on mineralogy, three units were identified. The easternmost unit - an Amphibolite Gneiss (1.Xag) below the tree line and in contact with the proposed range/basin-bounding fault (WCTF) defining the eastern limit of the field area; the central unit - a Quartzofeldspathic Gneiss (2. Xqfg); and the westernmost unit - a Felsic and Hornblendic Gneiss (3.Xfh), at the higher elevations at the western limit (Figures 30 & 31; Plate I). The total number of lithologic units for the ridgelines, including the subdivisions, amounts to three (3) units, six (6) sub-units and eleven (11) overall subdivisions (Figure 30; Appendix B; Plate I). Of the six sub-units, the three sub-units of the Amphibolite Gneiss are the Black Amphibolite Gneiss, Gray Compositionally-banded Amphibolite Gneiss, and Quartzofeldspathic Schist. The three sub-units of the Felsic Hornblendic Gneiss are the Hornblendic Amphibolitic Gneiss, Felsic Quartzofeldspathic Gneiss and Feather Amphibolite (Figure 30). The remaining five subdivisions of the total overall eleven rock unit subdivisions are a Calc-Silicate Gneiss, Hornblende Pods, Whiteschist, Porphyroblastic Rocks, and Igneous Intrusions. As mentioned previously, a total of 69 hand specimens were collected in the field from both ridgelines and the Interridge saddle, with 30 specimens collected from the North Ridgeline (NR), 38 specimens collected from the South Ridgeline (SR), and one (1) collected from the Interridge Saddle (see Appendix A, Appendix B, Appendix C & Appendix D; Plate I).

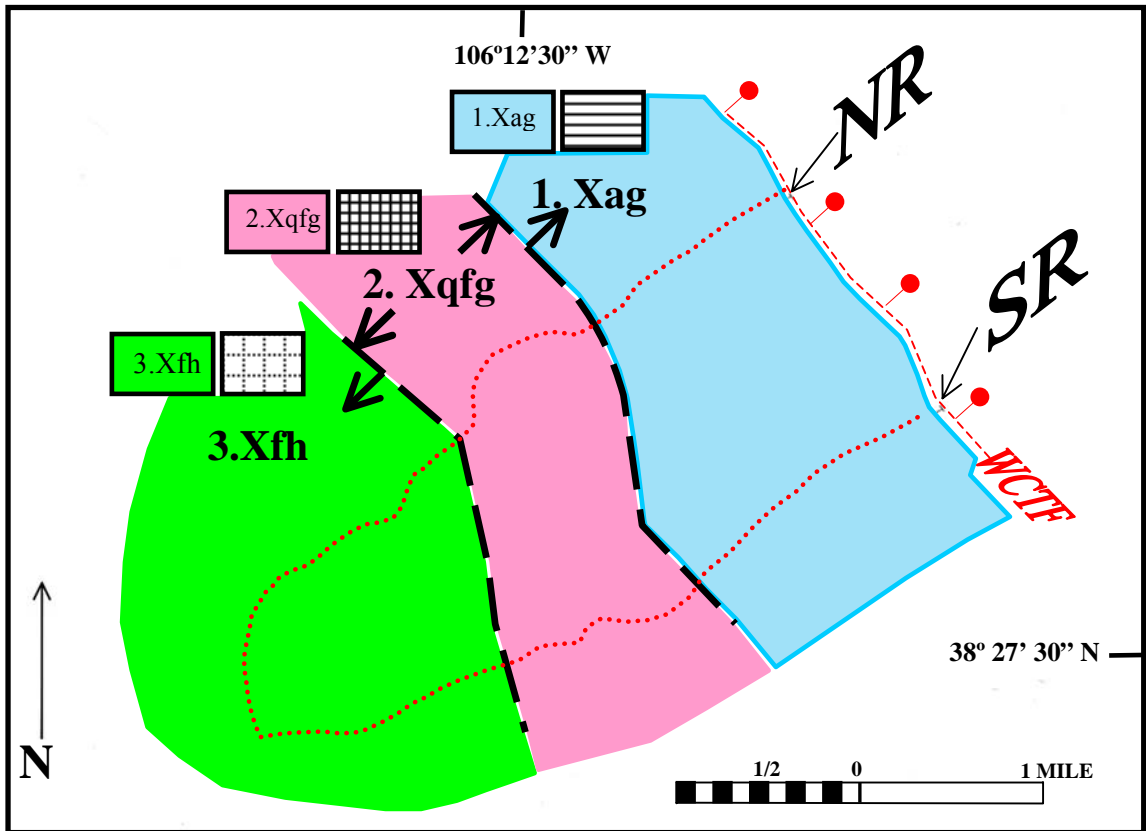


Figure 31. Simplified Geologic Map of both ridgelines showing the three broad mappable lithologic units throughout the field area.

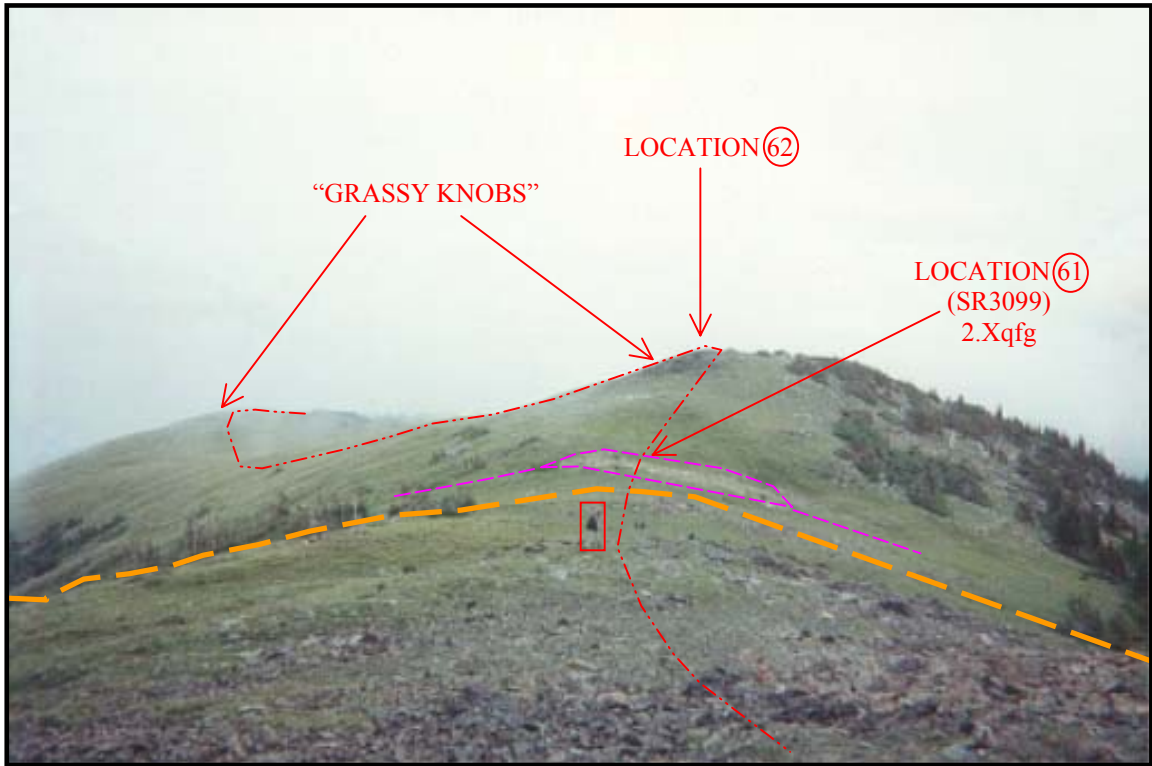


Figure 32. Surficial Expression of Lithologic Units. Looking east-northeast from location 60 on SR at the “Grassy Knobs.” Also shown is the suspected fault “Pass Creek Fault” (bold dashed line) on the SR where the hand specimen SR3099 was extracted at location 61. Field assistant is shown in rectangle for scale.

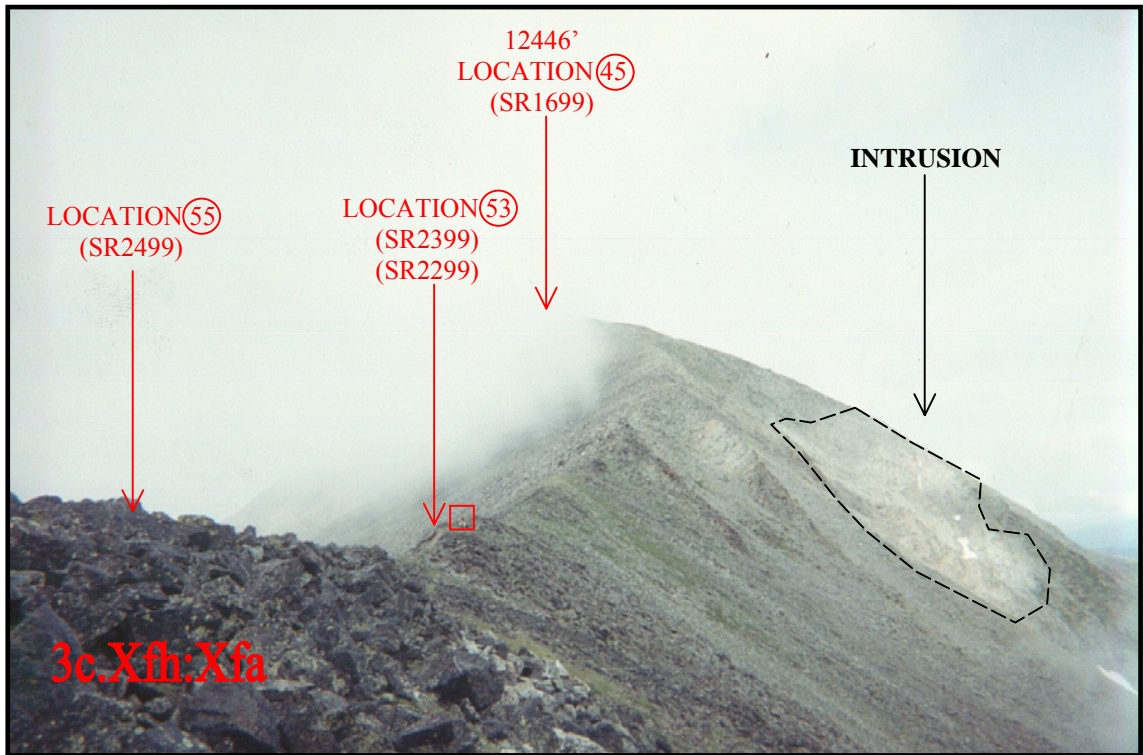


Figure 33. Surficial expression of lithologic units. Looking west-southwest up the south ridgeline (SR) at the light and dark striped appearance of the quartzofeldspathic gneiss and amphibolite gneiss exposures. Field assistant is shown in square for scale.

THREE BROAD LITHOLOGIC UNITS

AMPHIBOLITE GNEISS

The easternmost unit, classified as amphibolite gneiss (1.Xag) (Figure 31), is exposed in the lower elevations of the ridgelines and is fine-grained relative to the amphibolites exposed in the western higher elevations. There are three sub-units within the Amphibolite Gneiss which interlayer (Plate I):

1. Black Amphibolite Gneiss (1a.Xag:Xh), being the easternmost;

2. Gray Compositionally-Banded Amphibolite Gneiss (1b.Xag:Xf), upslope from Xh; and
3. Quartzofeldspathic Schist (1c.Xag:Xfs), at the western limit of the Amphibolite Gneiss.

BLACK AMPHIBIOLITE GNEISS (Xh)

The Black Amphibolite Gneiss (1a. Xag:Xh) (Figure 30 & 34a) weathers a brown to black and has a black fresh surface (Figures 34b).



Figure 34a. Looking south-southwest on NR at location 72 at an Amphibolite Gneiss (Xag) Black Amphibolite Gneiss (Xh) exposure (1a.Xag:Xh). Rock hammer is shown for scale. (NR2199).

The massive, blocky amphibolite is fine- to coarse-grained, gneissic and banded, very dark in color with alternating amphibolitic- and quartz-rich layers, and contains many quartz veins (some crosscutting each other, but most parallel to foliation).

Hornblende grains are coarse relative to the overall fine-grained rock. Surficial expression is blocky due to weathering out along planes of foliation and quartz veins. Hand specimens SR3899, SR3999, NR2699, NR2599, NR2499 & NR2199 are from this unit.



Figure 34b. A hand specimen of the Black Amphibolite Gneiss (Xh) sub-unit of the Amphibolite Gneiss (Xag) unit (1a.Xag:Xh). A marker (13.5 cm) is shown for scale. (NR2699).

Specimen NR2699 (Appendix A-E; Plate I) is a representative sample of Black Amphibolite Gneiss (1a.Xag:Xh) (Figures 34b & 34c). The rock weathers gray and has a black fresh color, is fine-grained gneissic with veins predominantly parallel to foliation (some crosscutting) and composed of calcite, quartz (ribbon quartz veins (Figure 34c), sericite and microcline. The rock is composed predominantly of hornblende, comprising

roughly 75% of the total rock. This variety of hornblende is relatively coarse-grained, ranging from 1.0 to 3.0 mm in average grain size, nematoblastic in texture, brown in color, slightly altered, and occur as elongated grains along the plane of foliation. Xenoblastic plagioclase is the next abundant component, comprising approximately 10% of the rock and has an average grain size of approximately 0.3 to 0.6 mm. Quartz, microcline and biotite comprise the remaining 15% of the rock (~5% each) and have roughly a 0.2 to 0.5 mm average grain size. The quartz is polygonal granoblastic, while the microcline is xenoblastic (confined to the veins) and the biotite is lepidoblastic in shape and texture. Other mineral constituents of the rock include calcite, chlorite, apatite and sphene. The overall texture is granolepidoblastic, with gneissic layering of hornblende and plagioclase.

The Black Amphibolite is not classified as a hornblende gneiss as other authors have defined because the quartz content is too low. The Black Amphibolite is found downslope from the Gray Compositionally-Banded Amphibolite Gneiss (1b.Xag:Xf) and closer to the transfer fault WCTF. The eastern limit of my field area, the basin-bounding fault (WCTF), is marked on the surface by massive blocks of Black Amphibolite Gneiss (Xh), which produce a steep drop-off. Some of these blocks have slid far downslope toward the east for some distance. On the SR, both specimens SR3999 (location 82) and SR3899 (location 81) appear to be massive, fault-related boulders located down by a campsite along Stumpy Creek (Appendix C & Appendix E; Plate I), and, on the NR, at location 79, the fault scarp is overlain and obscured by large boulders, which form a cliff on the descent.



Figure 34c. A photomicrograph of a thin section of Black Amphibolite Gneiss (Xh) of the Amphibolite Gneiss (Xag) unit (1a.Xag:Xh), showing a ribbon quartz vein parallel to the foliation plane of the fabric. Long axis of photomicrograph = 4 mm. (NR2699; hand specimen featured in Figure 34b).

GRAY COMPOSITIONALLY-BANDED AMPHIBOLITE GNEISS (Xf)

The Gray Compositionally-Banded Amphibolite Gneiss (1b.Xag:Xf) (Figure 35a) is a fine-grained and gneissic-layered amphibolite gneiss, with a fresh color of gray (fine-grained black and white) and a weathered color of gray. Weathering occurs along foliation planes that form thin plates and is slightly fissile (breaking along the contacts between banding planes of foliation and resilient veins) (Figure 35a), unlike the black amphibolite gneiss (1a.Xag:Xh, to the east) that weathers in a blocky manner (Figure 34b). Hand specimens SR3599 (ignoring pods), SR3699, NR2399 & NR2299 all outcrop in this unit.

Specimen NR2399 (Figures 35a, 35b & 35c) is a representative gray compositionally-banded amphibolite gneiss that exhibits a gray weathered color and a



Figure 35a. Amphibolite Gneiss (Xag) Gray Compositionally-Banded Amphibolite Gneiss (Xf) exposure (1b.Xag:Xf). Looking southeast on NR at location 75 at the tabular, platy unit with a N12W fracture pattern due to prominent weathering out along the planes of foliation, more fissile than the neighboring units, Xh & Xfs. Field assistant is shown for scale. (NR2399).

black and white fresh color, with hornblende and quartz bands/layers respectively. The rock has a fine-grained to very fine-grained matrix, veins parallel to and crosscutting foliation, a thin and platy appearance with weathering along veins. Hornblende (~40% of the rock, ~0.2-0.5 mm average grain size) is the major mineral constituent that is nematoblastic, slightly altered (producing a greenish cast), and elongated in the direction of foliation. Microcline is the second most common mineral in the rock at approximately 30% of the rock (xenoblastic; ~0.1-0.8 mm average grain size). Quartz and plagioclase, at 15% and 10% of the rock, respectively, are both roughly 0.1 to 0.8 mm in average

grain size. The average grain size of the matrix is approximately 0.1 to 0.3 mm (compared to the porphyroblasts at approximately 0.6 to 0.8 mm in average grain size), with the quartz crystals in the veins ranging in size from approximately 0.6 to 1.0 mm average grain size. Other mineral constituents are biotite, muscovite, chlorite, epidote, apatite, zircon and sphene, all consisting of small proportions and grain sizes.



Figure 35b. A hand specimen of the Gray Compositionally-Banded Amphibolite Gneiss (Xf) of the Amphibolite Gneiss (Xag) unit (1b.Xag:Xf). Marker (13.5 cm) is shown for scale. (NR2399).

With the increase in the amount of quartz, this specimen could be classified as a hornblende gneiss, however, the amount of hornblende decreased relative to the increase of microcline while the amount of plagioclase remained roughly the same. Hornblende is less common (and smaller in grain size) and quartz is more common in this unit, as

compared to the Black Amphibolite Gneiss unit downslope (1a.Xag:Xh) (e.g. NR2699) where hornblende is more common (and of a medium grain size) and quartz is less common.



Figure 35c. A photomicrograph of a thin section of the Gray Compositionally-Banded Amphibolite Gneiss (Xf) sub-unit of the Amphibolite Gneiss (Xag) unit (1b.Xag:Xf). Long axis of photomicrograph = 4 mm. (NR2399).

Specimen SR3699 is another representative gray compositionally-banded amphibolite gneiss that contains a few porphyroblasts of quartz with quartz intergrown, quartz veins crosscutting foliation forming slight lineaments across the subtle metamorphic fabric, and brittle deformation with veins offset.

QUARTZOFELDPATHIC SCHIST (Xfs)

The Quartzofeldspathic Schist (1c.Xag:Xfs) (Figure 34a) is a weathered orange-yellow-light brown, glittery, coarse-grained, brittle schistose quartzose rock (Figure 36a). Concentrations of biotite and muscovite are greater relative to quartz and feldspar. Weathering does not occur predominantly along foliation planes but rather between the



Figure 36a. A hand specimen of the Quartzofeldspathic Schist (Xfs) sub-unit of the Amphibolite Gneiss (Xag) unit (1c.Xag:Xfs). Marker (13.5 cm) is shown for scale. (SR3499).

mineral grains, forming a crumbly surface. Hand specimens SR3799, SR3499, SR3399, NR499, ~NR4*99(ignoring pods) are from this unit.

Specimen SR3499 (Figure 36a) is a representative quartzofeldspathic schist that exhibits an orange-light brown weathered color, a yellowish-light brown fresh color, and contains roughly 75% potassium feldspar (microcline). Specimen NR499 (Figure 36b) is another representative quartzofeldspathic schist that exhibits an orange-light brown

weathered color and a yellowish-light brown fresh surface color. It is granolepidoblastic in texture overall and excessively poikiloblastic (a phase of porphyroblastic formation which is the texture of a quartzofeldspathic porphyroblastic rock (Pfs) [NR4*99]).

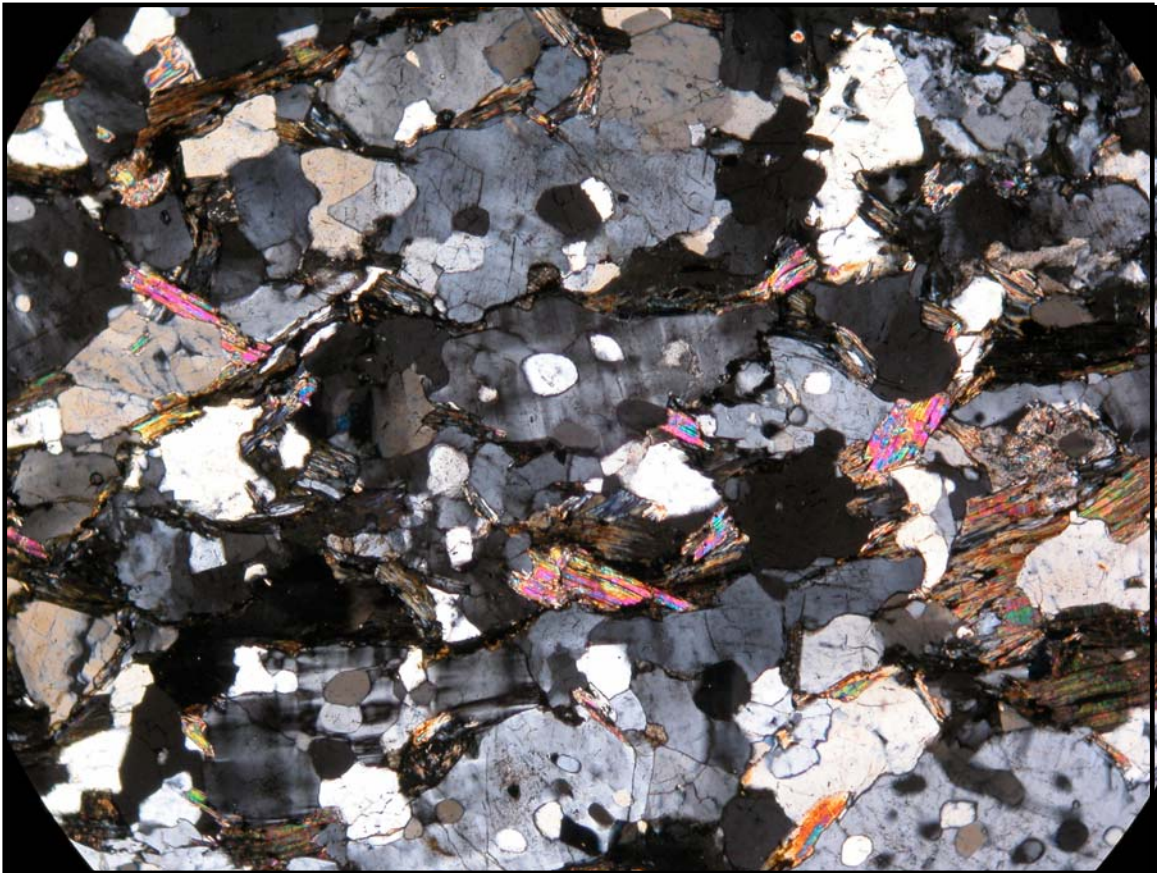


Figure 36b. A photomicrograph of a thin section of the Quartzofeldspathic Schist (Xfs) of the Amphibolite Gneiss (Xag) unit (1c.Xag:Xfs). Long axis of photomicrograph = 4 mm. (NR499).

Specimen NR499 has a brittle, crumbly appearance and feel. It has a coarse-grained equigranular matrix with microcline (~50% of the rock, ~0.2-0.5 mm average grain size, xenoblastic) as the major mineral constituent (which exhibits a poikiloblastic texture with quartz inclusions). Quartz is the second most common mineral in the rock at approximately 20% (~0.1-0.2 mm average grain size; xenoblastic) and is both poikiloblastic and granoblastic in texture. Plagioclase is the third most abundant mineral

in the rock at approximately 15% (~0.3-0.5 mm average grain size). Biotite and muscovite comprise 10% of the rock (~5% each), having roughly a 0.5 mm average grain size each, and are lepidoblastic in texture. Other mineral constituents are chlorite, epidote, calcite, apatite, zircon and sphene, all of small proportions and grain sizes (Figure 36b).

QUARTZOFELDSPATHIC GNEISS

The Quartzofeldspathic Gneiss unit (2.Xqfg) covers a huge portion of the area and the central portion of the ridgelines. A total of 16 specimens of this unit were collected from both ridgelines. The quartzofeldspathic or leucocratic gneiss is a fine-grained (~0.1-0.4 mm average grain size) gneiss, granolepidoblastic in texture, that weathers to a



Figure 37a. Quartzofeldspathic gneiss (2.Xqfg) exposure. Field notebook is shown for scale. Photo courtesy of Dr. Mary Hubbard.

pink-orange-light brown color and has a fresh surface color of gray to black (Figures 37a, 37b & 37c).

The quartzofeldspathic gneiss is rich in quartz (~40-75%) and feldspars (microcline ~5-20% and plagioclase ~5-25%) relative to the fine-grained hornblende (~0-10%), biotite (~2.5-5%) and muscovite (~1-15%) mineral grains. Sericite accounts for ~20% of the specimen's total rock portion, being altered from both microcline and plagioclase.

The quartzofeldspathic gneiss weathers to an orange-brown to pinkish-light brown-orange (Figure 37b) and has a light gray fresh surface color.



Figure 37b. A hand specimen of Quartzofeldspathic Gneiss (2.Xqfg) showing the orange weathered color. Marker (13.5 cm) is shown for scale. (SR2799)

This unit exhibits a “wavy” appearance along the planes of foliation in some exposures (Figure 37a) and fractures into thin plates and, in some locations, has fractured into massive cubic blocks.

The “porphyroblasticity” was found to vary throughout this unit along the traverse of both ridgelines (NR1099, SR3199, SR3099 & SR2899), with quartz porphyroblasts oriented both along and crosscutting foliation. Specifically, specimens SR3199 and SR3099 contain quartz porphyroblasts, specimen NR1099 contains large quartz aggregates (quartz grains mantled by finer grains of quartz) and specimen SR2899 contains porphyroblasts of quartz and microcline, mantled by fine-grained ribbon quartz. Compared to the other two units, the quartzofeldspathic unit has minimal igneous intrusions throughout and contains a lens of an exotic calc-silicate gneiss exposure, only found in this unit.

Specimens NR599, NR1*99, NR899, NR199, NR399, NR799, NR999, NR1099, SR3299, SR3199, SR3099, SR2999, SR2899, SR2799, and SR2699 are from this unit (Appendix A; Appendix B; Appendix C; Appendix D; & Plate I).

Specimen SR2799 is a representative quartzofeldspathic gneiss specimen on the SR that is fine-grained, weathers to an orange-light brown color (Figure 37b), has a fresh surface color of gray (fine-grained black and white) and exhibits a blocky fracture pattern (Figure 37b).

Specimen NR399 is a representative quartzofeldspathic gneiss specimen of the quartzofeldspathic unit on the NR. This quartzofeldspathic gneiss weathers to a pinkish-light brown color and has a fresh surface color of gray to black. The major mineral

constituent is quartz, which is fine- to med-grained, ranges from 0.1 to 0.4 mm in average grain size and comprises roughly 40% of the total rock. The next abundant minerals are microcline and plagioclase, each comprising approximately 25% of the total rock and ranging from 0.2 to 0.4 mm in average grain size. Hornblende and biotite are the next abundant minerals, each comprising 5% of the rock, ranging from approximately 0.1 to

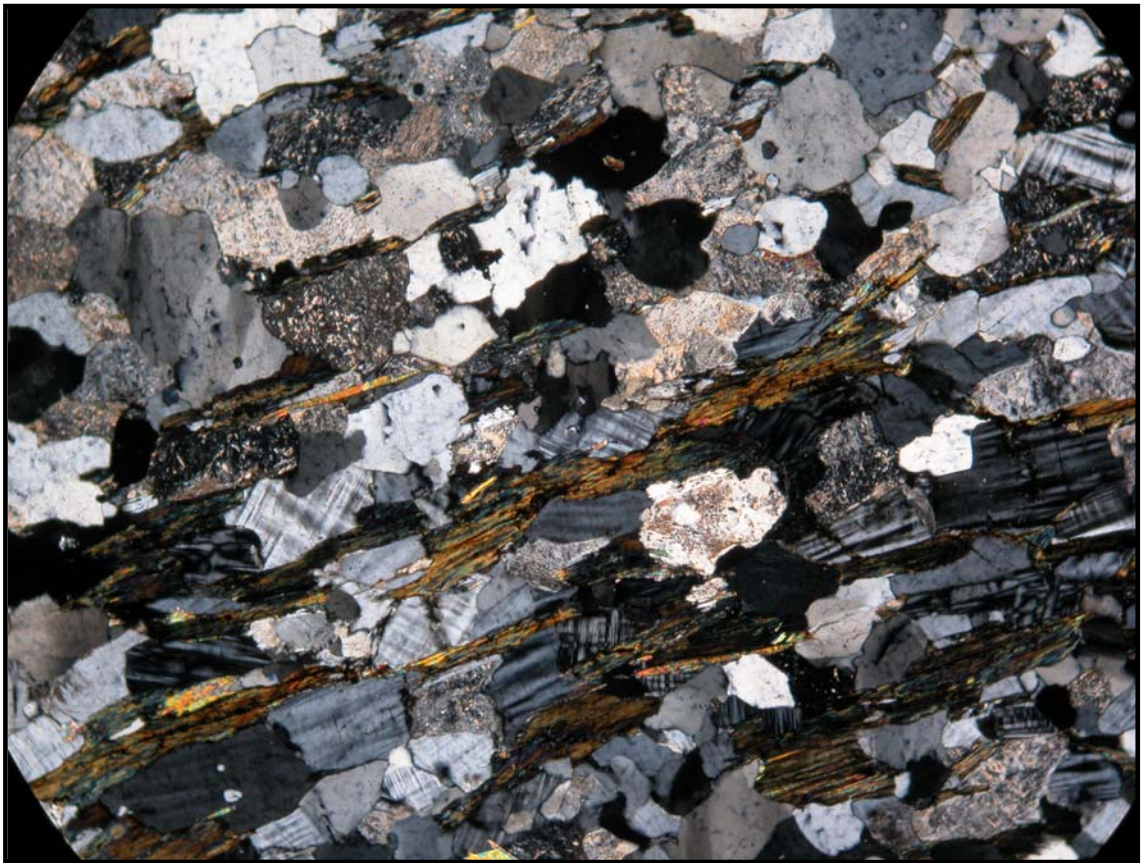


Figure 37c. A photomicrograph of a thin section of Quartzofeldspathic gneiss (2.Xqfg). Long axis of photomicrograph = 4 mm. (NR399).

0.2 mm in average grain size each. Other mineral constituents include muscovite (~1%; 0.1-0.2 mm average grain size) and apatite (~1%) (Figure 37c). This specimen has a thin and platy fracture pattern (not blocky like SR2799).

FELSIC HORNBLENDIC GNEISS

This unit of felsic hornblende gneiss (3.Xfh) (Figure 31 & Plate I) is best viewed and most representative in the westernmost exposures at the higher elevations. The contact between the central unit (2.Xqfg) and westernmost unit (3.Xfh) is based on the sudden decrease in spacing distance between the felsic and hornblende “stripes” (or layers/fingers). In the western high elevations, the stripes are thin and closely-spaced and the interval between the felsic rich and the hornblende layers is decreased. The three sub-units within the felsic hornblende gneiss unit (3.Xfh) are: an amphibolite gneiss (3a. Xfh:Xa), quartzofeldspathic gneiss (3b. Xfh:Xqf) and feather amphibolite (3c. Xfh:Xfa). There are two additional sub-units that are located throughout and within the 3.Xfh units: a hornblende porphyroblastic unit (3d. Xfh:Xhb [amphibolite (3a. Xfh:Xa)]) and a quartz mica schist “whiteschist” (3e. Xfh:Xqms), which crop out as sparse lenses. Generally, the amphibolite gneiss units are fine to coarse-grained, the quartzofeldspathic gneiss units are fine-grained and the feather amphibolites are coarse-grained. The quartzofeldspathic gneiss has both a wavy and a blocky fracture pattern. These amphibolite gneiss and quartzofeldspathic gneiss sub-units contain many quartz and epidote veins (giving a foliated texture to the rock), as well as many intrusive bodies throughout the layers (Figure 38a).

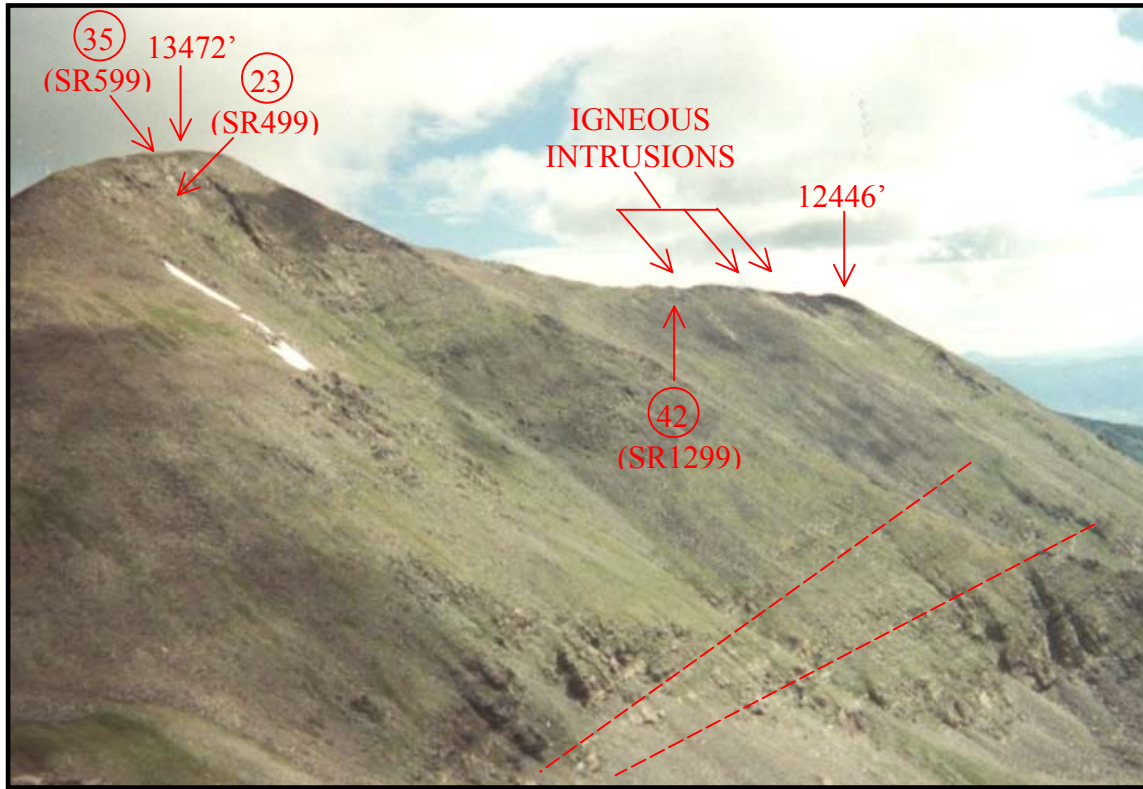


Figure 38a. Looking north-northeast at the northeast-striking and northwest-dipping strata and exposures on the south face and apex of the SR in the western high elevations. Locations 35 (SR599) & 23 (SR499), igneous intrusions and Location 42 are shown. Dashed line indicates surficial expression of exposures towards the base. Field of view = 1 mile [1610 m]

(HORNBLENDIC) AMPHIBOLITE GNEISS

One stripe within the interstriped unit Xfh is a (hornblendic) amphibolite gneiss (3a.Xfh:XA) (Figures 38b & 38c). The amphibolite gneiss is a dense, fine- to coarse-grained amphibolite, with a weathered color of orange-maroon-brown-black-gray, with iron oxide deposits. It has a fresh surface color of dark gray to 'black and white', with green epidote veins and white quartz veins. The veins are randomly oriented with respect to the foliation of the subtle gneissic fabric. The amphibolite gneiss weathers into rhombohedron-like blocks, cubes, elongated rod-like shards and, occasionally, into foliated plates. Hornblende and plagioclase comprise approximately 70% and 25% of the



Figure 38b. Looking northeast downstrike (northeast-striking and northwest-dipping) of an amphibolite gneiss (3a.Xfh:Ya) exposure at location 35 near the 13,472' apex of SR (shown in Figure 38a). Pencil is shown for scale. (SR599)

rock, respectively, while the prevalence of microcline is minimal. Small amounts of biotite and muscovite give a micaceous sheen to the exposures and hand specimens. Fourteen hand specimens (NR1199, NR2099, NR1899, NR1699, SR2599, SR2299,

SR2199, SR1999, SR1899, SR1699, SR1399, SR1099, SR599 & IS199) are all classified as amphibolite stripes within this interstriped unit.

Specimen SR1699 is a representative specimen of a (hornblendic) amphibolite gneiss (3a.Xfh:XA) that weathers a grayish black (Figure 38c) and has a fresh surface color of black, with green epidote veins.



Figure 38c. A hand specimen of an amphibolite gneiss (XA) of the felsic hornblendic gneiss (Xfh) unit (3a.Xfh:XA). Marker (13.5 cm) is shown for scale. (SR1099)

The rock consists primarily of nematoblastic coarse-grained hornblende (~75%; 0.4-0.8 mm average grain size). Plagioclase is sericitized and accounts for ~10% of the rock. Microcline is minimal (~5%; ~0.2-0.4 mm average grain size) and lepidoblastic biotite (~5%; ~0.2-0.4 mm average grain size) is low in amount. The other mineral constituents are granoblastic quartz (~2.5%), lepidoblastic muscovite (~1%), epidote (~1%) in veins, diopside (~1%) and apatite (~1%). The overall texture of the rock is granolepidoblastic (Figure 38d).

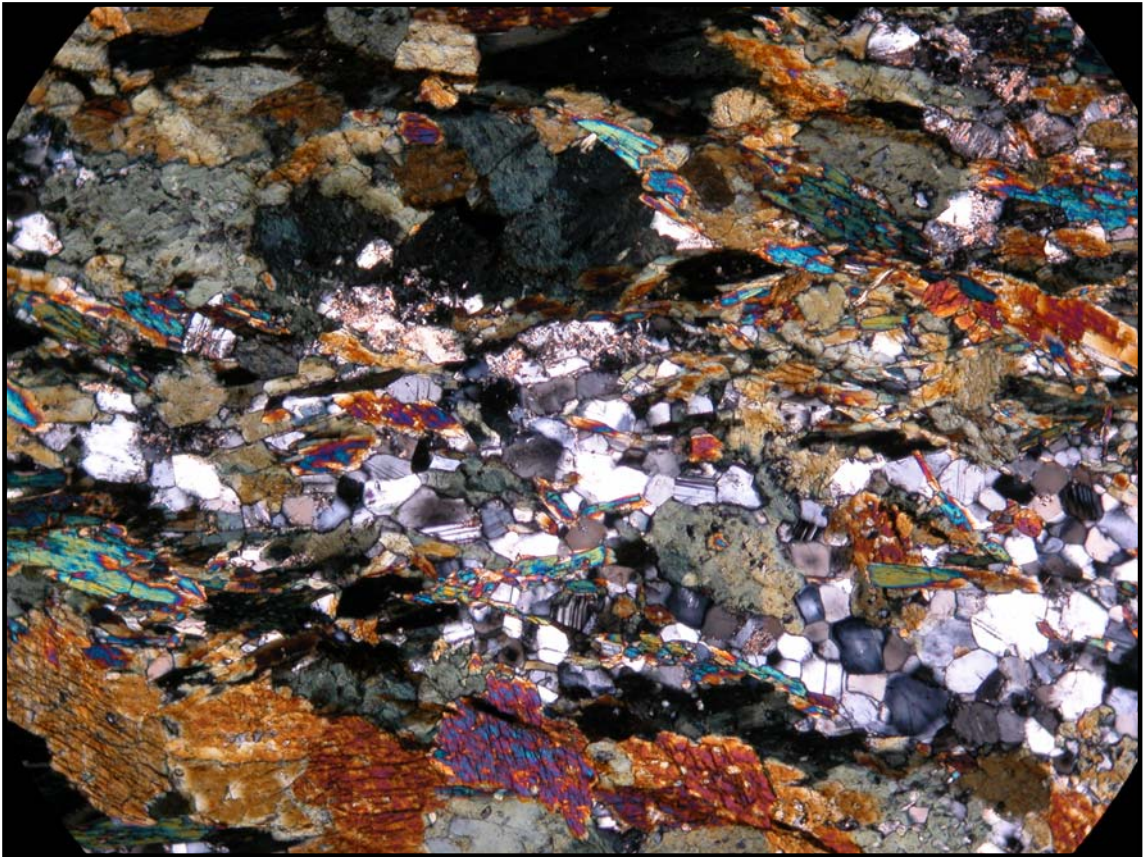


Figure 38d. A photomicrograph of a thin section of a hornblende amphibolite gneiss (Xa) in the felsic hornblende gneiss (Xfh) unit (3a, Xfh:Xa). Long axis of photomicrograph = 4 mm. (SR1699)

Specimen NR2099 contains quartz and epidote veins that appear to have formed porphyroblasts and segregated the gneissic texture parallel to foliation.

(FELSIC) QUARTZOFELDSPATHIC GNEISS

Another stripe within the interstriped unit Xfh is a (felsic) quartzofeldspathic gneiss (3b.Xfh:Xqf), similar to the central unit of quartzofeldspathic gneiss. A fine-grained rock with a grano-nemato-lepidoblastic texture, quartz and iron oxide-filled veins parallel, perpendicular and crosscutting foliation and a quartzite appearance. The rock



Figure 38e. A hand specimen of a quartzofeldspathic gneiss (Xqf) of the felsic hornblending gneiss (Xfh) unit (3b. Xfh:Xqf), showing both the weathered and fresh surfaces. Marker (13.5 cm) is shown for scale. (SR899)

exhibits a weathered color of pink-brown-orange-gray and a fresh surface color of gray (fine grains of black and white gneissic banding) that weathers predominantly into thin brittle platy, triangular and arcuate shards (Figures 38e & 38f). Eight (8) hand specimens (NR1799, SR2399, SR2099, SR999, SR899, SR799, SR499, and SR399) are all felsic

quartzofeldspathic gneiss specimens. All the specimens are fine-grained, with the exception of the coarse-grained specimen SR399.



Figure 38f. A photomicrograph of a thin section of felsic quartzofeldspathic gneiss (Xqf) of the felsic hornblendic gneiss (Xfh) unit (3b. Xfh:Xqf). Long axis of photomicrograph = 4 mm. (SR999).

Specimen SR799 is a representative felsic quartzofeldspathic gneiss, weathers to a splotchy, brownish-orange to black color, has a fresh surface color of gray and has a weathered shape of thin and platy. Fine-grained quartz is the dominant mineral of the rock (~60%; ~0.1-0.2 mm average grain size). The next abundant minerals are microcline and plagioclase, both at 10% of the rock, with an average grain size of roughly 0.2 to 0.4 mm. The rock is also slightly micaceous, with biotite and muscovite composing ~5% of the rock, with an average grain size of ~0.2 to 0.4 mm each.

FEATHER AMPHIBOLITE

The third and final stripe within the interstriped westernmost unit (3.Xfh) is a feather amphibolite (3c.Xfh:Xfa), also known as a garbenschiefer, a coarse-grained granoblastic amphibolite with the hornblende being very coarse-grained (unlike the easternmost amphibolites (1.Xag)) (Figure 38g).

Some specimens are heterogranular and still contain a fine-grained hornblende within the matrix. The random equigranular and fan-shaped radiating clusters of hornblende grains comprise ~75% of the rock and exhibit a texture described as “artwork”. Seven hand specimens (NR1499, NR1999, NR1599, SR2499, SR1599, SR1499, and SR699) are all of feather amphibolite.



Figure 38g. A hand specimen of feather amphibolite (Xfa) of the felsic hornblende gneiss (Xfh) unit (3c.Xfh:XA), showing the weathered gray color. Elongate breakage into shards is also visible. Marker (13.5 cm) is shown for scale. (NR1999)

Specimen NR1999 is a representative feather amphibolite (3c.Xfh:Xfa), with a weathered color of gray and a fresh surface color of black (Figure 38g). The rock is granoblastic with radiating crystal clusters of coarse-grained hornblende (70%; 2.0-4.0 mm average grain size). Microcline and plagioclase, both sericitized, each amount to ~10% of the rock and ~0.2-1.0 mm in average grain size. Other minerals are quartz (25%; ~0.2-0.5 mm average grain size), biotite (2.5%; ~0.8-1.0 mm average grain size), epidote (1.5%; ~0.1-0.2 mm average grain size), diopside (1%; ~0.1-0.2 mm average grain size), and apatite (1%; ~0.1-0.2 mm average grain size) (Figure 38h).

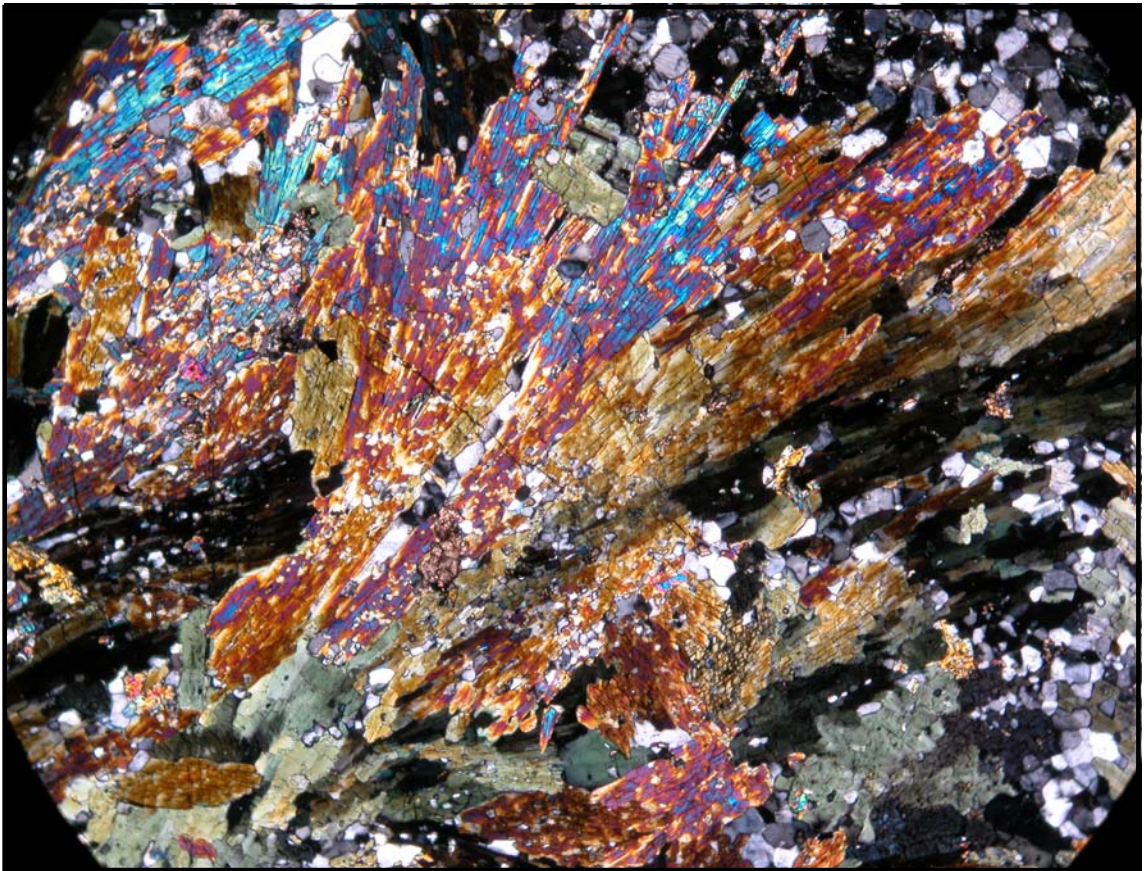


Figure 38h. A photomicrograph of a thin section of a feather amphibolite (Xfa) of the felsic hornblendic gneiss (Xfh) unit (3c.Xfh:Xfa). Long axis of photomicrograph = 4 mm. (NR1999)

Specimen SR699 is a black feather amphibolite located between two quartzofeldspathic gneiss exposures, with a weathered color of black-brown and a fresh surface color of dark gray. The texture is granoblastic with randomly oriented grains, not quite as foliated and gneissic in fabric. Hornblende (~70%) and sericitized plagioclase (~10%) comprise the matrix. A large prominent fine-grained microcline (~10%; in both vein and matrix) vein, along with some epidote (~1%), quartz (~5%) and diopside (~1.5%) veins, exist within the fabric. Apatite accounts for ~1% of the rock.

Specimen NR1499 is a feather amphibolite that weathers into rhombohedron-shaped blocks. It is fine-grained, heterogranular and consists of hornblende grains of two average grain sizes (coarse-grained fan-shaped bands of hornblende and fine-grained hornblende) within the matrix. Microcline and quartz veins, parallel to and crosscutting foliation, appear to be offset, faulted and subjected to brittle deformation and reverse movement.

Specimen SR2499 (Figure 33) is a black and green feather amphibolite with feathery artwork of massive (~0.3-0.4 average grain size) hornblende (~75%) grains and biotite (~5%) grains. Plagioclase (15%) is abundant while quartz (~2.5%) is minor in amount and present in veins that are stretched out. Epidote (<1%) and diopside (<1%) give a greenish cast to the rock.

OTHER LITHOLOGIC UNITS

CALC-SILICATE GNEISS

Within the quartzofeldspathic gneiss unit, there was a sliver of a coarse-grained calcareous-aluminous-siliceous “calc-silicate” gneiss (4. Xcs ; AKA 2a.Xqfg:Xcs).



Figure 39a. An exposure of the calc-silicate gneiss (4.Xcs)(a.k.a. 2a.Xqfg:Xcs) which outcrops within the quartzofeldspathic gneiss unit (2.Xqfg). Brunton is shown for scale. (NR699)

Specimen NR699 (Figures 39a & 39b) of the NR and specimen SR299 of the SR are the calc-silicate gneiss specimens found in the field from these exposures. This unit is exposed on the NR and was found along strike on the SR, but only as float.

Specimen NR699 is an exemplar representative specimen of the calc-silicate gneiss. The calcite has been dissolved and overlain by a ferrous oxide, which gives it a rust brown weathered color. However, when scraped with a knife and subjected to an application of hydrochloric acid, the fresh surface effervesced.

Specimen NR699 is a coarse-grained gneissic (white calcite bands with black/green hornblende bands), granonematoblastic rock that weathers to a dolomitic appearance of grayish-green and has a fresh surface color resembling a greenish black matrix, with pink-red calcite grains (Figure 39b). The main component is calcite (30%;



Figure 39b. A hand specimen of a calc-silicate gneiss (4.Xcs (a.k.a 2a.Xqfg:Xcs)), which is exposed within the quartzofeldspathic gneiss (2.Xqfg) unit, showing the fresh color. Marker (13.5 cm) is shown for scale. (NR699).

~2.0-5.0 mm average grain size), forming large idioblastic crystal grains (Figure 39c).

Recrystallized metamorphic quartz, the second most abundant mineral by comprising approximately 30% of the rock (~0.2-0.8 mm average grain size), shows evidence of stretching. Green hornblende (~25%; ~0.8-1.0 mm average grain size) is altering to trace amounts of epidote, biotite and chlorite. Sericitized feldspars (~5%; ~1.0-2.0 mm average grain size) compose the remainder of the rock. There is dissolved calcite that is

highly iron stained and vuggy on the surface of the weathered specimen. Iron oxide (opaques/FeO/FeOxides/rust) (~5%; ~0.3mm average grain size) is deposited within and lines the dissolution veins through the calcite grains and bands (Figure 39c). Other mineral constituents include microcline (~3%; ~0.3mm average grain size), epidote (<1%; ~0.2-0.3 mm average grain size), plagioclase laths (~1%; ~0.3mm average grain size), untwinned orthoclase (~1%; ~0.3mm average grain size), diopside (<1%; ~0.3mm average grain size); sphene (<1%; ~0.3mm average grain size), zircon (<1%; ~0.3mm average grain size) and apatite (<1%; ~0.3mm average grain size).

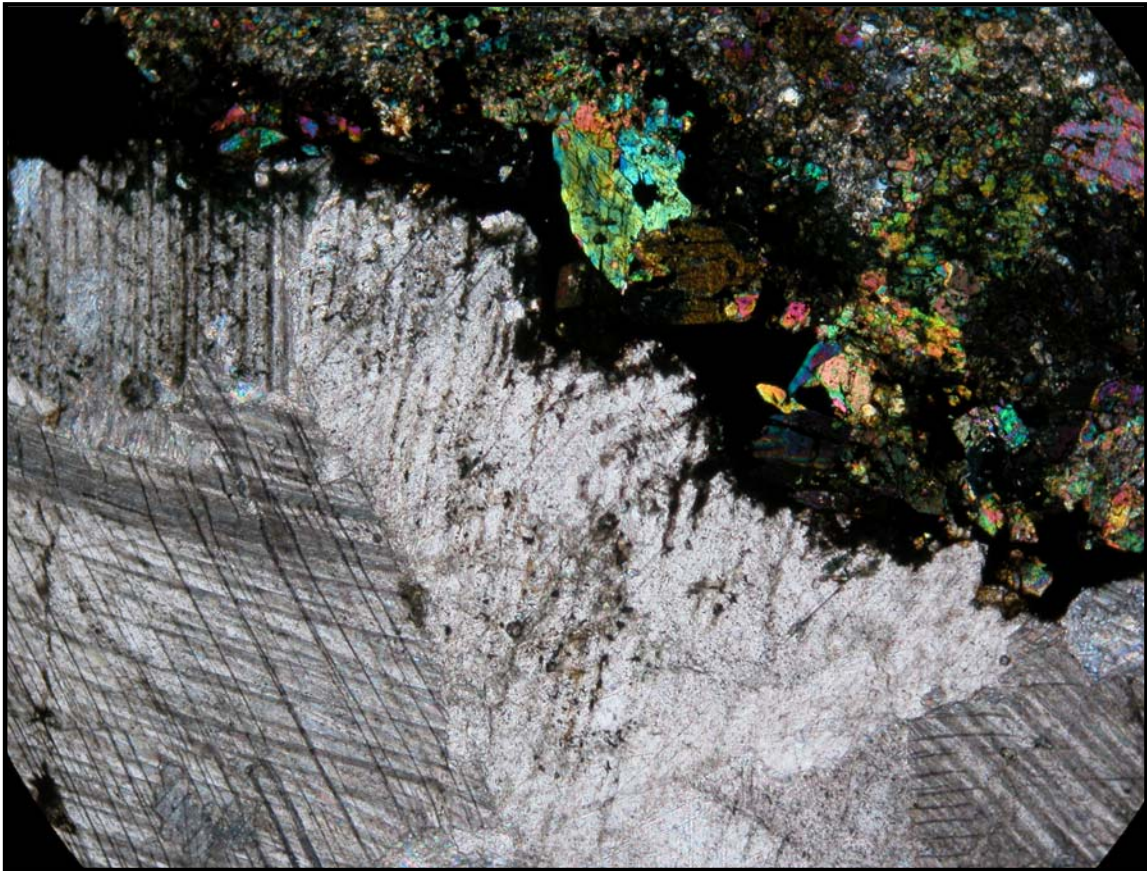


Figure 39c. A photomicrograph of a thin section of the calc-silicate gneiss (4.Xcs) (a.k.a. 2a.Xqfg:Xcs). Long axis of photomicrograph = 4 mm. (NR699).

PORPHYROBLASTIC “POD” ROCKS

Throughout the ridgeline units, there are select exposures within which the texture of the amphibolite is porphyroblastic. The “pods” are porphyroblasts that are recrystallized and have grown to consist of crystals larger than the minerals of the matrix. It is thought that they are not porphyroclasts because they are not grains of the protolith, which have been pulverized, broken and crushed. The porphyroblasts are most pronounced near an area thought to be a shear zone, but exist throughout various lithologies along the entire traverse of the ridgeline. The porphyroblasts vary in mineral composition and are not confined solely to one lithology. In some locations, the porphyroblasts were unstable within the matrix and weathered out easily (especially near the proposed shear zone), resulting in the ridgeline surface being strewn with orbicular particles. The mineral that mantles the porphyroblast, such as muscovite, can make the porphyroblast more susceptible to instability and cause it to weather out of the matrix.

One porphyroblastic rock, specimen SR3599 (5a.Pf), is located within the gray compositionally-banded amphibolite gneiss unit (1b.Xag:Xf) and is a fine-grained, heterogranular granoblastic porphyroblastic amphibolite gneiss with a gray (black & white) weathered color and a gray (with white “pods” within) fresh surface color (Figure 40a). The huge porphyroblasts exhibit a core-mantle structure, with fine-grained muscovite and quartz (>5.0mm) in the core, mantled by finer grains of both muscovite and quartz. The zonation of the mantling minerals muscovite and quartz forms large concave lens-shaped discs, roughly 5 cm in diameter and 1.82 cm in height, that are contained within an aluminous schistose matrix fabric of hornblende, biotite and muscovite flakes. This unit outcropped on the SR at location 69 at 10,840-10,880', just



Figure 40a. A hand specimen of the Gray compositionally-banded amphibolite gneiss porphyroblastic rock (5a. Pf), including weathered out porphyroblasts. Marker (13.5 cm) is shown for scale. (SR3599).

east of the quartzofeldspathic porphyroblastic unit (5b. Pfs), and on the NR west of location 73, between NR2299 (location 73) and NR2199 (location 72). Quartz (~40%; >5.0 mm average grain size; polygonal granoblastic) is the main mineral component, located in large concave-shaped porphyroblasts with muscovite (~15%; >5.0 mm average grain size) within a hornblende (~20%; ~0.1-0.2 mm (matrix) average grain size; nematoblastic), plagioclase (~10%; ~0.1-0.2 mm (matrix) average grain size), biotite (~10%; ~0.1-0.2 mm (matrix) average grain size; lepidoblastic), and muscovite (~5%; ~0.1-0.2 mm (matrix) average grain size; lepidoblastic) micaceous schistose matrix. Microcline (~1%, ~0.1-0.2mm (matrix) average grain size), apatite (~1%) and opaques

(~1%, ~0.1-0.2mm (matrix) average grain size) comprise the remainder of the matrix (Figure 40b).

The fine-grained muscovite mantling the porphyroblasts of muscovite and quartz causes susceptibility to being weathered out of the aluminous, micaceous (biotite and muscovite) matrix (with hornblende).

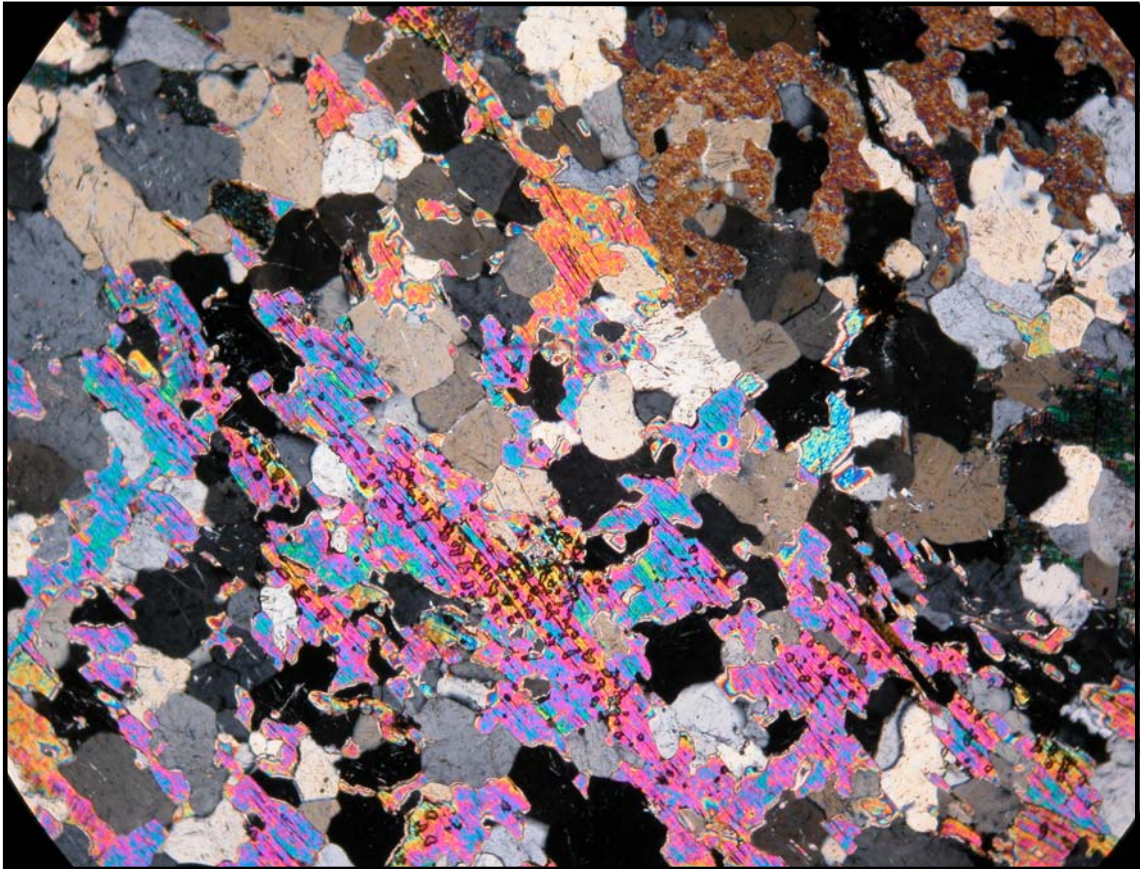


Figure 40b. A photomicrograph of a thin section of the gray compositionally-banded amphibolite gneiss porphyroblastic rock, showing the quartz and poikiloblastic muscovite within the of porphyroblasts (5a. Pf). Long axis of photomicrograph = 4 mm. (SR3599)

Another porphyroblastic rock specimen is a quartzofeldspathic schist (5b. Pfs), a pinkish-tan schist with elongated porphyroblasts (compared to the others that are discs) that have weathered out of the schist quite easily. Many of them lay on the surface downslope and near the base of the exposure. This quartzofeldspathic porphyroblastic

specimen unit is located in the quartzofeldspathic schist (1c.Xag:Xfs) unit and forms a prominent hilltop (10,807') [NR4*99] on the NR, just south of the Cinderella South Mine along Green Creek road, and on the south ridgeline as float, at 10,920'.

Specimen NR4*99 (5b.Pfs) (aka NR4a99/NR4'99) is a heterogranular, granolepidoblastic, fine-grained, pinkish-orange-brown-gray quartzofeldspathic schist porphyroblastic rock (Figure 41a), with porphyroblasts of dark gray sillimanite in the core, mantled by a finer grained, white ribbon quartz. The weathered color is pink to light brown and has a fresh surface color of pink to gray. The texture is more schistose than gneissic and the micaceous matrix is more susceptible to weathering.



Figure 41a. A hand specimen of Quartzofeldspathic schist porphyroblastic rock (5b. Pfs). Marker (13.5 cm) is shown for scale. (NR4*99 & SR3799)

Consequently, encompassed porphyroblasts easily weather out of the fine-grained potassium feldspar(kspar)-rich and micaceous (biotite and muscovite) schistose matrix. The micas are expressed on the surface and throughout the fine-grained micaceous groundmass with maroon kspar veins throughout (Figure 41a). This unit is also exposed on the SR at location 65 (SR3799).

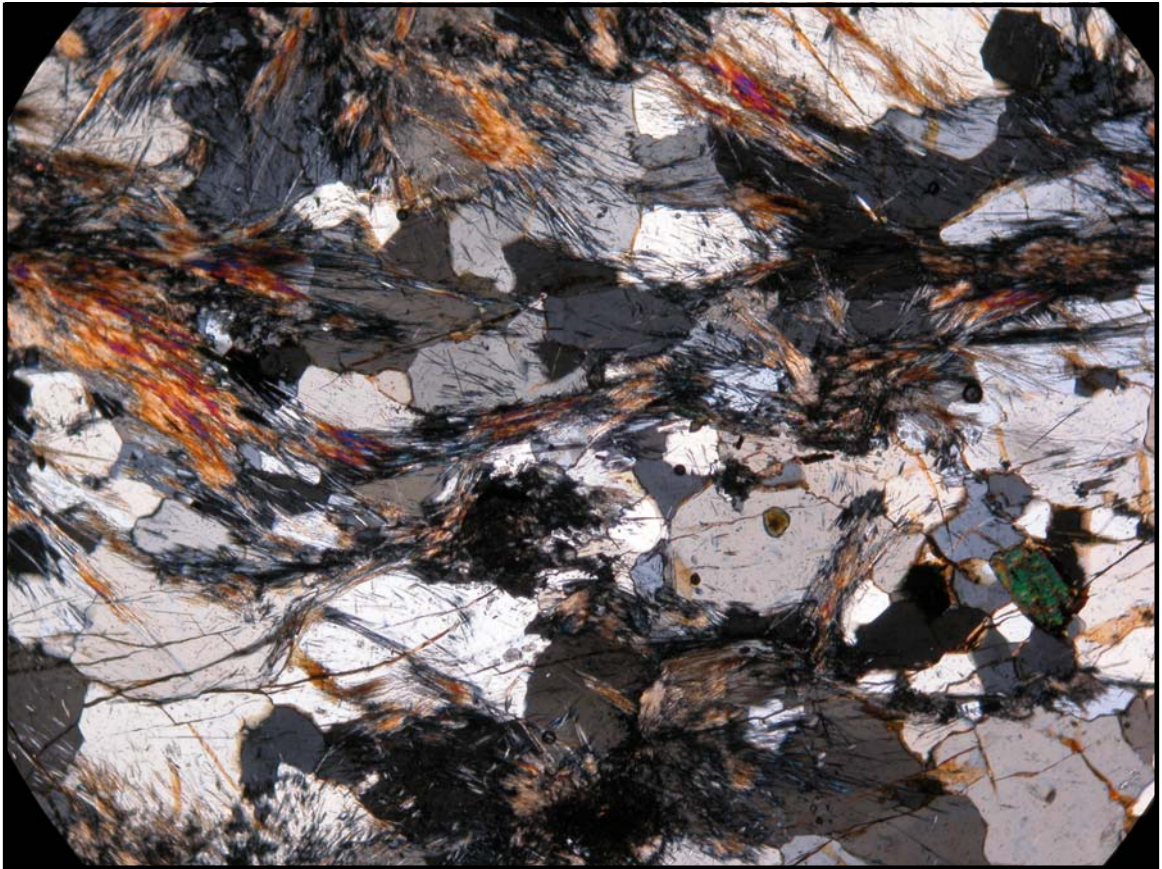


*Figure 41b. A photomicrograph of a thin section of the porphyroblasts within the quartzofeldspathic schist porphyroblastic rock (5b. Pfs). Long axis of photomicrograph = 4 mm. (NR4*99)*

Elongate (2.75 cm in length by 1.25 cm in diameter) porphyroblasts, composed of predominantly coarser quartz (~1.0mm), is cored by masses of acicular fibrous (fibrolitic) dark gray sillimanite (~10%; ~0.5 mm (porphyroblasts) average grain size) being

replaced and overgrown in the core by muscovite (from both the outside in and the inside out), and mantled by muscovite (~0.4 mm average grain size) and finer grained polygonal ribbon quartz (~ 60%; ~0.2-0.4 mm (porphyroblasts) & 0.1-0.4 mm(matrix) average grain size) (Figure 41b).

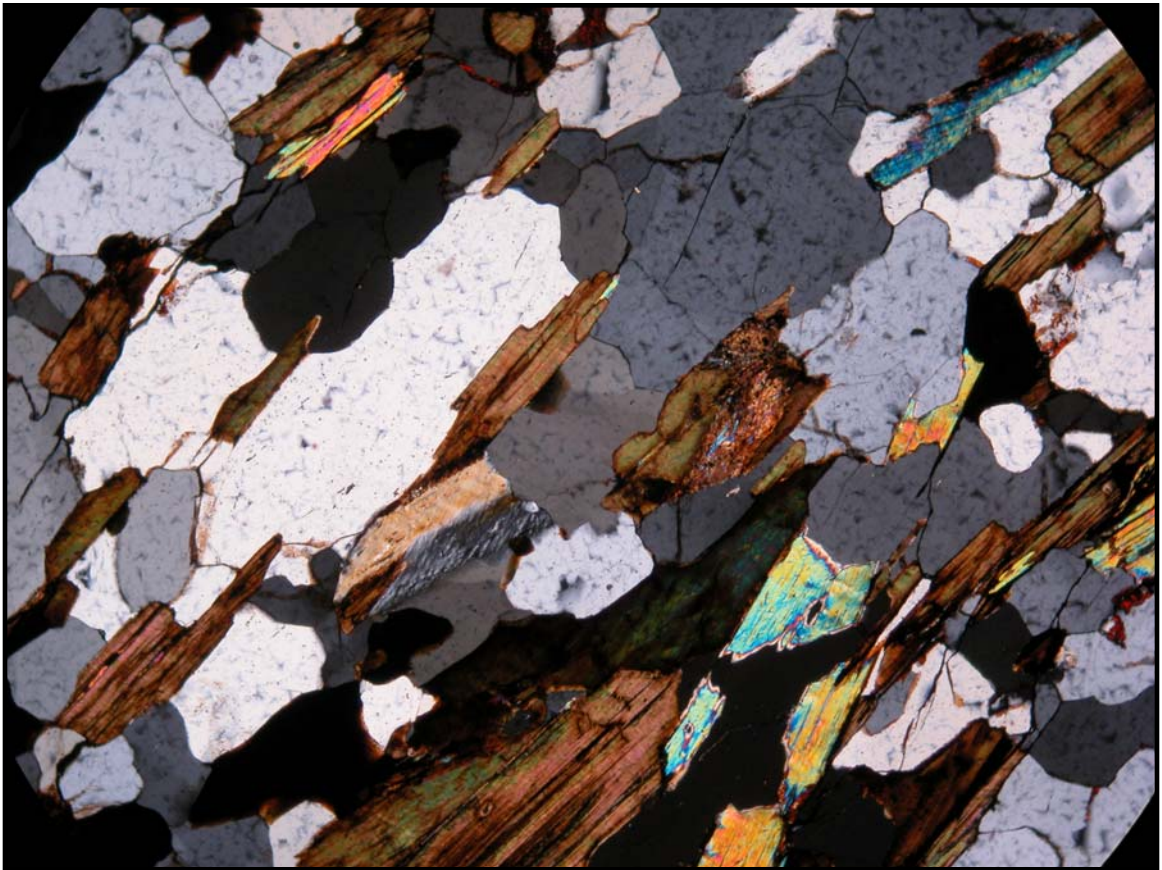


*Figure 41c. A photomicrograph of a thin section showing the matrix of the Quartzofeldspathic schist porphyroblastic rock (5b. Pfs). Long axis of photomicrograph = 4 mm. (NR4*99)*

A granolepidoblastic matrix of biotite (~5%; ~0.2-0.4 mm average grain size (porphyroblasts)), muscovite (~5%; ~0.5 mm (porphyroblasts) and 0.1-0.4 mm (matrix) average grain size; lepidoblastic), microcline (~10% (between porphyroblasts & in matrix); ~0.1-0.2 mm (porphyroblasts) & 0.1-0.4 mm (matrix) average grain size, granoblastic), hornblende (~5%; 0.2-0.4 mm (porphyroblasts) & 0.1-0.4 mm (matrix)

average grain size), quartz (~0.1-0.4 mm average grain size) and plagioclase (~0.1%) almost fully altered to sericite (<1%). Apatite (<1%) and iron oxides/opaque (<1%) comprise the remainder of the rock (Figure 41c). The quartz contains rutile needles, while the feldspars are altering to sericite and compose the microcline veins that parallel the schistose fabric.

Specimen SR3799 is a heterogranular coarse-grained porphyroblastic quartzofeldspathic schist with a pinkish-tan weathered color and a pinkish-gray fresh surface color (Figure 41a).

In the western high elevations, the “porphyroblasticity” in the weathered exposures increased in some locations, becoming pronounced in the outcrops.



Figure 42a. Looking southwest on the SR at location 59 at the massive quartzofeldspathic gneiss blocks, which contain large porphyroblasts/pods of quartz (outlined in photo) mantled by quartz, elongated along SE/NW plane; ENE & WNW fractures. Field of view = 10 feet [3 m]. (SR2899)

As the ridgeline was further traversed, the porphyroblastic rocks were found to be increasingly tolerant to weathering and were truncated by either an abrupt change in lithology or an igneous intrusion.

Specimen SR2899, obtained from an exposure higher in the range, on the SR within the quartzofeldspathic gneiss [2.Xqfg] unit, contained many large coarse-grained elongate porphyroblasts, stretched into ovals (about the size of footballs), embedded within the rock. They were well established and stable, showing no signs of being susceptible to being weathered out of the fine-grained matrix (Figures 42a & 42b).



Figure 42b. A hand specimen of the quartzofeldspathic gneiss porphyroblastic rock, showing the porphyroblasts that have been sliced through outlined with a dashed line. Marker (13.5 cm) is shown for scale. (SR2899)

SR2899 is a fine-grained, granolepidonematoblastic quartzofeldspathic gneiss that weathers a pinkish-gray and has a fresh surface color of gray to white, and contains porphyroblasts, with fine-grained ribbon quartz (~15%; ~4.0 mm average grain size) mantling the microcline porphyroblasts (~13%; ~1.0-2.0 mm (core) average grain size). The 5.0mm+ average grain size porphyroblasts are contained within a fine-grained matrix of quartz (~45%; ~0.1-0.2 mm average grain size), sericitized plagioclase (~10%; ~0.2-0.4 mm average grain size), hornblende (~5%, ~0.2-0.3 mm average grain size), biotite (~5%; ~0.2-0.4 mm average grain size),



Figure 42c. A photomicrograph of a thin section of the quartzofeldspathic gneiss “blocks with pods” porphyroblastic rock, showing the pod/matrix contact with a dashed line, with the edge of the porphyroblast in the lower left and the matrix in the upper right of the photomicrograph. Long axis of photomicrograph = 4 mm. (SR2899)

microcline (~2%, ~0.1-0.2 mm average grain size) and muscovite (~1.5%, ~0.1-0.2 mm average grain size). Iron oxides/opaque (~1%) in veins crosscutting foliation, epidote (~1%), and apatite (~1%) comprise the remainder of the rock (Figure 42c).

HORNBLLENDE PODS

Specimens NR1299 and NR1399 (3d.Xfh:Xhb) both contain hornblende (~40-60%; ~0.3-0.6 mm average grain size) porphyroblasts (pods) mantled by biotite (~5%; ~0.1-0.2 mm average grain size) within a fine-grained granoblastic quartzofeldspathic matrix of quartz (~15-50%; ~0.1-0.2 mm average grain size), plagioclase (~2.5-15%; ~0.2-0.4 mm average grain size) and microcline (~1-1.5%; ~0.1-0.2 mm average grain size). Other mineral constituents include iron oxide opaques (~1%; <0.1 mm average grain size) and apatite (~1%; <0.1 mm average grain size). These hornblende porphyroblasts appear to have been once hornblende phenocrysts of a metavolcanic protolith that was succumbed to forces, resulting in parallel and isolated blasts oriented along subtle foliation within the foliated gneissic matrix of the amphibolite. The porphyroblasts are oriented diagonally across the slide as well as the cut face of the hand specimen (Figure 43a). There were no specimens of this lithology discovered on the south ridgeline.

Specimen NR1299 is a fine-grained, granolepidoblastic, amphibolite gneiss with a weathered color of brown to gray (black & white) and a fresh surface color of black. Hornblende (~65%; ~0.3-0.6 mm average grain size, nematoblastic) and biotite (~5%; ~0.1-0.2 mm average grain size; lepidoblastic) porphyroblast grains reside in a fine-grained matrix of quartz (~15%; ~0.1-0.2 mm average grain size; polygonal granoblastic)

and plagioclase (~ 5%; ~0.2-0.4 mm average grain size; xenoblastic) matrix. Other mineral constituents include microcline (~1%; ~0.1-0.2 mm average grain size; granoblastic), iron oxides (~1%) and apatite (~1%).

Specimen NR1399 (Figure 43a) is a granolepidoblastic, fine-grained amphibolite gneiss that has a weathered color of brown to gray and a fresh surface color of gray (black and white fine-grained). The rock contains hornblende (~40%; ~0.3-0.6 mm average grain size; nematoblastic) porphyroblasts (pods) mantled by biotite (~5%; ~0.1-0.2 mm average grain size; lepidoblastic) within a finer grained quartz (~50%; ~0.1-0.2 mm average grain size; polygonal granoblastic) and plagioclase (~2.5%; ~0.2-0.4 mm



Figure 43a. A hand specimen of hornblende "pods" (outlined in circles) (3d.Xfh:Xhb) in a fine-grained matrix. Marker (13.5 cm) is shown for scale. (NR1399).

average grain size; xenoblastic) matrix. Other constituents of the matrix are microcline (~1.5 %; ~0.1-0.2 mm average grain size; granoblastic), apatite (~1%) and iron oxides/opaque (~1%)(Figure 43b).

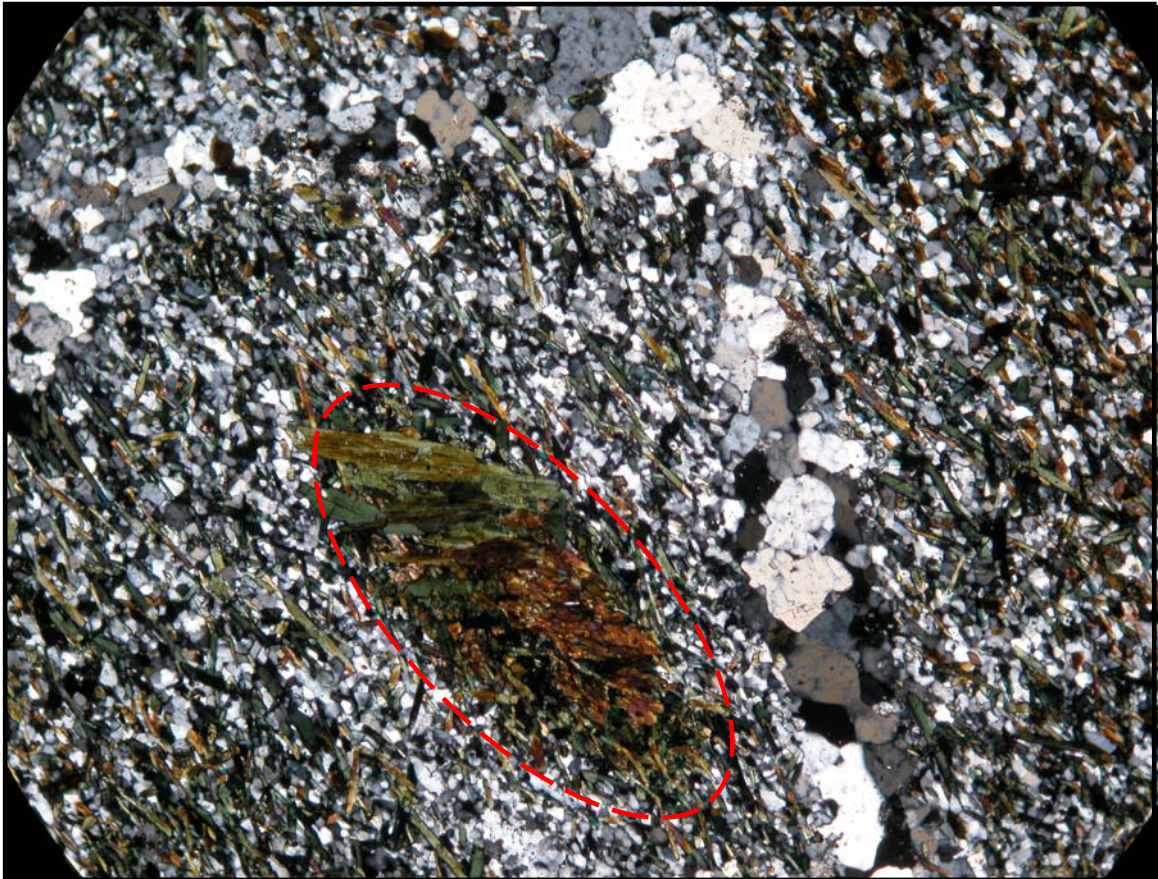


Figure 43b. A photomicrograph of a thin section of a hornblende “pod” outlined by dashed line adjacent to quartz veins. Long axis of photomicrograph = 4 mm. (NR1399).

The porphyroblasts are oriented along a subtle foliation, similar to the adjacent specimen NR1299 located downridge. The specimen appears as a dense and massive rhombohedron-like block with thick quartz veins both perpendicular to and diagonally crosscutting the plane of foliation of the hornblende porphyroblasts. There are more quartz veins than the neighboring nearly-identical specimen, NR1299. The

porphyroblasts are sparse, with only about twelve parallel grains oriented both diagonally and across the thin section (Figure 43a).

QUARTZ PODS

Specimen NR1099 “quartz pods” is a coarse-grained and granolepidoblastic quartzofeldspathic gneiss, with a weathered color of light pink to gray to black-brown-orange (including gray lenticular quartz “pods”), and a fresh surface color of gray (fine-grained quartz matrix). The large quartz porphyroblasts (mineral aggregates of coarse grains mantled by fine grains) are oriented parallel to each other, stretched out (36° N21°W) and elongated, both along and

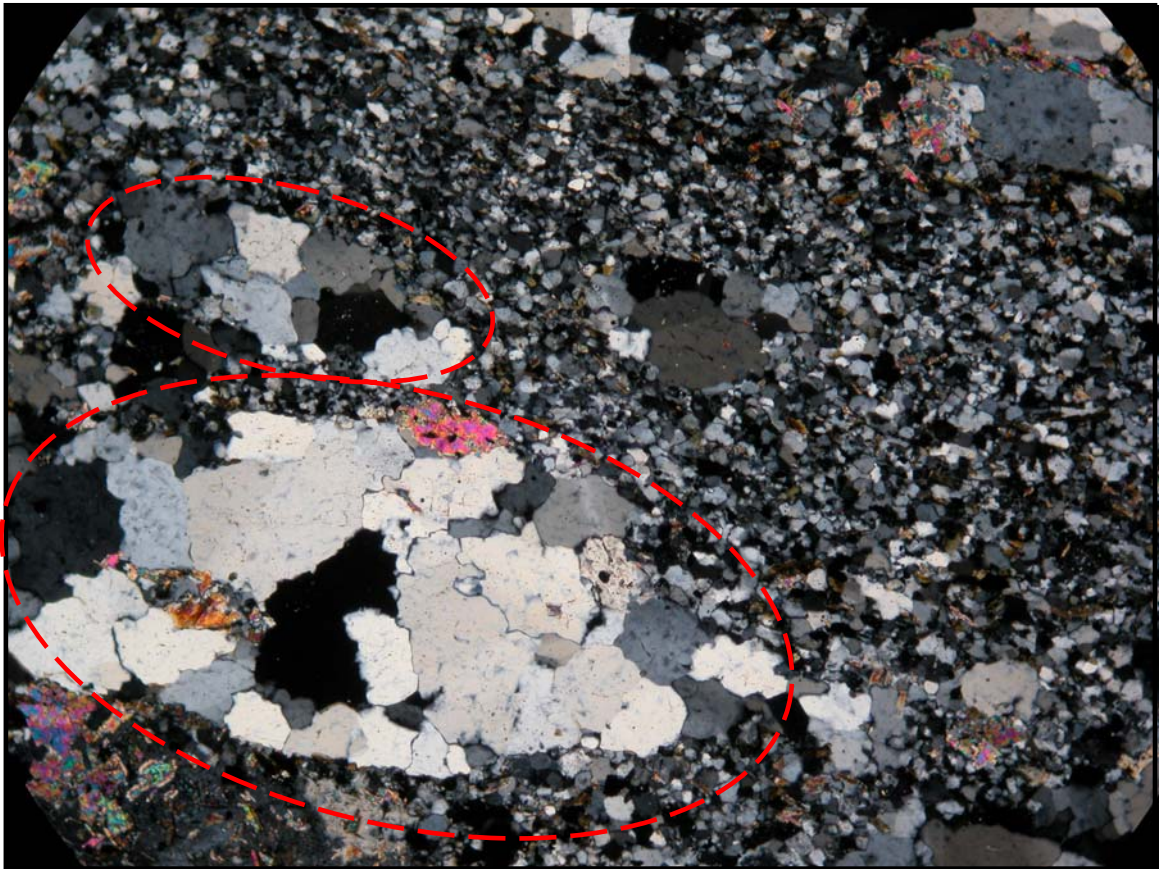


Figure 43c. A photomicrograph of a thin section of the “quartz pods” with the pods outlined with dashed line. Long axis of photomicrograph = 4 mm. (NR1099).

crosscutting, the plane of foliation (N45°E 35°SE) of the metamorphic fabric. Although quartz (~25% (pods & matrix); ~0.7-1.0mm average grain size; polygonal poikiloblastic) composes the porphyroblasts and part of the matrix, the majority of the matrix is composed of sericitized plagioclase (~60% total rock mass; ~0.5mm average grain size; xenoblastic). Other constituents of the matrix are muscovite (~15%; ~0.5-0.9 mm average grain size; lepidoblastic), microcline (~1%; ~0.2-0.3 mm average grain size; xenoblastic) and apatite (<1%). The quartz porphyroblasts appear to be former veins that have been stretched out. The specimen lacks hornblende and has a granitic appearance due to the high concentration of plagioclase and quartz (Figure 43c).

IGNEOUS INTRUSIONS

There were multiple leucocratic igneous intrusions, especially pegmatites, that cut through the basement, which, from a distance, appear as light stripes within the dark gneissic rock (Figure 44a). Both the amphibolite gneiss and quartzofeldspathic gneiss within the interlayered gneiss unit, weather to a dark color making the contrast quite discernable from a distance (Figures 23, 24, 25, 28, 33, 38a & 44a). Although intrusions occurred in all units along the traverse, they occurred predominantly throughout the westernmost unit (3.Xfh), were not as abundant throughout the central unit (2.Xqfg) and were somewhat common throughout the easternmost unit (1.Xag). Veins (quartz, sericite, epidote, calcite & microcline) were common throughout the traverse as well. In the easternmost unit, the veins were predominantly quartz and calcite in composition; while in the westernmost unit, they were quartz and epidote in composition. The presence of epidote gives the rock a greenish cast.

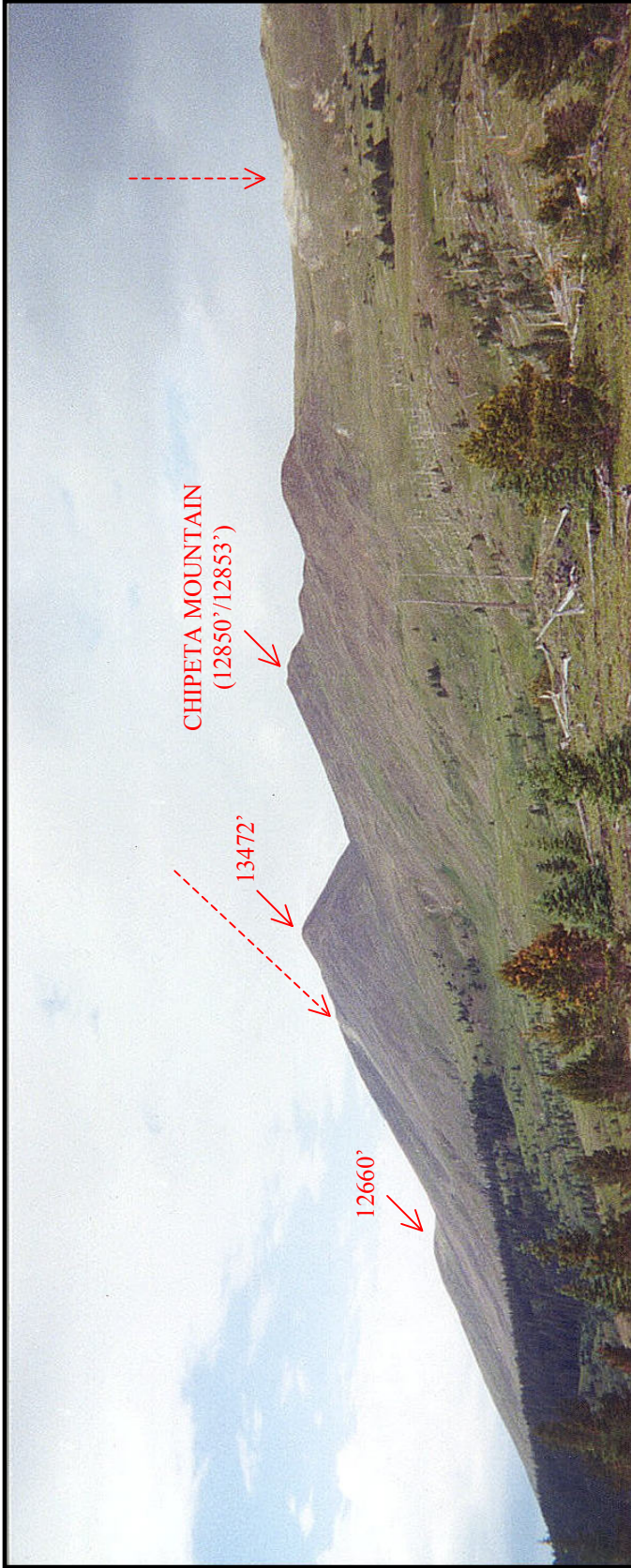


Figure 44a.. Looking northeast at both the 13,472' and 12,660' apices and igneous intrusion exposures (dashed arrows). Field of view = 2.75 miles [4440 m].

Specimen SR1299 is a representative specimen of the igneous intrusive rocks. It is a felsic, coarse-grained, pegmatitic, graphic intrusive that weathers to a light pink to light brown color and has a fresh surface color of light pink (Figure 44b).

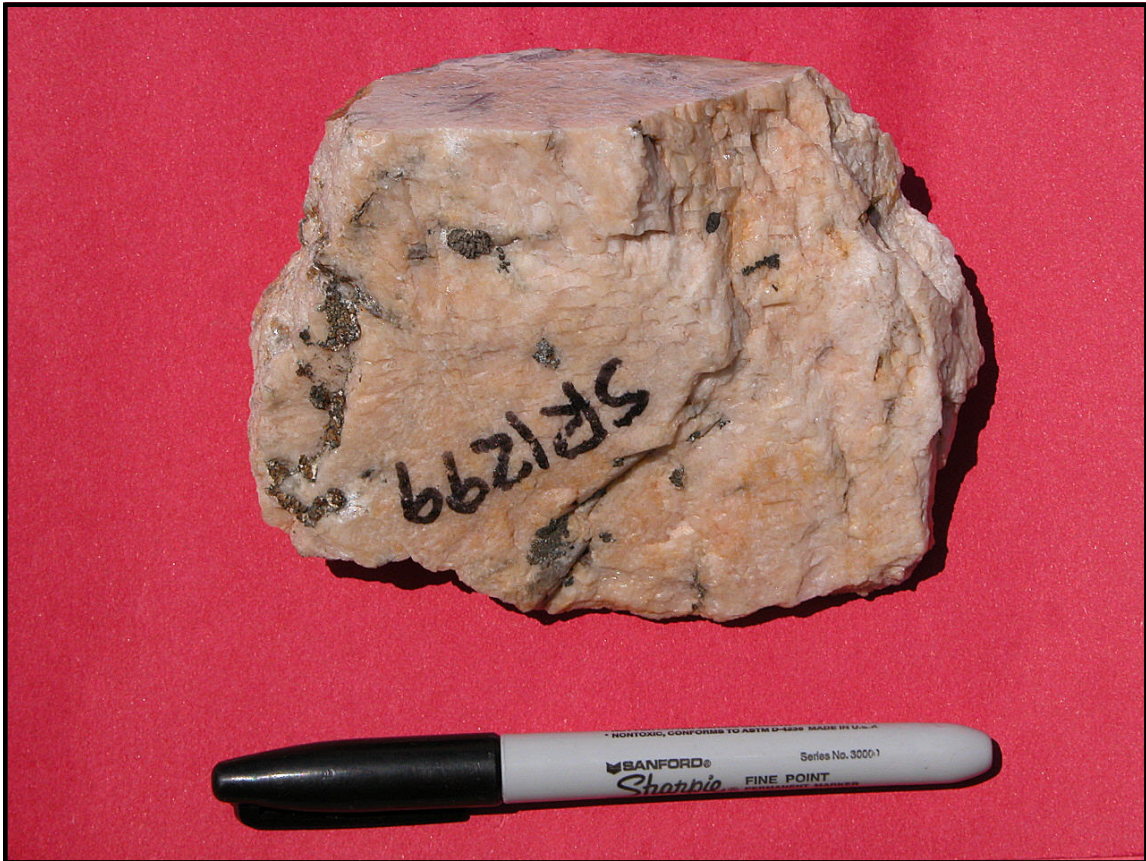


Figure 44b. A hand specimen of the graphic intrusive rock (6.i). Marker (13.5 cm) is shown for scale. (SR1299)

Large crystal grains of graphic quartz (~50%; ~5.0-10.0 mm average grain size; euhedral) are fused together as intergrowths within perthitic potassium feldspar. These large perthitic intergrowths within micrographic microcline (~15%; ~2.0-5.0 mm average grain size; euhedral) are the result of the potassium-rich host of exsolved sodium-rich phase [albite])(Figure 44c). Untwinned orthoclase (~15%; ~2.0-5.0 mm average grain size; euhedral) is also present, along with muscovite (~15%; ~1.0-2.0 mm average grain



Figure 44c. A photomicrograph of a thin section of an igneous intrusive rock (6.i), showing the graphic quartz intergrowths within perthitic microcline. Long axis of photomicrograph = 4 mm. (SR1299).

size) as parallel books (especially visible in the hand specimen) and plagioclase (~5%; ~0.4-0.8 mm average grain size). Micrographic quartz (<0.1mm average grain size) and apatite (< 1%) are also present within the matrix and comprise the remainder of the rock.

Specimen SR1799 is a felsic, coarse-grained, granitic intrusive that weathers brown and has a fresh surface color of white to pinkish white (Figure 44d). This light-colored leucocratic intrusive contains the distinct texture of radiating myrmekitic quartz (~32%; ~1.0-2.0 mm average grain size)(Figure 44e). Quartz is replacing microcline (~32%; ~0.8-1.0 mm average grain size) and plagioclase (~32%; ~0.8-1.0 mm average



Figure 44d. A hand specimen of a granitic intrusive rock (6.i). Marker (13.5 cm) is shown for scale. (SR1799)

grain size) in a plagioclase-rich matrix. Other constituents in the matrix are muscovite (~1%; ~1.0-2.0 mm average grain size), biotite (~1%; ~1.0-2.0 mm average grain size), hornblende (~1%; ~1.0-2.0 mm average grain size) and small reddish apatite (~1%; ~1.0-2.0 mm average grain size) grains.

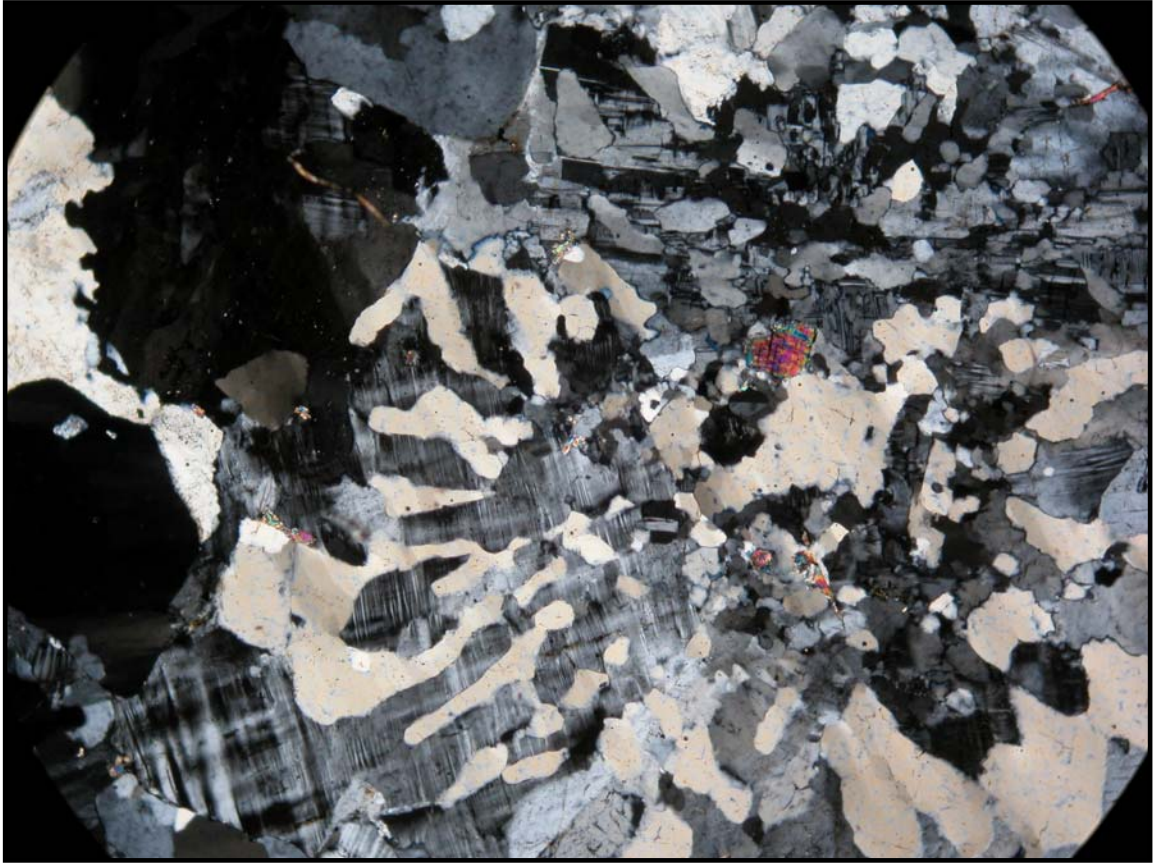


Figure 44e. A photomicrograph of a thin section of an igneous intrusive rock (6.i), showing radiating myrmekitic quartz. Long axis of photomicrograph = 4 mm. (SR1799).

WHITESCHIST

Specimen NR13a99 (3e.Xfh:Xqms) (AKA NR13*99) came from a sliver of the Xfh unit along the north face of the NR. This lithology was discovered only on the NR and no specimen was discovered on the SR. This “Quartz Mica schist” is a white, quartzofeldspathic, muscovite-rich, micaceous schistose rock that weathers to a gold-light brown-light pink and has a fresh surface color of white to pinkish-white (Figure 44f). It is both granolepidoblastic and relatively fine-grained in texture and appears to be a metamorphosed pegmatite. The quartz grains are of two general sizes, with both coarse

quartz grains (~15%; ~0.4-0.8 mm average grain size; hypidioblastic) and fine quartz grains (~15%; ~0.1-0.2 mm average grain size; hypidioblastic).



Figure 44f. A hand specimen of quartz mica schist “whiteschist” (3e.Xfh:Xqms). Marker (13.5 cm) is shown for scale. (NR13a99).

The coarse quartz grains are pitted out with muscovite flakes, both within and on the edges, and the smaller quartz grains exhibit grain migration boundaries within the matrix. Plagioclase (~30%; ~0.2-0.3 mm average grain size; hypidioblastic) is the next most abundant mineral. The matrix also contains the elongate tabular mineral of muscovite (~25%; ~0.1-0.2 mm average grain size; lepidoblastic) and microcline grains (~10%; ~0.1-0.2 mm average grain size; xenoblastic) both of which line the outer weathered edge of the specimen (Figure 44g). Sillimanite (~10%; ~0.2-0.3 mm average grain size) and

apatite (~1%; ~0.1 mm average grain size) finalize the contents of this white, layered, glittery, micaceous schistose rock.

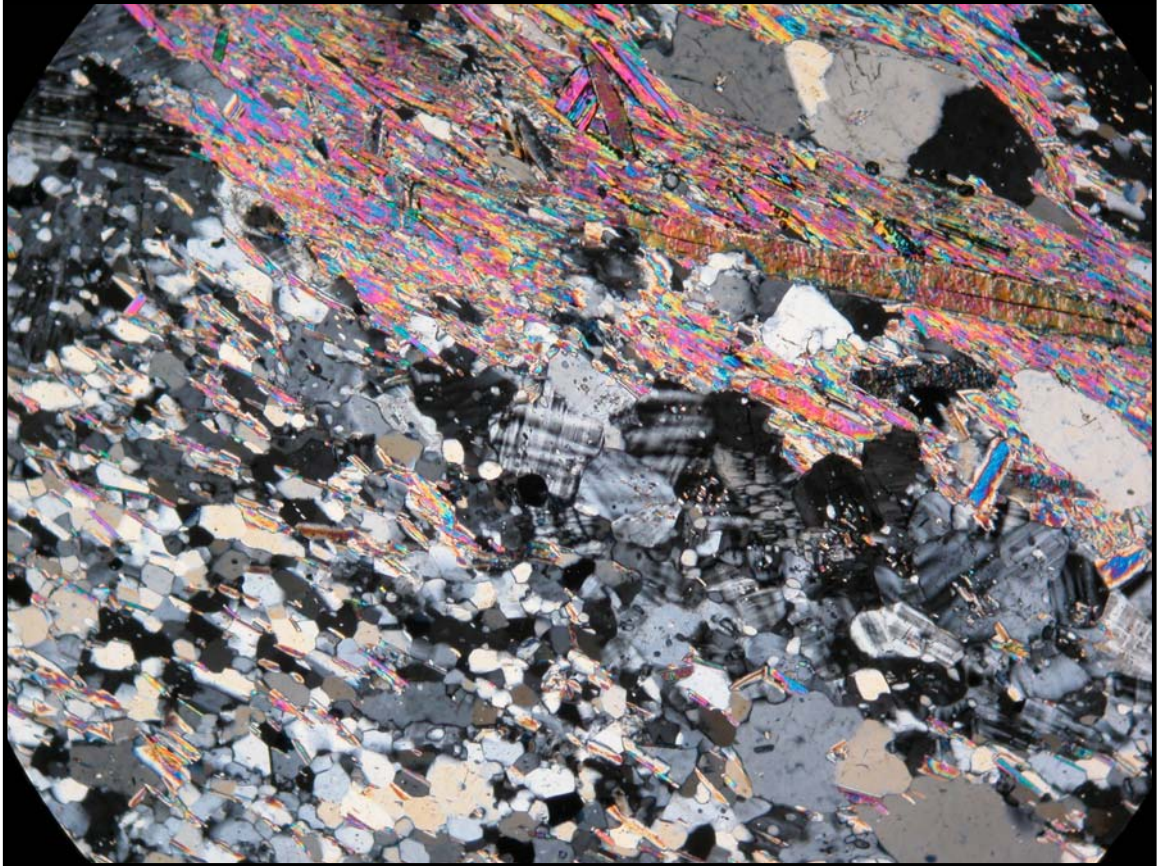


Figure 44g. A photomicrograph of a thin section of the quartz mica schist "whiteschist" (3e.Xfh:Xqms). Long axis of photomicrograph = 4 mm. (NR13a99)

DISCUSSION

This region of the southern Sawatch Mountains has been mapped by Tweto (1979) as being Precambrian crystalline basement (bedrock) of high-grade amphibolite facies, comprising the footwall of the boundary fault called the WCTF by Dippold (1999), the Poncha Pass Transfer Zone (PPTZ) of the upper Arkansas basin (uAb) of the Rio Grande rift (RGr) (Dippold, 1999). The unit is mapped as “Precambrian X Felsic and Hornblendic gneisses (Xfh)”, which, according to Tweto (1977, 1979, 1987a & 1987b), are “either separate or interlayered/interfingered – includes metabasalt, metatuff,

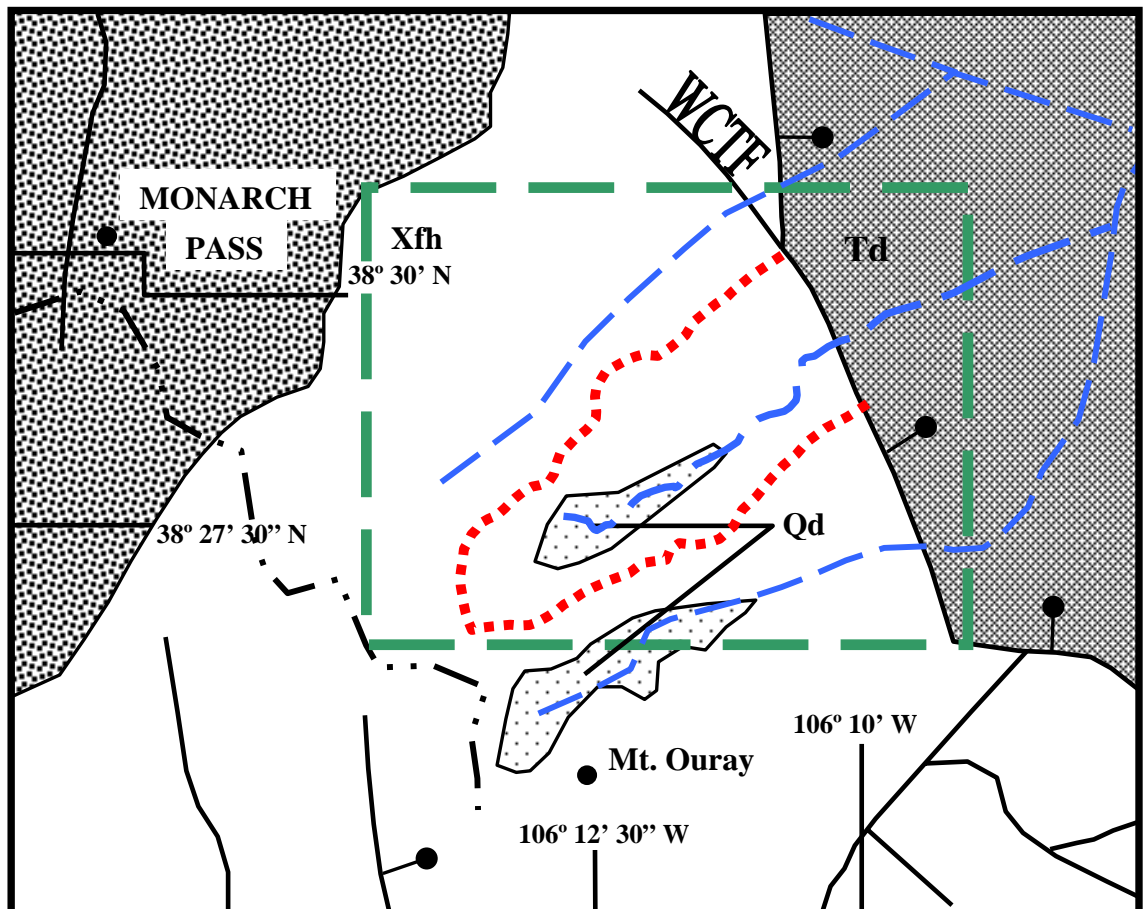


Figure 45. Simplified geologic map of South-Central Colorado showing Field Area (dashed rectangle), ridgeline traverse (dotted line) and three primary units of Xfh (Precambrian Felsic and Hornblendic Gneisses), Td (Tertiary deposits east of the WCTF) and Qd (Quaternary deposits within the Pass Creek and the Little Cochetopa Creek drainages). Also shown is the Monarch Pass (Proterozoic granite YXg) (modified from Tweto, 1979).

and interbedded metagreywacke” which are undifferentiated Xf and Xh of the Xfh (feldspathic hornblende gneisses) unit (Tweto, 1961; Boardman, 1971) (Figure 45).

The X was implemented to describe the Precambrian, which is of a set age limit of ~1.8-1.6 Ga (Tweto, 1977) and is used in place of PC that describes the whole era. The Xfh unit also locally contains interlayered biotite gneiss and is derived principally from volcanic rocks, none of which were located within the field area (Tweto, 1979).

Kouther (1969)(Figure 12b) and Dippold (1999)(Figure 12c) reported similar mineralogical assemblages and metamorphic traits for the two ridgelines of the field area as found in this study. Kouther’s and Dippold’s field areas were focused to the east of this study.

On the NR traverse, Kouther (1969) designated the easternmost lower unit as a muscovite quartz schist (PCqms), the middle unit as an amphibolite gneiss (PCag) and the upper unit a quartz-feldspar gneiss (PCfqg) (Figure 12b). On the SR traverse, Kouther designated the easternmost lower unit as an amphibolite gneiss, which transitioned into a muscovite quartz schist (at the proposed Pass Creek Shear Zone (PCSZ) porphyroblastic rocks outcropping location), then into the PCfqg near the unit I have designated as Xfs. The PCfqg unit is silicified in the PCSZ and epidotization is less compared to the PCag. The PCag contains 50-70% hornblende, as compared to the PCfqg(+silicification), which contains only 20% hornblende. The PCag was named an amphibolite gneiss because of its hornblende composition and gneissic fabric. This same naming convention was used in this study.

Dippold (1999) designated the NR easternmost limit as lower gneissic amphibolite (Xh; both gray compositionally banded and black) and upper

quartzofeldspathic gneiss (Xf) (Figure 12c). Dippold's quartzofeldspathic gneiss (Xf) is most likely equivalent to the quartzofeldspathic schist (Xfs) classified in this study, given the mica concentration relative to the quartz, the micaceous matrix and the overall schistosity. A quartzofeldspathic rock, found to be more gneissic than schistose, was located farther up the ridgeline beyond the limits of that study. As a result of the limitation of the study area, certain specimens were prematurely classified as quartzofeldspathic gneiss rather than a quartzofeldspathic schist, as evidenced by the considerable mica content within the specimens. Dippold (1999) identified the easternmost unit as a gneissic amphibolite and noted that this unit comprised the most common unit in the vicinity of the transfer fault (WCTF), which is similar to the amphibolite gneiss of this study. Dippold described the two amphibolites within the gneissic amphibolite unit as being compositionally-banded amphibolite and black amphibolite. I found this to be the case as well, with the compositionally-banded amphibolite gneiss farther up the ridgelines and to the west of the black amphibolites. The black amphibolites formed huge boulders at the base of the ridgeline, marked the eastern limit of the ridgeline traverse and were broken up by the fault. Some boulders moved rather far downslope to the east and existed atop the Tertiary unit. With these rocks being gneisses and of amphibolite composition, I chose the name amphibolite gneiss over gneissic amphibolite.

The lithology of the Precambrian Xfh unit is of a high-grade, highly-metamorphosed amphibolite-facies and is the result of regional dynathermal metamorphism. This Precambrian Xfh unit consists of felsic and hornblende gneisses that contain high concentrations of the amphibole hornblende. These felsic and

hornblende gneisses also contain the Al_2SiO_5 polymorph of sillimanite, which places them in the kyanite-sillimanite type facies series (Barrovian), the almandine-amphibolite facies and the sillimanite-almandine-orthoclase subfacies (Winter, 2001). The kyanite-sillimanite facies series varies over a range of intermediate temperatures (400 - 600° C) and a range of high pressures (3 to 6 kbar; 300 to 600 MPa) (Figure 46). Assuming a normal intermediate geothermal gradient (30° C /km) and taking into account these intermediate temperatures, the depth in the crust at the time of metamorphism could be estimated to be ~13-20 km. These amphibolite gneisses and quartzofeldspathic gneisses are deemed hydrous rocks and, with progressive metamorphism and increase in grade, dehydration is increasing (Williams et al., 1982).

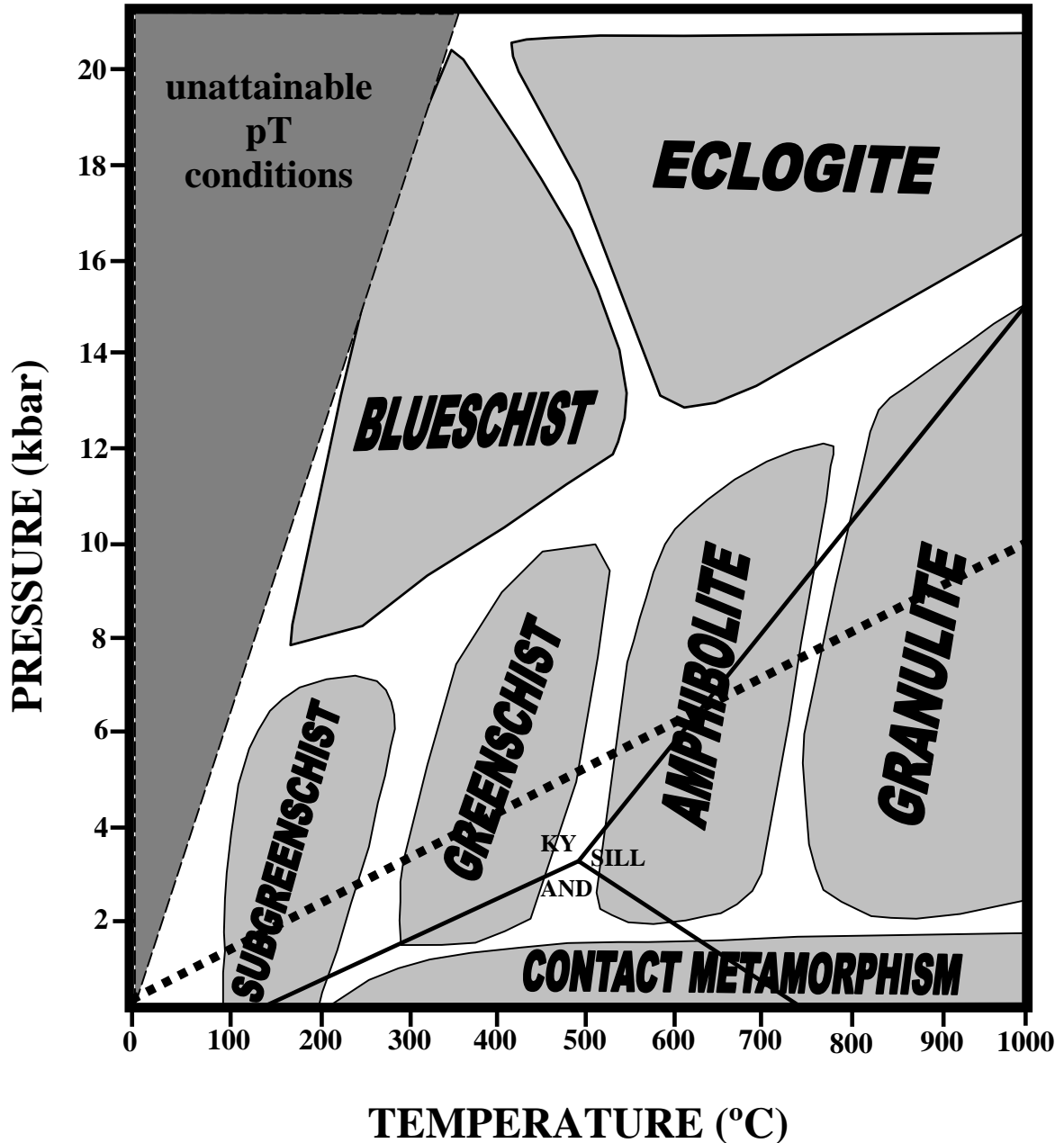


Figure 46. Pressure-Temperature Diagram of Metamorphic Facies showing the Al_2SiO_5 polymorphs of kyanite, sillimanite and andalusite. Sillimanite forms at high temperatures and high-low pressures, compared to kyanite at low temperatures and high pressures, and andalusite at high-low temperatures and low pressures. Given the ductile fabric having formed at temperatures greater than $400^\circ C$, the normal geothermal gradient ($\sim 30^\circ C/km$; high pressure & high temperature) shown with dotted line, regional metamorphism likely occurred at about $600^\circ C$ and 6 kbar. (modified from Bucher and Frey, 2002).

The occurrence of fibrolitic sillimanite (NR13*99, NR4*99 and SR3799), not the other two Al_2SiO_5 polymorphs of andalusite and kyanite, makes these rocks distinctive.

Sillimanite is the polymorph present in high temperatures and high to low pressure conditions, compared to kyanite, which is present at low temperatures and high pressures, and andalusite, which is present at high to low temperatures but low pressures (Figure 46). Sillimanite forms at the expense of biotite and its presence is thought to be due to long-sustained high temperatures and the possible influx of magmatic fluid activity (Williams et al., 1982).

These amphibolite gneissic rocks and quartzofeldspathic gneissic rocks could be either paragneiss (of sedimentary origin) or orthogneiss (of igneous origin) or perhaps, an intermixed sequence of both (Passchier et al., 1990; Myers, 1978; Kröner et al., 1994). The tectonic rock cycle setting of this interlayered unit is thought to be an island arc setting where sediments were accreted, then deformed slightly perpendicular to inherent weaknesses of these ancient sediments.

Similar to an amphibolite being rich in plagioclase and hornblende, amphibolite gneissic rocks are identical, simply containing some quartz to give it some compositional layering and gneissose structure. The protolith of these amphibolite specimens varies between the differentiated units. In the areas where the amphibolites are dark, black, coarser grained, poorer in micas and less schistose, the protolith was likely to have been an arenaceous sedimentary rock, a siliceous volcanic rock, a metagabbro and/or a metabasalt. In the areas where the gray (black and white) compositionally-banded amphibolite exists and grades into a gneissic texture, the protolith is more likely to be an acidic plutonic rock such as a metagranodiorite, metadiabase or metadiorite (Ehlers and Blatt, 1982).

The amphibolite is commonly of a mafic/basic igneous origin, thought to be derived from oceanic crust, with the parent rock (protolith) most likely being a gabbro or basalt (tholeiitic), granodiorite, diabase or diorite. The abundance of untwinned hornblende, the presence of a simple form with ragged terminations, and the presence of a sieve structure, allow an amphibolite to be distinguished from a diorite (Williams et al., 1982). Hornblende tends to be less abundant in extrusive igneous rocks compared to intrusive igneous rocks, so the protolith is more likely a metagabbro compared to a metabasalt. Van Alstine (1971) found that an amphibolite close to the area contained a chemical signature value similar to that of a metagabbro sill and proposes that it is of an igneous origin, an orthoamphibolite and not of sedimentary-origin. Sidman (1998) located a unit he called “zebra rock” that is similar to the striped appearance of Xfh and the sampling site noted by Van Alstine (1971).

The protolith of the quartzofeldspathic gneiss (2.Xqfg) could possibly be a metagranite, metarhyolite, metaquartzmonzonite or metaarkosic sandstone. These protoliths are all feldspar-rich, high in aluminum and silicon content and derived mainly from arenaceous sediments, siliceous volcanic rocks or predominantly acidic plutonic rocks (Williams et al., 1982). This Xqfg appears to be similar to what Sidman (1998) identified as a granite gneiss. Granite gneisses are common in Archean terranes where plutonic bodies of the ancient crust have been repeatedly metamorphosed, however, this rock contains a dynamically imprinted gneissic fabric and its plutonic origin is still uncertain (Williams et al., 1982).

The calc-silicate gneiss (NR699 and SR299) is thought to be an aluminous metamorphosed, calcite-cemented sandstone, such as a metagreywacke,

metadirtysandstone, metadirtyquartzite or metaquartzarenite. Boardman (1971) suggested the protolith as being a metagreywacke sandstone or a dirty quartzite. Dippold (1999) located a calc-silicate gneiss in her field area farther north up by Willow Creek within the unit designated a quartz-biotite schist. A similar lithology called a "lime-silicate" (Boardman, 1971; Boyer, 1962), roughly identical to these exposures, was found in the adjacent areas of Salida (Boardman, 1971) and the Wet Mountains to the southeast of the field area (Boyer, 1962).

The porphyroblastic rocks are not necessarily blastoporphyratic, because that would imply they were definitely of an igneous porphyritic protolith, which has yet to be determined. Furthermore, it can be concluded that they are not porphyroclastic because these minerals were created during retrograde metamorphism by recrystallization, not by breaking and fragmentation. The porphyroblasts are not large idioblastic crystals but rather mineral aggregates with a Rapakivi-ish zonation of core-mantle rim structure (Passchier and Trouw, 1996) as the coarse grains within the finer matrix (Winter, 2001). The feather amphibolite (garbenschiefer) is even a porphyroblastic amphibolite gneiss with stellate and shieflike hornblende crystals oriented along the plane of foliation.

The dominant porphyroblastic/pod rock exposures outcrop near and are most pronounced in an area suggested and thought to contain a shear zone, Pass Creek Shear Zone. Kouter (1969) mapped a northwest-trending shear zone (Pass Creek Shear Zone) of brecciation and mylonitization in the eastern region of the north ridgeline near Cinderella South Mine. This happens to coincide with the lithological change from 1.Xag to 2.Xqfg and of an adjacent unit of distinct rocks containing porphyroblasts within the foliation. Kouter (1969) based this shear zone on the presence of cataclastic

rocks with elongated quartz embedded in silicic cementing material (silicification). I found this proposed zone to overlay the locations of the pod exposures adjacent to the prominent lithologic change. The proposed shear zone, if present, affected more than one lithology (e.g. 1b.Xag:Xf and 1c.Xag:Xfs) so it doesn't comply with a contact.

The quartzofeldspathic schist porphyroblastic rock (Pfs) appears to be the same lithology that Boardman (1971) identified. He proposed that sillimanite replaced muscovite from the outside in. Dippold (1999) proposed that they were the result of pressure solution and shear. Boardman (1971) found that there were pods similar in appearance located to the east of Salida, which is NE of the field area. He hypothesized that they were actually relict bedding of the sedimentary rock protolith. The leading hypotheses as to formation of the porphyroblastic rocks are: a gradational/transitory unit, pressure solutions (Dippold, 1999; Koutner, 1969), relict primary sedimentary (bedding) and igneous textures (Boardman, 1971), an orbicular granite protolith, and an inherent Rapakivi texture (Van Schmus, 2003). Given the lack of kinematic indicators (rotated grains) throughout the traverse of the ridgelines up into the western high elevations, it seems unlikely that the porphyroblasts are the product of shear, but rather the result of grading into lithologies that had preexistent features (e.g. quartz veins, phenocrysts) that, through deformation, had been stretched, isolated, contorted and eventually pinched off, segmenting into porphyroblasts. The thermal effects are facilitated through pressurized hydrothermal fluids and are incurred at shallow depths. Given the variation in size of these porphyroblasts, becoming rather large to the west (Figure 42a), along with the variation in the lithologies, it appears to be a subtle thermal effect. The Mt. Princeton batholith has hydrothermally-altered kaolinite "Chalk Cliffs", so the presence of

hydrothermal fluids in the area have affected adjacent rocks, making this a likely cause of the porphyroblasticity.

The hornblende blobs (3d.Xfh:Xhb) appear to be a porphyritic igneous protolith with stretched out phenocrysts and the quartz blobs appear to be stretched out relict sedimentary structures in a conglomerate or sandstone.

Other than near the proposed shear zone, the “porphyroblasticity” was found to increase along the ridgelines near suspected faults, such as with SR2399 and SR2299 near the Hump Jut Fault (HJF), and SR3099, SR2999 and SR2899 near the Pass Creek Fault (PCF).

Colin Shaw (personal communication, 2003) located another exposure of highly-aluminous pod rocks farther north within the northern Sawatch Range and specifically within the Gore Range. He said that, despite the inconclusive evidence denoting their genesis, the hypotheses mentioned are the accepted and proposed ideas.

Other porphyroblastic pod rocks that have been located include: “Siliceous pod rocks” in the Park Range (Snyder et al., 1988), leucosomes with similar textures (Nabelek, 1997), and sillimanite pod-rock the Farwell Mountain-Lester Mountain Suture/Shear Zone (Tyson et al., 2002; Tyson et al., 2001).

The igneous intrusions contained many unique textures and features, such as the radiating myrmekitic quartz, graphic granite and perthitic intergrowths in microcline (MacKenzie et al., 1982), making them quite contrasting, despite their concordance and proximity. Kouter (1969) discovered intrusive diorite, pegmatite (discordant with amphibolite gneiss), graphic granite and a light gray to green granodiorite, as igneous lithologies. He believed the graphic granite to be Precambrian-aged due to fault

dissection. Boardman (1971) identified intermediate and mafic dikes, pegmatites, aplite and quartz monzonite, trending sub-parallel with foliation and crosscutting in dip. Van Alstine (1969) identified aplites, pegmatites, lamprophyres, dacite porphyry and diabase intrusions near the field area, and of these only pegmatites were found in the field area. The age of the individual intrusions in the field area is still uncertain.

The lens of quartz mica schist discovered in the westernmost unit, appears to be an exotic sparse exposure, different from the quartz muscovite schist (PCqms) mapped by Kouter (1969) in the eastern segment of the ridgelines. Despite being nicknamed a “whiteschist” it is not a true whiteschist (which is composed of talc (Winter, 2001)). It was only called such based on the color and texture, and the nomenclature of a previous author (Sidman, 1998).

STRUCTURE

The goal of the structural analysis was to determine the orientations of structural features in the Precambrian basement rocks in an effort to assess the role that basement structures had in influencing Laramide and rift-related structures.

METHODS

Prior to fieldwork, aerial photography, satellite imagery and digital elevation models were used to identify large-scale structural features in the study area. Fieldwork was carried out by mapping and sample collecting along two major ridgelines. A combination of GPS (Global Positioning System) readings and topographic maps were used to specify field locations. The strike and dip of metamorphic foliation, fractures, faults and shear zones, and the bearing and plunge of the fabric lineation (elongations of mineral grains and stretching penetrative mineral lineations) were measured throughout the field area. The foliation, lineation and fracture orientation data were entered into StereoWin (Stereonet for Windows) v. 1.2.0., created by Dr. Richard W. Allmendinger, and the resultant graphically displayed, lower-hemisphere equal area plots were compared across and along ridgelines by both lithologic unit and location by noting the elevation along the traverse. The foliation data was displayed as poles-to-planes by both ridgeline and lithologic unit (see Appendix F for individual stereonet) and when plotted in lower hemisphere projections, the slight variations in crystalline basement orientations were noted along with changes in dip magnitude.

Throughout the traverse of the ridgelines, roughly 200 single orientation measurements were taken by the Brunton compass (Appendix E; Appendix F & Appendix G: Plate II). The results are presented according to lithology and location

along the ridgeline of the traverse in the field. The average measurements of the Precambrian bedrock metamorphic foliation are compared along the ridgelines among the prominent lithologic units and across the ridgelines. This comparison allowed a pinpointing of variations in values within the study area on a relatively small scale.

The strike and dip of metamorphic foliations, the plunge and bearing of both stretching lineations and slickenlines data, and the strike and dip of fractures were averaged, both mathematically and graphically, by stereonet (by both lithologic unit and ridgeline). In the amphibolite gneiss, foliation fabric is defined by the compositional gneissic layering of hornblende and quartz with parallel veins. In the quartzofeldspathic gneiss, platy minerals define the planar texture. In the felsic and hornblende gneisses the gneissose structure is defined by banding and porphyroblast alignment.

Lineations were found in the form of ductile (stretching) penetrative mineral lineations (spml's), which occur with stretching and elongating minerals through elevated thermal conditions and/or mineral regrowth, a ductile fold axis found at the mid-ridge elevations and brittle slickenlines ("slicks"). The fracture patterns varied throughout the lithologies, with most forming rectilinear orthogonal blocks with sets of fractures as joints. The mathematically averaged data is displayed in Tables 2 and 3 (individual detailed data is displayed in Appendix E). Individual orientation data for foliations, lineations and joints/fractures were entered into the software and the results are graphically averaged and displayed in Figures 56, 57 and 58 (see Appendix F for individual stereonet).

Oriented samples were collected throughout the field area. In order to be analyzed for sense of shear, five of these oriented samples were cut parallel to stretching lineations and perpendicular to the foliations of the metamorphic fabric.

Kinematic indicators, such as asymmetrical fabrics (shear bands, asymmetric grain-tail complexes and asymmetric grains) and the stretching of grains in potential shear zones, were sought in the thin sections. Ductile indicators were minimal and porphyroblasts of mineral aggregates, not idioblastic crystals, showed no rotation, asymmetrical grains or grain tails. Brittle indicators, in the form of tension fractures, gashes and vein fillings, were abundant (Passchier and Trouw, 1996; Simpson and Schmid, 1983).

Exposure is moderate and excessive physical weathering and erosion has often left outcrops highly fractured and/or slightly displaced, making structural measurements a challenge throughout the field area (Figures 47, 48 & 49). Even beneath the tree line, it was extremely difficult to denote exposures and the presence of the WCTF due to the scree marring the surface and the overgrowth of aspens, ponderosa pines and other dense vegetation.

Metamorphic foliations were measured in the field and then compared with both lithologic unit and ridgeline. The ridgelines were compared to each other (between the eastern low elevations and the western high elevations) and the three (3) broad lithologic units within: 1. Xag, 2. Xqfg, & 3. Xfh. The Precambrian bedrock measurements were both mathematically and graphically averaged (Appendix F; Figures 50, 51 56, 57 & 58; Tables 2 & 3). When compared between the ridgelines, the Interridge Saddle (IS) was both averaged with the NR and omitted from the comparison (see Tables 2 & 3).



Figure 47. South Ridgeline profile, showing humps potentially derived by faulting. Field of view = 360 ft (110 m).



Figure 48. Looking west from location 60 back up the SR, showing how an exposure of amphibolite [outlined by rectangle] appears in relation to the jumbled, loose blocks of float, which overlies and masks the surface. Field of view = 5 ft.(1.5 m).

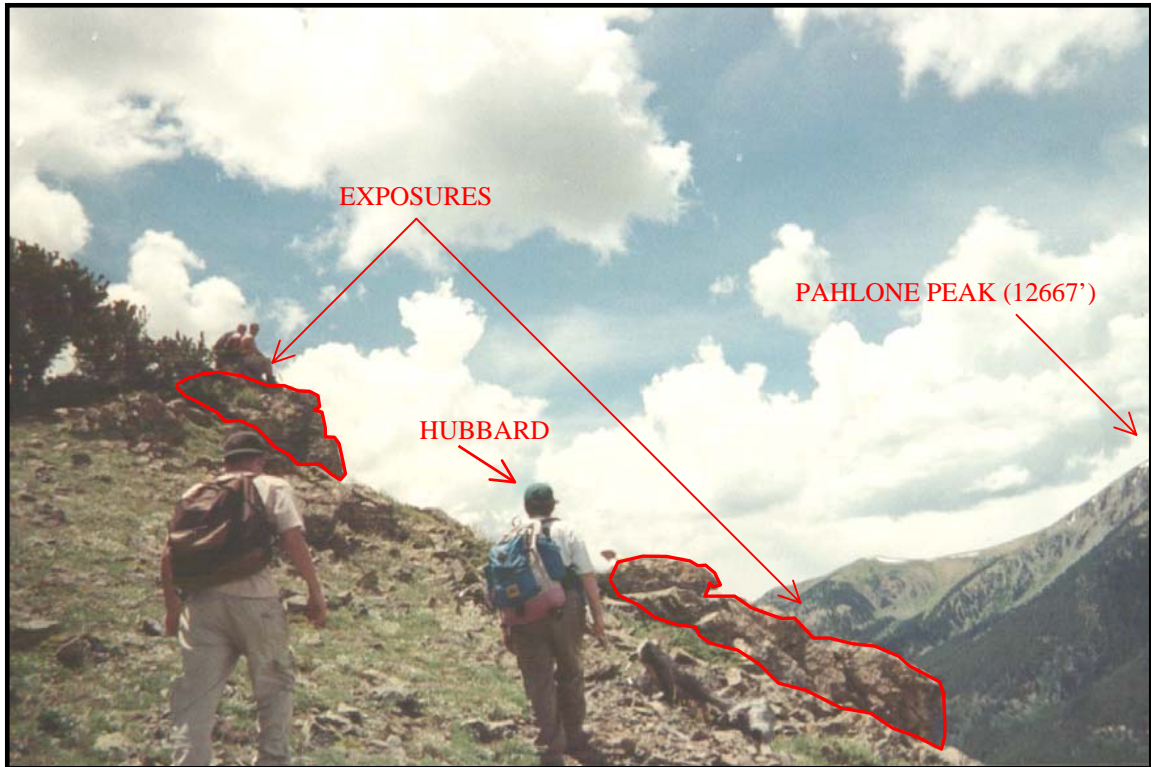


Figure 49. Looking west-northwest at an exposure/outcrop, showing an exposure jutting out to the northeast on the NR with Pahlone Peak (12,667') visible in the background. Dr. Hubbard is shown for scale.

RESULTS

STRUCTURAL FEATURES BY RIDGELINE & LITHOLOGIC UNIT

My structural analysis consisted of characterizing structural features in the Precambrian igneous and metamorphic rocks, in order to evaluate the role that basement structures had in the development of Laramide or rift structures. Mapping the locations of structures by lithologic unit and ridgeline, measuring the strike and dip of both the metamorphic foliations and fractures of the Precambrian bedrock and measuring the plunge and bearing of both stretching penetrative mineral lineations (spml's) and slickenlines, was completed in the field.

When viewed from the side and from afar, the ridgelines conform in shape, with major drop-offs traceable across ridgelines that could be fault-derived (Figures 19, 20 & 47). It is unclear as to whether or not the present-day surficial expression of the anticlinal/antiformal striped appearance of these talus/scree slopes is a pattern due to the influence of underlying ancient inherent controls (Precambrian folding, Ancestral Rockies FrontRange uplift anticline or being on the west flank of the Laramide Sawatch Anticline), which created inherent weaknesses within the basement after being reactivated during the Rio Grande rifting episode. Other causes could be obscured structures and hidden faults or just simply the manner in which these Precambrian folded igneous and metamorphic rocks weather and erode. Locally, there are concordant igneous intrusions parallel to and along the prominent planes of foliation of the metamorphic fabric, within the exposures. The intrusions have an affect on how the rock weathers (either into a massive, blocky, rectilinear, orthogonal, fractured appearance, or into a thin and platy appearance) within the jumbled talus/scree slopes (Figures 19, 32 & 33).

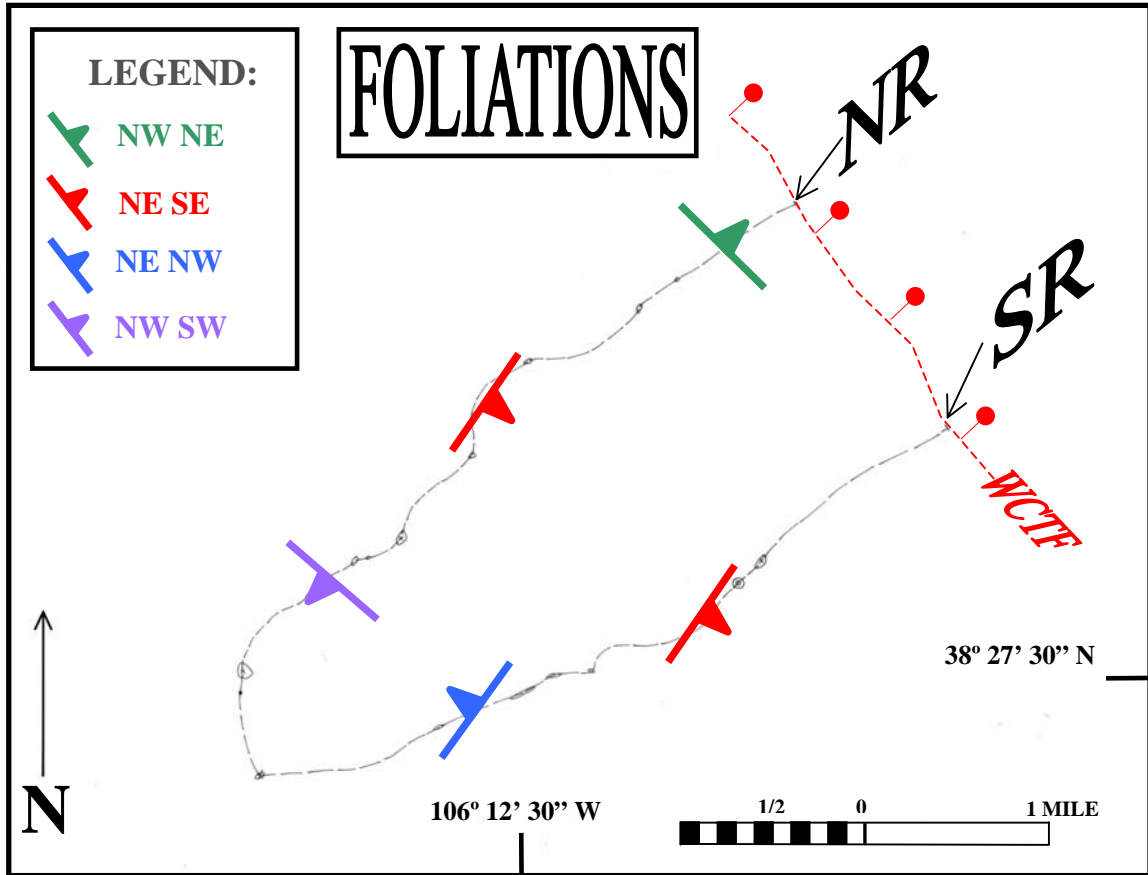


Figure 50. Map of the ridgelines, showing the locations of the dominant metamorphic foliation measurements.

METAMORPHIC FOLIATIONS AND ORIENTATION OF BASEMENT FABRIC

The overall averaging of metamorphic foliations (shear fabrics) revealed that both the NR and SR, at eastern low elevations in the Amphibolite Gneiss (1.Xag) unit, had a dominant northwest strike & northeast dip (Figure 50). When traversing upridge from the eastern unit, the strikes are predominantly northwest but then become random. In the western high elevations, in the Felsic Hornblendic Gneiss (3.Xfh) unit, the NR and SR still had a predominant northwest strike and northeast dip, but had much more dispersion (Figure 51). The SR tends to have a northeast strike at the western end of the traverse (northeast strike and northwest dip to the west and northeast strike and southeast dip

down-ridge to the east), yet a northwest strike at the eastern end of the traverse (Figure 50).

When foliations are compared by both unit and ridgeline (Table 2) with the due north-south and east-west measurements categorized relative to adjacent values and lithologic unit, the values were found to be predominantly NW-striking and NE-dipping (56%), NE-striking and SE-dipping (16%), NW-striking and SW-dipping (14%) and NE-striking and NW-dipping (14%). The NW-striking and NE-dipping (56%) values were primarily on the NR (75%) in the eastern unit at low elevations; the NE-striking and SE-dipping (16%) values were equal amongst NR (54%) and SR (46%), both in the central unit at mid-ridge elevations; the NW-striking and SW-dipping (14%) values were predominantly on the NR (64%) at the western high elevations in the hornblende amphibolite gneiss unit (3a.Xfh:XA); and the NE-striking and NW-dipping (14%) values were predominantly on the SR (91%) at the western high elevations in the felsic quartzofeldspathic gneiss unit (3b.Xfh:Xqf) (Figure 50). Overall, the average strike and dip of metamorphic foliation is N35°W 47°NE (56%) with dispersion in other values up ridgeline of N44°E 55°SE (16%), N38°W 58°SW (14%) and N50°E 58°NW (14%)(Tables 2 & 3).

With northwest being the average strike, the forces that created these attitudes were from the northeast and southwest, whether they were compressional or extensional. The northwest-striking, steeply-dipping metamorphic foliations in the Precambrian gneisses and schists defines the structural grain in these basement exposures and has been slightly overprinted in certain locations due to localized events.

FOLIATIONS

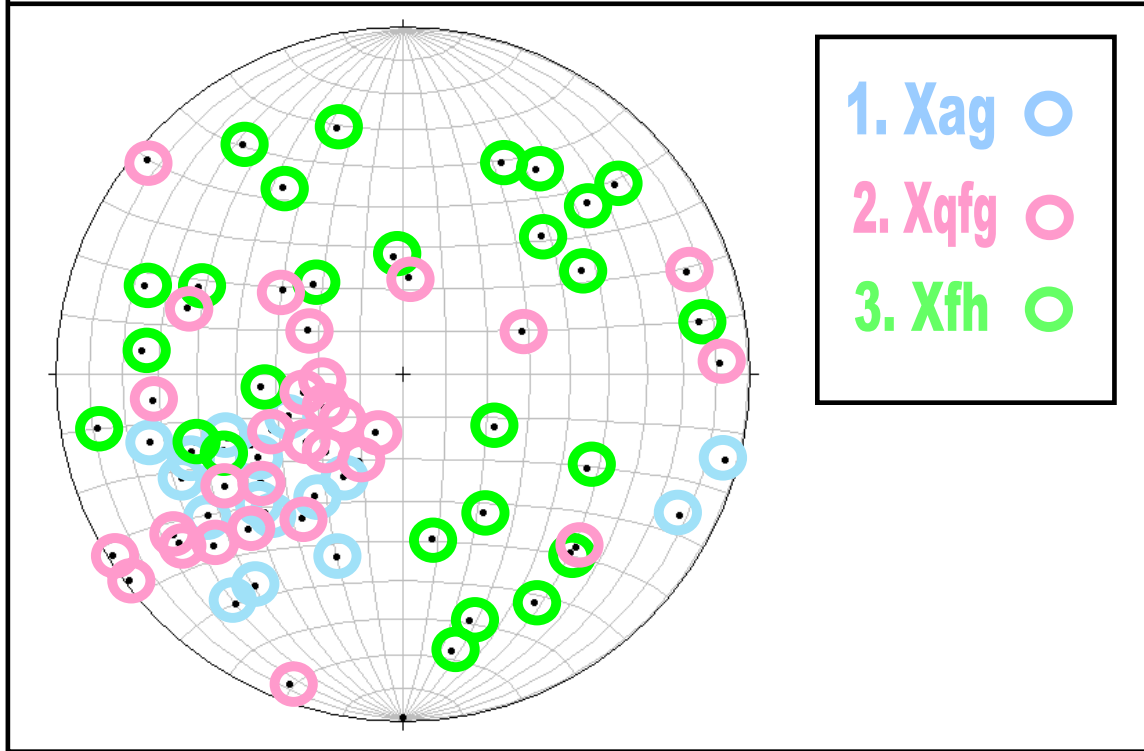


Figure 51. A stereonet of pole-to-planes for foliations, showing the three broad mappable units. The dispersion in values upridge is thought to be due to greater frost action, measurement of loose blocks of talus/scree or the measurement of unrecognizable limbs of folds (See Figures 56a, 56b, 56e & 56h).

When graphically averaged by stereonets and mathematically averaged by calculations, the foliations of the porphyroblastic rocks were averaged with the subunit within which they occurred (the parent rock). The exotic lithologies were omitted from the graphical averaging and considered individually, but were mathematically-averaged in Tables 2 & 3 and shown in brackets.

LINEATIONS

Lineations were found in the form of ductile stretching, penetrative mineral lineations (spml's) and/or growth of elongate minerals and brittle slickenlines. Nineteen values were measured in the field, with eleven brittle slickenlines and eight ductile

stretching penetrative mineral lineations (spml's) and/or elongate growth of minerals (Figures 52 & 57; Appendix E & Appendix F). Penetrative mineral lineations, formed from elevated temperatures and pressures by deformation and/or recrystallization, can resemble slickenlines (Davis and Reynolds, 1996), making the ductile and brittle lineations overall hard to discern, but in these crystalline rocks the slickenlines were distinctive.

The average bearing and plunge of lineations for slickenlines and stretching penetrative mineral lineations (spml's) is 36° N 27° E (63%), with other values of 34° N 14° W (26%) and 33° S 14° E (11%) (Tables 2 & 3). Most lineations were brittle slicks (58%) with average values of 42° N 34° E (45%) and 34° N 14° W (45%), the others being ductile spml's (37%) with an average value of 31° N 22° E and the fold (5%).

The average bearing and plunge of brittle lineations ("slicks") were found to be N 34° E bearing and 42 degrees plunge to N 14° W bearing and 34 degrees plunge. An example of a prominent lineation found and measured in the field was found in the calc-silicate gneiss (NR699) at location 14, which contained slicks that plunge 42 degrees and bear more westerly towards \sim N 07° W, relative to the average foliation trend.

The average bearing and plunge of ductile stretching penetrative mineral lineations (spml's) were found to be N 22° E bearing and 31 degrees plunge. An example of a prominent stretching lineation found and measured in the field was in the porphyroblasts of the quartzofeldspathic schist at location 11a. The stretched grains plunge 40 degrees toward \sim N 11° E, relative to the average foliation trend. The fold was found to be of a S 20° E bearing and 11 degrees plunge and will be discussed later.

The brittle down-dip lineations are largely oriented in the northeast quadrant and are attributed to the rifting event of the Rio Grande rift, even though there were a few low-angle brittle features not oriented down-dip (Figure 52), indicating a potential strike-

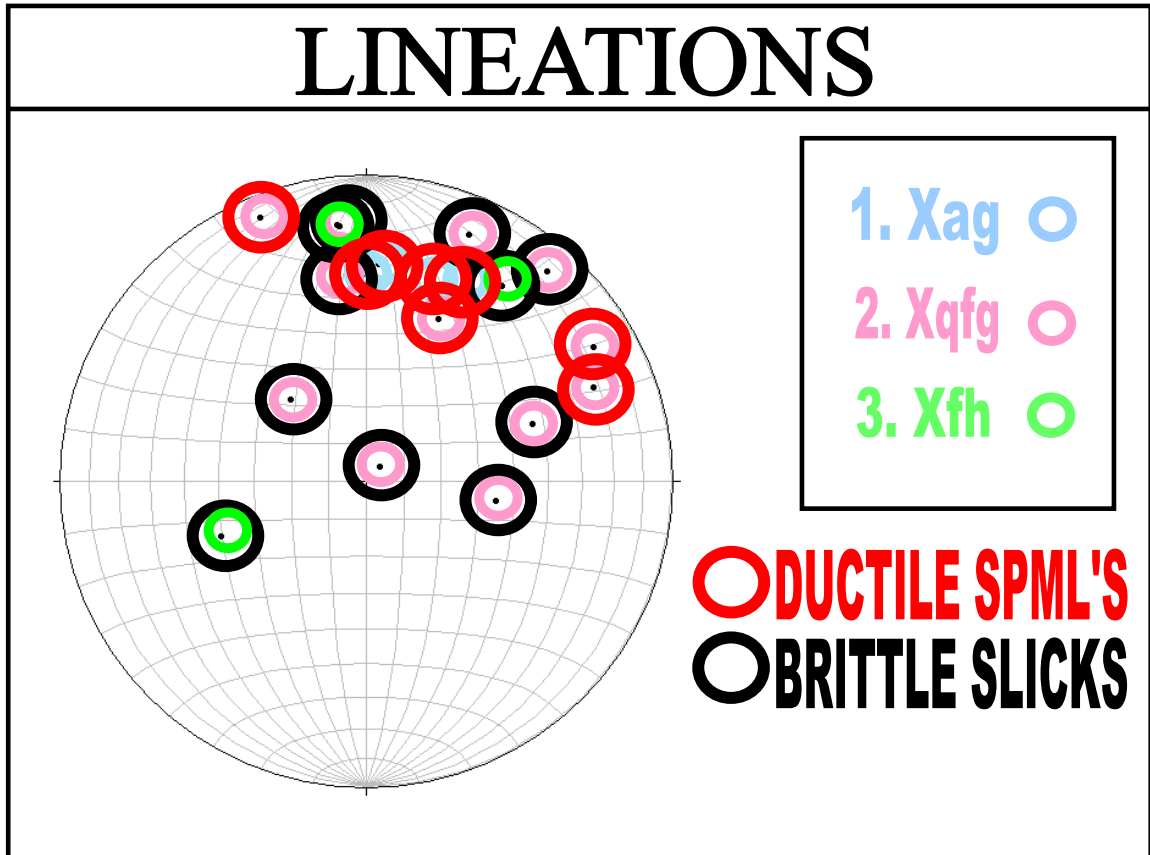


Figure 52. A stereoplot of pole-to-planes for lineations showing the three broad mappable units and the differentiation between the brittle slickenlines and ductile stretching penetrative mineral lineations (spml's). (See Figures 57a, 57b, 57c and 57d for individual stereonets).

slip displacement along these planes (mentioned in fractures). The ductile lineations are somewhat conclusive in the northeast quadrant and most likely represent early deformational features, possibly coeval with metamorphism. Although it is difficult to determine how the ductile lineations relate to other deformational events, they are not likely related to Rio Grande rifting or the Laramide orogeny (Figure 52). The ductile spml's are parallel to the direction of shearing (Davis and Reynolds, 1996) and in this scenario, southeast-northwest shearing occurred.

FRACTURES

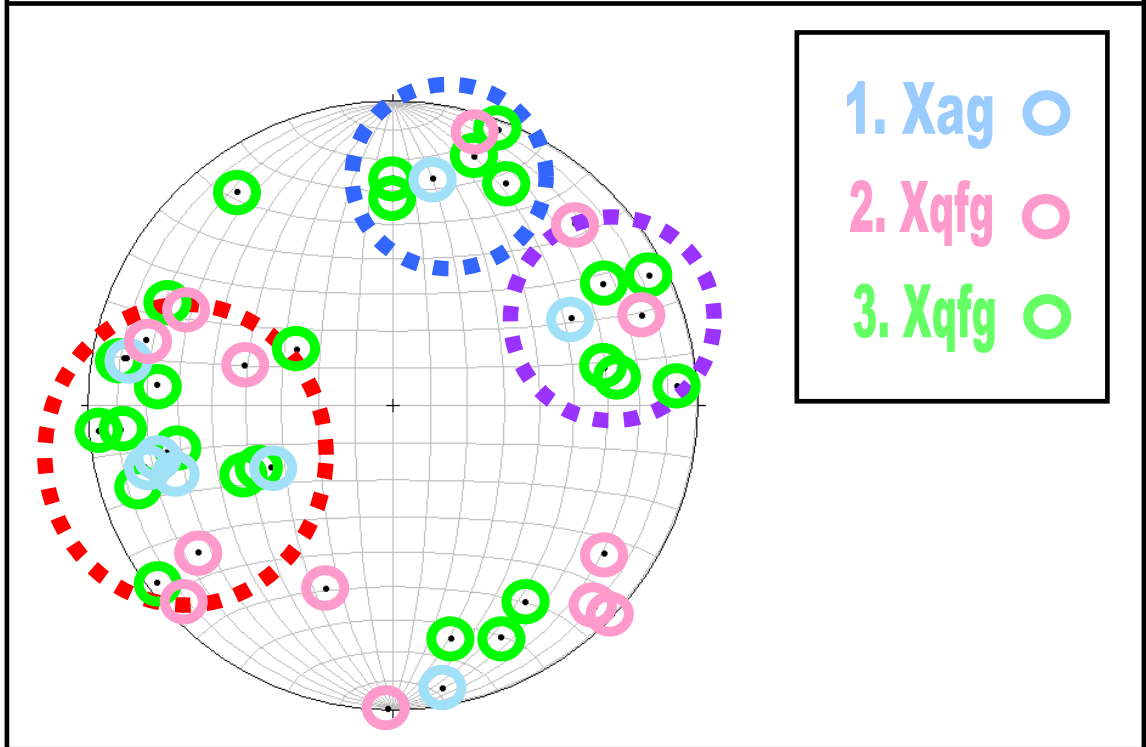


Figure 53a. Fractures of the all three units of the field area (See Figures 58a, 58b, 58c & 58d for individual stereonets).

FRACTURES

Fracture analysis was performed to deduce the influence of the metamorphic foliation on the breakage pattern in the Precambrian exposures. The brittle fracture pattern throughout the area created a system of brittle structures and brittle fault planes (bfp's), resulting in planar faces, which displayed minimal to no movement. The resultant weathering pattern was commonly massive, cubic, rectilinear, orthogonal blocks (Figure 42a).

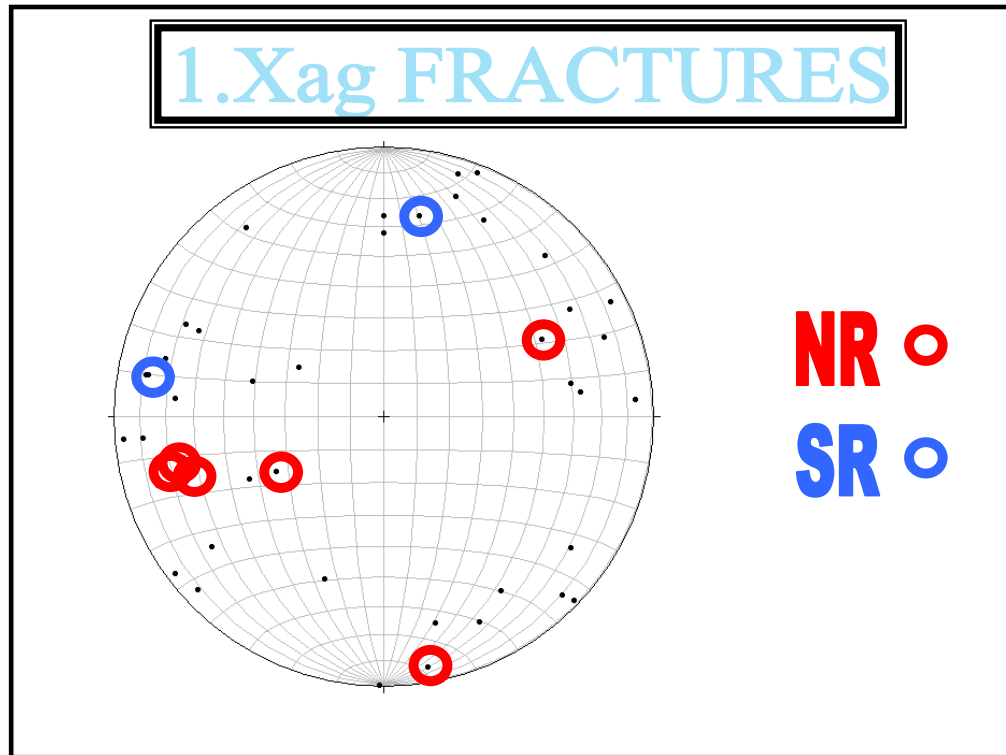


Figure 53b. Fractures of the Amphibolite Gneiss (1.Xag) unit at lower elevations at the eastern limit (See Figures 58b, 58e & 58h and Appendices f29-33 for individual stereonets).

The dominant fracture plane was the same as the foliation plane and formed a conjugate set of planes of breakage, with average northwest and northeast strikes (Figure 53a { shown in red and purple circles }). An additional plane of breakage, oriented ~north-south, was also found throughout the area (Figure 53a { shown in blue circle }). The average strike and dip of the fractures, brittle fracture planes (bfp's) or joints is N29°W 68°NE (33%), N40°W 73°SW (28%), N28°E 64°SE (22%) and N61°E 75°NW.

The fracturing was more common throughout the western higher elevations and along the south ridgeline (Figure 53d), compared to the lower elevations and the north ridgeline, respectively (Figures 53b & 53c). In the western higher elevations, there also appeared to be some underlying influence in the fracture pattern that was not specific to

the lithology and indeterminate in controls. This shuffling and jostling of crustal blocks is most likely due to a loss of cohesion as a result of frost action and/or the rifting of the Rio Grande rift. Intragranular fractures oriented parallel to the gneissic foliation defined by platy mineral grains can influence the brittle deformation of the fabric (Evans, 1998) as were found in these amphibolite gneiss and quartzofeldspathic gneiss rocks.

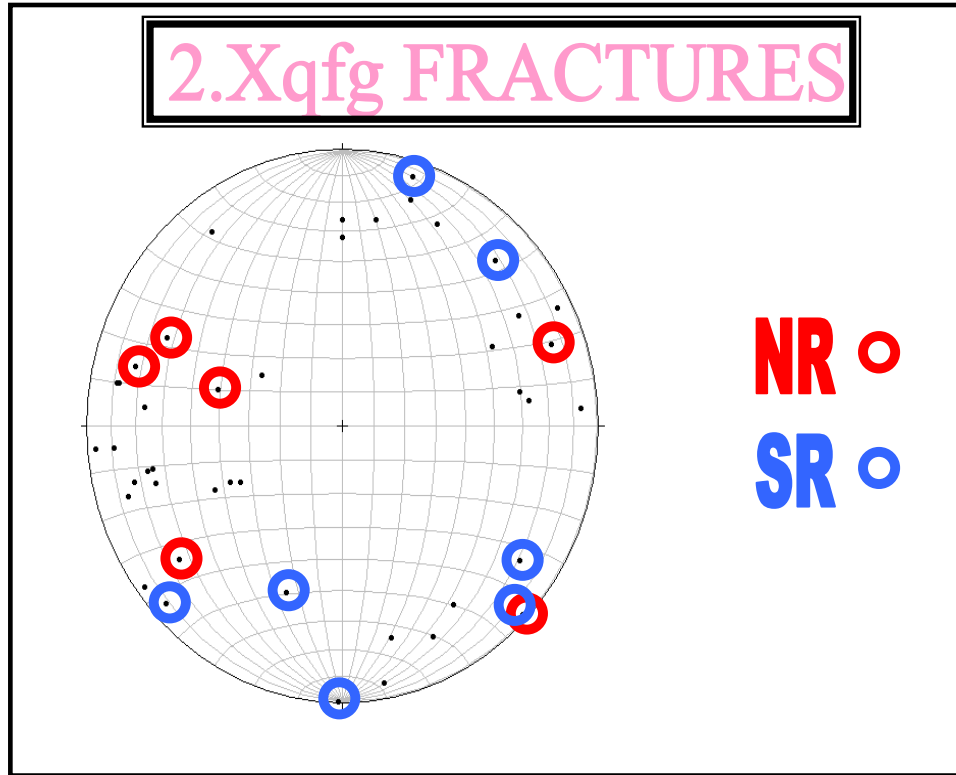


Figure 53c. Fractures of the central unit at mid-ridge elevations (Figures 58c,58f &58i).

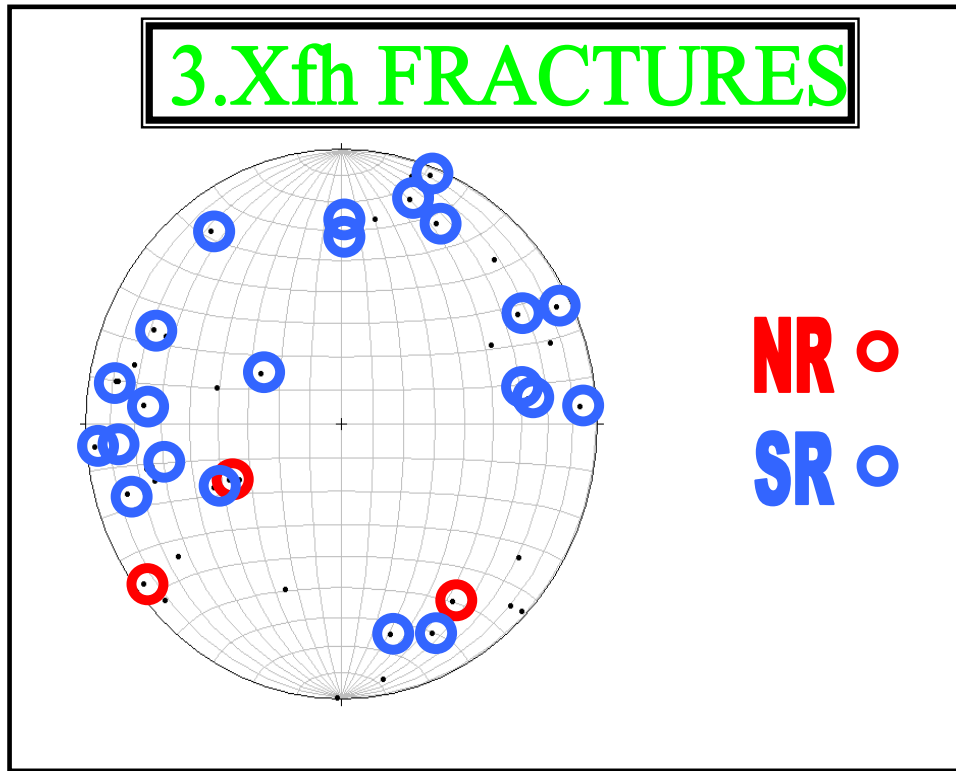


Figure 53d. Fractures of the western unit at high elevations (See Figures 58d, 58g & 58j and Appendices f34-38).

Joints may be the result of compression, tension or shear stress (Davis & Reynolds, 1996). A series of parallel planes of breakage, forming a joint set, were discovered within some fracture faces in the western high elevations. These joints govern the parting in the rock into blocks, not plates, when coupled with the fracture planes they are visible within. With tension joints forming a regular pattern at right angles to the direction of tension and, given the northeast-east joint planes, it can be deduced that some extension occurred to the northwest-southeast. It is unknown if these distinct jointed fracture faces are the result of fracturing, faulting, shearing, or perhaps, a combination of the three (Figures 54 & 55).

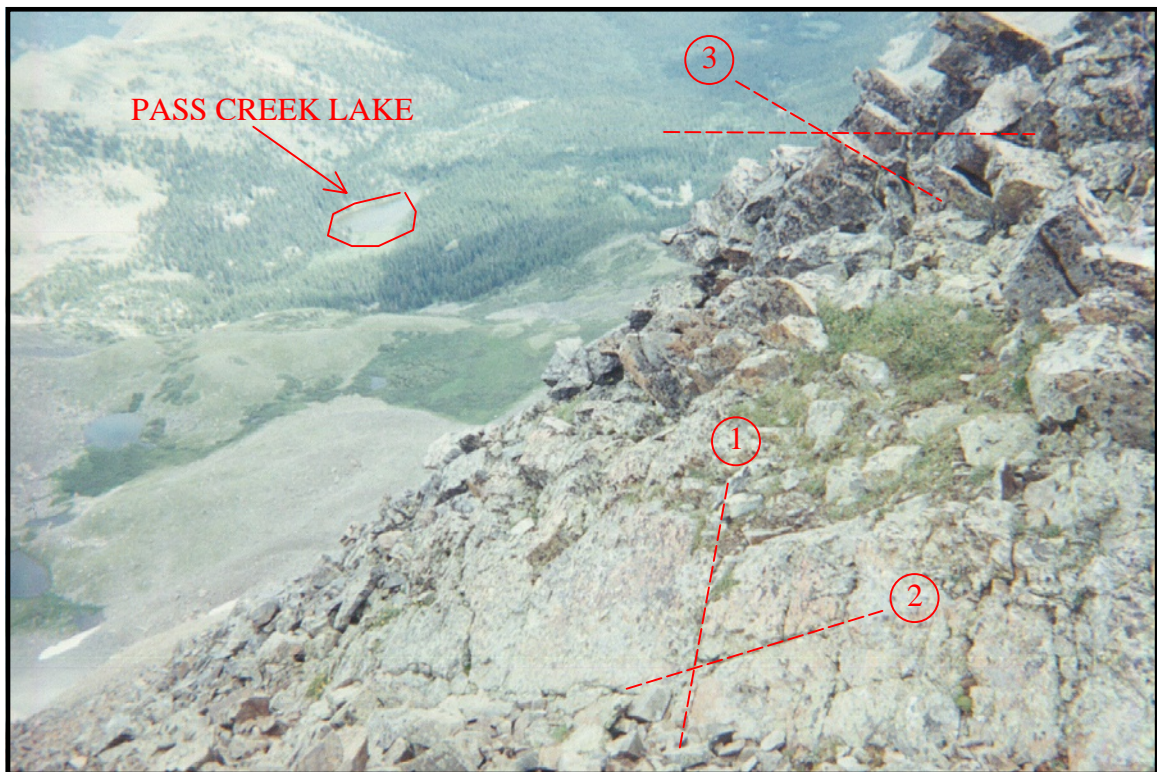


Figure 54. Looking northeast on SR down into Pass Creek at a prominent plane within the felsic quartzofeldspathic gneiss (3b.Xfh:Xqf) with no slicks present, therefore possibly a joint or fracture plane and not a shear face. The northwest-striking and southwest-dipping face/plane (N30W 69SW) contained two joint sets, one at N27E{~N/S} (line marked with 1 in circle) and the other at N87E{~E/W} (line marked with 2 in circle). The exposure strikes N45E and dips 60SE (line marked with 3 in circle). Field of View = 10 feet. (SR799 [location 37])

Some brittle structures (in the form of slickenlines) actually showed evidence of sub-horizontal, not down-dip, movement, indicating a strike-slip component of displacement in this area (Figure 55).

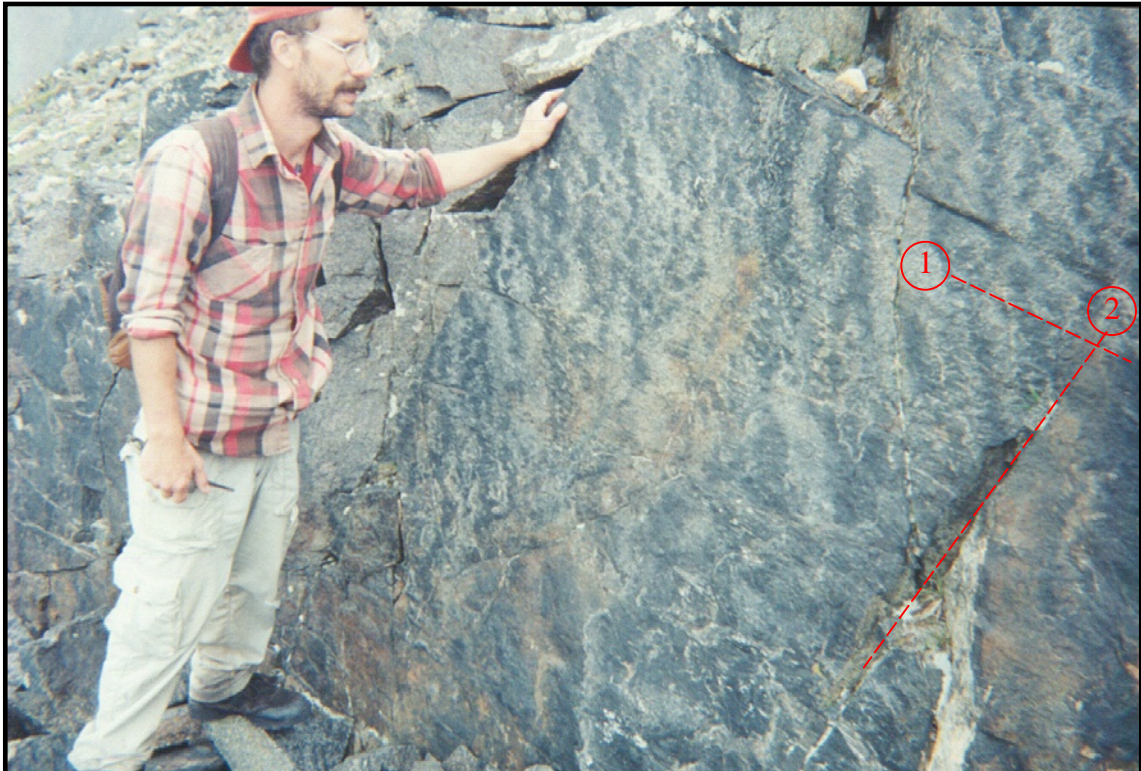


Figure 55. Looking ~southwest on the SR at a prominent northwest-striking and northeast-dipping (N10W 79NE) face/plane of an amphibolite gneiss exposure. A lineation of slicks (17plunge & n07e bearing) shows right-lateral movement; two joint sets are shown with one joint set at N30E 30SE (line marked with 1 in circle) & the other set at N72W 75SW (line marked with 2 in circle). Field assistant is shown for scale. (SR1499 [location 44])

LINEAMENTS/TRENDS/CONTACTS [T]

Bearings were taken for major lineaments and trends, such as contacts and linear vegetation growth and mineral veins. Fifteen (15) measurements were taken, with nine (9) from the NR and six (6) from the SR (Tables 2 & 3). Thirteen (13) of the fifteen (15) were northwest lineaments, with an average value of N36W (87%). The majority of the type of measurements and the corresponding values were mineral veins/bands (54%)

which trended N30W (75%) and N57E (25%), contacts of N39W (33%) and linear vegetation growth (13%) of N47W.

The majority of the lineaments measured were noted within the central unit at mid-ridge elevations. At location 3' (3a) on the SR, for example, a north-northwest lineament of vegetation was observed, both in the field and in aerial photos. This northwest trend conforms to the general trend of the metamorphic foliation and faulting which may influence placement of vegetation along planes of breakage where percolation of fluids may occur.

Table 2. Mathematically averaged measurements for Precambrian basement foliations and lineations by both lithologic unit and ridgeline (NR vs. SR vs. IS); dashed line implies no applicable measurement; {with exotic lithology averaged}; [corresponding stereonet figure: 56a-m/57a-d/58a-m/AppendixF:f1-f41].

RIDGELINE (UNIT)	NUMBER OF MEASUREMENTS: METAMORPHIC FOLIATIONS; LINEATIONS; FRACTURES; LINEAMENTS {w/P/Xcs/Xhb/Xqms/IS}	AVERAGE (AZIMUTH) STRIKE AND DIP OF METAMORPHIC FOLIATION/FABRIC [F] (F=79 [Figure 56a])	AVERAGE BEARING AND PLUNGE OF LINEATION [L] (L=19 [Figure 57a])	AVERAGE (AZIMUTH) STRIKE AND DIP OF FRACTURE/JOINT [J] (J=46 [Figure 58a])	AVERAGE BEARING OF TREND/LINEAMENT [T] (T=15)
NR (1.Xag)	8{9}; 2{3}; 5; 3	(328) N32W 53NE {(328) N32W 53NE} [56c]	29° n05e {32° n07e} [f19]	(080) N80E 84NW, (334) N26W 55SW & (342) N18W 56NE [58e]	(341) N19W
NR (1a.Xag:Xh)	5; 1; 2; 1	(333) N27W 52NE [f04]	30° n03e [f20]	(080) N80E 84NW & (334) N26W 55SW [f29]	(347) N13W
NR (1b.Xag:Xf)	2; 0; 2; 1	(315) N45W 62NE [f05]	-----	(346) N14W 66NE [f30]	(344) N16W
NR (1c.Xag:Xfs)	1{2}; 1{2}; 1; 1	(330) N30W 40NE {(329) N31W 46NE} [f06]	27° n07e {34° n09e} [f21]	(333) N27W 37NE [f32]	(333) N27W
NR (2.Xqfg)	24{27}; 11{12}; 6; 5	(321) N39W 45NE {(323) N37W 44NE}, (029) N29E 50SE, (349) N11W 79SW & (045) N45E 60NW [56f]	39° n37e, 37° n19w {38° n16w} & 33° s14e	(335) N26W 71NE, (022) N22E 54SE, (044) N44E 88NW & (340) N20W 76SW	(312) N48W

				[58f]	
NR (3.Xfh)	9{13}; 1; 3; 0	(331) N29W 50NE {(332) N28W 48NE}, (005) N05E 65SE {(016) N16E 62SE} & (321) N39W 63SW {(313) N47W 57SW} [56i]	23° n35e [f22 & f23]	(323) N37W 87NE {(329) N31W 64NE} & (056) N56E 67NW [58g]	-----
NR (3a.Xfh:XA)	7{11}; 0; 0; 0	(319) N41W 59NE {(324) N36W 52NE}, (005) N05E 65SE {(016) N16E 62SE} & (322) N38W 67SW {(312) N48W 58SW} [f13]	-----	-----	-----
NR (3b.Xfh:Xqf)	1; 0; 0; 0	(315) N45W 47SW [f14]	-----	-----	-----
NR (3c.Xfh:Xfa)	1; 1; 2{3}; 0	(355) N05W 34NE [f15]	23° n35e	(323) N37W 87NE {(329) N31W 64NE} & (056) N56E 67NW [f37]	-----
NR (4.Xcs)	3; 1; 0; 0	(335) N25W 43NE	42° n07w	-----	-----
SR (1.Xag)	9{10}; 1; 2; 0	(313) N47W 44NE {(315) N45W 50NE} & (021) N21E 83NW [56d]	28° n27e [f24 & f25]	(010) N10E 78SE & (280) N80W 65SW [58h]	-----
SR (1a.Xag:Xh)	3; 0; 0; 0	(310) N50W 46NE [f07]	-----	-----	-----
SR (1b.Xag:Xf)	3{4}; 0; 0; 0	(320) N40W 48NE {(322) N38W 58NE} [f08]	-----	-----	-----
SR (1c.Xag:Xfs)	3; 1; 2; 0	(300) N60W 28NE & (021) N21E 83NW [f09]	28° n27e	(010) N10E 78SE & (280) N80W 65SW [f33]	-----
SR (2.Xqfg)	3{4}; 0; 7; 3	(340) N20W 30SW, (337) N23W 34NE {(346) N14W 27NE} & (090) N90E 89SE [56g]	-----	(293) N67W 76NE, (301) N59W 79SW, (045) N45E 83NW & (015) N15E 73SE [58i]	(330) N30W
SR (3.Xfh)	16; 2; 21; 3	(057) N57E 51NW, (063) N63E 49SE, (350) N10W 79NE & (313) N48W 54SW [56j]	17° n07w & 48° n21e [f26]	(321) N39W 76SW, (036) N36E 63SE, (347) N13W 71NE & (077) N77E 68NW [58j]	(057) N57E & (353) N07W
SR (3a.Xfh:XA)	7; 1; 15; 1	(313) N48W 54SW, (062) N62E 62SE & (070) N70E 68NW [f16]	48° n21e [f27]	(326) N34W 78SW, (345) N15W 68NE, (050) N50E	(353) N07W

				67SE & (077) N77E 68NW [f34]	
SR (3b.Xfh:Xqf)	8; 0; 4; 2	(053) N53E 46NW & (065) N65E 29SE [f17]	-----	(330) N30W 69SW, (355) N05W 87NE & (018) N18E 75SE [f35]	(057) N57E
SR (3c.Xfh:Xfa)	1; 1; 2; 0	(350) N10W 79NE [f18]	17° n07w [f28]	(288) N72W 75SW & (030) N30E 30SE [f38]	-----
SR (4.Xcs)	1; 0; 0; 0	(355) N05W 20NE	-----	-----	-----
SR (6. i)	0; 0; 2; 1	-----	-----	(035) N35E 74NW & (350) N10W 60SW [f41]	(290) N70W
IS (3a.Xfh:Xa)	1; 0; 0; 0	(273) N87W 23SW	-----	-----	-----

Stereonet of foliations, lineations and fracture/joint orientations were displayed in Stereonet for Windows v.3. Stereonets allow one to display and then analyze the relationships between directional data. Lower hemisphere equal-area projected plots of foliation, lineation and fractures/joints were generated for both lithologic unit and ridgeline (the western high elevations compared to the eastern low elevations). The data was plotted as poles-to-planes (Figures 56, 57 & 58; for additional stereonet, see Appendix F).

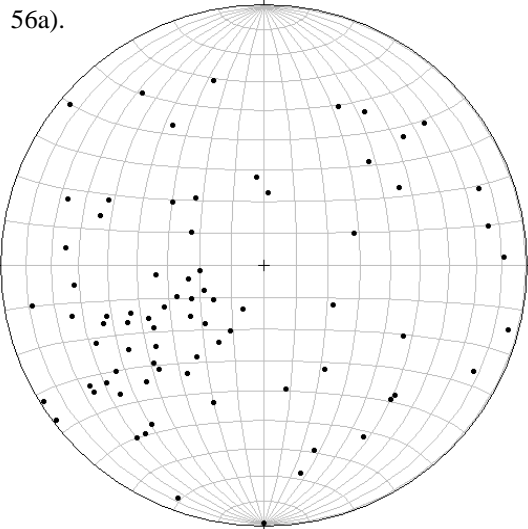
When comparing by ridgeline, the average strike and dip of metamorphic foliation for the NR (61% of the foliations) is N34°W 47°NE (69%) and SR (38% of the foliations) is N36°W 48°NE (37%). The average strike and dip of the brittle fracture planes or joints for the SR (69% of the fractures) are N44°W 74°SW (34%), N33°W 73°NE (25%) and N30°E 66°SE (25%), and for the NR (31% of the fractures) is N24°W 63°NE (50%). The average bearing and plunge of lineations for slickenlines and stretching penetrative mineral lineations (spml's) for the NR (84% of the lineations) is 36° N27°E (63%) and SR (16% of the lineations) is 38° N24°E (67%). The average bearing of the

trends/lineaments for the NR (53% of the trends) is N41°W (100%) and for the SR (33% of the trends) is N24°W (67%) and N57°E (33%).

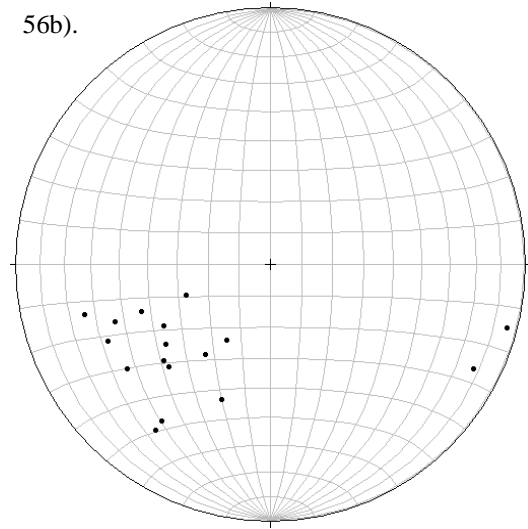
Table 3. Mathematically averaged measurements for Precambrian basement foliations and lineations by only lithologic unit along ridgeline (western high elevations (whe's) vs. eastern low elevations (ele's); dashed line implies no applicable measurement{with exotic lithology averaged}; [corresponding stereonet figure: 56a-m/57a-d/58a-m/AppendixF:f1-f41].

UNIT (FOR BOTH RIDGELINES)	NUMBER OF MEASUREMENTS: FOLIATIONS; LINEATIONS; FRACTURES; LINEAMENTS {w/P/Xcs/Xhb/Xqms/IS}	AVERAGE (AZIMUTH) STRIKE AND DIP OF METAMORPHIC FOLIATION/FABRIC (F=79 [Figure 56a])	AVERAGE BEARING AND PLUNGE OF LINEATION (L=19 [Figure 57a])	AVERAGE (AZIMUTH) STRIKE AND DIP OF FRACTURE/JOINT (J=46 [Figure 58a])	AVERAGE BEARING OF TREND/LINEAMENT (T=15)
1.Xag	17{19}; 3{4}; 7; 3	(283) N77W 43NE {(288) N72W 46NE} & (021) N21E 83NW [56b]	28° n12e {31° n12e} [57b]	(342) N18W 56NE, (307) N53W 60SW, (080) N80E 84NW & (010) N10E 78SE [58b]	(341) N19W
1a.Xag:Xh	8; 1; 2; 1	(325) N35W 50NE [f01]	30° n03e	(080) N80E 84NW & (334) N26W 55SW	(347) N13W
1b.Xag:Xf	5{6}; 0; 2; 1	(318) N42W 53NE {(320) N40W 59NE} [f02]	-----	(346) N14W 66NE	(344) N16W
1c.Xag:Xfs	4{5}; 2{3}; 3; 1	(315) N45W 34NE {(319) N41W 40NE} & (021) N21E 83NW [f03]	28° n17e {32° n15e}	(333) N27W 37NE, (280) N80W 65SW & (010) N10E 78SE [f31]	(333) N27W
2.Xqfg	27{31}; 11{12}; 13; 8	(322) N38W 44NE {(325) N35W 43NE}, (041) N41E 58SE & (045) N45E 60NW [56e]	39° n37e, 37° n19w {38° n16w} & 33° s14e [57c]	(309) N51W 74NE, (314) N46W 78SW, (045) N45E 86NW & (018) N18E 60SE [58c]	(318) N42W
3.Xfh	25{29}; 3; 24; 3	(057) N57E 51NW, (054) N54E 52SE {(046) N46E 54SE}, (318) N42W 60SW {(313) N47W 56SW} & (336) N24W 58NE {(336) N24W 54NE} [56h]	17° n07w & 36° n28e [57d]	(321) N39W 76SW, (342) N18W 69NE, (036) N36E 63SE & (072) N72E 68NW [58d]	(057) N57E & (353) N07W
3a.Xfh:xa	14{18}; 1; 15; 1	(048) N48E 63SE {(039) N39E	48° n21e	(326) N34W 78SW, (345)	(353) N07W

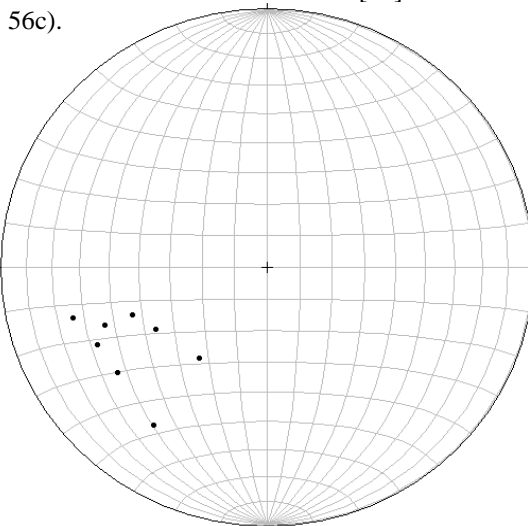
		39SE}, (319) N41W 63SW {(312) N48W 57SW}, (319) N41W 59NE {(324) N36W 52NE} & (070) N70E 68NW [f10]		N15W 67NE, (077) N77E 68NW & (050) N50E 67SE	
3b.Xfh:Xqf	9; 0; 4; 2	(315) N45W 47SW, (063) N63E 49SE & (057) N57E 51NW [f11]	-----	(018) N18E 75SE, (355) N05W 87NE & (330) N30W 69SW [f35]	(057) N57E
3c.Xfh:Xfa	2; 2; 4{5}; 0	(353) N07W 57NE [f12]	23° n35e & 17° n07w	(056) N56E 67NW, (323) N37W 87NE {(329) N31W 64NE}, (288) N72W 75SW & (030) N30E 30SE [f36]	-----
3d.Xfh:Xhb	2; 0; 1; 0	(335) N25W 40NE & (019) N19E 68SE	-----	(335) N25W 40NE [f39]	-----
3e.Xfh:Xqms	1; 0; 0; 0	(023) N23E 54SE	-----	-----	-----
4.Xcs (2a.Xqfg:Xcs)	4; 1; 0; 0	(340) N20W 37NE	42° n07w	-----	-----
5.P (5a.Pf) (1b.Xag:Xf)	1; 0; 0; 0	(328) N32W 89NE	-----	-----	-----
5.P (5b.Pfs) (1c.Xag:Xfs)	1; 0; 0; 0	(328) N32W 51NE	-----	-----	-----
6. i	0; 0; 2; 1	-----	-----	(350) N10W 60SW & (035) N35E 74NW [f40 & f41]	(290) N70W



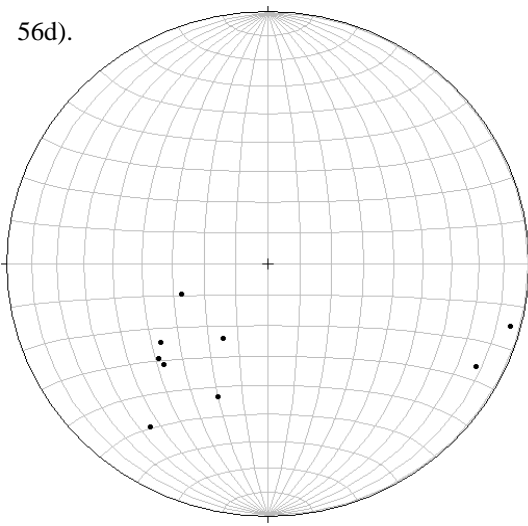
56a. foliations NRSR [79]



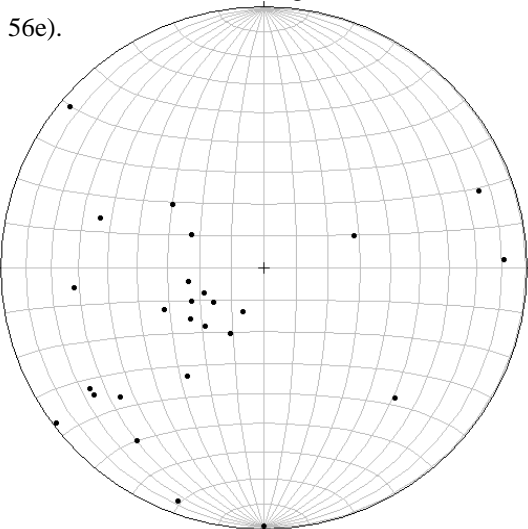
56b. foliations NRSR 1 Xag wo5aPf5bPfs [17]



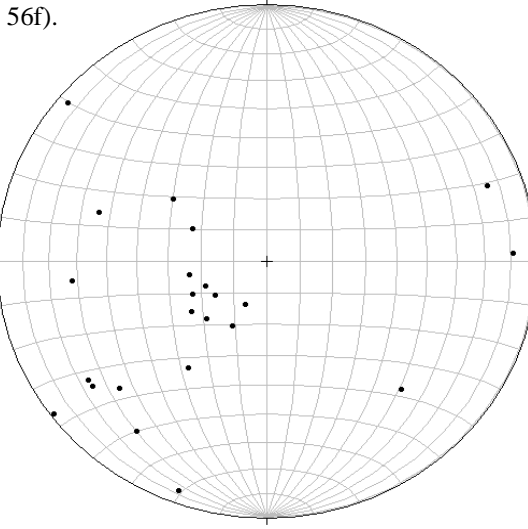
56c. foliations NR 1 Xag wo5aPf5bPfs [8]



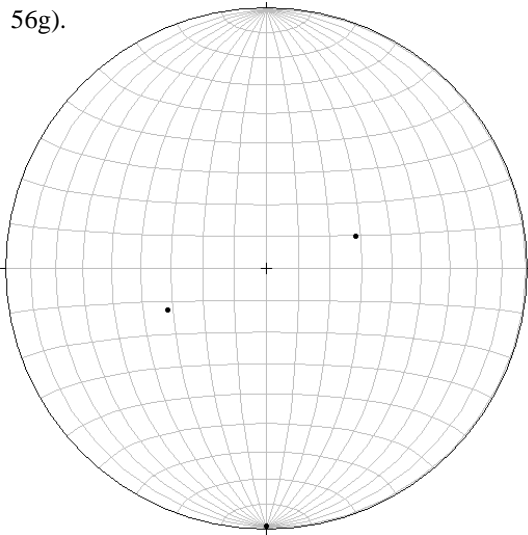
56d. foliations SR 1 Xag



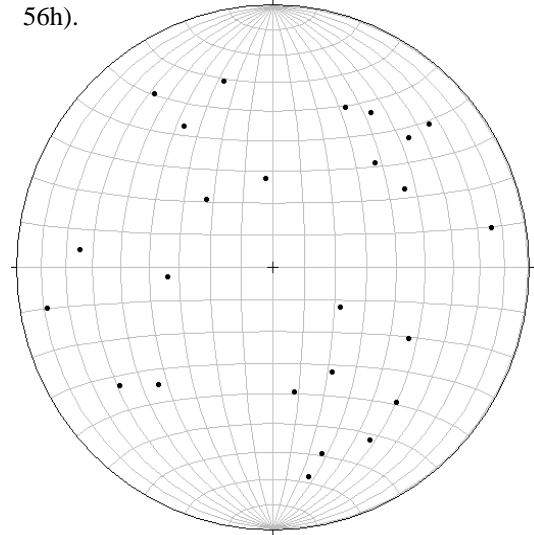
56e. foliations NRSR 2 Xqfg [27]



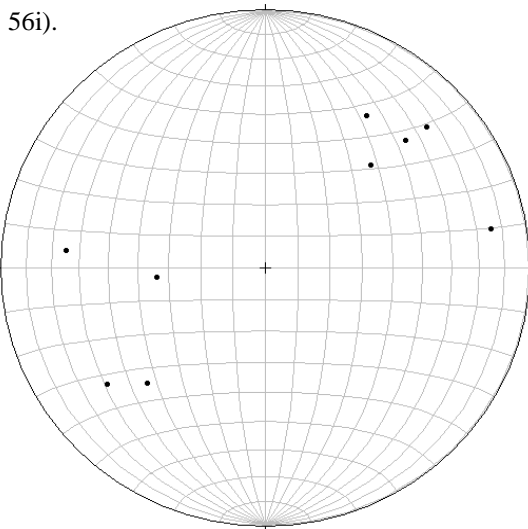
56f. foliations NR 2 Xqfg [24]



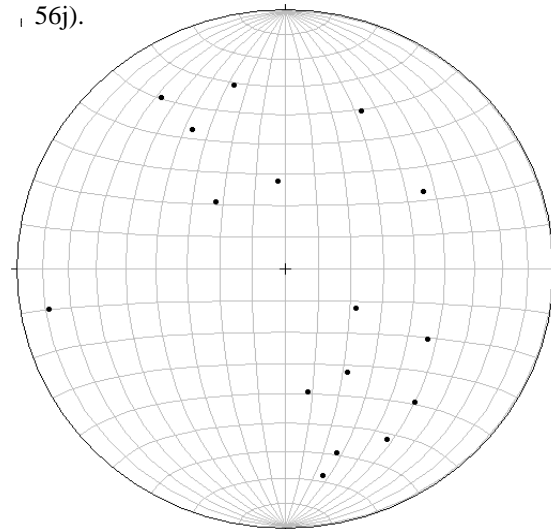
56g. foliations SR 2 Xqfg [3]



56h. foliations NRSR 3 Xfh [25] (3a, 3b & 3c)

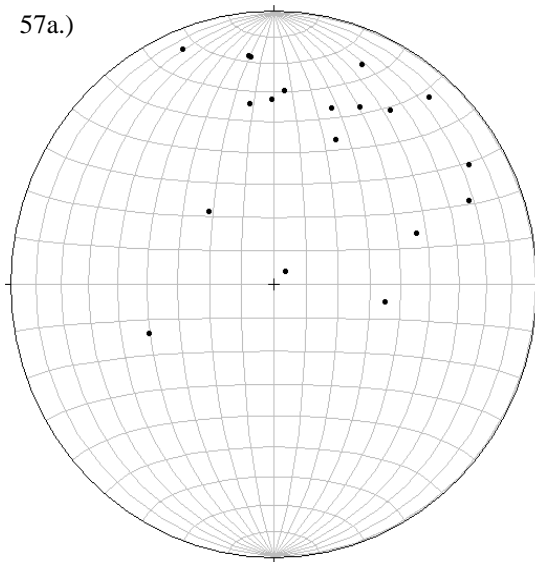


56i. foliations NR 3 Xfh [9] (3a, 3b & 3c)

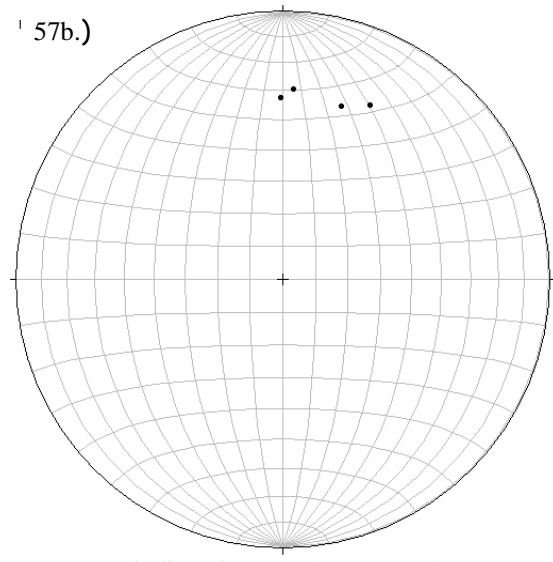


56j. foliations SR 3 Xfh [16] (3a, 3b & 3c)

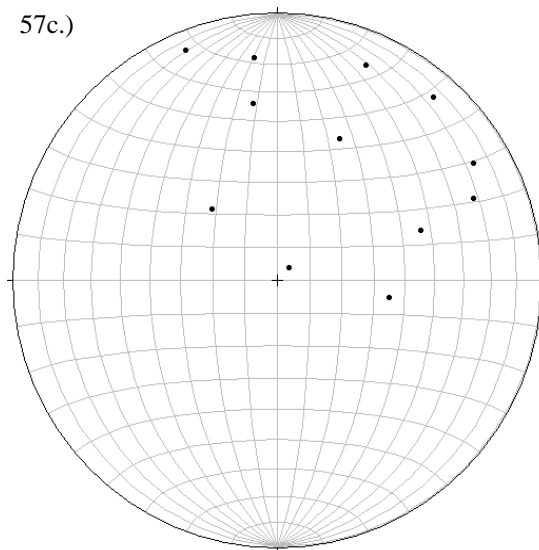
Figure 56. Lower Hemisphere Equal-Area projected plots (a-j) of field area for metamorphic foliation by both unit and ridgeline.



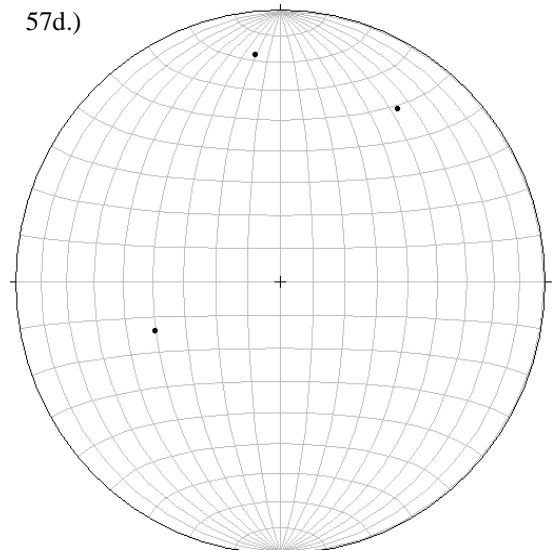
57a. lineations NRSR [19]



57b. lineations NRSR 1 Xag [4]

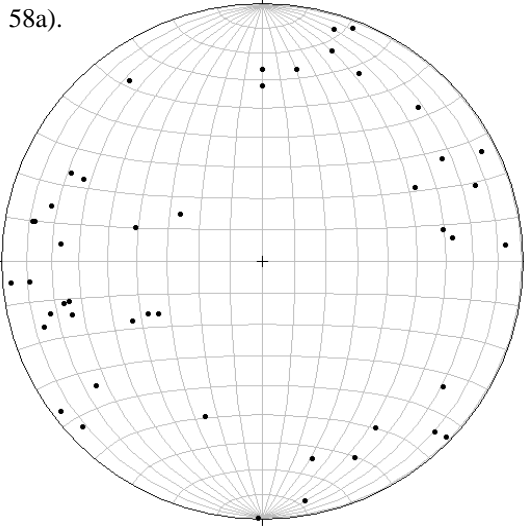


57c. lineations NRSR 2 Xqfg [12]

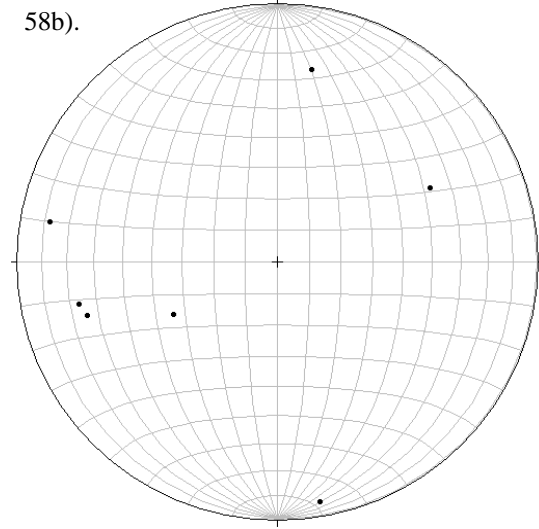


57d. lineations NRSR 3 Xfh [3]

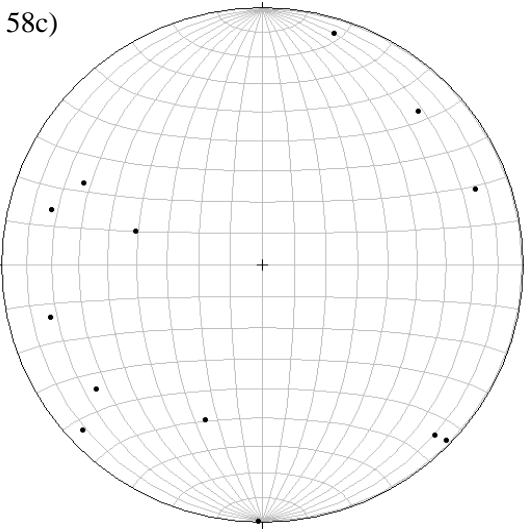
Figure 57. Lower Hemisphere Equal-Area projected plots (a-d) of units for lineations: both ductile stretching penetrative mineral lineations and brittle slicks.



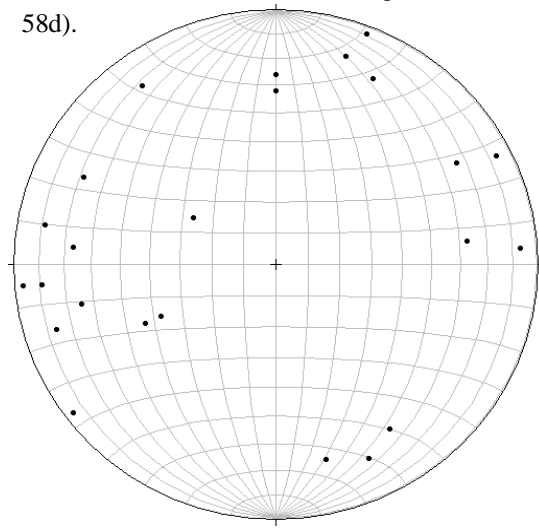
58a. fractures NRSR [46]



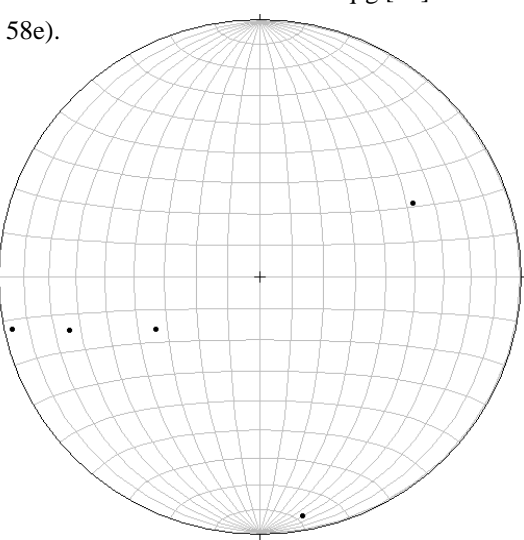
58b. fractures NRSR 1 Xag [7]



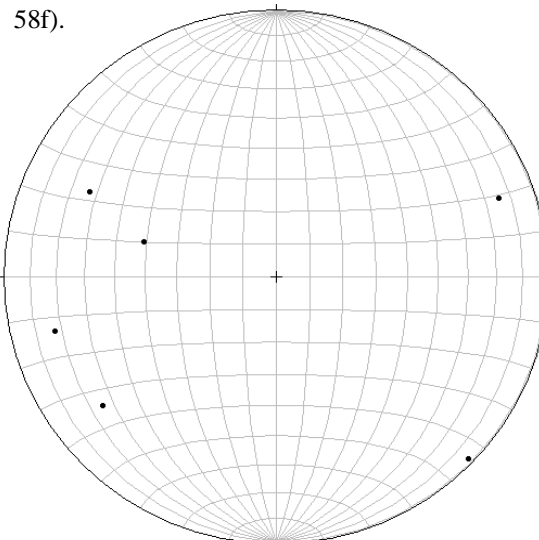
58c. fractures NRSR 2 Xqfg [13]



58d. fractures NRSR 3 Xfh [24]



58e. fractures NR 1 Xag [5]



58f. fractures NR 2 Xqfg [6]

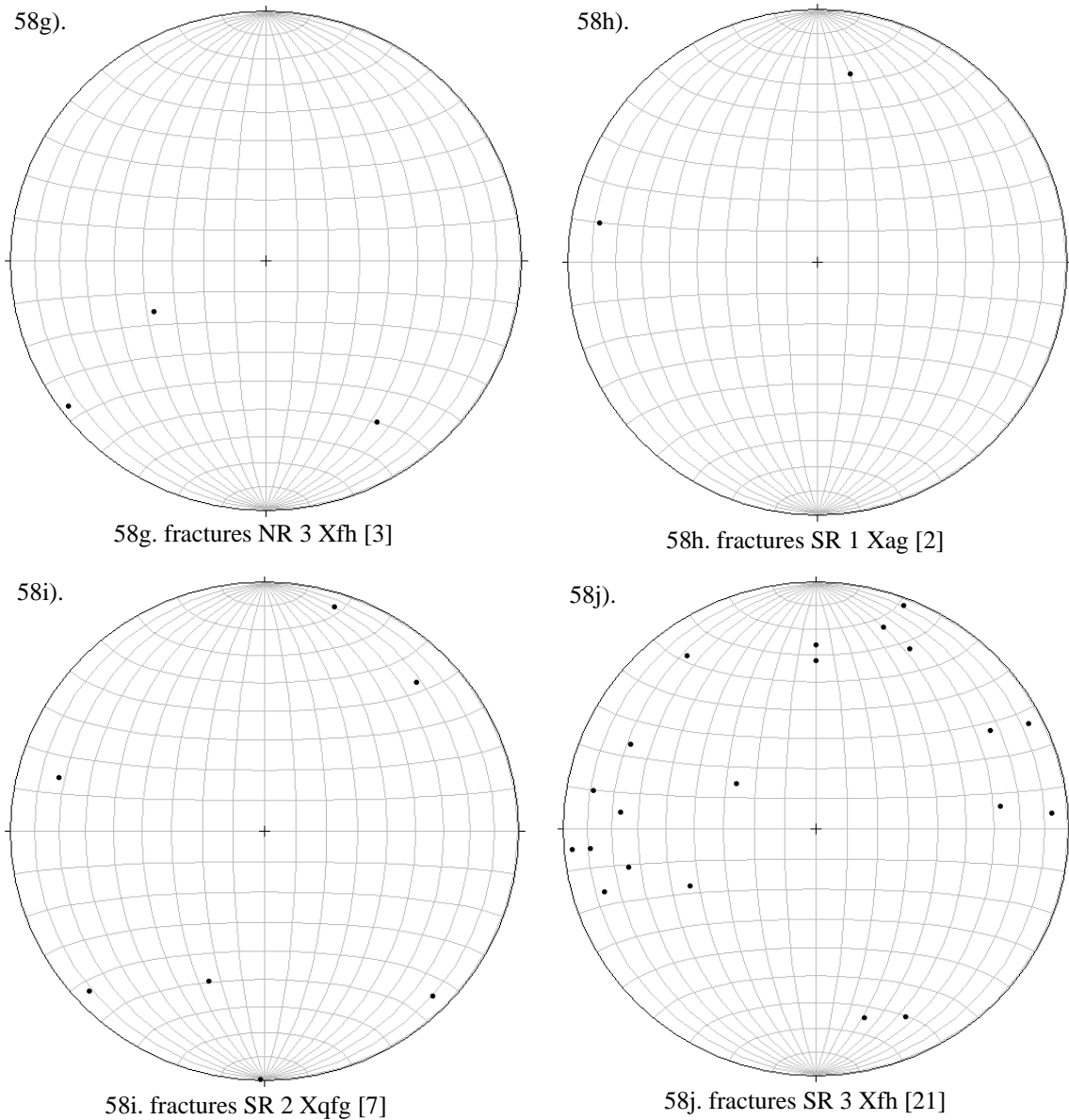


Figure 58. Lower Hemisphere Equal-Area projected plots (a-j) of field area for metamorphic foliation by both unit and ridgeline.

FAULTS

An attempt was made to identify large-scale structural features in the study area by the use of aerial photography, satellite imagery and digital elevation models (prior to the field season). By observing the linear features of the field area, some potential faults

were inferred (Figures 59 & 60). These suspected faults were inferred based on irregularity in the profile, change in slope, jog in the traverse and/or change in lithology (Figures 15 and 20). Although investigation of these faults in the field revealed no surficial evidence of offset, scarps or fault gauge, slickenlines were noted at some locations (locations 14, 14a, 16, 20, 21, 27, 44 and 51), signifying movement. Some indicators of movement that were noted were: normal (stepping down to the north) (location 21; location 16), right-lateral dextral movement (SR1599[location 44]; NR599[location 12]), vertical movement (NR1799 [location 14a]) and normal and

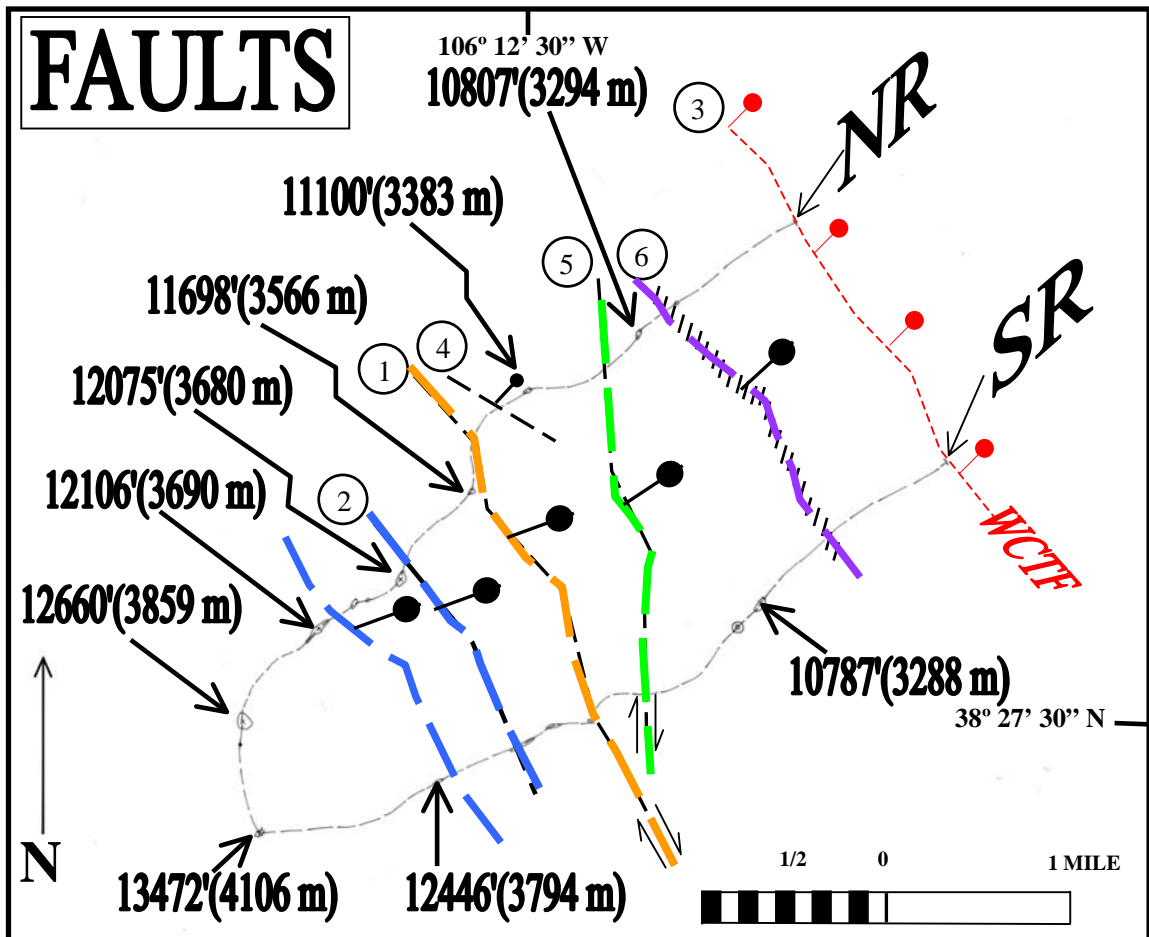


Figure 59. Simplified Geologic Map showing structural features of interest from Plate II. Features shown and described in text: 1. PCF (Pass Creek Fault); 2. HJF (Hump Jut Fault); 3. WCTF (Basin-bounding fault Willow Creek Transfer Fault); 4. Normal splay Fault; 5. Drainage Divide Fault; 6. Pass Creek Shear Zone Fault; Bar and ball on downthrown side of faults and inferred horizontal arrows.

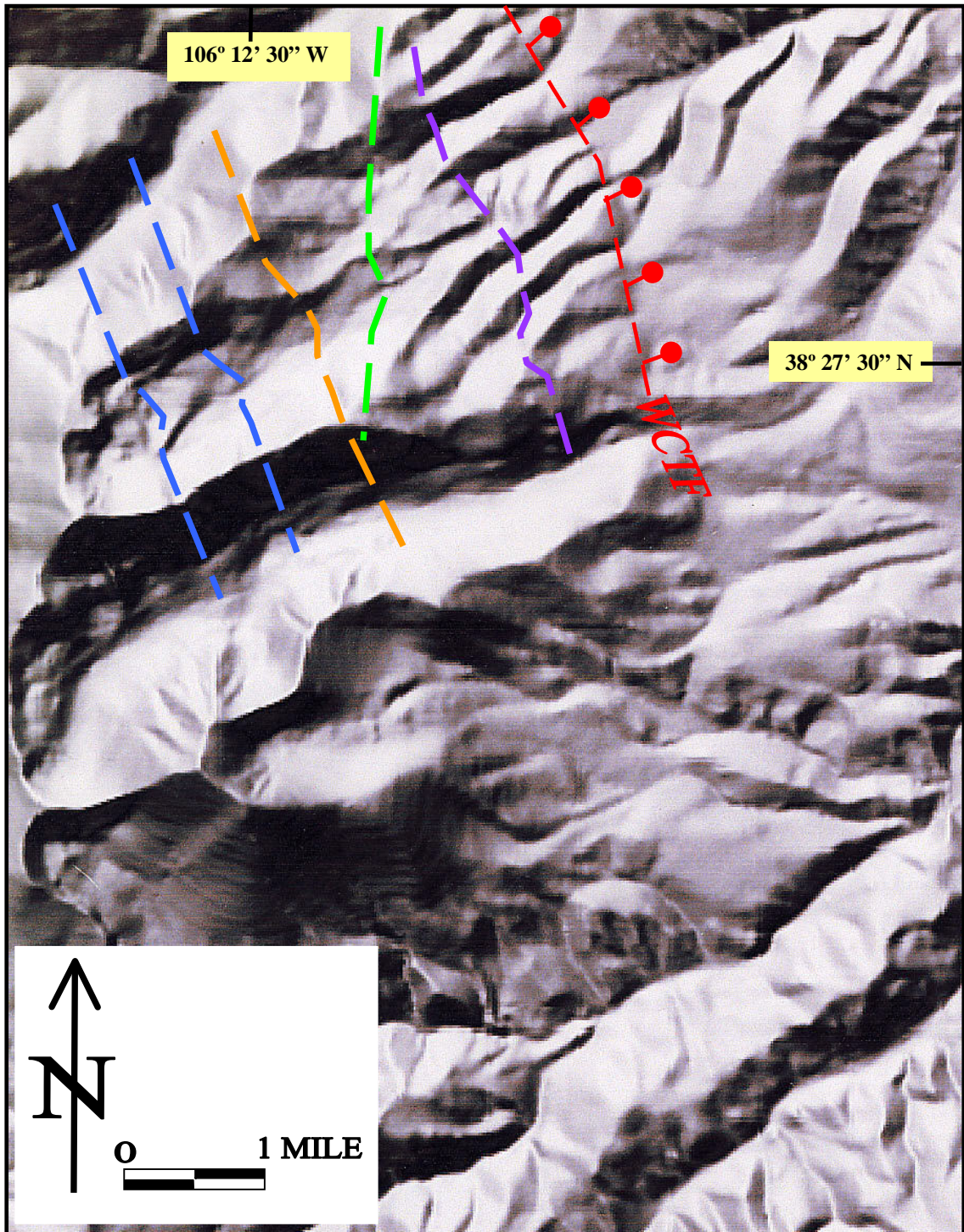


Figure 60. A Digital Elevation Model showing the relief of the area and the inferred faults relative to surficial expression.

reverse movement (NR1499[location 27]). Brittle deformation (NR2699[location 78]; SR3699 [location 71]) was found throughout the traverse, at both western high elevations and eastern low elevations.

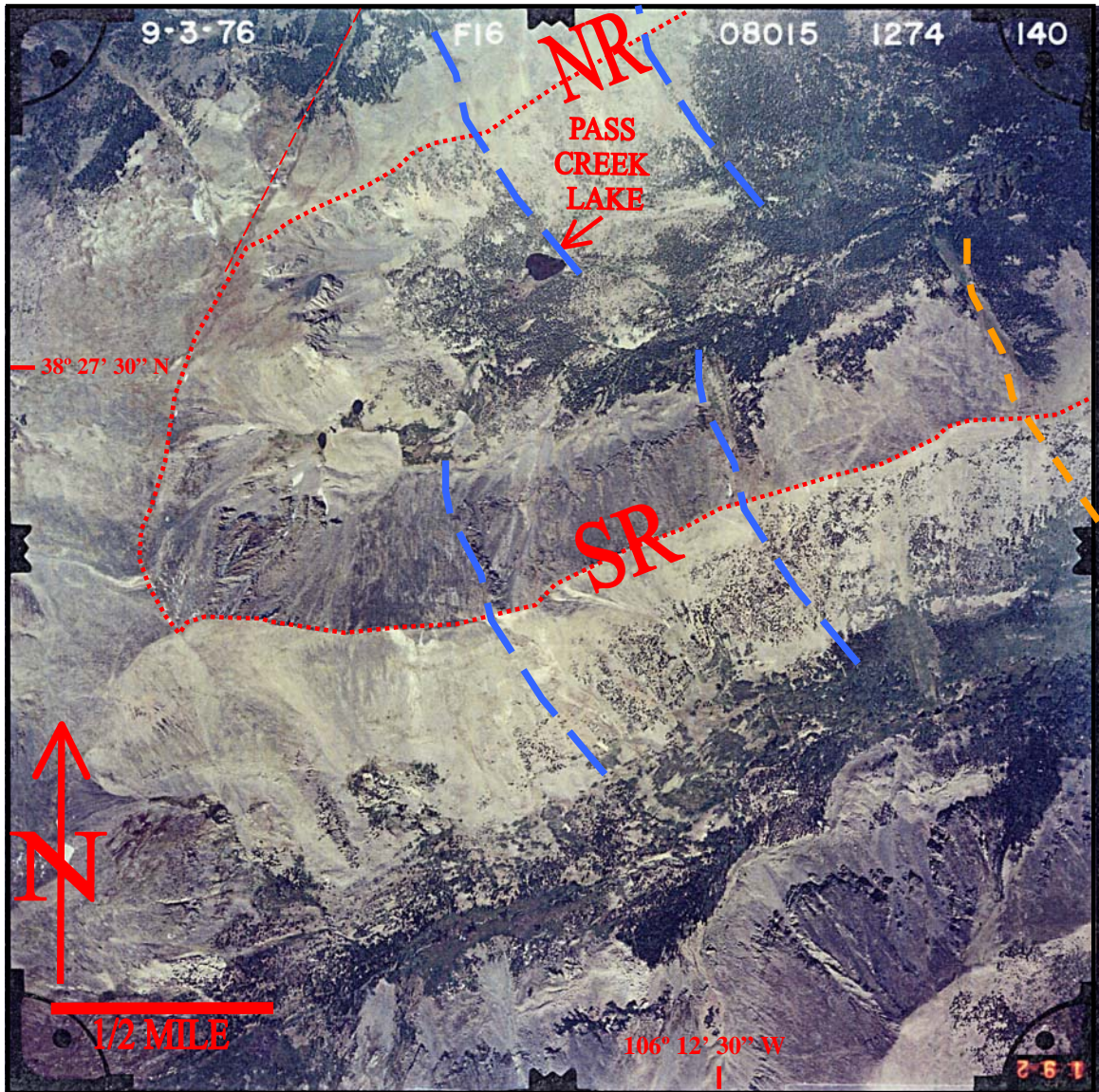


Figure 61. Aerial photo showing Pass Creek Lake and both the North and South Ridgelines at the western high elevations. Also shown are the Hump Jut Faults to the west (blue dashed lines) and the Pass Creek Fault to the east (orange dashed line).

Although, six (6) inferred faults were noted through the use of digital imagery, aerial photo notations and field observations, typical evidence of faulting was possibly

obscured in the subsurface and/or had been removed by denudational processes. Therefore, it was difficult to confirm that these inferred faults were actual faults, not just the jostling or shuffling of crustal blocks. Although it remains unclear as to how important a role they play, having noted the locations of these inferred faults and potential planes of movement was important in assessing the exhumation and cooling history of the study area.

PASS CREEK FAULT (PCF) (1)

This inferred fault, referred to as the “Pass Creek Fault” (“PCF” and ①), is located up in the higher elevations of the range, east of the 11,698’ hilltop (at ~11,560’) on the NR and at ~12,080’-12,120’, on SR (Figure 59). This fault is near locations 19, 20, and 21, on the NR and 61 & 62, on the SR. This fault is sub-parallel to the trend of the WCTF downslope to the east. This fault is assumed to have an associated component of dextral normal sense of shear. Five brittle lineations (slickenlines) were measured on the NR at locations 19-21, revealing both down-dip (L11, L12 & L13) and down-strike movement (L14 & L15), while one ductile lineation (spml) showed down-strike movement (L10). It is possible that this component of oblique strike-slip displacement on this proposed fault is related to movement within the Poncha Pass Transfer Zone, where similar displacement was discovered by Petrina (1992).

The presence of this fault was inferred based on a prominent change in the topography (jog in the traverse), a prominent lineament and change in lithology (Figures 22 & 24). The traverse of the south ridgeline jogs northward, where the ridgelines appeared to be slightly incised and turning southward at location 61 (SR3099), establishing a feature nicknamed “Grassy Knobs” (Figure 32). The prominent lineament

trends northwest and coincides with a drainage feature that possibly formed along this fault plane (Figures 29a, 29b & 32). A conspicuous pink exposure located on the SR (at the “Grassy Knobs”), indicated a change in lithology, possibly as a result of movement along this fault (Figure 32). The porphyroblasticity of the petrologic samples was found to increase at this location with specimens SR3099, SR2999 and SR2899, thought to be a fault indicator.

HUMP JUT” FAULT (HJF) (2)

The “Hump Jut” Fault (2) was inferred based on a feature referred to as a “hump”. Visible across ridgelines, this feature “juts” out into the Pass Creek drainage (Figure 59) and is suspected of being fault-induced (Figures 19, 22, 24, 33, 47, 59, 60, 61 and 62). This proposed plane of movement (HJF#2) cuts across the ridgelines from location 53 on the SR to the 12,075’ peak on the NR (Figure 61). It is thought that the plane of movement passes through locations 51-56 on the SR and 26a & 27 on the NR, and the resultant hump is downslope at locations 47-48. Slickenlines were found at location 51 (L18) and location 27 (L17), both of which show down-dip displacement. Prominent fractures contribute to the change in slope on the SR, with an additional set of north-south and east-west oriented planes of breakage, becoming more prevalent down ridge. A change in lithologic unit, along with a contact between the central unit (quartzofeldspathic gneiss) and the western unit (felsic hornblendic gneiss), were also noted just downslope of this location. On the NR the exotic lithologies are located just downslope of this proposed fault plane and the hump believed to be generated by this fault is just upslope, and on the SR the fault plane is not located along a contact but parallels the contact (Plates I & II). Aerial photos 139 (Figures 29a & 29b) and 140

(Figure 61) show the contorted traverse between the HJF (2) and the PCF (1), located down ridge. A parallel splay (HJF#1) is thought to exist farther upridge from just downslope of the 12,446' peak on the SR (locations 44-45) to the northeast of the 12,106' peak on the NR, between locations 27 and 34. The HJF#1 hump is upslope of the fault at location 44 slightly southwest of the 12,446' peak, with 3 intrusions upslope and 1 downslope of the fault plane (Plates I & II). Slickenlines were found in the feather amphibolite at location 44 (SR1599), indicating right lateral movement. Some

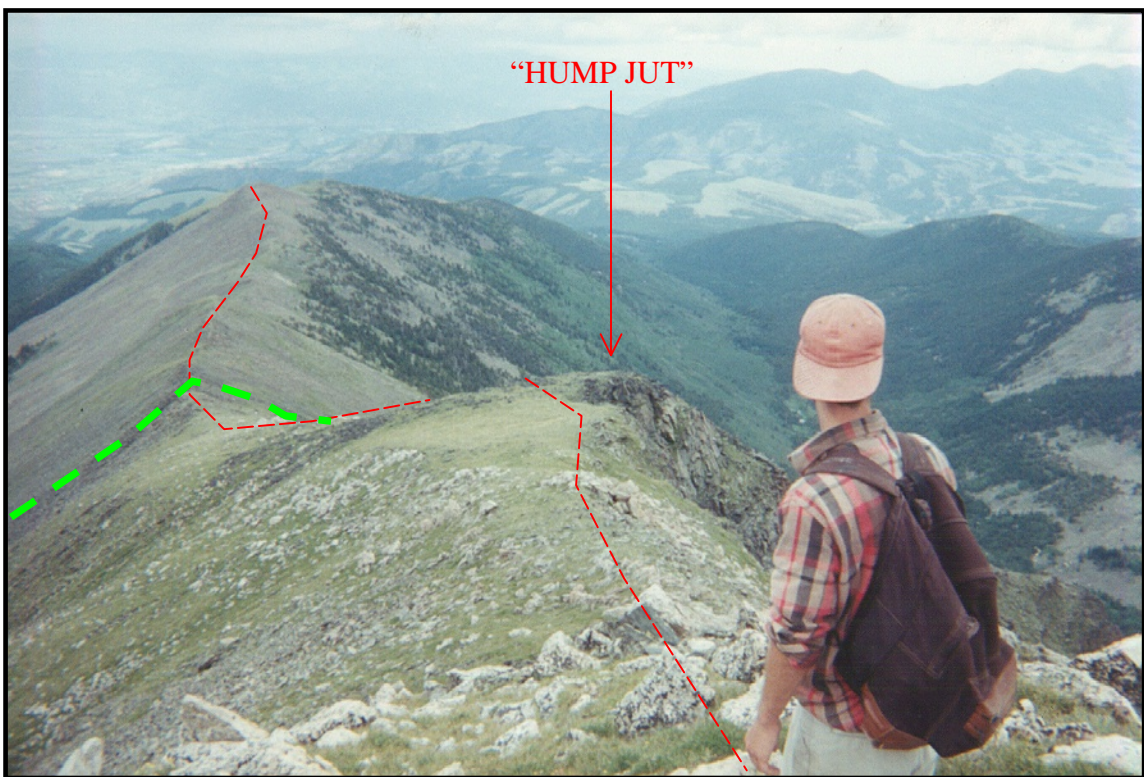


Figure 62. Looking east-northeast down NR just upridge from the Hump Jut Fault #2 at 12,075' at the prominent jutting out ("hump jut") into Pass Creek to the SE that is suspected as being fault-induced. Field assistant is shown for scale. See also Figure 19 (looking SE @ the same feature across ridgelines). Dashed green line shows 2.Xqfg/3.Xfh contact.

porphyroblastic rocks (SR2399 and SR2299) were noted near this proposed fault, similar to porphyroblastic rocks being found near the proposed Pass Creek Fault. These humps (Figure 47) could have been generated from a component of strike-slip faulting to the

south coupled with a component of normal faulting to the east along pre-existent planes of weakness and possible inversion, with the latter the result of the youngest episode of Rio Grande rifting.

WILLOW CREEK TRANSFER FAULT (WCTF) (3)

This northwest-striking and northeast-dipping dip-slip fault, conforms to the metamorphic fabric and foliation (Figure 63) and is thought to exhibit normal movement. It is the southernmost basin/range-bounding fault of the upper Arkansas basin/valley (uAb/uAv) contained within the Poncha Pass Transfer/Accommodation Zone (PPTZ/PPAZ). It is considered to be a northeast-vergent fault of a north-striking east-vergent fault system (Dippold, 1999) (Figure 59).

Dippold (1999) identified and named the WCTF based on a change in slope and colluvium, which incidentally was due to the lack of exposure of the contact between the Dry Union Formation (Tertiary sediments/Tertiary gravels) to the east and the Precambrian basement to the west. This change in slope and colluvium, along with the change in vegetation-type, was the basis for which I used to designate the eastern limit of both traverses and the location of the southernmost basin-bounding fault. Indeed, a contact between the (east-dipping) Precambrian basement and the (west-dipping) Tertiary sediments was not found on the ascents or descents of either ridgeline. However, there was a prominent change in slope at the lower elevations near this proposed major basin-bounding fault (WCTF), marked by a change of colluvium (large blocks of the Black Amphibolite (1a.Xag:Xh), which trended northwest-southeast) (Figure 63). The change



Figure 63. Looking south-southeast down the WCTF scarp on NR where large blocks of Black Amphibolite Gneiss (1a.Xag:Xh) cause a rapid drop in elevation. Note the dense vegetation, both up and downslope, but the lack of vegetation where these colossal boulders rest. Brunton, GPS & clipboard are shown for scale. The fault is considered evidence of brittle deformation during the rifting episode. (location 78; NR2699)

in slope is indicated on a topographic map by a discernable difference in the shape and spacing of the contour lines at the point of this prominent decrease in elevation (Plate II). These differences in elevation appear as knobs projecting out toward the basin. Although the prominent change in slope is quite visible on a topographic map, aerial photos and digital elevation models (used to delineate the limits of the traverse), the ridgelines were still traversed way beyond the limit, ensuring that no additional structural features were present. The drop-off was subtle on the SR, but far more noticeable and drastic on the NR. The change in vegetation type, from pines to aspens, could possibly reflect a change in soil moisture as a result of percolation along the fault plane. The difference in vegetation type, the change of colluvium and a prominent change of slope all serve as indicators of a potential fault.

NORMAL SPLAY FAULT (4)

At location 16 on the NR, slickenlines were found on a prominent quartzofeldspathic gneiss (2.Xqfg) exposure, which jutted out to the northeast into Green Creek, exhibiting normal movement and a stepping down to the north (Figures 49 & 59). Movement resulted in a dropping down of the northeast side of the fault and formed the northeast-facing scarp. The northwest trend parallels the fold found ~800 feet (~244 m) up the ridgeline at location 17 (10,217'/3114 m). This stepping down to the north was also discovered at location 21, where the PCF is proposed.

DRAINAGE DIVIDE FAULT (5)

The "Drainage Divide" fault is located across the ridgelines, from location 07 on the NR to location 61 on the SR (Figure 15 & 20). The strike of the fault is north-south

to northwest-southeast, conforming to the WCTF downslope (Figure 59). The apparent dip on the Drainage Divide fault is ~90 degrees. This feature was denoted in aerial photos, satellite and DEM imagery (Figure 60) as well as by abrupt changes in vegetation and the branching of the ridgeline (where the SR divides into three sub-ridges to the immediate east of this location (Figure 60)). The intersection of this feature on the SR coincides with and approaches the inferred Pass Creek Fault (PCF(1)) at location 61, at a feature called “Grassy Knobs” where there is a noticeable jog in the traverse. When looking at the ridgelines from afar, this feature is visible as a change in profile (Figures 15, 20 and 24). This Drainage Divide Fault is located along a fault predicted by Kouter (1969). The Drainage Divide Fault is thought to intersect the Pass Creek Fault on the SR and then continue to the south onto the Arm of Mt. Ouray’s “Devil’s Armchair.”

PASS CREEK SHEAR ZONE NEIGHBOR FAULT (6)

This proposed fault, at location 13 on the NR and 64-65 on the SR, is thought to coexist with the proposed Pass Creek Shear Zone. This fault and shear zone are in roughly the same location as the Cinderella South Mine (along the NR). This fault is thought to have both a component of normal displacement (like the WCTF to the east) and, based on the shear this area is thought to have experienced, a component of right-lateral (dextral) displacement. This proposed fault trends ~N35°W 19°NE and parallels the PCF to the southwest (Figure 59) and the WCTF to the northeast. A noticeable change in lithology, which happens to coincide and correspond with the area Kouter (1969) proposed as having a northwest-trending shear zone, is noted by an outcropping of porphyroblastic pod-like schistose rocks. The pods appear to be stretched out, intrusive features or relict bedding of an arkosic conglomerate, both of which would have occurred

with the assistance of hydrothermal pressure solutions and some element of shear. Petrina (1992) estimated that a shear zone trends ~N55°W, while Dippold (1999) estimated a little more easterly at N45°W.

FOLD

A fold was found in the central unit quartzofeldspathic gneiss (2.Xqfg) on the NR, at location 17. The axial plane strikes N20°W and parallels both the WCTF and the PCF. This northwest-trending and southwest-vergent asymmetrical fold contains a gently-plunging axial plane that plunges 11° and bears S20°E. This was the only notable sign of compression and plastic deformation within the field area. Northwest-striking fractures were found parallel to the axial plane and propagating outward, suggesting formation during the Eocene extension (Figure 64). The northwest-striking axial plane suggests that forces that had occurred during this contraction and shortening were from the northeast-southwest. It is thought that this compressional deformation and shallow exposure is temporally linked to older deformational events (most likely, during the Precambrian following the formation of the northwest-striking foliation, but not during the Laramide orogeny).



Figure 64. Looking northeast from the NR down the northwest axial plane of a fold in the Xqfg that veers to the left. Evidence of plastic compressional anticlinal deformation. Fold axis bearing S20°E and plunge 11°. Pencil is shown for scale. (location 17)

KINEMATIC INDICATORS

An analysis of the metamorphic fabric and foliation attitudes was performed to determine the kinematics in the basement gneissic and schistose rocks. The results indicate that, due to brittle deformation and the jostling of the blocks (predominantly), the basement was rotated by an undeterminable amount. There has been brittle deformation at the extreme high elevations, with the exposures weathering along the planes of foliation within the fabric. This brittle deformation has given rise to microscopic fractures, vein fillings and tensional gashes, formed crosscutting the mineral grains. The kinematic indicators were minimal throughout this predominantly brittle deformed rock. Ductile kinematic indicators (e.g. asymmetric grains, asymmetric grain-tail complexes, shear bands, C'' fabrics and C-S fabrics) were roughly nonexistent. Brittle kinematic indicators were slightly more abundant in the form of small-scale faults and fractures with slight movement (Hanmer and Passchier, 1991; Passchier and Trouw, 1996; Simpson and Schmid, 1983). Even in thin sections of specimens harvested and located near suspected faults (e.g. SR3199), there were no indicators present. This would mean that the indicators recrystallized, the specimen was out of place or the suspicion was incorrect.

BRITTLE INDICATORS

Fractures formed by brittle deformation were common throughout specimens along the ridgelines, but especially near the basin/range-bounding fault. Specimen NR1499, for example, exhibited reverse movement in a faulted vein (NR1499; Figure 38j; Figure 65). Other signs of offset were seen with breakage of crystals, with subsequent vein fillings. An example of this offset, specimen NR2699, was displayed

within a hornblende crystal, where the offset could be attributed to either vein filling, faulting or both. Given that this specimen was not oriented, the displacement was undeterminable (NR2699, Figure 66). Tensional gashes (NR1099; Figure 67a, Figure 67b) were found in a ductile-deformed specimen (Figure 43d). Although tensional gashes and curvilinear microfractures were found in specimens SR699 and NR399, along with vein fillings, it is undeterminable as to whether or not they post-date the faulting of the WCTF.



Figure 65. A photomicrograph of a thin section showing faulting of veins in NR1499 and showing dextral reverse movement. Arrows on bottom left indicate up-direction and direction down lineation. With a NWstrike & NEdip, the slip appears to be NE-down-dip slip. The long axis of photomicrograph = 4 mm. (NR1499 [hs# 23/ts# 12/location 27])

Brittle deformation was also noted in specimens SR3699 and NR2399, along with vein fillings, parallel, perpendicular and crosscutting foliation. Despite the NR599

specimen being oriented and exhibiting dextral sense of shear in the field, no evidence was found in the thin section.

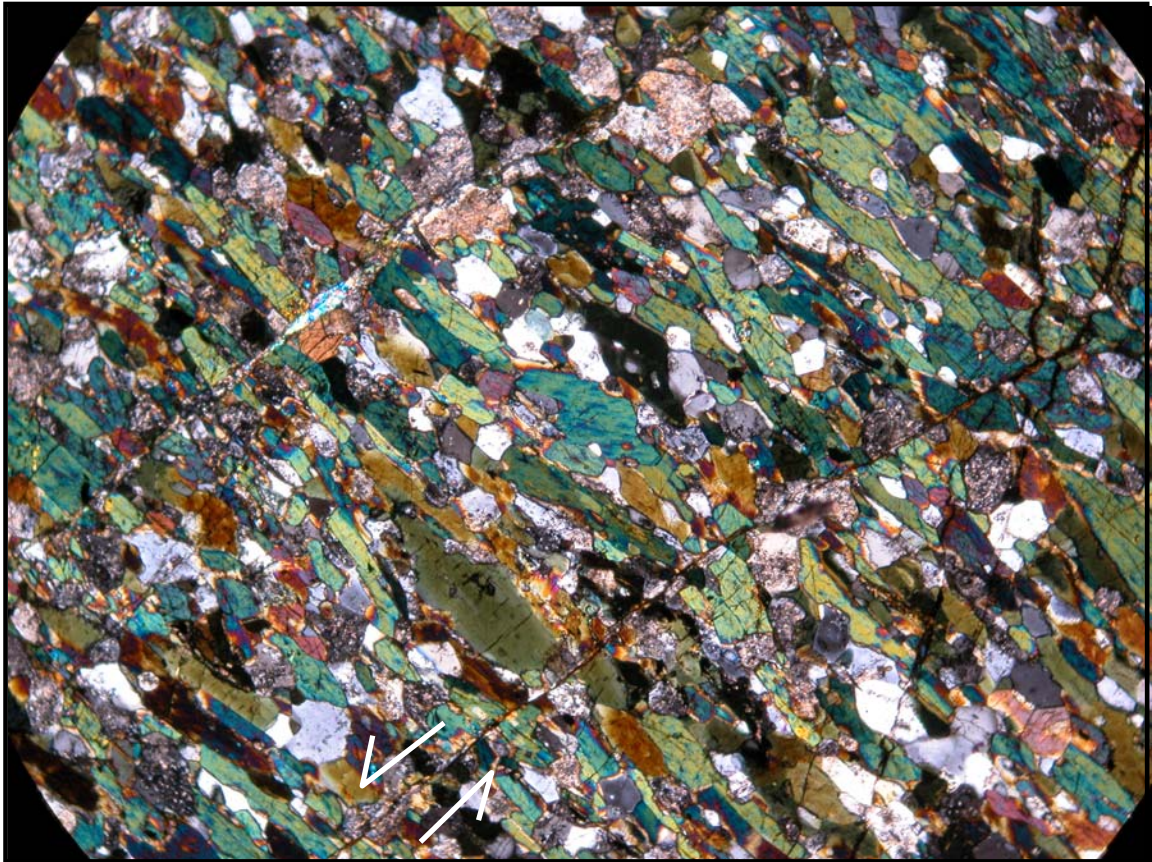


Figure 66. A photomicrograph of a thin section showing extensional feature. Long axis of photomicrograph = 4 mm. (NR2699).

DUCTILE INDICATORS

The only ductile indicators were found in the porphyroblastic (pod) rocks along the ridgelines. One specimen, NR1099, contained porphyroblasts of quartz aggregates that appeared slightly asymmetrical (Figure 67a). The Pf and Pfs exposures in the eastern low elevations (SR3599, SR3799 & NR4*99) showed no asymmetric grains. Likewise, the hornblende porphyroblast specimens (NR1299 and NR1399) (Figure 43c) and

quartzofeldspathic gneiss porphyroblast specimen (SR2899) in the western high elevations, also showed no asymmetrical grains.

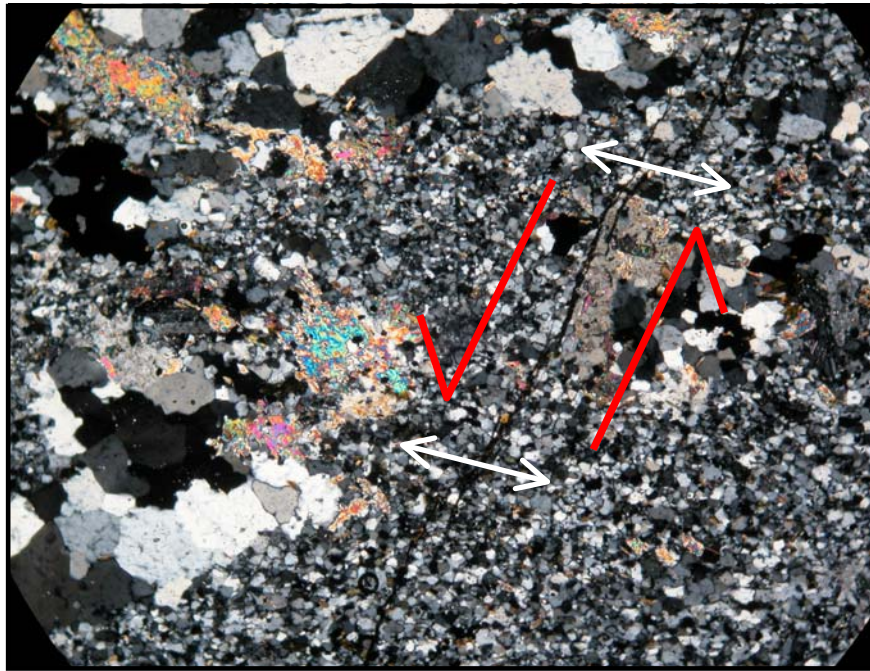


Figure 67a. A photomicrograph of a thin section of NR1099. Long axis = 4mm.

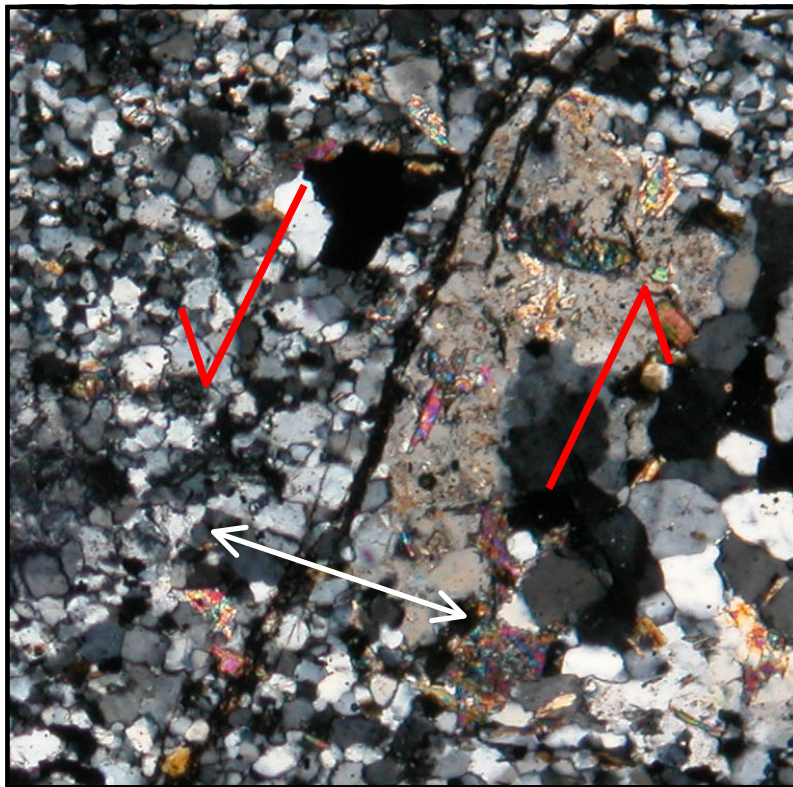


Figure 67b. Close up of fractured and extended grain of NR1099. Long axis of photomicrograph = 0.8 mm.

STRUCTURAL FEATURES BY LITHOLOGIC UNITS

The three broad mappable lithologic units were compared from the low to high elevations along both ridgelines (Plates II & III).

AMPHIBOLITE GNEISS (1.Xag)

The easternmost unit that forms the eastern limit and is of lower elevation, the amphibolite gneiss (1: Xag) was found to contain both ductile and brittle features throughout the traverse. The ductile attributes of metamorphic foliations (Figures 51, 56b, 56c & 56d; Appendix F: 1-9) and true stretching lineations (Figures 52 & 57b; Appendix F: 19-21 & 24-25) were both measured. The metamorphic foliations had an average northwest strike and northeast dip and conformed to the trend of the basin/range-bounding fault (WCTF) to the immediate east, which formed the eastern limit of the field area. Despite the proposed Pass Creek Shear Zone (PCSZ) and porphyroblastic textured rocks collected, no mylonitic ductile zones were discovered. The brittle attributes of faults and fractures with minimal movement (bfp's) (Figures 53a, 53b, 58b, 58e & 58h; Appendix F: 29-33) showed breakage along foliation planes and planes orthogonal to the foliation. No brittle slickenlines (Figure 52 & 57b) were found. Moreover, brittle structures were not abundant, possibly minimized due to movement along the WCTF. The Willow Creek Transfer Fault (WCTF; 3) (Figure 63) and the Pass Creek Shear Zone Fault (PCSZF; 6) were the planes of movement. The inferred faults discovered in this unit (Figure 59 & 60), though no outward visible indicators were displayed in the field, were based on work by previous authors and image analysis (Plates II & III).

QUARTZOFELDSPATHIC GNEISS (2.Xqfg)

The central unit, the quartzofeldspathic gneiss (2. Xqfg), is located at mid-ridge elevations (Figure 49). The ductile attributes of metamorphic foliations (Figures 51, 56e, 56f & 56g) and true stretching lineations (Figures 52 & 57c) were both measured in the field. The metamorphic foliations were predominantly northwest-striking and northeast-dipping, with the values becoming slightly scattered upridge. A total of four (4) ductile stretching penetrative mineral lineations (spml's) were measured and found to have a variance in values. No mylonitic ductile zones were discovered in this unit. A fold was discovered and given the orientation relative to foliation, it is deduced that this buckle in the quartzofeldspathic gneiss formed in the Precambrian, just prior to shallow exposure (Figure 64). The brittle attributes of faults, fractures with minimal movement (bfp's) (Figures 53a, 53d, 58c, 58f & 58i) and slickenlines (Figures 52 & 57c) were also measured throughout the central unit. The faults and planes of movement are the Pass Creek Fault (PCF; 1), the Normal Splay Fault (NSF; 4) and the Drainage Divide Fault (DDF; 5), all of which were found to parallel along a northwest strike and exhibit possible dextral normal movement. The fractures predominantly occurred along the northwest-striking planes of foliation (Figure 37a). They exhibited a secondary northeast-striking plane of breakage, giving a conjugate fracture pattern to this unit. A total of seven (7) brittle slicks were measured and found to display northeast down-dip trends (Plates II & III).

FELSIC HORNBLENDIC GNEISS (3.Xfh)

The westernmost unit, felsic hornblende gneiss (3. Xfh), forms the western limit and is located within the highest elevations of the study area. The striping is more pronounced compared to the other units and the foliation planes form the rough contacts between the stripes, with weathering common along these planes. The ductile attributes of metamorphic foliations and true stretching lineations were measured. The results of the values were found to be unreliable. The metamorphic foliations (Figures 51, 56h, 56i & 56j; Appendix F: 10-18) were found to be more scattered at the higher elevations and have various orientations, despite the northwest-striking and northeast-dipping trend found at the opposite lower elevations of the field area. The cause of this dispersion could be due to greater frost action, the measuring of loose blocks or the measuring of unrecognizable limbs of folds. Only a few stretching penetrative mineral lineations (Figure 52 & 57d; Appendix F: 22-23 & 26-28) were measured and found to be scattered in values. No mylonitic ductile zones were discovered throughout this unit. The brittle attributes of faults, fractures with minimal movement (bfp's) and slickenlines (Figure 47) were measured and found to be rather inconclusive, similar to the ductile attributes. Although the fractures (Figures 53a, 53d, 58d, 58g & 58j; Appendix F: 34-38) had a plethora of values, no trend was established. This could be the result of erosion and/or frost action that jostled these blocks. The inferred fault in this unit is the Hump Jut Fault (HJF; 2). Only a few brittle slicks were measured in this unit and were found to display an element of strike-slip displacement (Plates II & III)

DISCUSSION

The metamorphic foliations of this gneissose structure of the fabric could be contributory to both the faulting and fracture patterns throughout this Precambrian basement. The Precambrian bedrock foliation fabric strikes generally northwest and dips northeast, with slight variations throughout the traverse. An increase interval of stripes in the western high elevations resulted in more metamorphic foliations being measured and a dispersion of values. The northeast-trending Precambrian provinces could have influenced the increase of northeast average strikes of the metamorphic foliations in the western high elevations. Dippold (1999) found the entire area of the WCTF footwall Precambrian basement to be on the average N45°W 35°NE orientation in metamorphic foliation. Yet, in the proximity of the Pass Creek footwall segment, it was on the average N53°W, 39°NE, slightly greater in magnitude for both measurements. I found this to be consistent along both the SR and NR and along the eastern elevations near the fault, where a northwest strike and northeast dip prevailed. As Kouter (1969) noted, the Precambrian bedrock exhibited two structural trends: primary older northwest-trending faults; and younger northeast-trending faults, located near the drainage of Pass Creek. He proposed that these might be influential in creating the northwest and northeast fracture patterns throughout the area. Major northwest-trending regional Precambrian-age faults were reactivated in the late Paleozoic and the late Cretaceous to early Tertiary, with many episodes of deformation along potential weaknesses that pre-date the Cenozoic extensional event.

When viewed around the traverse from the SR eastern limit to the NR eastern limit, the strike appears to rotate clockwise from NW(5:00) at the SR eastern limit to

N(6:00) at mid-ridge; then NE (7:00) up in the western high elevations of the SR; then to ~ENE(8:00) at the interridge saddle; then to NW (10:00) at the NR western limit; and finally, to NW(11:00) at the NR eastern limit (Plate I). When viewed in the opposite direction (from the NR eastern limit to the SR eastern limit), the rotation is reversed and there is a counterclockwise rotation of strike. This analysis of foliation attitudes in basement gneisses and schists, and the clockwise rotation of strikes, where the strike becomes more easterly to both the west and south, indicates that the basement has been rotated by an amount could possibly be caused by an inherent Precambrian influence. Other potential causes include clockwise rotation of the Colorado Plateau, to the immediate west of the Rio Grande rift (Figure 50) (Chapin et al., 1996; Steiner, 2004), having unknowingly measured fold limbs or tectonic rotation due to dextral strike-slip displacement (Dippold et al., 1999; Hubbard et al., 1999). Rotation to the east (clockwise) was also found in the Mosquitos, on the other side of the Upper Arkansas Basin (Nehring and Geismann, 2001).

I interpreted that this older fabric of the Precambrian basement formed at the time of metamorphism, roughly 1750 to 1700 m.y. ago. Early fabrics with gently-dipping, west- to northwest-striking, tectonic foliation, that paralleled the compositional layering and planar arrangement, appeared to have become overprinted by a steeper tectonic fabric, south of the Mazatzal front (Shaw and Karlstrom, 1999). Steeply-dipping northeast- and northwest-striking fabrics, west and southwest of the field area, appeared to be caused by folding, similar to this area in the western high elevations (Shaw and Karlstrom, 1999). The northern limit of the Mazatzal front is still poorly defined, but might represent some structural discontinuity (Shaw and Karlstrom, 1999) in fabrics.

Another possibility in this area is that the intracratonic deformation of these previous orogenic episodes could all be influenced by the inversion of Proterozoic faults (northwest-striking extensional faults) (Marshak et al., 2000), reactivating then in the reverse/opposite motion. The ancestry of structures and Proterozoic trends are all influential in the later deformational events and orogenic episodes. Tectonic inversion (extensional collapse) of Laramide structures, which were influenced by older northeast (1.65 to 1.4 Ga), northwest (1.1 Ga) and north-south (0.8 Ga) lineaments, both structural and tectonic grains, may have been influential in this Paleoproterozoic area (Karlstrom et al., 1999). Positive inversion tectonics in the reversal of extensional fault movement during contractional tectonics (Williams et al., 1989) could have influenced the pre-rifting faulting. The proposed faults of the field area strike roughly northwest and during the older compressional events, inversion may have occurred to produce folding and reverse motion as noted in some thin sections (Figure 65).

The trace of the major northwest-trending fault at the eastern margin of the Sawatch Range was identified by a conspicuous break in topography (Kouther, 1969; Van Alstine, 1968; Dippold, 1999). The eastern extent of the traverse was the WCTF, which separates the west-dipping tertiary sediments from the east-dipping Precambrian bedrock and was mapped and named by Dippold (1999). It is thought that the WCTF fault plane complies with the adjacent foliation fabric ~N45W and that the incline varied from steep (70°) to shallow (40°) (Dippold, 1999). Dextral normal displacement was found along the WCTF, the southernmost basin-bounding fault of the Upper Arkansas Basin, which has only existed (and been active) for the last ~30-20 Ma (Hubbard et al., 2001) (Figure 57). The total slip of the fault was immeasurable in the field.

In addition to the dextral normal displacement on the WCTF, other dextral components to deformation have recently been documented adjacent to this area. On the east side of the southern Sawatch Range, a ductile fabric indicated a reverse dextral sense of shear (Hubbard et al., 1999). Dextral components of displacement have been analyzed between the Colorado Plateau and the North American craton, along the eastern margin of the Colorado Plateau, immediately west of the field area (Wawrzyniec et al., 2002). The northern part of the upper Arkansas valley is a pull-apart type basin, bound by right-stepping, dextral, extensional faults (Hubbard and Wawrzyniec, 2000). A component of strike-slip deformation that may have accompanied compressional (early) and/or extensional (late) deformation could be a product of inherited zones of weakness responding to deformational events (Hubbard et al., 1999). Many of the structures appear to be gravity-driven and are late syn-rift in their evolution. Precambrian northwest-striking faults, with both dextral and normal components of displacement, have been found in the vicinity (Hubbard and Wawrzyniec, 2000). Kinematic indicators suggest a rotational or lateral, as well as, a vertical component of movement (Denesha, 2003).

Other faulting discovered adjacent to the field area was found to exhibit strike-slip, oblique-slip and normal dip-slip displacement. Miller (1999) noted northwest-trending fault segments near the major basin-bounding normal fault up on the western margin of the upper Arkansas basin. Sidman (1998) identified a northwest-trending brittle, strike-slip fault in crystalline rocks that parallels the major fault, delineating the northernmost boundary of the transfer zone. Petrina (1992) found no brittle evidence for strike-slip faulting and found only one fault exhibiting oblique slip. All other faulting attributed to normal dip-slip displacement, has been suggested that the geometry of the

fault zone reflects a subsurface dextral shear zone, where perhaps all the extensional strain was accommodated and lateral movement was expressed at the mid-crust (Petrina, 1992).

The possibility of the existence of a shear zone seems likely near the basin-bounding fault, as Koutner (1969) proposed, based on cataclastic rocks. These rocks, which lack foliation, contain little or no evidence of frictionally generated thermal changes and are often impregnated with thermal waters into a “gouge” (Wise et al., 1984). The quartzofeldspathic schist unit (1c.Xag:Xfs) sounds very similar in lithology to cataclastic rocks and might be an indicator of brittle faulting, with high rates of strain, near the precise location of the shear zone. However, given that the porphyroblasticity is thought not to be the product of shear, and given the lack of kinematic indicators (rotated grains) and no shear-related fabrics, a shear zone might not be located in the subsurface of this unit. Pressure solutions and hydrothermal fluids were contributory to the formation of the porphyroblastic rocks found in the area proposed to contain a shear zone. Given that the formation of this texture took place at shallow depths, it is possible that only a brittle fault with fluids is present at this proposed shear zone location. There is the possibility, however, that this proposed shear zone is Proterozoic in age and located at mid-crustal levels (Petrina, 1992), but given the predominant northeast trend of Proterozoic shear zones (Figure 4a), this northwest-trending zone is unlikely to be Proterozoic in age.

The fracture analysis revealed that the fractures were influenced predominantly by metamorphic foliation. Dippold (1999) did not analyze the fracture system in the vicinity of the WCTF due to the assumption that displacement on the southernmost range/basin-

bounding fault would be the cause of the brittle deformation in such close proximity to the fault. Precambrian joints and NE-trending faults are thought to exert and partially influence local control of the incision of the Arkansas River, with no single isolated controlling structure (Leonard et al., 2002). The crust was segmented into blocks by both joints and fractures, with the joints being in parallel sets and the majority of the scree resulting from orthogonal, rectilinear blocks donning the surface. The fracture system within the western high elevations was abundant and the majority of the measurements taken in this area were of fractures. Spencer and Kozak (1974) performed an analysis of fracture patterns and orthogonal joint orientations within Precambrian basement rocks. Their study found that the metamorphic fabric and crustal lineaments were influential on these planes of breakage. Koutner (1969) identified a northwest system of joints parallel to a major fracture trend in the area and a younger northeast-trending system, with random deformation of the country rocks.

Ductile features were minimal within the western high elevations. Locally, ductile penetrative fabric attributed to shear deformation was found within the gneissic layering and schistosity. Brittle features were abundant in the form of extensional tension fractures and slickenlines. Both ductile and brittle deformation was exhibited by structures, with a component of motion oblique to the tensional axes of the rift ranges and basins (Hubbard et al., 1999). No hornblende deformation features (e.g. jagged terminations, zonations, mechanical twinning, translation gliding, lamellae or cleavage distortions (Passchier and Trouw, 1996)) were visible, as noted by Rooney et al., (1975), so deformation was overridden or relatively minor in amount.

Stretching lineations found on Precambrian bedrock through the central portion of the WCTF were shallow and plunging $\sim 35^\circ$ towards the northeast and were found to have a reverse dextral sense of shear in microstructures. This reverse dextral sense of shear is thought to be reflective of an older shear event, such as the Ancestral Rockies or Laramide orogenies, but not the Rio Grande rifting (which exhibited predominantly brittle features) (Dippold, 1999).

EXHUMATION

The exhumation was assessed to determine when the area was cooled through the low range of temperatures (relative to the deformational events this area has experienced) in an attempt to better define this Precambrian basement.

METHODS

MINERAL SEPARATION

From the suite of collected samples, representative unweathered specimens were selected for fission-track analysis, based on appropriate mineralogy for the method. The separation of the mineral grains from the rock specimen was done at the Isotope Geoscience Laboratory (IGL) at the University of Kansas, in Raymond Nichols Hall.

The mineral separation process consisted of magnetic separation and heavy liquid separation in order to isolate the apatite mineral grains. Samples were first crushed through a series of three crushers, reducing the grain size to about 70-250 μ m (Wagner and Van den Haute, 1992), washed with water, submerged and rinsed with an acetone wash, and finally, dried. Next, electromagnetic separation and heavy liquid separation was used to separate the minerals. The main procedure consisted of a heavy liquids separation. The dry specimen was placed into a liquid of a specific gravity. The two heavy liquids utilized for this separation of apatite were "Bromo" (Bromoform or Tribromomethane [CBr₃H]) to separate out the minerals with a density less than 3.2 grams/cc, and "MeI" (Methylene Iodide or Diiodomethane [CH₂I₂]) to separate out the minerals with a density greater than 3.2 grams/cc. Apatite, the mineral being separated out, has a specific gravity of 3.3 grams/cc. Bromo has a specific gravity of 2.85

grams/cc, while MeI has a specific gravity of 3.32 grams/cc. Using Bromo first, the apatite grains were isolated by sinking and, by using MeI second, the apatite grains were isolated by floating. Once the “heavies” and “lights” fractions were separated, based on specific gravity, the fractions were sieved, based on size, and ran through a Frantz Isodynamic Magnetic Separator to separate, based on magnetism. Finally, the purified apatite fraction was again washed with both acetone and alcohol in an ultrasonic bath to insure that the sample was entirely cleaned. Individual apatite grains were finally handpicked to be used in the Apatite Fission-Track (AFT) dating. The apatite grains were separated out of seven (7) specimens (NR599, NR1*99, NR899, NR17*99, NR1899, NR1799, & SR399) of Precambrian igneous and metamorphic rocks, located both close to the flanks of the rift along the eastern limit at lower elevations near the margin, and up in the higher elevations in the western limit of the traverse of the ridgelines. The apatite grains were sent to New Mexico Tech for age-dating.

APATITE FISSION-TRACK (AFT) THERMOCHRONOLOGY

The fission-track method, referred to as an ‘age’ determination method, is where the ‘age’ is defined as the instant the radioactive system (i.e. fission tracks) becomes stable and fixed into the mineral, evaluating the time-temperature cooling history of rocks below ~110°C. Thermochronology is the time-temperature history, based on age, as a result of the radioactive nuclide decay (geochronology) (Jackson, 1997). A fission track is a narrow trail of crystallographic damage that occurs as a result of a fast charged particle being emitted through nuclear fission. Given that the event of fission is rare, fission-track thermochronology uses uranium-rich minerals, such as apatite, sphene and

zircon, in which fission is more common. The basis of fission track thermochronology dating is the decay of ^{238}U by spontaneous nuclear fission (Naeser, 1979, 1976), which releases $\sim 200\text{MeV}$ of kinetic energy. This substantial amount of energy of alpha particles moves through the apatite grain, stripping electrons from atoms in the crystal, causing small channels to be produced. As the ionized atoms repel each other, portions of the crystal are destroyed (Wagner and Van den Haute, 1992). The damage is visible in tracks that form along the trajectory of the particle in the solid mineral and are retained in the solid mineral (Figure 68). The fission track “dating” technique entails mounting the apatite grains in an epoxy wafer, polishing them, etching them in nitric acid (HNO_3) at room temperature for a certain amount of time (~ 45 seconds) and then irradiating them (Kelley et al., 1992; Wagner and Van den Haute, 1992). These etching conditions allow the fission tracks to appear needle-like, regardless of the crystallographic orientation, for an accurate quantification (Wagner and Reimer, 1972) (Figure 68).

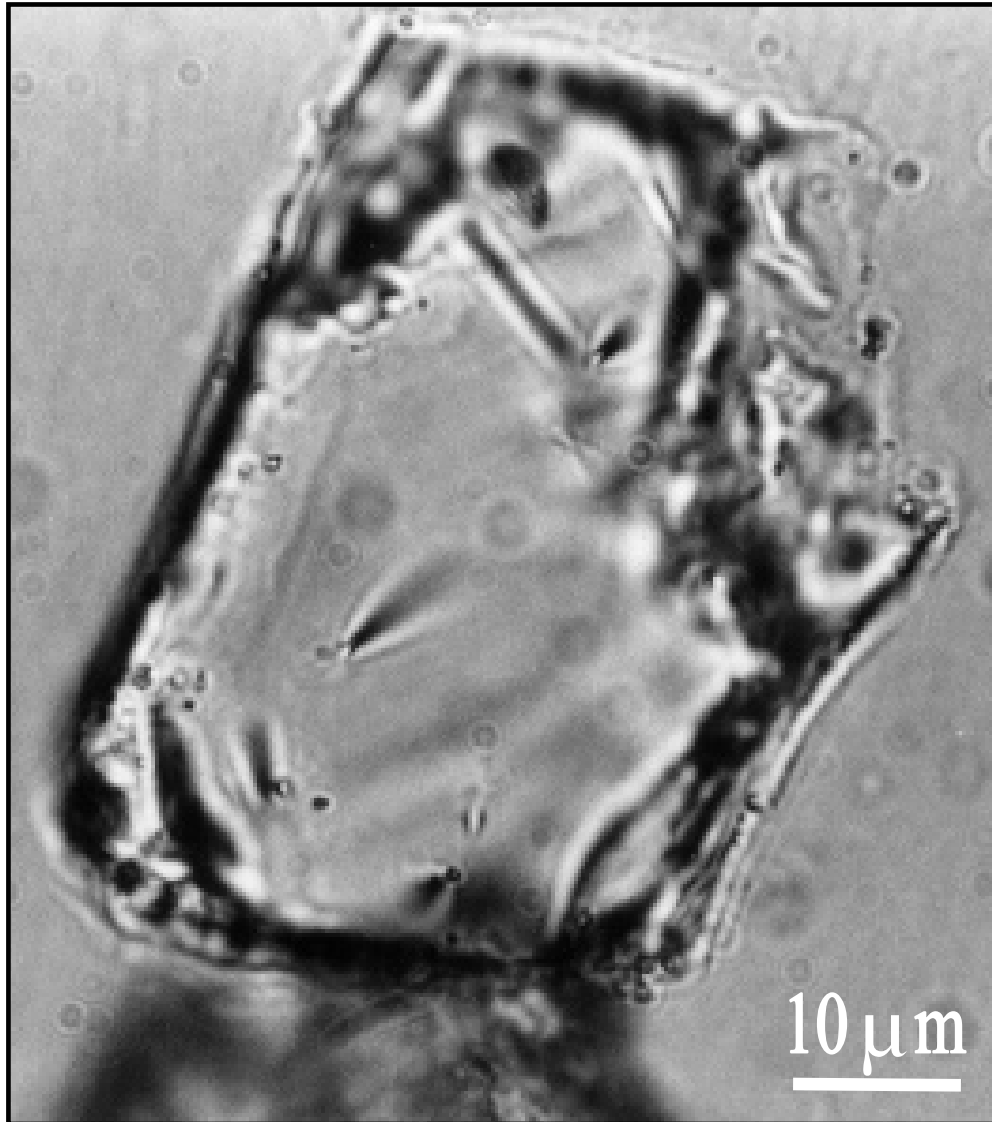


Figure 68. Etched fission tracks confined in the basal plane of an apatite grain observed with oil immersion (etchant: 65% HNO_3 at 20 °C for 15s). 10 μm across grain (image courtesy of Shari A. Kelley <http://www.ees.nmt.edu/Geol/Structure/fission.JPG>).

Fission tracks vary in type, size, shape, mean track length, geometry and density. There are both latent tracks and etched tracks. There are two types of etched tracks that can be considered for track-length investigations: those which are spontaneous and cut the mineral surface to record an age; and those which are confined by the crystal interior, due to existent tracks or cleavage planes (Wagner and Van den Haute, 1992).

FISSION TRACK		
MINERAL	CLOSURE TEMPERATURE	REFERENCES
Apatite	$\sim 100 \pm 20^\circ \text{C}$	Dickin, 1997 Faure, 1986
Zircon	$\sim 175 \pm 25^\circ \text{C}$	Dickin, 1997

$^{40}\text{Ar}/^{39}\text{Ar}$		
MINERAL	CLOSURE TEMPERATURE	REFERENCES
Biotite	$\sim 280 \pm 40^\circ \text{C}$	McDougall and Harrison, 1999
Muscovite	$\sim 320 \pm 40^\circ \text{C}$	McDougall and Harrison, 1999
Hornblende	$\sim 525 \pm 25^\circ \text{C}$	McDougall and Harrison, 1999

Figure 69. Closure temperatures for retention of fission tracks. (Modified from Dickin, 1997; McDougall and Harrison, 1999; Faure, 1986).

The closure temperatures for fission tracks are generally below those of conventional isotope geochronometers, making them particularly useful in determining cooling histories and low-temperature events. The closure temperatures for fission tracks are basically the temperatures at which the fission tracks are retained in the mineral (Dodson, 1973). For apatite, specifically, it is the temperature at which the fission tracks are retained and no longer annealed or healed. When the temperature of a mineral exceeds its closure temperature, the fission tracks anneal. Once the temperature of the mineral decreases, the fission tracks are retained and the mineral tracks are closed. When

a mineral anneals, it undergoes partial to complete erasure of tracks (Naeser, 1979). The closure temperature for apatite is $\sim 100^{\circ} \pm 20^{\circ}\text{C}$ (Figure 69) (Faure, 1986; Dickin, 1997; Wolf et al., 1996).

The apatite fission-track ages in Precambrian basement rocks reflect the low temperature cooling history of the basement. Mean track length and distribution can differ depending on the cooling history (Figure 70). For example, it was found that with longer mean track length and a smaller variance in track-length distribution, the resultant ages were older, signifying that the rock underwent a pulse of cooling, rather than a long duration of cooling (Figure 70 (e) and (f)). On the other hand, track-length data, which indicates that the fission tracks were partially annealed, is indicative of younger tracks and a longer cooling span in the Partial Annealing Zone (PAZ) (Figure 70 (g) and (h)). The Partial Annealing Zone (PAZ), formerly known as the “Zone of Partial Stability (for apatite)”, is a wide range of temperatures over which the track annealing gradually increases (Figure 71(a)). The base of the PAZ corresponds to the 100°C paleoisotherm (Figure 71(a)) and within a relatively stable geologic environment, the apatite fission-track (AFT) age and track length decrease systematically with depth (Kelley et al., 2000). The PAZ can be preserved and if not affected by later thermal events, can be exhumed and exposed on the surface (Figure 72). The cooling is affected by uplift and denudation, rotation and post-volcanism isotherm relaxation (Kelley et al., 1992). In order to relate AFT ages to exhumation, it must be assumed that no episodic heating of the area has occurred (Wagner and Van den Haute, 1992).

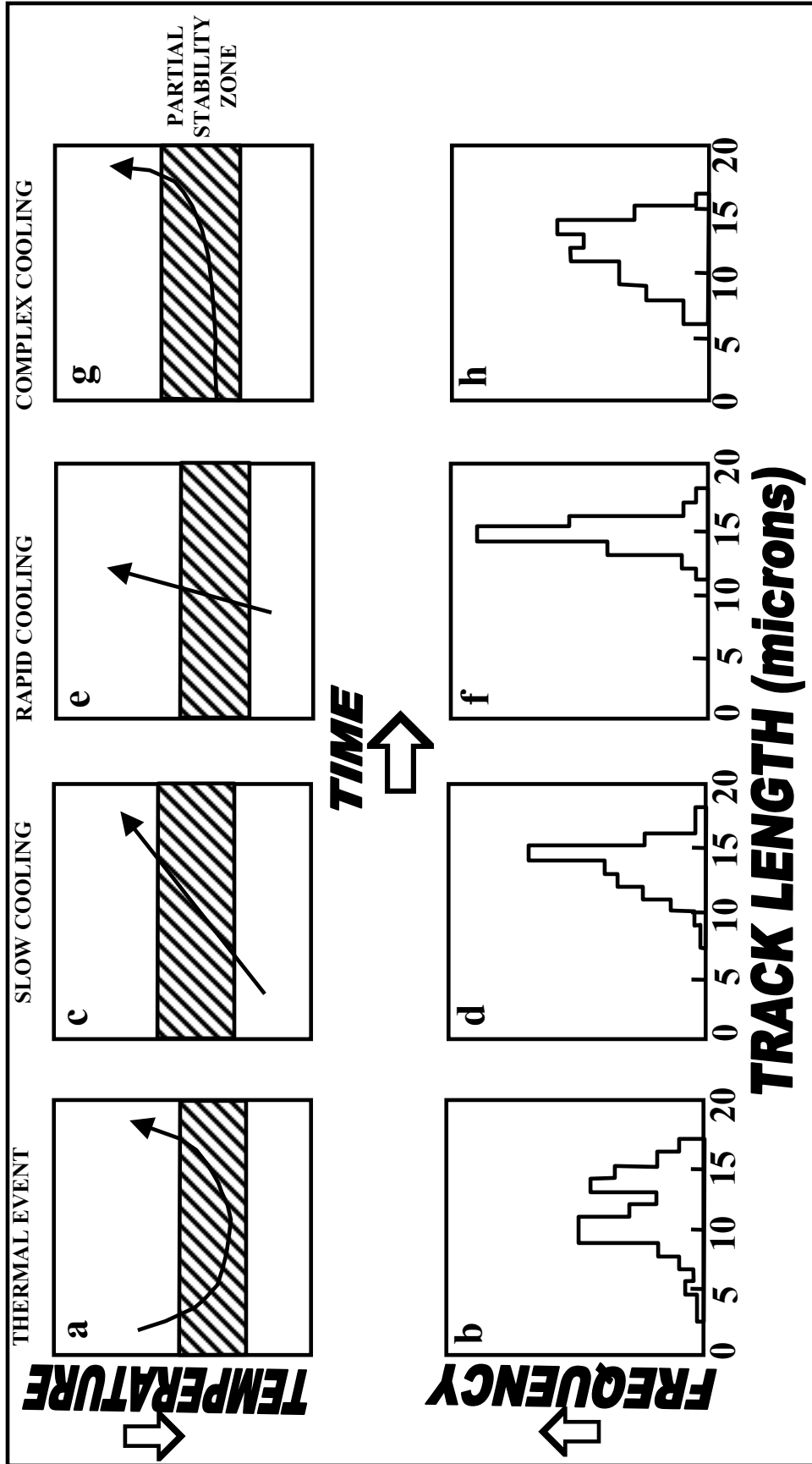


Figure 70. Hypothetical time-temperature curves (a,c,e&g) showing associated resultant track-length patterns and distributions (b,d,f&h) (modified after Kelley, 1990).

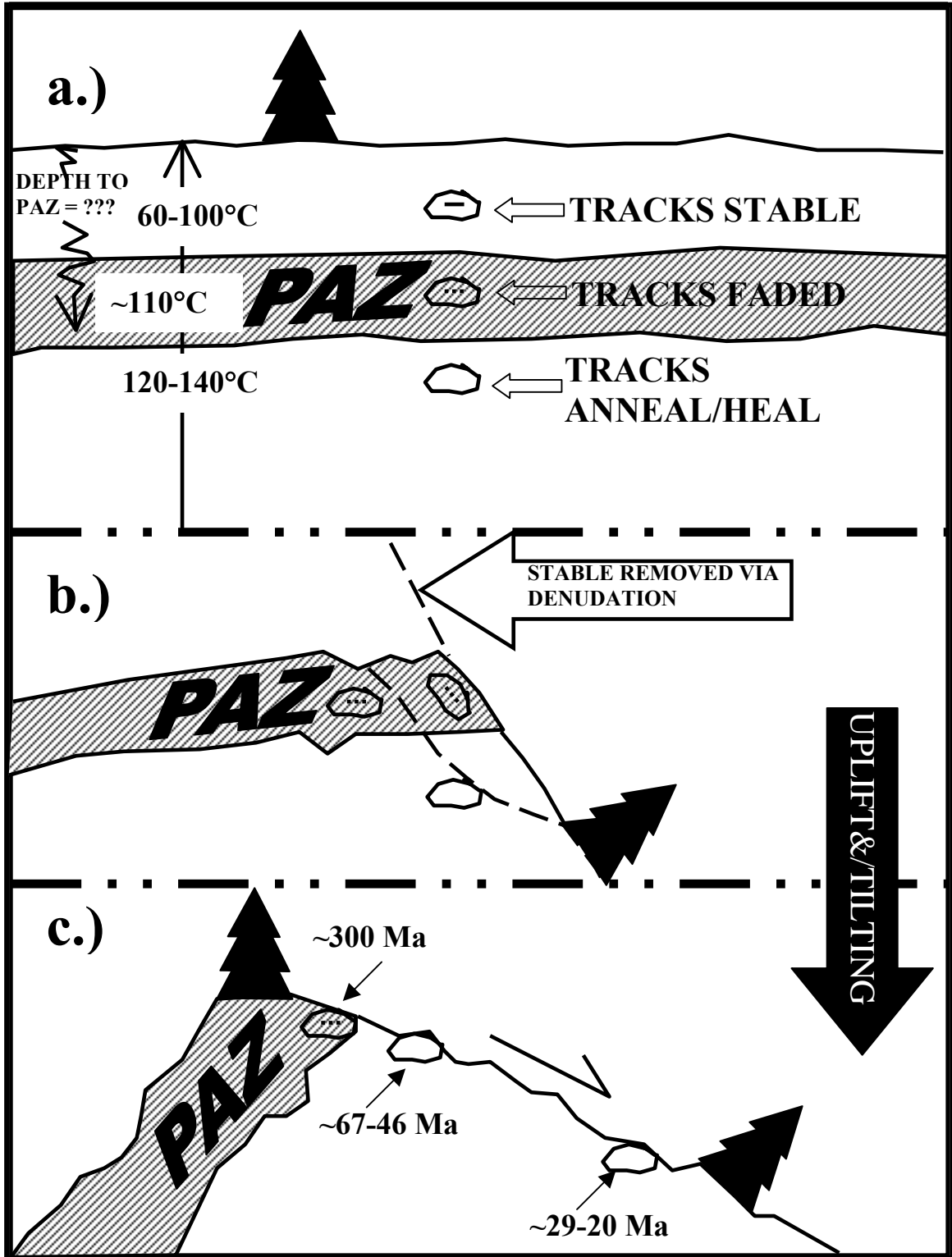


Figure 71. Cartoon depiction of formation, preservation and exhumation of the PAZ. a.) Some tracks annealed in PAZ at ~110°C; b.) denudation to expose a PAZ; c.) uplifting & tilting.

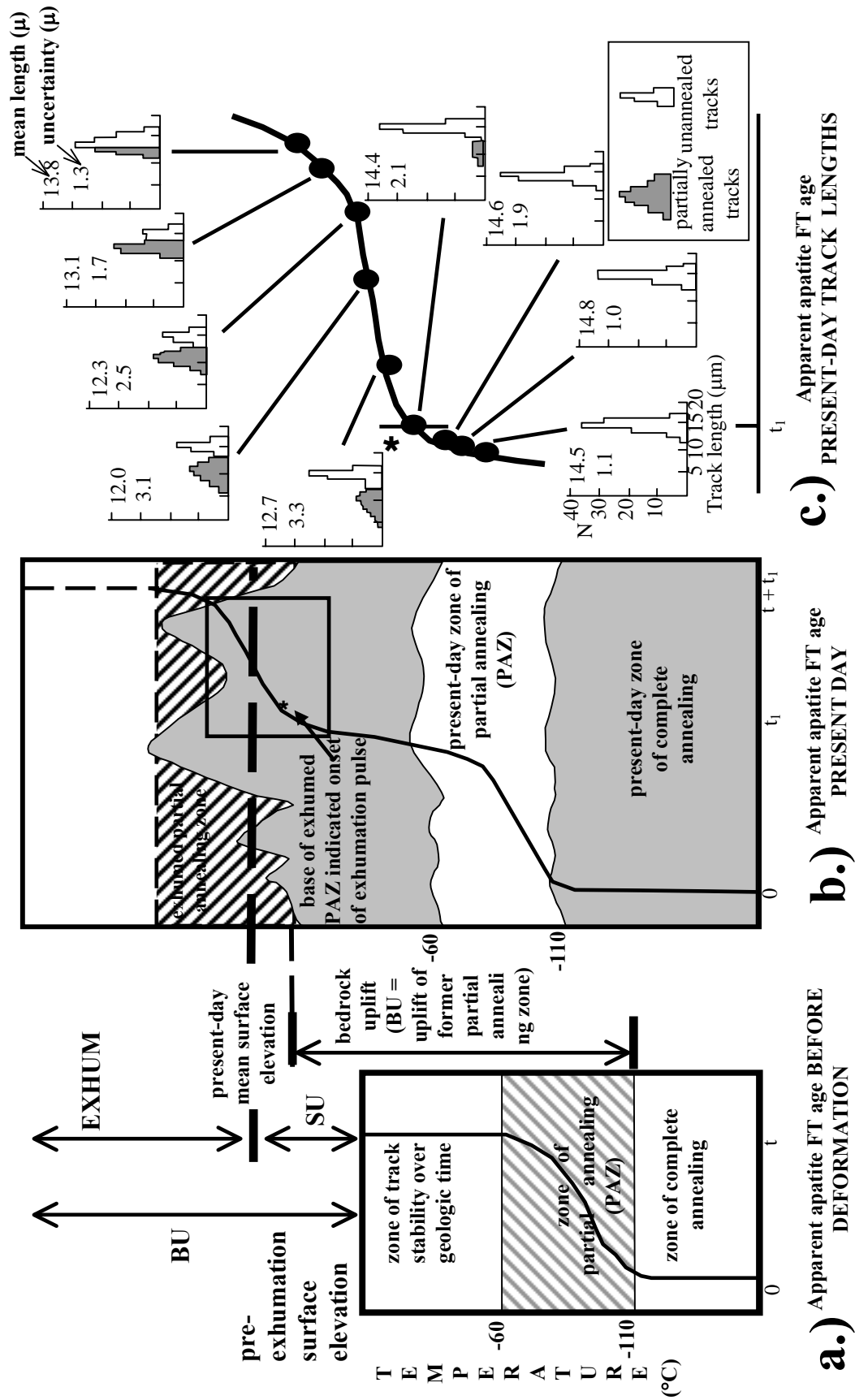


Figure 72. Apatite fission-track dating utilizing the Partial Annealing Zone (PAZ) before deformation (a.), present day (b.) and present day resultant track length distributions (c.) showing how to estimate denudation, exhumation (EXHUM), surface uplift (SU) and bedrock uplift (BU) (modified after Burbank and Anderson, 2001).

Apatite, $\text{Ca}_5(\text{PO}_4)_3(\text{F},\text{Cl},\text{OH})$, is a common accessory mineral in a wide array of rocks. It can be found within ore veins, metamorphic schists and gneisses, sediments, both volcanic and plutonic igneous rocks. Because of the diversity of this mineral, it is frequently used in fission-track dating (Wagner and Van den Haute, 1992). Fission tracks in apatite can help determine uplift rates and erosion rates (when combined with geothermal gradient estimates), regional uplift trends and time constraints, for both fault movement and uplift (Wagner and Reimer, 1972).

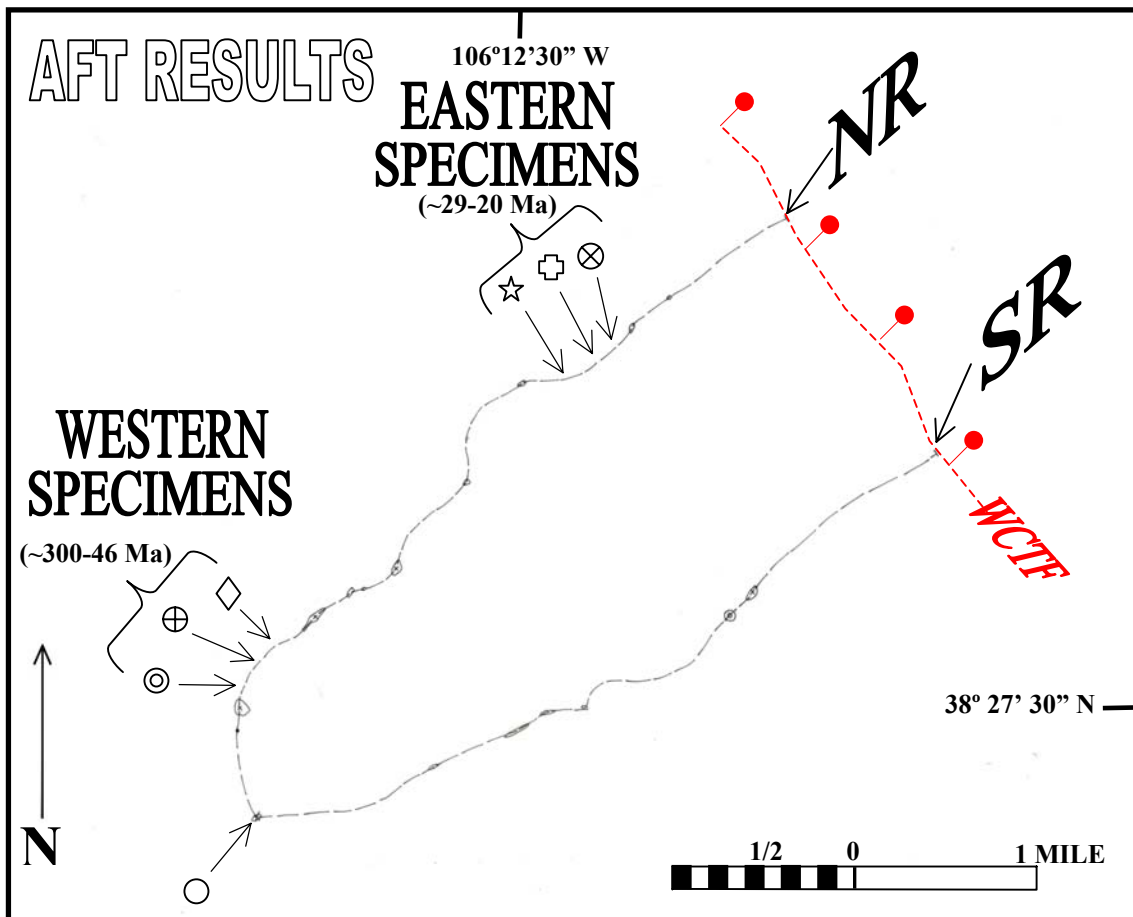


Figure 73. Simplified Geologic Map showing sample locations along ridgelines relative to the range/basin-bounding fault (WCTF). Refer to Table 4 for sample location symbols and resultant Apatite Fission-Track (AFT) ages.

RESULTS

Samples were harvested from prominent emplaced outcrops based on lithology and neighboring structures. There were two samples harvested from the western highest elevations and the SR specimen (SR399) was omitted and the NR specimen (NR1799) was selected to be age-dated given that the other specimens were all located on the NR. Only one igneous specimen was age-dated (NR17*99) and found to be similar in age to other igneous rocks of the northern Sawatch Range (Church and Bickford, 1971). The apatite grains were age-dated at New Mexico Tech by Shari A. Kelley and found to be of roughly two sets of apparent apatite fission-track (AFT) ages: ~20-29 Ma along the eastern margin (Figures 73, 74, & 75; Table 4) down near the basin-bounding fault; and ~46-299 Ma, up in the western high elevations (Hubbard et al., 2001) (Figures 73, 74 & 76; Table 4). This AFT age and length data imply that these apatite mineral grains cooled through the cooler range of temperatures (100-150°C) following the regional dynathermal metamorphism and deformational event and were succumbed to three separate episodes of cooling. The timing of the exhumation of the footwall of these ridgelines, within the southern Sawatch Mountains of the southern Rocky Mountains in south-central Colorado, were exhumed at ~300, ~67-46 and ~29-20 Ma.

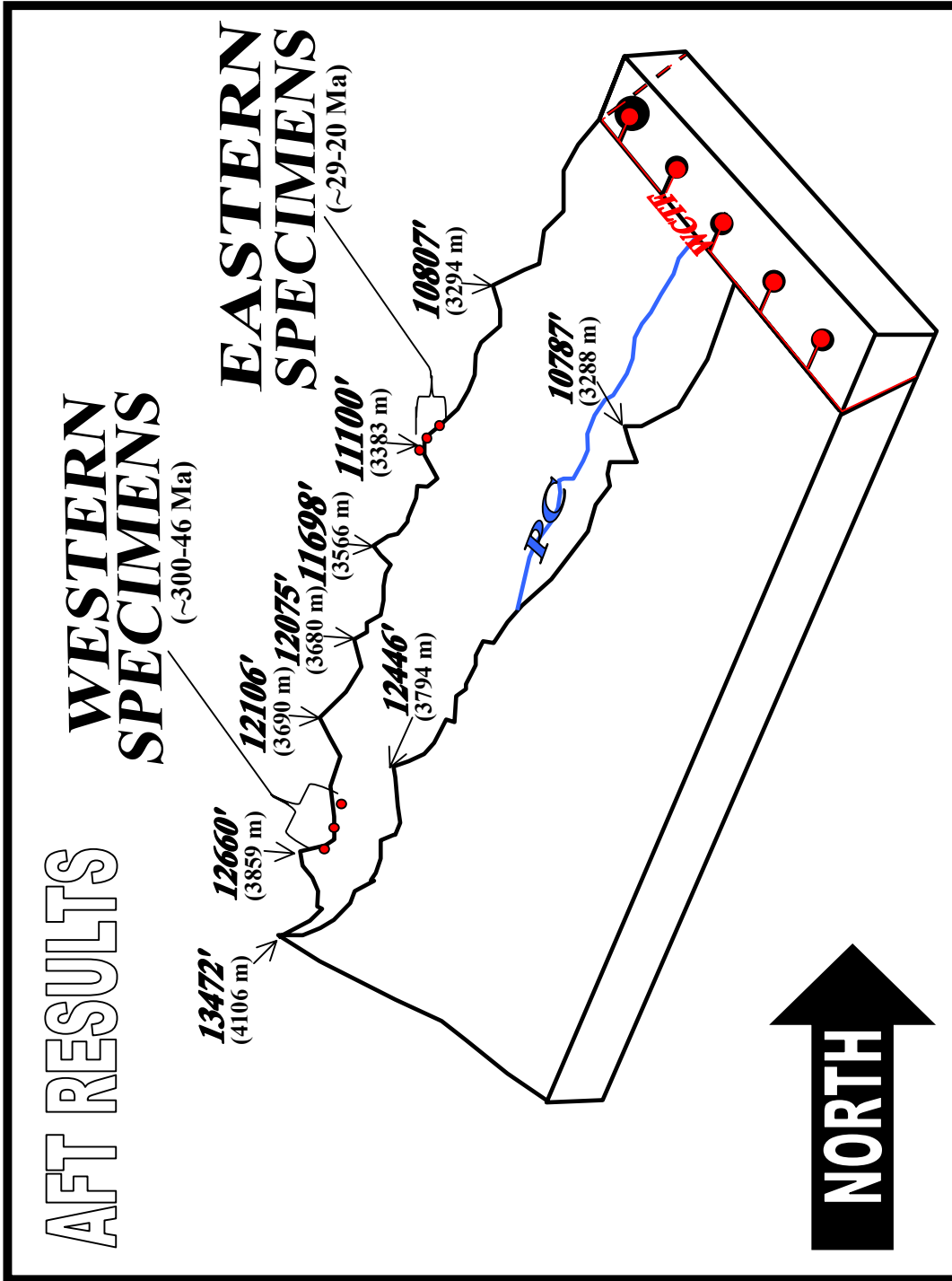


Figure 74. Simplified Orthogonal Cartoon Block Diagram Geologic Cross-section looking ~west-northwest, showing the Apatite Fission-Track (AFT) sampling locations and resultant ages for western high elevations and eastern low elevations.

The resultant apatite fission-track (AFT) ages varied along the ridgelines. The oldest ages were in the western high elevations (whe), with one of the apatites (NR1899) contained an age of roughly 300 Ma (299.6 ± 23.3 Ma), which corresponds with the late Paleozoic to early Mesozoic (middle Pennsylvanian to early Permian) Ancestral Rockies Orogeny (Figures 76). Throughout these oldest-exhumed rocks in the western high elevations (Figures 23, 24 and 35), there were two AFT ages of ~40 Ma and ~60 Ma

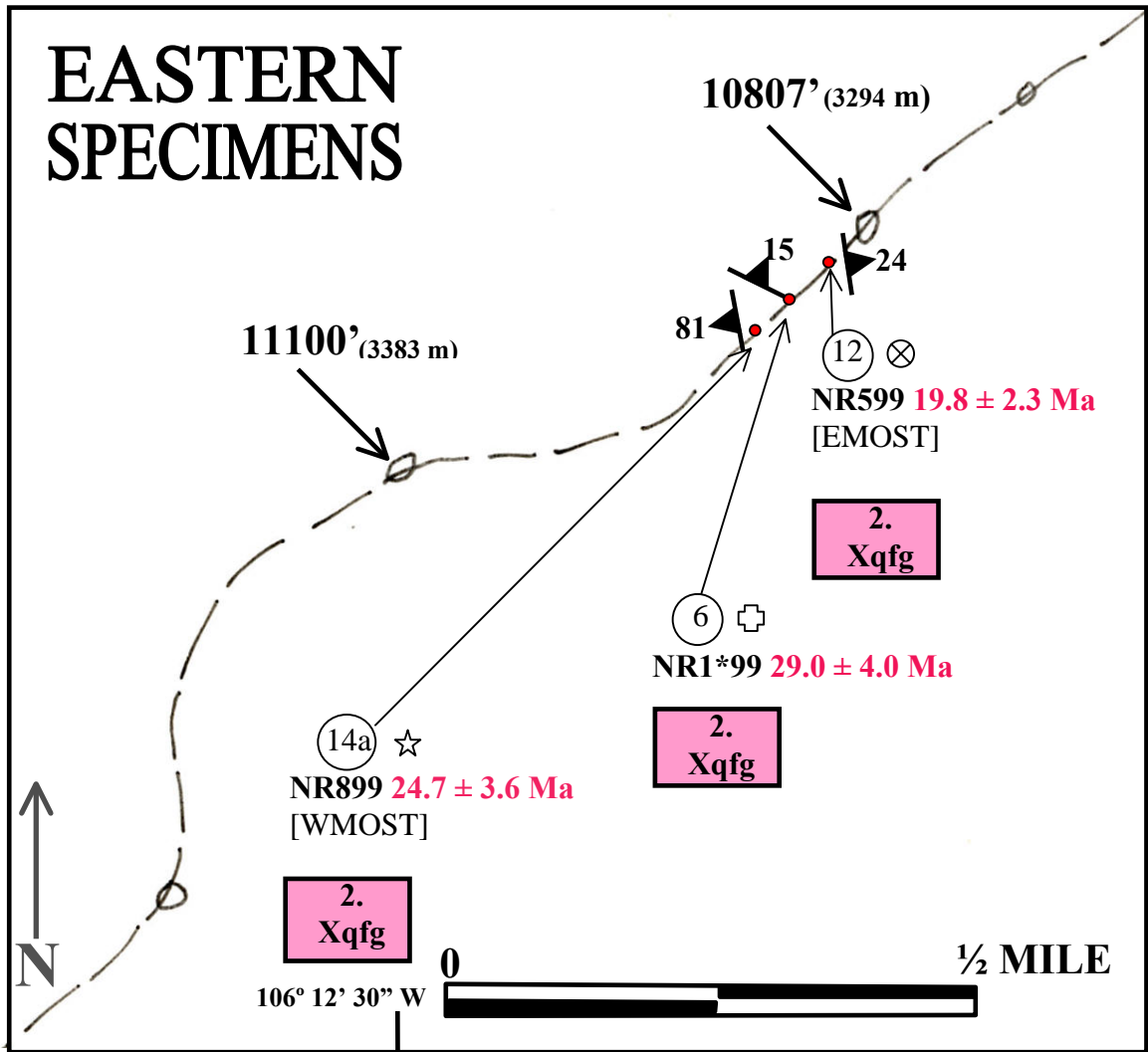


Figure 75. AFT results for the eastern low elevations, showing distribution along the ridgeline by location number, symbol, petrologic specimen, resultant age and lithologic unit.

(46.2 ± 4.6 Ma and 67.3 ± 7.9 Ma) of the apatites of a quartzofeldspathic gneiss unit (NR1799) and an intrusive unit (NR17*99), respectively. These ~40 Ma and ~60 Ma specimens coincide with being exhumed during the late Cretaceous to early Tertiary episode of compression and transpression along the western margin of North America, during the Laramide Orogeny (Figure 76). The youngest ages were within the easternmost specimens (NR599, NR1*99 and NR899), located at eastern low elevations

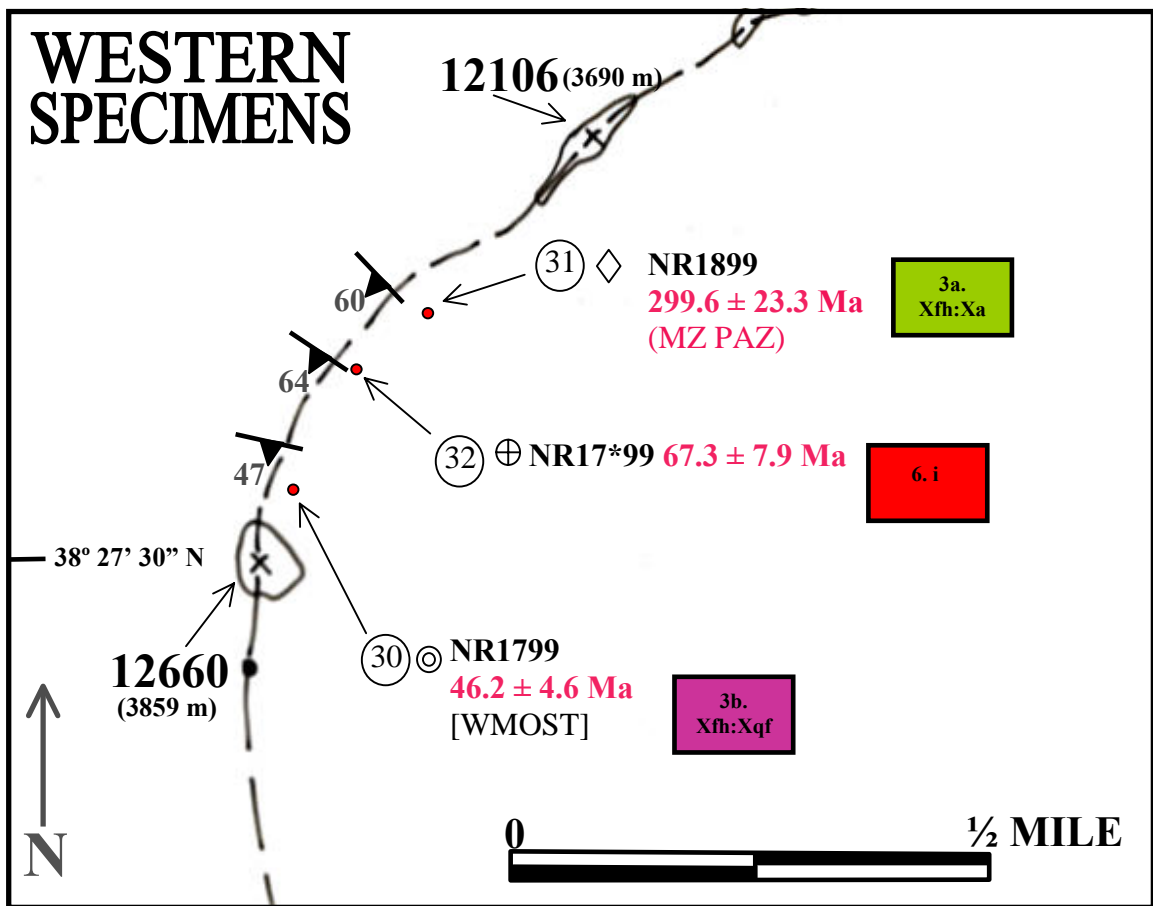


Figure 76. AFT results for the western high elevations.

(ele's) near the WCTF, adjacent to the Rio Grande rift flank. The apatites in these quartzofeldspathic gneissic rocks (19.8 ± 2.3 , 29.0 ± 4.0 and 24.7 ± 3.6 Ma) were

exhumed approximately 22 Ma and coincide with the earliest phases of rifting (20-29 Ma) that occurred during the late Oligocene to early Miocene extensional event, forming the Rio Grande rift (Figure 75). The rifting began about 30 Ma and continues into the present (Chapin and Cather, 1994; Kluth and Schaftenaar, 1994).

The mean (confined) track lengths convey cooling rates. Longer tracks (*asymmetric* track-length distribution) indicate slow cooling ($\sim 1\text{-}5^\circ\text{C}/\text{Ma}$) (Figure 70 (d)), while the longest tracks (*symmetric* track-length distribution) indicate rapid cooling, $\sim 5\text{-} >10^\circ\text{C}$ (Figure 70 (f)). Shortened tracks were affected by a thermal event and were not completely erased (Figure 70 (b)).

The eastern low elevation specimens (NR599, NR1*99 and NR899), closest to the basin-bounding fault, were determined to be of Oligocene to early Miocene age, reflecting cooling that followed volcanism in the area. Given the mid-12 to low $13\mu\text{m}$ ($12.6\text{-}13.5\mu\text{m}$) range and tracks of less length, these specimens did not undergo a rapid cooling ($>14\mu\text{m}$) (Figure 70 (f)), but rather a slow cooling ($\sim 1\text{-}5^\circ\text{C}/\text{Ma}$) through the PAZ or perhaps, a reheating by the Oligocene episode of volcanism (Figure 70 (d)).

The specimens in the western high elevations displayed two different trends. First, the westernmost specimens (NR1799 & NR17*99) (Figure 23) yielded Laramide cooling ages, exhibited short mean track lengths of $\sim 12\text{-}13\mu\text{m}$, and were likely partially reset during volcanism (Figure 70 (b)). Second, specimen NR1899 (Figure 23) yielded the shortest mean track lengths ($10.2 \pm 2.9 \mu\text{m}$) and an old anomalous age. Given that specimen NR1899 was found in the lowest elevation (of the western high elevations) and closer to the fault than NR1799 & NR17*99, it should have contained longer track lengths and be younger than or the same age as, the aforementioned specimens.

However, due to the contrary, it has been interpreted as containing a preserved partial annealing zone (PAZ), as indicated by the presence of a set of ancient, partially erased tracks. The base of the late Mesozoic apatite PAZ, both preserved and exposed on the surface of crystalline rocks, roughly corresponds to the 110°C paleoisotherm. This could possibly be due to the specimen residing within the PAZ for some time, cooling very slowly (~1 °C/Ma) (Kelley, personal communication) (Figures 70 (h), 71 & 72). This Proterozoic basement was cooler and buried more shallowly, which allowed preservation of the PAZ in the subsurface where heat and deep burial was not pronounced enough to destroy and erase this feature. The base of the Mesozoic PAZ, similarly, was also found to be preserved in the Front Range (Kelley et al., 2000). The Laramide AFT ages, at higher elevations to the west (from below the base of the PAZ), mimics the pattern seen in the Front Range (Kelley and Chapin, 2002). The fission-track, east-dipping Partial Annealing Zone has also been found preserved on the eastern limb of the broad Sawatch Anticline, in the southern Mosquito Range (north of Salida, in the Whitehorn Granodiorite) (Nehring and Geissman, 2001).

Both an “Age-vs.-Elevation” plot (Figure 77) and an “Age-vs.-Distance from Range/Basin-Bounding Fault” plot (Figure 78) were generated, based on the AFT ages derived from specimens harvested along the traverse of the ridgelines, from the basin-bounding fault (WCTF) in the eastern low elevations to the western high elevations. The apparent fission track ages increased as the distance from the basin-bounding fault within the transfer zone and the elevation to the west increased, with the exception of the preserved Mesozoic PAZ (Figures 77 & 78). The age-elevation traverse showed that the base of the apatite PAZ, which equates to the ~110°C paleoisotherm, is preserved at the

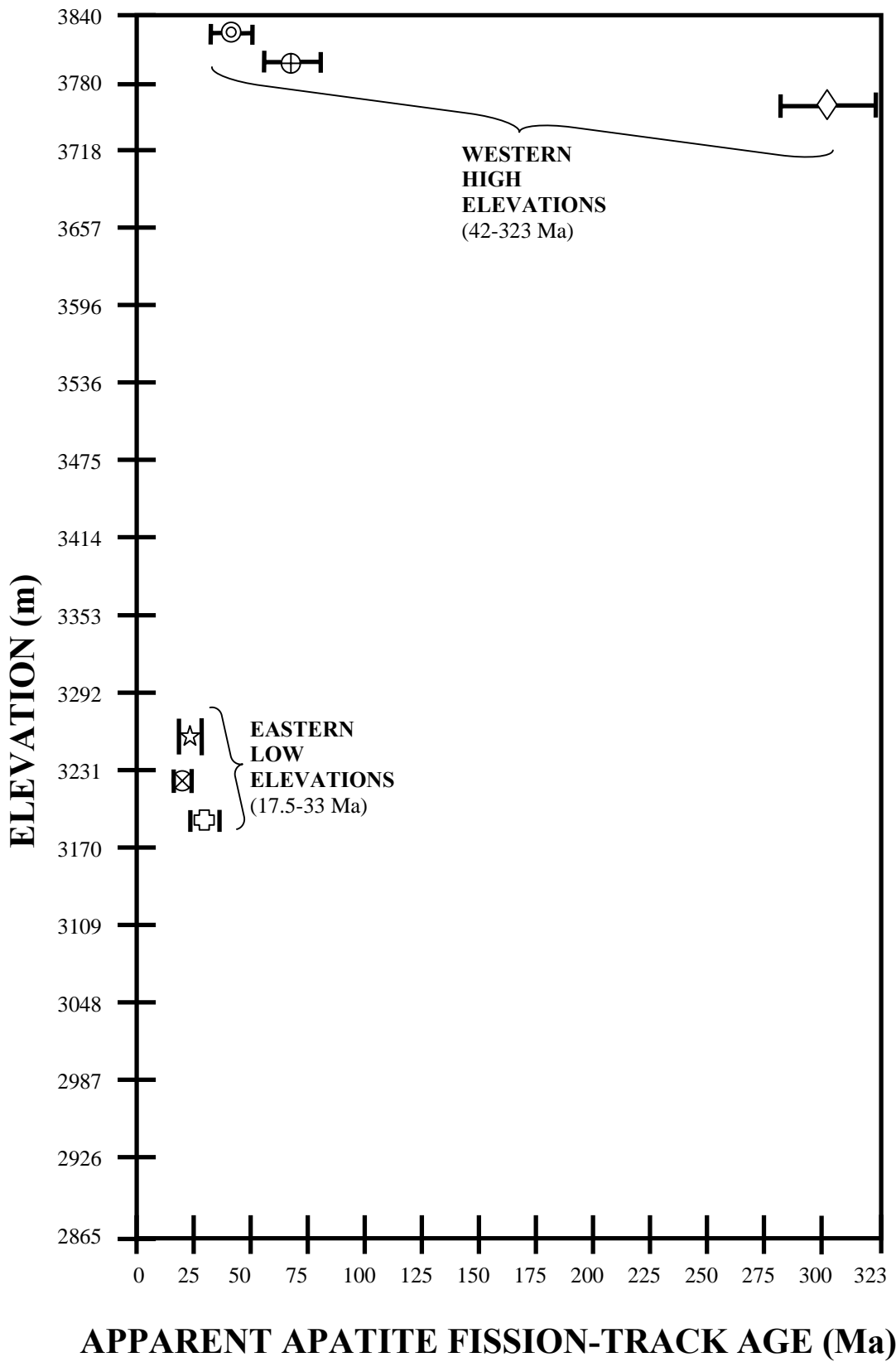


Figure 77. Age (Ma (BP)) versus Elevation (m) plot of results of AFT dating.

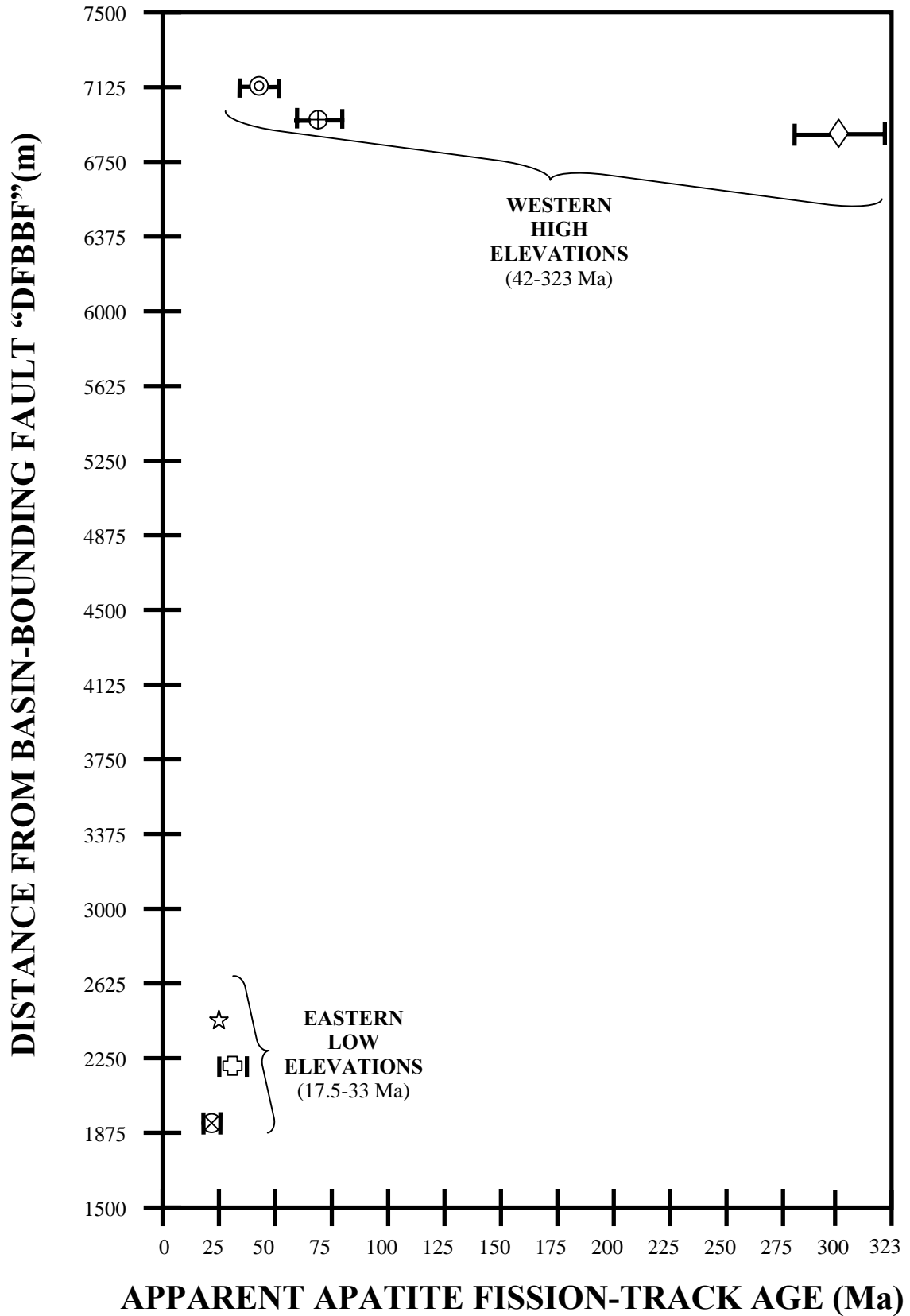


Figure 78. Age (Ma(BP)) versus Distance From Basin-Bounding Fault ("DFBBF")(m) plot of AFT results.

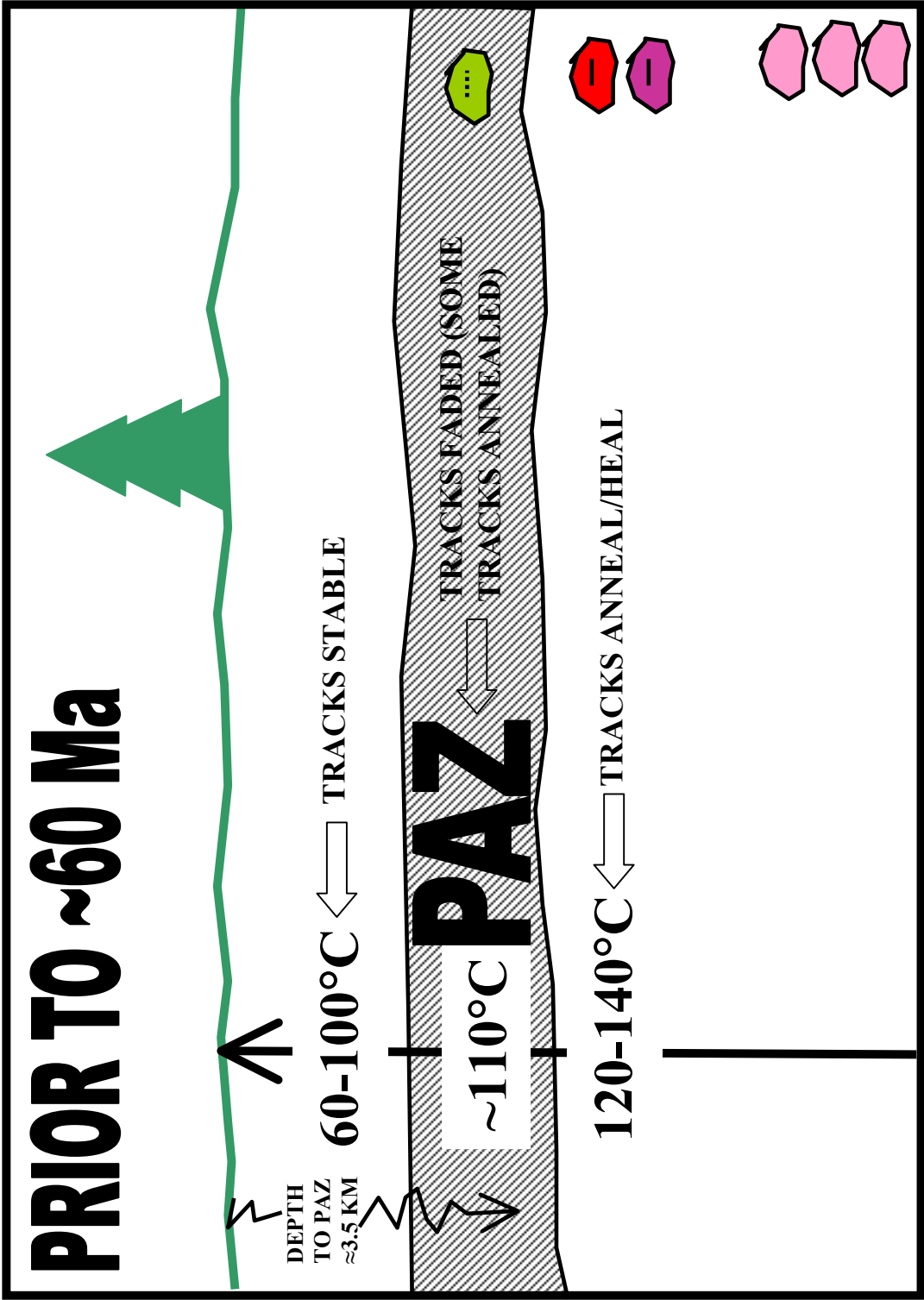


Figure 79. Explanation of results.

high elevation of ~12,360' in the footwall block.

The schematic of the AFT results (Figure 79) shows that prior to ~60 Ma (67.3 Ma) the old anomalous age specimen was in the PAZ while partially annealing the tracks created by the fission of ^{238}U (the depth of the PAZ is deduced based on the geothermal gradient of these amphibolite-facies metamorphic rocks which equates to ~3.5 km). At ~46 Ma (46.2 Ma) the adjacent specimens cooled through the PAZ and both specimens (67 Ma & 46 Ma) cooled relatively rapidly to become stable fast enough to not retain any older tracks. The youngest specimens (29-19 Ma) were still relatively deep within and annealing tracks, and not exhumed yet through and above the PAZ until ~17 Ma later.

These observed AFT age patterns are similar to the trend of rocks at higher present day elevations cooled before the rocks at lower present-day elevations resulting in the apparent ages at higher elevations being older (Kelley et al., 1992). These observed AFT age patterns were similar to those of the Mt. Princeton quartz monzonite (~30 km to the north), with older (~18–23 Ma) ages of samples from the high elevations and younger (~10–14 Ma) ages for samples closer to the basin margin (Kelley et al., 1992). The pattern found in this study could be due to the folding and tilting of the PAZ, also observed on the south side of Pikes Peak, where track lengths below the PAZ show a two-stage Laramide cooling (Leonard et al., 2002) (Figure 79).

Precambrian amphibolite-gneissic rocks were collected adjacent to the Willow Creek Transfer Fault (WCTF) and within the Poncha Pass Transfer Zone (Dippold, 1999). Hornblende, biotite and muscovite grains were separated out, isotopically dated by the $^{40}\text{Ar}/^{39}\text{Ar}$ method and found to be of Precambrian age. The hornblende ages imply that these rocks have remained at temperatures lower than ~500°C (Figure 80)

$^{40}\text{Ar}/^{39}\text{Ar}$ DATA =

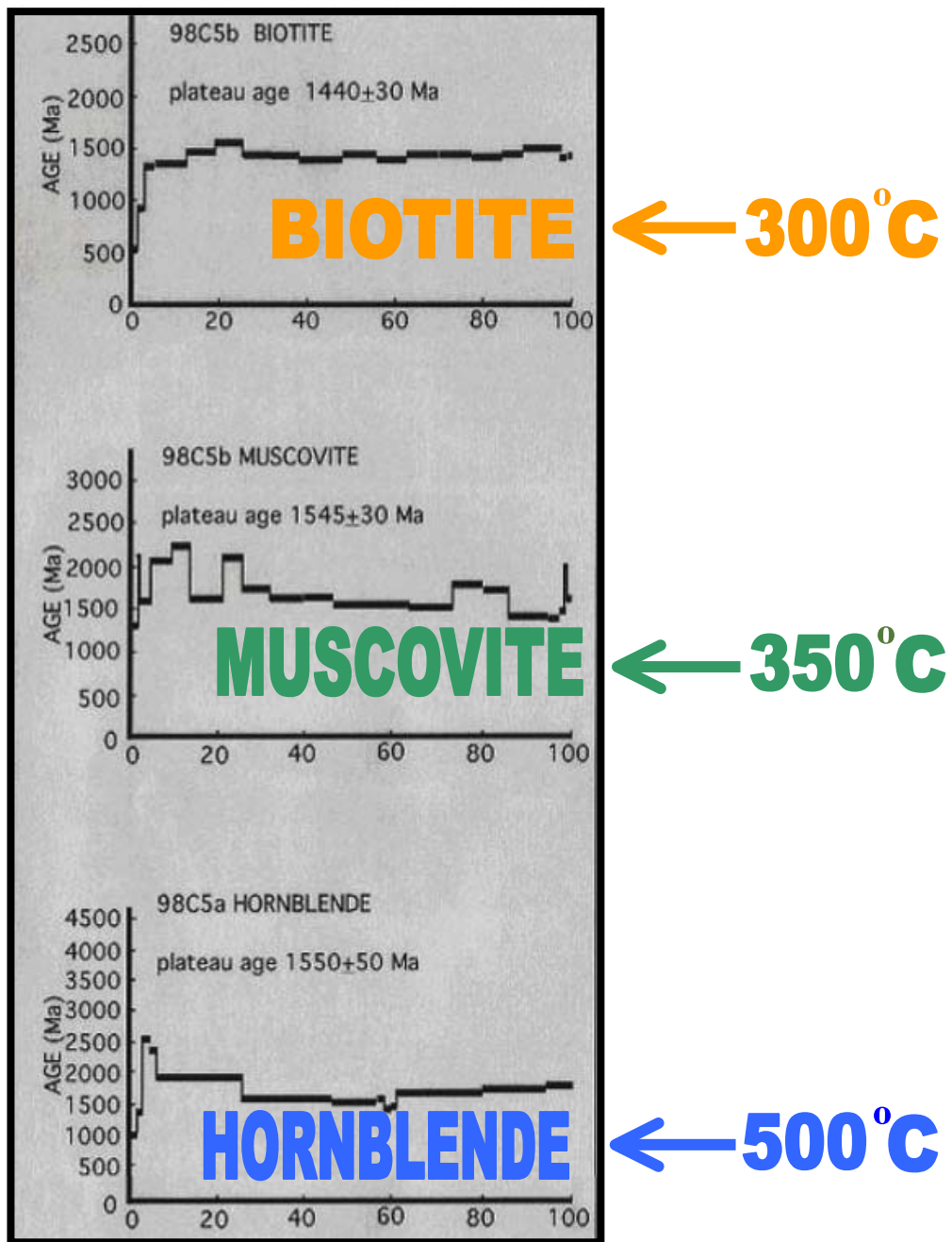


Figure 80. Dippold (1999) $^{40}\text{Ar}/^{39}\text{Ar}$ data.

since ~1600 Ma. In addition, the muscovite and biotite ages imply that these rocks have remained at temperatures lower than ~350°C and ~300°C, respectively (Figure 69), since

~1300 to ~1400 Ma (Figure 80). Following the profound heating and regional cooling at ~1600 - ~1300 Ma, these rocks have remained below ~300°C. Given the lowest temperature mineral and the geothermal gradient based on facies, these results constrain the timing and reveal that the rocks have been and imply that no heating above greenschist-facies settings (300°C at 1300 Ma) has occurred during tectonic activity throughout the Phanerozoic (Hubbard et al., 2001). These rocks had already cooled down through the extreme temperatures that existed just prior to the Paleozoic. Given the fact that these rocks have remained below 300°C since the beginning of the Paleozoic and assuming an average geothermal gradient (30°C/km), there has been minimal displacement (roughly 10 km) and throw on this northernmost basin-bounding fault (WCTF), causing the fault to remain shallower than 10 km for a long time. The rifting of the Rio Grande rift produced downdropping of the hanging wall, resulting in <10 km of footwall exhumation (Hubbard, personal communication, 2004). The thermal history of the rocks near the basin-bounding fault (WCTF) recorded a regional cooling through 300 °C following deformation and metamorphism associated with a 1.75-1.70 Ga event, all of which occurred prior to ~1300 Ma. Cooling with erosion occurred between ~1300 Ma and ~67 Ma, bringing the samples to cooler temperatures during a long period. The Laramide Orogeny exhumed and caused the rocks to cool below at least 125 °C. The rocks continued to be exhumed and remained nearly in the same crustal position following the Laramide activity. The AFT data does not support significant throw on the fault during the Laramide Orogeny, so the crustal elevation remained roughly the same between these episodes. The rock was subsequently cooled to ~110°C, forming the PAZ, and later annealed (Figure 81).

By combining the $^{40}\text{Ar}/^{39}\text{Ar}$ data with the AFT data (without the zircon FT and feldspar $^{40}\text{Ar}/^{39}\text{Ar}$ age data), a cooling curve ($^{\circ}\text{C}/\text{Ma}$) can be generated to show that, given the slope of the curve, most cooling in the last 20 Ma in this area could be attributed to normal faulting (Figure 81). The cooling rates can be deduced from the slope of the cooling curve to show slow rates with gradual portions and fast rates with steep portions.

Based on the difference in elevation and resulting apparent AFT ages of the eastern low elevations and western high elevations a rough uplift rate (aka denudation rate), during the late Laramide to early Rio Grande rifting, can be calculated and is found to be ~ 35 m/Ma. The exhumation rate can be calculated by cooling rate ($^{\circ}\text{C}/\text{Ma}$) over geothermal gradient ($^{\circ}\text{C}/\text{km}$), and in this case the value is ~ 0.033 km/Ma.

The AFT sample sites along the eastern low elevations are located southwest and up ridgeline from the proposed Pass Creek Shear Zone (3), lending no clues as to its existence. Specimen NR599, located to the east of the inferred Drainage Divide Fault (5), resulted in such a young age (19.8 ± 2.3 Ma) that motion and slip, if any, was horizontal, not vertical (which would have affected the resetting of the thermal signature). Specimen NR1*99 (29.0 ± 4.0 Ma) exhibited a slightly older age sandwiched between two relatively younger ages. This pattern may have been influenced by this proposed fault by exposing these slightly older apatites (Figure 59).

$^{40}\text{Ar}/^{39}\text{Ar}$ & AFT DATA =

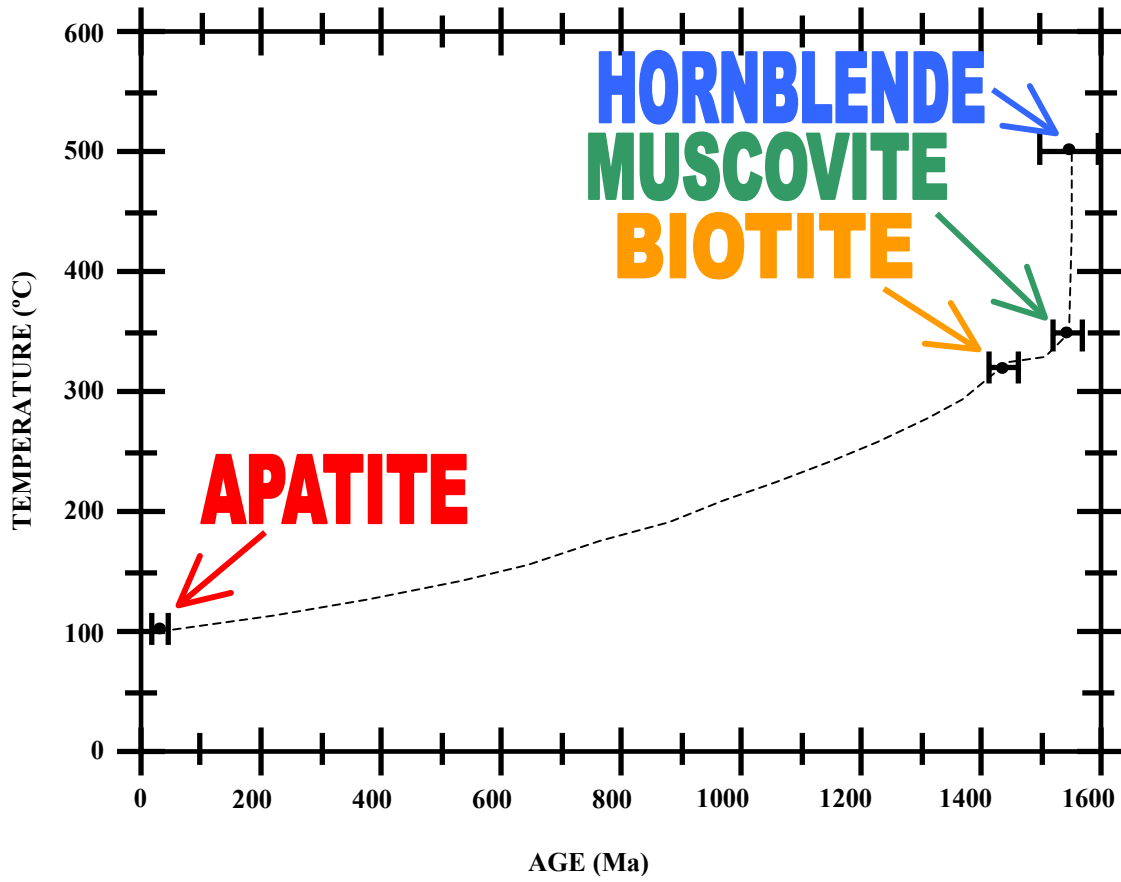


Figure 81. Cooling curve.

LOCATION (SYMBOL)	SAMPLE	AF-T AGE (Ma)	MEAN TRACK LENGTHS (μm)	LITHOLOGY	ELEVATION feet [m]	DF B-BF* km (m) <ft> {mile}
12 (⊗)	NR599	19.8 ± 2.3 Ma [18-22 Ma]	13.2 ± 2.2 [11.0-15.4]	2. Xqfg (quartzofeldspat hic gneiss)	10720' [3267m] Emost of ele of NR	1.9km (1900m) <6234'> {1.18mi}
06 (⊞)	NR1*99	29.0 ± 4.0 Ma [25-33 Ma]	13.5 ± 2.6 [10.9-16.1]	2. Xqfg (quartzofeldspat hic gneiss)	10600' [3231m]	2.15km (2150m) <7054'> {1.36mi}
14a (☆)	NR899	24.7 ± 3.6 Ma [21-28 Ma]	12.6 ± 2.7 [9.9-15.3]	2. Xqfg (quartzofeldspat hic gneiss)	10820' [3298m] Wmost of ele of NR	2.55km (2550m) <8367'> {1.58mi}
31 (◇)	NR1899	299.6 ± 23.3 Ma [276-323 Ma]	10.2 ± 2.9 [7.3-13.1]	3a. Xfh: Xa (amphibolite gneiss)	12360' [3767m] Emost of whe of NR	6.85km (6850m) <22475'> {4.26mi}
32 (⊕)	NR17*99	67.3 ± 7.9 Ma [59-75 Ma]	13.1 ± 3.6 [9.5-16.7]	6. i (intrusive)	12470' [3801m]	7.0km (7000m) <22967'> {4.35mi}
30 (⊙)	NR1799	46.2 ± 4.6 Ma [42-51 Ma]	12.4 ± 1.8 [10.6-14.2]	3b. Xfh: Xqf (quartzofeldspat hic gneiss)	12540' [3822m] Wmost of whe of NR	7.125km (7125m) <23377'> {4.43mi}
22 (○)	SR399	N/A	N/A	3b. Xfh: Xqf (quartzofeldspat hic gneiss)	13472' [4106m]	7.4km (7400m) <24279'> {4.60mi}

Table 4. AFT Results (*DFB-BF = Distance From Range/Basin-Bounding Fault (WCTF of the PPTZ of the RGr); ele = eastern low elevations & whe = western high elevations).

DISCUSSION

The field area consisted of ridgelines of Precambrian basement juvenile gneissic rocks exposed at the surface that were 1.8 to 1.6 Ga (1,800-1,600 Ma) in age. These ancient rocks were brought to the surface or exhumed through tectonics and/or erosion. Exhumation is the process described as “the uncovering or exposure by erosion of a pre-existing surface, landscape, or feature that had been buried” (Jackson, 1997), or the unroofing history of a rock caused by tectonic processes, such as normal faulting and ductile thinning, along with surficial processes (e.g. erosion) (Ring et al., 1999).

England and Molnar (1990) state that the exhumation of rocks can be determined by geothermometry coupled with the ambient geothermal gradient. Exhumation is the displacement and exposure, whereas uplift is the process by which the land surface and rock column are raised above sea level. Exhumation is the displacement of rocks with respect to the surface that involves the rock uplift (BU/Bedrock Uplift) (displacement of rocks with respect to the geoid) displacement, less the surface uplift (SU) (displacement of Earth’s surface with respect to the geoid) displacement (Figure 72a).

The rate of exhumation is simply the rate of erosion or the rate of removal of overburden by tectonic processes (England and Molnar, 1990). Exhumation of orogenic systems causes mountain chains to expose rocks formed at depth and, as exhumation proceeds, the isostatic forces cause readjustment and retrieval of rocks from depth (Ring et al., 1999). Fission-track geochronology is a temperature sensitive isotopic dating system based on the assumption that, as overburden is eroded off, the underlying host rock cools through a range of temperatures (geothermal gradient), which can yield clues to the exhumation.

The cooling ages of bedrock in the orogenic system, the cooling ages of detrital sediments and the amount of sediment removed during exhumation, can all yield clues to the evolution and exhumation of orogenic systems (Ring et al., 1999). The cooling ages of bedrock was chosen for this study, given the active tectonic setting of the Rio Grande rift. Apatite fission track (AFT) dating of minerals with lower closure temperatures, coupled with the radiometric-dating scheme of $^{40}\text{Ar}/^{39}\text{Ar}$ of high closure temperatures, allowed the thermal history to be ascertained for the southern Sawatch Range (Figure 81). Pre-rifting AFT cooling ages were preserved in rift-flank ranges, where rift-related exhumation is relatively shallow (less than 3 to 4.5 km in crustal depth). The fission tracks are annealed and erased at greater crustal depths, where the temperature exceeds 110°C (Kelley et al., 1992).

The AFT data helped constrain the timing of footwall exhumation adjacent to the range/basin-bounding fault and revealed that the earliest phases of rifting exhumed the amphibolite gneisses in close proximity to the rift. By coupling AFT data with (U-Th)/He ages in apatite, the chronology of rift-flank exhumation and deformation can be refined beyond the reconstruction, based on basin sedimentary record and footwall thermal history (House et al., 2003).

The post-Laramide ages in this region, for this field area the eastern low elevations, are thought to be influenced by the low-velocity mantle beneath the Southern Rocky Mountains and within preexistent Proterozoic crustal sutures (Pazzaglia and Kelley, 1998; Karlstrom and Humphreys, 1998).

CONCLUSION

The interlayered Precambrian gneissic rocks were subdivided into amphibolite gneiss, quartzofeldspathic gneiss and felsic hornblendic gneiss, based on microfabric analysis and mineralogical assessment. Throughout this interlayered unit of predominantly amphibolite gneiss and quartzofeldspathic gneiss, other lenses of exotic exposures (combined with igneous intrusions) gave a striped appearance to these basement rocks. Given the ductile fabric of porphyroblastic textures (having formed at temperatures greater than 400° C), the typical Barrovian high-grade amphibolite-facies assemblage of minerals (e.g. sillimanite), and the fact that fractures don't cut across the mineral boundaries, all suggest that metamorphism occurred at ~600° C, 6kbar pressure and 20 km depth.

The coincidence of the average northwest-striking and northeast-dipping metamorphic foliation and brittle structures suggests that the metamorphic foliation influenced the development of the younger structures and faulting, most notably the basin-bounding Willow Creek Transfer Fault (WCTF), during the Cenozoic extension of the Rio Grande rift. Lineations indicate normal down-dip movement on inferred faults throughout the field area, with a few dextral strike-slip slickenlines. Kinematic indicators on brittle fabrics were difficult to assess, therefore, reverse movements could not be ruled out completely.

Following the formation of the rocks within the study area, during the Paleoproterozoic (1750-1700 Ma) and at ~20 km depth, these gneissic rocks cooled through to the mid-crust (~10 km). The high-temperature minerals of hornblende, biotite

and muscovite grains cooled down through temperature ranges of 300-500°C at ~1500-1300 Ma. These basement rocks gradually moved from the mid-crust to the upper crust and, based on the geothermal gradient, surpassed the 10 km depth at the beginning of the Phanerozoic. Since the beginning of the Phanerozoic, temperatures of these rocks did not exceed the temperatures of the greenschist facies (~300°C). The western high elevations were cooled to ~100° C during the Laramide Orogeny (67-46 Ma). Apatite Fission-track data indicates that some samples resided in the Partial Annealing Zone (PAZ) prior to, and during the Laramide. The eastern low elevations, located near the Rio Grande rift, were cooled below ~100° C during the rifting episode as a result of displacement on the basin-bounding fault at ~30-20 Ma.

The Thermochronologic (AFT) data, coupled with the petrologic data and the structural constraints, convey that these rocks cooled during older deformational events (particularly the Laramide Orogeny) at the higher elevations and during the youngest and most recent event at the lower elevations. Age was found to increase with both elevation and distance from the basin-bounding fault, complying with the “age as a function of elevation” trend, where rocks found at higher elevations are older than those found at lower elevations. This is based on the premise that rocks at higher elevations cooled before rocks at lower elevations. Although it is commonly thought that these mountains were exhumed during the rifting episode, the results of this study indicate that older events also played a significant role in the exhumation and cooling.

For future analysis of this Precambrian basement, it is recommended that: remotely-sensed imagery, by applying edge enhancements, be utilized. This method of analysis can convey additional information about the metamorphic fabric and assist

researchers in accurately discerning exposures from talus. Chemical analysis of the basement could help specify the protoliths of this metagneous, metasedimentary unit. Finally, (U-Th)/He apatite ages could help further refine the exhumation and cooling history.

REFERENCES:

- Anderson, J.L., and Cullers, R.L., 1999, Paleo- and Mesoproterozoic granite plutonism of Colorado and Wyoming: *Rocky Mountain Geology*, v. 34, p. 149-164.
- Baars, D.L., and Stevenson, G.M., 1984, The San Luis Uplift, Colorado and New Mexico - An enigma of the Ancestral Rockies: *The Mountain Geologist*, v. 21, no. 2, p. 57-67.
- Barnes, F.F., 1935, The Pre-Cambrian Rocks of the Sawatch Range, Colorado, Ph.D., Northwestern University, Evanston, Illinois, 199 pp.
- Barnes, F.F., and Butler, J.W., Jr., 1935, The Pre-Cambrian rocks of the Sawatch Range, Colorado: Doctoral, Northwestern University. Evanston, IL, United States.
- Beacom, L.E., Holdsworth, R.E., McCaffrey, K.J.W., and Anderson, T.B., 2001, A quantitative study of the influence of pre-existing compositional and fabric heterogeneities upon fracture-zone development during basement reactivation, in Holdsworth, R.E., et al, eds., The nature and tectonic significance of fault zone weakening, *Journal of the Geological Society of London Special Publication*, v. 186, p. 195-211.
- Bird, P., 1998, Kinematic history of the Laramide orogeny in latitudes 35 degrees to 40 degrees north, western United States: *Tectonics*, v. 17, October No. 5, p. 780-801.
- Boardman, S.J., 1971, Precambrian Geology and Mineral Deposits of the Salida Area, Chaffee County, Colorado: Doctoral, University of Michigan, PhD Dissertation, 4 plates, 126 pp.
- Bowring, S.A., and Karlstrom, K.E., 1990, Growth, stabilization, and reactivation of Proterozoic lithosphere in the southwestern United States: *Geology*, v. 18, no. 12, p. 1203-1206.
- Boyer, R.E., 1962, Petrology and Structure of the Southern Wet Mountains, Colorado: *Geological Society of America Bulletin*, v. 73, no. 9, p. 1047-1070.
- Brown, W.G., 1988, Deformational Style of Laramide Uplifts in the Wyoming Foreland: *Geological Society of America Memoir* 171, p. 1-25.
- Bryant, B., and Naeser, C.W., 1980, The significance of fission track ages of apatite in relation to the tectonic history of the Front Range and the Sawatch Range, Colorado: *Geological Society of America Bulletin*, Part I, v. 91, p. 156-164.
- Bucher, K., and Frey, M., 2002, Petrogenesis of metamorphic rocks, 7th edition, Springer-Verlag, Berlin, www.springer.de, ISBN 3540431306, QE475.A2 B84 2002, 341 pp.

Burbank, D.W., and Anderson, R.S., 2001, *Tectonic geomorphology*: Malden, Blackwell Science, 274 pp.

Burchfiel, B.C., Lipman, P.W., and Zoback, M.L., 1986, eds., *The Cordilleran orogen: Conterminous U.S.*, Geological Society of America, *The Geology of North America: Decade of North American Geology*, v. G-3, 724 pp., QE71.G48 1986.

Burrett, C. and Berry, R., 2000, Proterozoic Australia-Western United States (AUSWUS) fit between Laurentia and Australia, *Geology*, 28, 2, p 103-106.

Burrett, C., and Berry, R., 2001, A statistical approach to defining Proterozoic crustal provinces and testing continental reconstructions of Australia and Laurentia - SWEAT or AUSWUS? *Gondwana Research*, 5, 1, p 109-122.

Butler, R.W.H, Holdsworth, R.E., and Lloyd, G.E., 1997, Introduction: The role of basement reactivation in continental deformation, *in* Butler, R.W.H., Holdsworth, R.E. and Lloyd, G.E., eds., *The Role of Basement Reactivation in Continental Deformation*, *Journal of the Geological Society of London*, v. 154, part 1, p. 69-71.

Chapin, C.E., 1971, The Rio Grande rift, Part I: Modifications and additions: New Mexico Geological Society, *Guidebook 22, 22nd Field Conference Guidebook*, p. 191-201.

Chapin, C.E., and Cather, S.M., 1994, Tectonic setting of the axial basins of the northern and central Rio Grande rift, *in* Keller, G.R., and Cather, S.M., eds., *Basins of the Rio Grande Rift: Structure, Stratigraphy, and Tectonic Setting*, Geological Society of America Special Paper 291, p. 5-25.

Chapin, C.E., Cather, S.M., and Kelley, S.A., 1996, Overprinting of the Rio Grande Rift on the Laramide Southern Rocky Mountains: Geological Society of America, *Abstracts with Programs*, 28th annual meeting, v. 28, no. 7, p. 271.

Church, S.E., and Bickford, M.E., 1971, Spontaneous fission-track studies of accessory apatite from granitic rocks in the Sawatch Range, Colorado: *Geological Society of America Bulletin*, v.82, p. 1727-1734.

Davis, G.H., and Reynolds, S.J., 1996, *Structural Geology of Rocks and Regions*, 2nd edition, John Wiley & Sons, Inc., New York, QE601.D3, ISBN 0-471-52621-5, 776 pp.

Denesha, C.V., 2003, *Tertiary Faulting and Its Relation to Basin Architecture in the Upper Arkansas Basin, Northern Rio Grande Rift*, Masters Thesis, Kansas State University, 50 pp.

Dickin, A.P., 1997, *Radiogenic Isotope Geology*, Second Edition, Cambridge University Press, ISBN: 0521598915 506 pp.

Dickinson, W.R., Klute, M.A., Hayes, M.J., Janecke, S.U., Lundin, M.A., McKittrick, M.A., and Olivares, M.D., 1988, Paleogeographic and paleotectonic setting of Laramide sedimentary basins in the central Rocky Mountain region: Geological Society of America Bulletin, v.100, p. 1023-1039.

Dickinson, W.R., and Snyder, W.S., 1978, Plate tectonics of the Laramide orogeny, in Matthews, V., III, ed., *Laramide folding associated with basement block faulting in the Western United States*: Geological Society of America Memoir 151, p. 355-366.

Dippold, C.L., Goodin, D.G., Hubbard, M.S., and Oviatt, C.G., 1999, Identification of Fault Structures in the Poncha Pass Transfer Zone, northern Rio Grande rift, using field reconnaissance and NDVI of Landsat 5 Satellite Imagery (abs.): Eos (Transactions, American Geophysical Union), v. 80, p. S316.

Dippold, C.L., 1999, The Geometry and Kinematics of the Poncha Pass Transfer Zone, northern Rio Grande Rift, Southern Colorado, Masters Thesis, Kansas State University, 90 pp.

Dodson, M., 1973, Closure temperature in cooling geochronological and petrological systems: Contributions to Mineralogy and Petrology, v.40, p. 259-274.

Doe, B.R., and Pearson, R.C., 1969, U-Th-Pb chronology of zircons from the St. Kevin Granite, northern Sawatch Range, Colorado: Geological Society of America Bulletin, v. 80, p. 2495-2502.

Dueker, K., Yuan, H., and Zurek, B., 2001, Thick-structured Proterozoic Lithosphere of the Rocky Mountain Region: GSA Today, v. ?, p. 4-9.

Ehlers, E.G., and Blatt, H., 1982, Petrology Igneous, Sedimentary and Metamorphic, WH Freeman and Co., San Francisco, ??p.

England, P., and Molnar, P., 1990, Surface uplift, uplift of rocks, and exhumation of Rocks: Geology, v. 18, p. 1173-1177.

Erslev, E., and Wiechelman, D., 1997, Fault and fold orientations in the central Rocky Mountains of Colorado and Utah, in Hoak, T.E., et al., eds., Fractured reservoirs: Characterization and modeling: Denver, Colorado, Rocky Mountain Association of Geologists, p. 131-136.

Erslev, E.A., and Gregson, J.D., 1996, Oblique Laramide Convergence in the Northeastern Front Range: Regional Implications from the Analysis of Minor Faults : Geological Excursions to the Rocky Mountains and Beyond; GSA Special Publications 44, p. 1-11.

Erslev, E.A., 1993, Thrusts, Back-Thrusts, and Detachment of Rocky Mountain Foreland Arches: in Schmidt, C.J., Chase, R.B, and Erslev, E.A., eds., Laramide Basement Deformation in the Rocky Mountain Foreland of the Western United States, Geological Society of America Special Paper 280, p. 339-358.

Evans, J.P., 1998, Influence of biotite and foliation on brittle deformation of gneiss: *in* Snoke, A.W., Tullis, J., and Todd, V.R., eds., Fault-related rocks: A Photographic Atlas, Princeton University Press, p. 40-41.

Faure, G., 1986, *Principles of Isotope Geology*, Wiley, Second Edition, ISBN 0471864129, 588 pp.

Fridrich, C.J., DeWitt, E., Bryant, B., Richard, S., and Smith, R.P., 1998, Geologic map of the Collegiate Peaks Wilderness Area and the Grizzly Peak Caldera, Sawatch Range, central Colorado: United States Geological Survey Miscellaneous Investigations Series, 29 pp., 1 sheet.

Fridrich, C.J., Smith, R.P., DeWitt, E., and McKee, E.H., 1991, Structural, eruptive, and intrusive evolution of the Grizzly Peak caldera, Sawatch Range, Colorado: Geological Society of America Bulletin, v. 103, p. 1160-1177.

Gaskill, D.L., Mutschler, F.E., Kramer, J.H., Thomas, J.A., and Zahony, S.G., 1991, Geologic map of the Gothic Quadrangle, Gunnison County, Colorado, U.S. Geological Survey Map GQ-1689, scale 1:24,000.

Green, P.F., Duddy, I.R., Gleadow, A.J.W., Tingate, P.R., and Laslett, G.M., 1986, Thermal annealing of fission tracks in apatite, 1. A qualitative description: Chemical Geology (Isotope Geoscience Section), v.59, p.237-253.

Gries, R.R., 1983, Oil and Gas Prospecting Beneath the Precambrian of Foreland Thrust Plates in the Rocky Mountains: American Association of Petroleum Geologists Bulletin, v. 67, no. 1, p. 1-28.

Hanmer, S., and Passchier, C., 1991, Shear-sense indicators: A review: Geological Survey of Canada, Paper 90-17, 72 pp.

Hill, B.M., and Bickford, M.E., 2001, Paleoproterozoic Rocks of Central Colorado: Accreted Arcs or Extended Older Crust?: *Geology*, v. 29, no. 11, p. 1015-1018.

Hoffman, P.F., 1988, United Plates of America, The Birth of a Craton: Early Proterozoic Assembly and Growth of Laurentia: *Annual Reviews of Earth and Planetary Sciences*, v. 16, p. 543-603.

Holdsworth, R.E., Butler, C.A. and Roberts, A.M., 1997, The recognition of reactivation during continental deformation: *in* Butler, R.W.H., Holdsworth, R.E. and Lloyd, G.E.,

eds., *The Role of Basement Reactivation in Continental Deformation*, Journal of the Geological Society of London, v. 154, part 1, p. 73-78.

House, M.A., Kelley, S.A., and Roy, M., 2003, Refining the footwall cooling history of a rift flank uplift, Rio Grande rift, New Mexico: *Tectonics*, v. 22, no. 5, 1060, p. 14-1-14-18.

Hubbard, M.S., Oviatt, C.G., Kelley, S., Perkins, M.E., Hodges, K.V., and Robbins, R., 2001, Oligocene-Miocene basin formation and modification in the northern Rio Grande rift: Constraints from $^{40}\text{Ar}/^{39}\text{Ar}$, fission-track, and tephrochronology: Geological Society of America Abstracts with Programs; 2001 Geological Society of America Annual Meeting, v. 33, no. 8, paper 108-8, p. A-257.

Hubbard, M.S., and Wawrzyniec, T., 2000, Pull-Apart sub-basins of the northern Rio Grande rift and/or eastern Colorado Plateau margin, Upper Arkansas valley, Colorado: Geological Society of America Abstracts with Programs, v. 32, no. 7, p. A-42.

Hubbard, M.S., Dippold, C.L., and Oviatt, C.G., 1999, Oblique deformation patterns in ductile and brittle fabrics, Rio Grande Rift, Southern Colorado [abs.]: *Eos* (Transactions, American Geophysical Union), Spring Meeting, v. 80, no. 17, p. S339.

Hutchison, C.S., 1974, *Laboratory Handbook of Petrographic Techniques*, John Wiley & Sons, p. 16-19.

Jackson, J.A., 1997, *Glossary of Geology*, 4th Edition: American Geological Institute, 727 p.

Karlstrom, K.E., Bowring, S.A., Chamberlain, K.R., Dueker, K.G., Eshete, T., Erslev, E.A., Farmer, G.L., Heizler, M., Humphreys, E.D., Johnson, R.A., Keller, G.R., Kelley, S.A., Levander, A., Magnani, M.B., Matzel, J.P., McCoy, A.M., Miller, K.C., Morozova, E.A., Pazzaglia, F.J., Prodehl, C., Rumpel, H.-M., Shaw, C.A., Sheehan, A.F., Shoshitaishvili, E., Smithson, S.B., Snelson, C.M., Stevens, L.M., Tyson, A.R., and Williams, M.L., 2002, Structure and Lithosphere Beneath the Rocky Mountains: Initial Results from the CD-ROM Experiment: *GSA Today*, v. 12, no. 3, march, p. 4-10. http://www.colorado.edu/GeolSci/faculty/pdf/karlstrom_et_al_0302.pdf

Karlstrom, K. E., Ahall, K., Harlan, S.S., Williams, M. L., McLelland, J., and Geissman, J. W., 2001, Long-lived (1.8-1.0 Ga) convergent orogen in southern Laurentia, its extensions to Australia and Baltica, and implications for refining Rodinia, *Precambrian Research*, 111, p 5-30.

Karlstrom, K.E., Cather, S.M., Kelley, S.A., Heizler, M.T., Pazzaglia, F.J., and Roy, M., 1999, Sandia Mountains and Rio Grande Rift: Ancestry of structures (Proterozoic to Laramide) and History of Deformation, in Pazzaglia, F.J., and Lucas, S., eds., *New Mexico Geological Society Guidebook, 50th Field Conference*, Albuquerque Geology, p. 155-165.

Karlstrom, K.E., and Humphreys, E.D., 1998, Persistent influence of Proterozoic accretionary boundaries in the tectonic evolution of southwestern North America: Interactions of cratonic grain and mantle modification events: in Karlstrom, K.E., ed., Lithospheric structure and evolution of the Rocky Mountains: Part I. ,Rocky Mountain Geology, v. 33, no. 2, p. 161-179.

Karlstrom, K.E., and Bowring, S.A., 1988, Early Proterozoic assembly of tectonostratigraphic terranes in southwestern North America: Journal of Geology, v. 96, p. 561-576.

Keller, G.R., and Baldrige, W.S., 1999, The Rio Grande Rift: A Geological and Geophysical Overview: Rocky Mountain Geology, v. 34, no. 1, p. 121-130.

Keller, G.R., and Cather, S.M., 1994, Introduction, *in* Keller, G.R., and Cather, S.M., eds., Basins of the Rio Grande Rift: Structure, Stratigraphy, and Tectonic Setting, Geological Society of America Special Paper 291, p. 1-3.

Keller, G.R., Khan, M.A., Morgan, P., Wendlandt, R.F., Baldrige, W.S., Olsen, K.H., Prodehl, C., and Braile, L.W., 1991, A comparative study of the Rio Grande and Kenya rifts: Tectonophysics, v. 197, p. 355-371.

Kelley, S.A., Chapin, C.E., and Karlstrom, K.E., 2000, Laramide cooling histories of the Grand Canyon, Arizona, and the Front Range, Colorado determined from Apatite Fission-Track Thermochronology: Canyon, Arizona, and the Front Range, Colorado, *in* Young, R., ed., Grand Canyon Monograph, p. 49-51. [www.flag.wr.usgs.gov]

Kelley, S.A., and Chapin, C.E., 1997, Cooling histories of mountain ranges in the Southern Rio Grande rift based on apatite fission-track analysis - a reconnaissance survey: New Mexico Geology, v. 19, no. 1, p. 1-14.

Kelley, S.A., Chapin, C.E., and Corrigan, J., 1992, Late Mesozoic to Cenozoic cooling histories of the flanks of the northern and central Rio Grande rift, Colorado and New Mexico: New Mexico Bureau of Mines & Mineral Resources, Bulletin 145, 40 pp.

Kelley, S.A., 1991, Constraints on the timing and magnitude of a mid-Miocene hydrothermal event in the Mt. Princeton Batholith, Colorado: Geological Society of America Rocky Mountain Section Abstracts with Programs, v. 23, no. 4, p. 38.

Kelley, S.A., 1990, Late Mesozoic to Cenozoic cooling history of the Sangre de Cristo Mountains, Colorado and New Mexico: New Mexico Geological Society, Guidebook 41, p. 123-132.

Kluth, C.F., and Schaftenaar, C.H., 1994, Depth and geometry of the northern Rio Grande rift in the San Luis Basin, south-central Colorado: *in* Keller, G.R., and Cather,

- S.M., eds., Basins of the Rio Grande Rift: Structure, Stratigraphy, and Tectonic Setting, Geological Society of America Special Paper 291, p. 27-37.
- Kluth, C.F., and Coney, P.J., 1981, Plate tectonics of the ancestral Rocky Mountains: *Geology*, v. 9, p. 10-15.
- Knepper, Jr., D.H., 1974, Tectonic analysis of the Rio Grande rift zone control, Colorado: Colorado School of Mines D.S. (Doctoral?) Thesis, T-1593, 237 pp.
- Kouther, M.J.H., 1969, Geology and mineralization of the northwest part of Bonanza Quadrangle, Chaffee and Saguache, Colorado: Master's Thesis, Colorado School of Mines, Golden, Colorado. 93 pp.
- Kröner, A., Kehelpannala, K.V.W., and Kriegsman, L.M., 1994, Origin of Compositional Layering and Mechanism of Crustal Thickening in the High-Grade Gneiss Terrain of Sri Lanka: *Precambrian Research*, v. 66, p. 21-37.
- Landon, S.M., 1994, Introduction & Summary: in Landon, S.M., ed., Interior Rift Basins, American Association of Petroleum Geologists Memoir 59, Tulsa, OK, 276 p., p. 1-4=intro & p. 259-269=summary.
- Leonard, E.M., Hubbard, M.S., Kelley, S.A., Evanoff, E., Siddoway, C.S., Oviatt, C.G., Heizler, M., and Timmons, M., 2002, High Plains to Rio Grande Rift: Late Cenozoic Evolution of Central Colorado: Geological Society of America Field Guide 3: Science at the Highest Level, p. 59-93.
- Livaccari, R.F., and Perry, F.V., 1993, Isotopic Evidence for preservation of Cordilleran Lithospheric Mantle during the Sevier-Laramide Orogeny, western United States: *Geology*, v. 21, p. 719-722.
- MacKenzie, W.S., Donaldson, C.H., and Guilford, C., 1982, Atlas of igneous rocks and their textures: Halsted Press, John Wiley & Sons, New York, 148 pp.
- Marshak, S., Karlstrom, K., and Timmons, J.M., 2000, Inversion of Proterozoic extensional faults: an explanation of Laramide and Ancestral Rockies intracratonic deformation, United States: *Geology*, v. 28, p. 735-738.
- Maxson, J., and Tikoff, B., 1996, Hit-and-Run collision model for the Laramide orogeny, western United States: *Geology*, v. 24, no. 11, p. 968-972.
- McCoy, A.M., 2001, The Proterozoic ancestry of the Colorado mineral belt: Ca. 1.4 Ga shear zone system in central Colorado: MS Thesis, University of New Mexico, Albuquerque, New Mexico, 158 pp.
- McDougall, I. and Harrison, T.M., 1999, Geochronology and thermochronology by the $^{40}\text{Ar}/^{39}\text{Ar}$ method, Oxford University Press, Second Edition, Oxford, 269 pp.

Miller, M.G., 1999, Active breaching of a geometric segment boundary in the Sawatch Range normal fault, Colorado, U.S.A.: *Journal of Structural Geology*, v. 21, p. 769-776.

Moore, E.M., 1991, Southwest U.S.-East Antarctic (SWEAT) Connection: A Hypothesis: *Geology*, v. 19, p. 425-428.

Munyanyiwa, H., Hanson, R.E., Blenkinsop, T.G., and Treloar, P.J., 1997, Geochemistry of amphibolites and quartzofeldspathic gneisses in the Pan-African Zambezi belt, northwest Zimbabwe: evidence for bimodal magmatism in a continental rift setting: *Precambrian Research*, v. 81, Issue 3-4, {1 February} p. 179-196.

Myers, J.S., 1978, Formation of Banded Gneisses by Deformation of Igneous Rocks: *Precambrian Research*, v. 6, p. 43-64.

Nabelek, P.I., 1997, Quartz-sillimanite leucosomes in high-grade schists, Black Hills, South Dakota: a perspective on the mobility of Al in high-grade metamorphic rocks: *Geology*, v. 25, no. 11, p. 995-998.

Naeser, C.W., 1979, Fission-track dating and geologic annealing of fission tracks; in Jäger, E., and Hunziker, J.C., eds., *Lectures in Isotope Geology*: Springer-Verlag, New York, QE501.4.N9 L42, p. 154-169.

Naeser, C.W., 1976, Fission track dating: United States Geological Survey, Open-File Report 76-0190, 65 pp.

Nehring, S.R., and Geissman, J.W., 2001, Paleomagnetism of the Latest Cretaceous Whitehorn Granodiorite and Host Strata, Southern Mosquito Range, Colorado: *Geological Society of America Abstracts with Programs*, paper no. 5248.

Passchier, C.W., and Trouw, R.A.J., 1996, *Microtectonics*, Springer, 289 pp.

Passchier, C.W., Myers, J.S., and Kröner, A., 1990, *Field Geology of High-Grade Gneiss Terrains*: International Union of Geological Sciences, Commission on Tectonics, Springer-Verlag, Berlin Heidelberg, 150 p.

Pazzaglia, F.J., and Kelley, S.A., 1998, Large-scale geomorphology and fission-track thermochronology in topographic and exhumation reconstructions of the southern Rocky Mountains: *Rocky Mountain Geology*, v. 33, p. 229-257.

Pearson, R.C., Hedge, C.E., Thomas, H.H., and Stern, T.W., 1966, Geochronology of the Saint Kevin Granite and neighboring Precambrian rocks, northern Sawatch Range, Colorado: Geological Society of America Bulletin, v. 77, no. 10, p. 1109-1120.

Pearson, R.C., 1962, Age of Laramide porphyries near Leadville, Colorado: in United States Geological Survey Research 1962: United States Geological Survey Professional Paper 450-C, p. C78-C80.

Peterman, Z.E., and Hedge, C.E., 1968, Chronology of Precambrian events in the Front Range, Colorado: Canadian Journal of Earth Sciences, v. 5, p. 749-756.

Petrina, C.H., 1992, Influence of pre-existing structure on the development of accommodation zones in continental rifts: San Luis and Upper Arkansas valleys, Colorado, University of Maryland, ?pp.

Reed, J.C., 2000, The secret of the Colorado 14ers: Why Colorado has 14ers and surrounding states don't: Trail & Timberline Magazine (Colorado Mountain Club newsletter), no. 956; http://www.cmc.org/tnt/trail_article.aspx?id=10.

Ring, U., Brandon, M.T., Willet, S.D., and Lister, G.S., 1999, Exhumation Processes, in Ring, U., Brandon, M.T., Lister, G.S., and Willet, S.D., eds., Exhumation Processes: Normal Faulting, Ductile Flow and Erosion, Geological Society of London Special Publication, v. 154, p. 1-27.

Rooney, T.P., Riecker, R.E., and Gavasci, A.T., 1975, Hornblende Deformation Features: Geology, v. 3, no. 7, p. 364-366.

Russell, L.R., and Snelson, S., 1994, Structure and tectonics of the Albuquerque Basin segment of the Rio Grande rift: Insights from reflection seismic data: in Keller, G.R., and Cather, S.M., eds., Basins of the Rio Grande Rift: Structure, Stratigraphy, and Tectonic Setting, Geological Society of America Special Paper 291, p. 83-112.

Schmidt, C.J., and Perry, W.J., Jr., 1988, eds., Interaction of the Rocky Mountain Foreland and the Cordilleran thrust belt: Geological Society of America Memoir 171, 582 pp.

Schneider, D.A., Bickford, M.E., Schulz, K., Cannon, W., 2002, Age of volcanic rocks and syn-depositional iron-formation in northern Michigan: Implications for the tectonic setting of Paleoproterozoic iron-formations of the Lake Superior region: Canadian Journal of Earth Science, v.39, p. 999-1012.

Shannon, J.R., 1988, Geology of the Mount Aetna Cauldron Complex, Sawatch Range, Colorado [Unpublished Ph.D. dissertation]: Colorado School of Mines, Golden, CO; 434 pp.

- Shannon, J.R., 1986, The Mount Antero and California Intrusions, Chaffee County, Colorado: *in* Colorado Pegmatites: abstracts, short papers, and field guides from the Colorado Pegmatite Symposium, Modreski, P.J., Fitzpatrick, J., Foord, E.E., and Kohnen, T.M., eds., p. 84-86.
- Shaw, C.A., Karlstrom, K.E., McCoy, A., Williams, M.L., Jercinovic, M.J., and Dueker, K., 2002, Proterozoic Shear Zones in the Colorado Rocky Mountains: From Continental Assembly to Intracontinental Reactivation: Geological Society of America Field Guide 3, p. 102-117.
- Shaw, C.A., Karlstrom, K.E., Williams, M.L., Jercinovic, M.J., and McCoy, A., 2001, Electron-microprobe monazite dating of ca. 1710-1630 Ma and ca. 1380 Ma deformation in the Homestake shear zone, Colorado: Origin and early evolution of a persistent intracontinental tectonic zone: *Geology*, v. 29, p. 739-742.
- Shaw, C.A., and Karlstrom, K.E., 1999, The Yavapai-Mazatzal crustal boundary in the Southern Rocky Mountains: *Rocky Mountain Geology*, v. 34, no. 1, p. 37-52.
- Sidman, D., 1998, Geology of a Rio Grande Rift transfer zone: Poncha Pass area, south central Colorado: Senior Thesis, Kansas State University, Manhattan, Kansas, 28pp.
- Simpson, C., and Schmid, S.M., 1983, Evaluation of criteria to deduce the sense of movement in sheared rocks: *Geological Society of America Bulletin*, v. 94, p. 1281-1288, 11 figs.
- Sims, P.K., and Stein, H.J., 2001, Tectonic history of the Proterozoic Colorado province: *Geological Society of America Abstracts with Programs*, v. 33, no. 5, p. A-4.
- Snyder, D.B., Clowes, R.M., Cook, F.A., Erdmer, P., Evenchick, C.A., van der Velden, A.J., and Hall, K.W., 2002, Proterozoic Prism Arrests Suspect Terranes: Insights into the Ancient Cordilleran Margin from Seismic Reflection Data: *GSA Today*, October, p. 4-10.
- Snyder, G.L., Brandt, E.L., and Smith, V.C., 1988, Precambrian petrochemistry of the northern Park Range, Colorado, and its implications for studies of crustal derivation: *United States Geological Survey Professional Paper 1343*, 116 p.
- Soreghan, G.S., Soreghan, M.J., and Eble, C.F., 2002, How High Were The Ancestral Rocky Mountains?: *Geological Society of America Abstracts with Programs*, v.32, paper no. 22-13.
- Spencer, E.W., and Kozak, S. J., 1974, Determination of Regional Fracture Patterns in Precambrian Rocks--A Comparison of Techniques, in Hodgson, R.A., Gay, Jr., S.P., and Benjamins, J.Y., eds., *Proceedings of the International Conference on Basement Tectonics*, v. 1, no.46, p.409-415.

Stark, J.T., and Barnes, F.F., 1935, Geology of the Sawatch Range, Colorado: Colorado Scientific Society Proceedings, v. 13, no. 8, p. 467-479.

Stark, J.T., 1935, Migmatites of the Sawatch Range, Colorado : Journal of Geology, v. 43, no. 1, p. 1-26.

Steiner, M.B., 2004, Is The Colorado Plateau Responsible for the Ancestral Rockies ?: A New Look At Old Mountains : Late Paleozoic Intra-plate tectonics of the Greater Ancestral Mountains : Geological Society of America Abstracts With Programs, Rocky Mountain (56th Annual) and Cordilleran (100th Annual) Joint Meeting, v. 36, no. 4, p. 27.

Thompson, T.B., and Pulfrey, R.J., 1973, The Mount Antero Granite, Sawatch Range, Colorado: The Mountain Geologist, v. 10, no. 4, p. 117-122.

Timmons, J.M., Karlstrom, K. E., Dehler, C.M., Geissman, J.W., and Heizler, M.T., 2001, Proterozoic multistage (ca. 1.1 and 0.8 Ga) extension recorded in the Grand Canyon Supergroup and establishment of northwest- and north-trending tectonic grains in the southwestern United States, GSA Bulletin, 113, 2, p 163-180.

Tweto, O., 1987a, Rock Units of the Precambrian Basement in Colorado: United States Geological Survey Professional Paper 1321-1, 54 p.

Tweto, O., 1987b, Geologic Map of the Precambrian Basement in Colorado, United States Geological Survey Professional Paper 1321-A, Plate 1.

Tweto, O., 1979, Geologic map of Colorado: United States Geological Survey, scale 1:500,000.

Tweto, O., 1977, Nomenclature of Precambrian Rocks in Colorado: United States Geological Survey Bulletin 1422-D.

Tweto, O., 1975, Laramide (Late Cretaceous-Early Tertiary) orogeny in the Southern Rocky Mountains, in Curtis, B.M., ed., Cenozoic history of the Southern Rocky Mountains: Geological Society of America Memoir, v. 144, p. 1-44.

Tweto, O., 1961, Late Cenozoic events of the Leadville district and Upper Arkansas Valley, Colorado: United States Geological Survey, Professional Paper 424-B, Art. 56, p. B133-B135.

Tyson, A.R., Morozova, E.A., Karlstrom, K.E., Chamberlain, K.R., Smithson, S.B., Dueker, K.G., and Foster, C.T., 2002, Proterozoic Farwell Mountain-Lester Mountain suture zone, northern Colorado: Subduction flip and progressive assembly of arcs: Geology, v.30, no.10, p.943-946.

Tyson, A.R., Karlstrom, K.E., Chamberlain, K.R., Foster, C.T., Morozova, E.A., and Smithson, S.B., 2001, Paleoproterozoic Suture (?) in Northern Colorado: Insights into the Geometry and Kinematics of Continental Assembly in the Southwestern U.S. In Geological Society of America Abstracts with Programs, Annual Meeting, Session No. 185, Booth #105, Paper No. 185-0.

Van den Haute, P., De Corte, F., 1998, eds., Advances in Fission-Track Geochronology, 1996 International Workshop on Fission-Track Dating, Kluwer Academic Publishers, Dordrecht, ISBN 0-7923-4904-0, 331pp.

Van Alstine, R.E., 1971, Amphibolites near Salida, Colorado: USGS Prof. Paper, No. 750-B, pp. B74-B81.

Van Alstine, R.E., 1970, Allochthonous Paleozoic blocks in the Tertiary San Luis-Upper Arkansas graben, Colorado: in Geological Survey Research 1968, United States Geological Survey, Professional Paper 700-B, p. B43-B51.

Van Alstine, R.E., 1969, Geology and mineral deposits of the Poncha Springs NE Quadrangle, Chaffee County, Colorado: United States Geological Survey, Professional Paper 626, p. 8-21 & p. 25-30, 52 pp.

Van Alstine, R.E., 1968, Tertiary trough between the Arkansas and San Luis Valleys, Colorado: in Geological Survey Research 1968, United States Geological Survey, Professional Paper 600-C, p. C158-C160.

Van Schmus, W.R., 2003, Geology of the Western Midcontinent Basement: USArray and The Great Plains: A Pre-Earthscope Workshop, Kansas State University Department of Geology, p. 30-31.

Van Schmus, W.R., Bickford, M.E., Anderson, J.L., Bender, E.E., Anderson, R.R., Bauer, P.W., Robertson, J.M., Bowring, S.A., Condie, K.C., Denison, R.E., Gilbert, M.C., Grambling, J.A., Mawer, C.K., Shearer, C.K., Hinze, W.J., Karlstrom, K.E., Kisvarsanyi, E.B., Likiak, E.G., Reed, J.C., Jr, Sims, P.K., Tweto, O., Silver, L.T., Treves, S.B., Williams, M.L., and Wooden, J.L., 1993, Transcontinental Proterozoic provinces: *in* Reed, J.C., Jr., Bickford, M.E., Houston, R.S., Link, P.K., Rankin, D.W., Sims, P.K., and Van Schmus, W.R. eds., Precambrian: Conterminous U.S.: Geological Society of America, The Geology of North America, Decade of North American Geology, v. C-2, p. 171-334.

Wagner, G.A., and Reimer, G.M., 1972, Tectonic interpretation of apatite fission track ages: Geological Society of America Abstracts with Programs, v. 3, no. 7, p. 141.

Wagner, G.A., and Van den Haute, 1992, *Fission track dating*, Solid Earth Sciences library, Kluwer Academic Press, Boston, ed.: v. 6, 285 pp. [QE508.W34]

Wawrzyniec, T.F., Geissman, J.W., Melker, M.D., and Hubbard, M., 2002, Dextral shear along the eastern margin of the Colorado Plateau—a kinematic link between Laramide contraction and Rio Grande rifting (ca. 75 Ma to 13 Ma): *Journal of Geology*, v. 110, p. 305–324.

Williams, G.D., Powell, C.M., and Cooper, M.A., 1989, Geometry and kinematics of inversion tectonics, in Cooper, M.A., and Williams, G.D., eds., *Inversion Tectonics: Geological Society Special Publication*, Blackwell Scientific Publications, Oxford, no. 44, p. 3-15.

Williams, H, Turner, F.J., and Gilbert, C.M., 1982, *Petrography: An introduction to the study of rocks in thin sections*, second edition, Wilson, J., ed., W.H. Freeman and Company, San Francisco.

Williams, M.L., and Karlstrom, K.E., 1996, Looping P-T Paths and High-T, Low-P Middle Crustal Metamorphism: Proterozoic Evolution of the southwestern United States: *Geology*, v. 24, no. 12, p. 1119-1122.

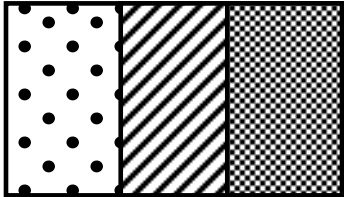
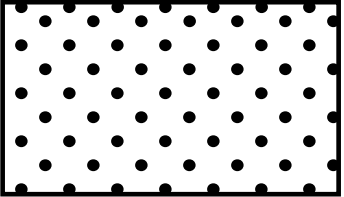
Winter, J.D., 2001, *An introduction to igneous and metamorphic petrology*, Prentice-Hall, Inc, Upper Saddle River, NJ, ISBN 0-13-240342-0; QE461.W735 2001.

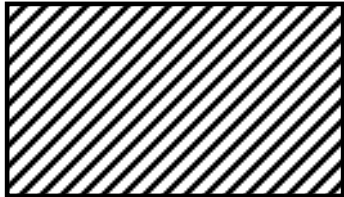
Wise, D.U., Dunn, D.E., Engelder, J.T., Geiser, P.A., Hatcher, R.D., Kish, S.A., Odom, A.L., and Schamel, S., 1984, Fault-related rocks: Suggestions for terminology: *Geology*, v. 12, p. 391-394.

Wolf, R.A., Farley, K.A. and Silver, L.T., 1996, Helium diffusion and low-temperature thermochronometry of apatite: *Geochimica et Cosmochimica Acta*, v. 60, p. 4231-4240.

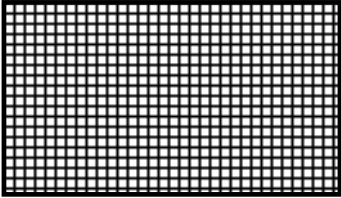
Ye, H., Royden, R.L., Burchfield, C., and Schuepbach, M., 1996, Late Paleozoic deformation of interior North America: The greater ancestral Rocky Mountains: *American Association of Petroleum Geologists Bulletin*, v. 80, p. 1397-1432.

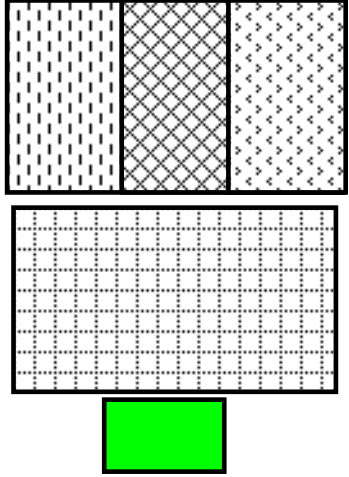
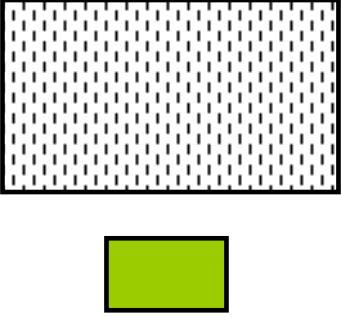
APPENDIX A: LITHOLOGIC UNITS

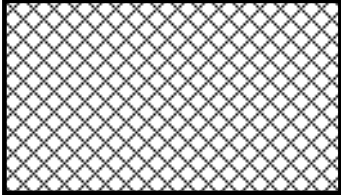
LITHOLOGIC UNIT	DESCRIPTION	NR SPECIMENS Representati ve sample in bold	SR SPECIMENS Representati ve sample in bold
 <p>1. PRECAMBRIAN AMPHIBOLITE GNEISS [Xag]</p> 	<p>AKA “BGA” (Black Gneissic Amphibolite)</p>		
<p>1a. PRECAMBRIAN AMPHIBOLITE GNEISS [Xag]: BLACK AMPHIBOLITE GNEISS [Xh]</p>  	<p>[1a. Xag; Xh] (black amphibolite gneiss/black a.g.); Xh=black blocky fine-grained amphibolite gneiss (a.g.) with very little white except quartz veins, most parallel to foliation; “hornblende gneiss”; in contact with WCTF farthest downslope in EMOST limit; upslope from the basin-bounding fault WCTF through the stumpy creek campsite & upridgeline; figures 34a-d; AKA hbgneiss (Xhb=hornblende gneiss) *black (& white) with occasional quartz (white) veins [veiny] which parallel foliation *massive and blocky *hornblendic/hornblende-rich/amphibolitic *hornblendes are fine-grained & foliated; gneissic black & white amphibolite *AKA: BAG/black</p>	<p>NR: NR2699 [hs#1/ts#1/location 78 (Figures 34b, 34c & 66)] ; location [79]; NR2599 [hs#2/location 77]; NR2499[hs#3/location76 (Figure 34a)]; & NR2199 [hs#6/location 72] (out of place?/another stripe?/float?)</p>	<p>SR: SR3899 [hs#68/location 81]; SR3999 [hs#69/location 82]; locations 68 & 67 = float?; SR2999 [hs#39/location 60] (within the 2.Xqfg but resembles 1.Xag;Xh... out of place?/another stripe?/float?)</p>

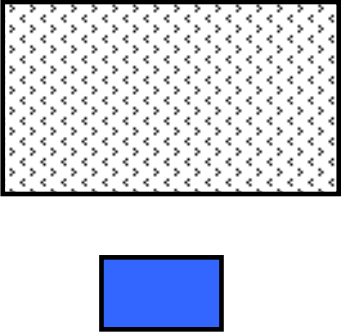
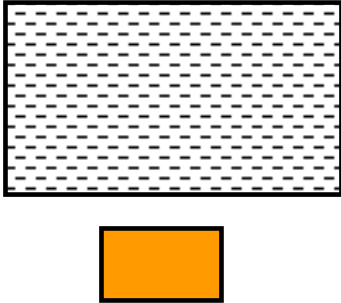
	<p>amphibolite gneiss/BGA/black gneissic amphibolite/black amphibolite/black amph./Xag/Xahg/Xhag/Xhg /PChg/PChag/PCahg/Xagh & PCh DIPPOLD: Gneissic Amphibolite : Black Amphibolite = Xh (gneissic amphibolite/hornblende gneiss) KOUTHER: PCag { amphibolite gneiss } & PCeag (epidotized amphibolite gneiss) FREDA: PCa {strikes ~NW in the N and then ~E/W in the S...similar to Dippold's change in s&d from N in the N to NW in the S...both due to CW rotation of the Colorado Plateau to the immediate W.</p>		
<p>1b. PRECAMBRIAN AMPHIBOLITE GNEISS [Xag]: GRAY COMPOSITIONALLY- BANDED AMPHIBOLITE GNEISS [Xf]</p>  	<p>[1b. Xag: Xf] (gray compositionally-banded amphibolite gneiss); Xf=thin & platy tabular (not fissile) gray compositionally-banded amphibolite gneiss (a.g.); gray gneissic amphibolite; Xqh? To Xfs; Xqfa? To Xf figure 35a-c; *compositionally-banded = gray (black & white) *flat thin platy tabular (not fissile) gray amphibolite gneiss *mica quartz hornblende amphibolite gneiss = quartz-biotite gneiss (Dippold)? *feels like a sandstone/quartzite and has an arcuate fabric AKA: [Xqhg/PCqhg] Quartzofeldspathic hornblende amphibolite gneiss [Xqfha]</p>	<p>NR: NR2399 [hs#4/ts#2/lo cation 75 (Figures 35a, 35b & 35c)]; NR2299 [hs#5/locatio n 73]</p>	<p>SR: SR3699 [hs#31/ts#14/ location 71]; location 70; SR3599 [hs#32/ts#15/ location 69]{Pf ignoring the pods}</p>

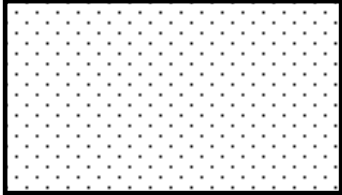
	<p>formerly “quartzhornblende amphibolite gneiss/quartzhornblende amphibolite gneiss” [Xqh] quartzofeldspathic amphibolite gneiss [Xqfa] feldspathic amphibolite gneiss/felsic amphibolite gneiss Xqh....Xqfa...Xf DIPPOLD: quartz-biotite gneiss; Xfh in NW & Xf in SE KOUTHER: PCeag, PCfqs+s[feldspathic quartz gneiss] (felsic; +silicification)</p>		
<p>1c. PRECAMBRIAN AMPHIBOLITE GNEISS [Xag]: QUARTZOFELDSPATHIC SCHIST [Xfs]</p>  	<p>[1c. Xag: Xfs] (qfschist); [Xfs = tan brittle schistose amphibolite gneiss (a.g.); figures 36a-b) *transitory unit from Xag to Xqfg”: the contact of the Xqfg to the W and Xag to the E is not precise and specific to a landform: green- redman=it’s on the E side of the 10807’ hilltop; redman-pass=it’s through the saddle, & pass- stumpy=it’s in the saddle *adjacent to prominent amphibolite/quartzofeldspat hic gneiss contact (1.Xag/2.Xqfg) *orangeish-tan glittery light-brown, orangeish- brown, schistose (not as gneissic) , brittle quartzitic amphibolite gneiss *AKA: tan schistose amphibolite gneiss/felsic schist/feldspathic schist/quartzofeldspathic schist[Xqfs/PCqfs] DIPPOLD: called Xf FREDA: PCs (Precambrian quartz-mica schist) KOUTHER: called PCqms (quartz muscovite schist)</p>	<p>NR: NR499 [hs#7/ts#3/lo cation 11 (Figure 36b)]; NR4*99 [hs#8/ts#4/lo cation 11:upridge {Pfs ignoring the pods} (Figures 41a, 41b & 41c)]</p>	<p>SR: SR3499 [hs#33/locati on 66 (Figure 36a)]; SR3399 [hs#34/locati on 66]; SR3799 [hs#35/locati on 65 {Pfs ignoring the pods} (Figure 41a)]; SR1*99 [hs#65/locati on 01]</p>

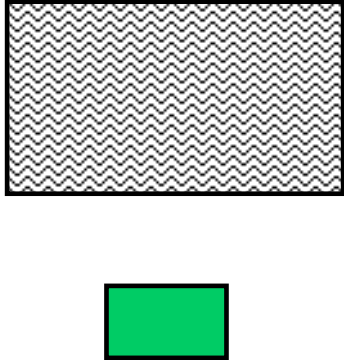
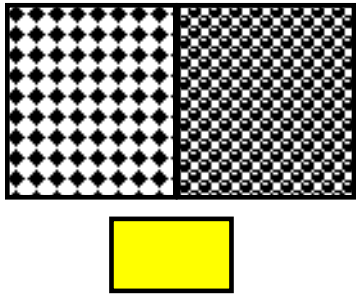
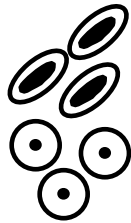
<p>2. PRECAMBRIAN QUARTZOFELDSPATHIC GNEISS [Xqfg]</p>  	<p>[2. Xqfg] (quartzofeldspathic [amphibolite?] gneiss); pinkish-tan [Xqfg/qfg/PCqfg] *surficial expression: massive & blocky AND thin, platy & wavy; *has pods on the SR at higher elevations and the podicity varies along the traverse (stretched orbs/pods formerly veins??); *silicic/felsic/leuco- {="light-colored"} *outcrops in a large area *weathers to a "pinkish- gray" to "pinkish-tan" or "orangeish-pinkish-tan" or "pink" (the weathered color tends to be gray and it is hard to decipher when traversing through the interfingering/interlayering of the amph (gray amphibolite gneiss; which also weathers to a gray hue) from the qfg stripes/fingers *granite gneiss?? (Sidman, Boyer?) DIPPOLD: Xf (or not mapped because too far upridgeline and out of field area therefore Xfh) FREDA: PCg KOUTHER: PCfqg OR PCfqF[F=float] SIDMAN: granite gneiss (gg)</p>	<p>NR: NR599 [hs#9/ts#5/ location 12/ AFTD#1/7 {separated&a ge-dated}]; & NR199 [hs#10/locati on 05]; NR1*99 [hs#11/locati on 06/AFT#2/7 (separated & age-dated)]; NR299 [hs#12/locati on 06]; NR399 [hs#13/ts#6/l ocation 07 (Figure 37c)]; NR799 [hs#15/locati on 14a]; NR899 [hs#16/locati on 14b/AFTD#3/ 7 {separated & age- dated}]; NR999 [hs#17/locati on 15] ; NR1099 [hs#18/ts#8/l ocation 19 (Figures 43c, 67a & 67b)]</p>	<p>SR: SR3299 [hs#36/locati on 64]; SR3199 [hs#37/ts#16/ location 63]; SR3099 [hs#38/ts#17/ location 61 (Figure 32)]; SR2999 [hs#39/locati on 60] (within the 2.Xqfg but resembles 1.Xag:Xh... out of place?/anothe r stripe?/float?) SR2899 [hs#40/ts#18/ location 59 (Figures 42a, 42b & 42c)]; SR2799 [hs#41/locati on 58 (Figure 37b)]; SR2699 [hs#42/locati on 57]</p>
--	---	--	---

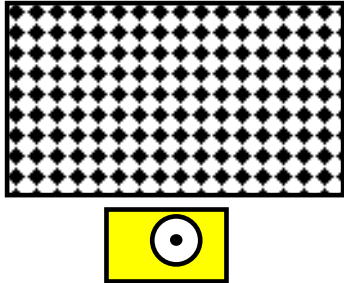
<p>3. PRECAMBRIAN FELSIC AND HORNBLENDIC GNEISS [Xfh]</p> 	<p>[3. Xfh] (felsic and hornblendic [amphibolite] gneiss); Xfh=hbf (hornblende feldspathic gneiss) *felsic/feldspathic-hornblendic/hornblende interlayered and interfingering & undifferentiated unit: 3a. Xa: Amphibolite (black, white & green gneissic amphibolite; hornblende and feldspar rich) 3b. Xqf: Quartzofeldspathic Gneiss 3c. Xfa: Feather Amphibolite Gneiss (e.g. NR1499, SR1499 & SR1599) 3d. Xhb: Hornblende Porphyroblasts 3e. Xqms: Quartz Mica Schist SIDMAN: "zebra rock" TWETO: Xfh</p>		
<p>3a. PRECAMBRIAN FELSIC AND HORNBLENDIC AMPHIBOLITE GNEISS [Xfh]: AMPHIBOLITE GNEISS [Xa]</p> 	<p>[3a. Xfh:Xa] (amphibolite gneiss); Amphibolite (black, white & green(BW&G); hornblende and feldspar rich) with subtle gneissic fabric ∴ amphibolite gneiss/gneissic amphibolite; quartz & epidote veins & dikes/intrusions with gneissic bands; EQUIVALENCIES ACROSS RIDGELINES: NR1999 & SR699</p>	<p>NR: NR1199 [hs#19/locati on 24]; NR2099 [hs#24/locati on 34 (Figure 19)]; NR1899 [hs#27/locati on 31/AFTD#5/7 {separated & age-dated}] (Figure 23); NR1699 [hs#29/locati on 29] (Figure 23); IS199 [hs#67/locati on 80("IS")]</p>	<p>SR: SR2599 [hs#43/locati on 56]; SR2299 [hs#46/locati on 53 (Figure 33)]; SR2199 [hs#47/locati on 50]; SR1999 [hs#48/locati on 48]; SR1899 [hs#50/locati on 47] {qfg-ish}; SR1699 [hs#52/ts#22/locati on 45 (Figures 33 & 38d)]; SR1399 [hs#55/locati on 43]; SR1099 [hs#57/locati on 40 (Figure 38c)]; SR599</p>

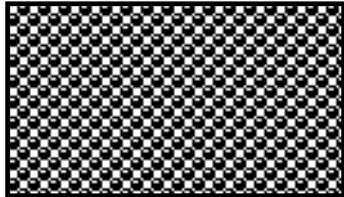
			[hs#62/locati on 35 (Figures 38a &38b)]
<p>3b. PRECAMBRIAN FELSIC AND HORNBLENDIC AMPHIBOLITE GNEISS [Xfh]; QUARTZOFELDSPATHIC GNEISS [Xqf]</p>  	<p>[3b. Xfh:Xqf] (Quartzofeldspathic Gneiss) wavy qfg</p>	<p>NR: NR1799 [hs#28/locati on 30/ATFD#6/7 {separated & age-dated} (Figures 23 & 24)]</p>	<p>SR: SR2399 [hs#45/locati on 53 (Figure 33)]; SR2099 [hs#48/ts#20/ location 49]; SR999 [hs#58/ts#24/ location 39 (Figure 38f)] SR899 [hs#59/locati on 38 (Figure 38e)]; SR799 [hs#60/locati on 37 (Figure 54)]; SR499 [hs#63/locati on 23 (Figure 38a)]; SR399 [hs#64/locati on 22/AFTD#7/7 {separated & age-dated} (Figure 21)]</p>

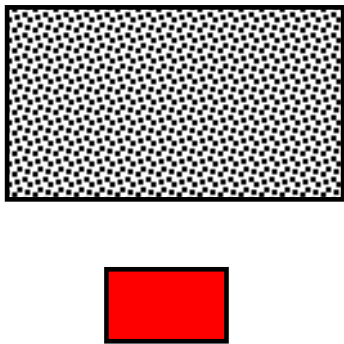
<p>3c. PRECAMBRIAN FELSIC AND HORNBLENDIC AMPHIBOLITE GNEISS [Xfh]: FEATHER AMPHIBOLITE [Xfa]</p> 	<p>[3c. Xfh:Xfa] (feather amphibolite) AKA "B&W&G AMPHIBOLITE GNEISS" (black & white & green amphibolite gneiss) Green = epidote up in core of range with interlayerings/interfingering s of qfg, amph and igneous rock bodies; amph. interlayered with wavy qfg) hornblende-feldspathic? hornblendic-feldspathic? feldspathic-hornblendic? feldspathic-hornblende?</p>	<p>NR: NR1499 [hs#23/ts#12/ location 27 (Figure 65)];</p> <p>NR1999 [hs#25/ts#13/ location 33] (Figures 38a & 38b);</p> <p>NR1599 [hs#30/locati on 28 {appeared to be Xqf in field}]</p>	<p>SR: SR2499 [hs#44/ts#19/ location 55] (Figure 33);</p> <p>SR1599 [hs#53/locati on 44];</p> <p>SR1499 [hs#54/locati on 44 (Figure 55)];</p> <p>SR699 [hs#61/ts#25/ location 36]</p>
<p>3d. PRECAMBRIAN FELSIC AND HORNBLENDIC AMPHIBOLITE GNEISS [Xfh]: HORNBLLENDE BLOBS (PORPHYROBLASTS) [Xhb]</p> 	<p>[3d. Xfh:Xhb] (amphibolite hb blobs) hornblende blobs in a fine-grained quartzofeldspathic matrix</p>	<p>NR: NR1299 [hs#20/ts#9/l ocation 25] (hbblobs1/2);</p> <p>NR1399 [hs#21/ts#10/ location 26] (Figures 43a & 43b) {hbblobs2/2}</p>	<p>SR: No SR</p>

<p>3e. PRECAMBRIAN FELSIC AND HORNBLENDIC AMPHIBOLITE GNEISS [Xfh]: QUARTZ MICA SCHIST [Xqms]</p>  	<p>3e.Xfh:Xqms (quartz mica schist "whiteschist"); Quartz Mica schist "whiteschist" Sillimanite & Quartzofeldspathic and micaceous muscovite-rich; white layered schistose lens/sliver in ridgeline traverse ;appears to be a metamorphosed pegmatitic intrusion</p>	<p>NR: NR13a99[hs #22/ts#11/location26a (Figures 44f & 44g)] AKA NR13*99 & "whiteschist")</p>	<p>SR: none</p>
---	--	---	-----------------

<p>4. CALC-SILICATE GNEISS [Xcs]</p> 	<p>“CS” [4. Xcs] (calc-silicate gneiss); (calc-silicate [amphibolite?]/quartzofeldspathic gneiss?; (AKA 4.(2a. Xqfg:Xcs (calc-silicate)) "lime-silicate" (Boardman, Boyer); *located in the qfg[Xqfg]; *iron stained with iron oxide opaques (FeO) deposited in the dissolution veins and cavities *fresh color = greenish black; biotite and chlorite; *Manitou-Fremont?? MOr DIPPOLD: altered to calcite (fizzes with HCl) and sericite like Dippold's; Dippold's was within the quartz-biotite schist; beings it's located in the zone Dippold designated as Willow Creek sheared maybe this is a product of faulting and deformation at depth of a limestone/calclitic cemented sandstone??...ancient shoreline? BOARDMAN: lime-silicate</p>	<p>NR: NR699 [hs#14/ts#7/locati ocation 14 (Figures 39a, 39b & 39c)]</p>	<p>SR: SR299 [hs#66/locati on 02]</p>
<p>5. PORPHYROBLASTIC "POD" ROCKS: [P]</p> 	<p>not Xp, but P</p> 		

<p>5a. FELSIC PODS [Pf](AMPHIBOLITE GNEISS GRAY COMPOSITIONALLY- BANDED AMPHIBOLTE GNEISS [Xag:Xf] PODS)</p> 	<p>5a.Pf(1b.Xag:Xf) PXf/Pgray c-b a.g.]; formerly Pag; located in the 1b.Xag:Xf unit; AKA: "UFO-POD SCHIST" "glitterball schist"; Xqhp {quartzhornblendic pods} /Xhp {hornblendic pods}/Xhas {hornblendic amphibolite schist} /Xqmsp {quartz muscovite schist pods}; Huge porphyroblasts 5cm diameter by 1.82 height; *quartz ufo pods flattened/squished and tabular patty-like discs; *a gradational unit or product of shear zone?; shear fabric; the "squished" pods; the pods have weathered out of the schist quite easily and many of them lay on the surface downslope and near the base of the exposure. SHAW: highly-aluminous schist (with plagioclase feldspar "ufo" pods) found in northern Sawatch/Gore Range by Colin Shaw exists on the eastern extreme of traverse</p>	<p>NR: none, west of location [73] between NR2299[73] & NR2199[72]</p>	<p>SR: SR3599 [hs#32/ts#15/ location 69 (Figures 40a & 40b)]</p>
--	---	--	---

<p>5b. QUARTZOFELDSPATHIC PODS [Pfs] (AMPHIBOLITE GNEISS [1c.Xag:Xfs] QUARTZOFELDSPATHIC SCHIST PODS)</p>  	<p>[5b. Pfs(1c.Xag:Xfs) (PXfs/Pqfschist)]; formerly Pqf; located in the Xag:Xfs unit *pinkish-tan gneiss/schist (foliated & not as banded) *product of shear zone? & shear fabric? OR relict bedding? *elongated (2.75 cm length by 1.25 cm diameter) torpedos pods/goobers *the pods have weathered out of the gneiss/schist quite easily and many of them lay on the surface downslope and near the base of the exposure; due to them laying on the surface and having a shape resembling elk turds gave rise to the phrase "elk poop gneiss"; they are elongated compared to the ufos; AKA: Xqfs (quartzofeldspathic schist)/Xqfsp (quartzofeldspathic schist pods)/ "LUMPY GOOBERS"; "ELK POOP GNEISS/SCHIST"; "elk poop pod schist"; "lumpys cored by goobers"; "good 'n plenty"; turds; green beans DIPPOLD: "masses of sillimanite { 17% total rock mass } surround rotated porphyroClasts of muscovite { 13% total rock mass }; in quartz-biotite gneiss unit"</p>	<p>NR: NR4*99 [hs#8/ts#4/location 11:upridge] AKA NR4a99</p>	<p>SR: SR3799 [hs#35/location on 65 (Figure 41a)</p>
---	--	---	---

<p>6. IGNEOUS INTRUSION/INTRUSI VE: [i]</p> 	<p>[6. i (intrusive)] (Precambrian?; Paleozoic?; Laramide/Cretaceous?; Tertiary?) *multiple igneous intrusions/intrusives {esp. pegmatites} cut through the bedrock/basement and appear as light streaks/stripes in the dark amphibolitic rock from a distance {photo 11} BOARDMAN(1971): intermediate and mafic dikes, pegmatites, aplite and quartz monzonite, trending sub-parallel with foliation and crosscutting in dip</p>	<p>NR: NR17*99 [hs#26/locati on 32/6.i (intrusive)/A FTD#4/7 {separated & age-dated} (Figure 23)]</p>	<p>SR: SR1799 [hs#51/ts#21/ location 46 (Figures 44d & 44e) (light pink graphic granitic leuco- intrusive pegmatite)]; SR1299 [hs#56/ts#23/ location 42 {pinkish intrusive} (Figures 38a, 44b & 44c)]</p>
---	---	--	--

**APPENDIX B:
HAND SPECIMENS ALONG AND ACROSS RIDGELINES**

NR HAND SPECIMENS	SR HAND SPECIMENS
NR2699 [hs#1/ts#1/location78(EMOST NR)/ 1a. Xag: Xh (black a.g.)]	SR3999 [hs#69/location 82(EMOST NR)/1a. Xag: Xh (black a.g.)]
NR2599 [hs#2/location77/1a. Xag: Xh (black a.g.)]	SR3899 [hs#68/location 81/1a. Xag: Xh (black a.g.)]
NR2499 [hs#3/location76/1a. Xag: Xh (black a.g.)]	SR3699 [hs#31/ ts#14/location 71/1b. Xag: Xf (gray c-b a.g.)]
NR2399 [hs#4/ts#2/location 75/1b. Xag: Xf (gray c-b a.g.)]	SR3599 [hs#32/ ts#15/location 69/5a.Pf (1b. Xag: Xf) (PXf/ Pgray c-b a.g.)]
NR2299 [hs#5/location 73/1b. Xag: Xf (gray c-b a.g.)]	SR3499 [hs#33/ location 66/1c. Xag: Xfs (qfschist)]
NR2199 [hs#6/location 72/1a. Xag: Xh (black a.g.)]	SR3399 [hs#34/location 66/1c. Xag: Xfs (qfschist)]
NR499 [hs#7/ts#3/ location 11/1c. Xag: Xfs (qfschist)]	SR3799 [hs#35/location 65/5b. Pfs (1c.Xag: Xfs)]

	(Pqfschist)
NR4*99 [hs#8/ts#4/location 11/5b.Pfs (1c. Xag: Xfs (Pqfschist))]	SR1*99 [hs#65/ location 01/1c. Xag: Xfs (qfschist)]
NR599 [hs#9/ts#5/ location 12/2. Xqfg/ AFTD#1/7(the only specimen thin sectioned, age dated & oriented (EMOST on NR of age date)!!]	SR299 [hs#66/ location 02/4. Xcs (calc-silicate)]
NR199 [hs#10/location 05/2. Xqfg]	SR3299 [hs#36/ location 64/2. Xqfg]
NR1*99 [hs#11/location 06/2. Xqfg/AFTD#2/7]	SR3199 [hs#37/ts#16/ location 63/2. Xqfg]
NR299 [hs#12/ location 06/2. Xqfg]	SR3099 [hs#38/ ts#17/location 61/2. Xqfg]
NR399 [hs#13/ ts#6/location 07/2. Xqfg]	SR2999 [hs#39/ location 60/2. Xqfg: Xh?]
NR699 [hs#14/ ts#7/ location 14/4.Xcs (calc-silicate)]	SR2899 [hs#40/ ts#18/ location 59/2. Xqfg]
NR799 [hs#15/ location 14a/2. Xqfg]	SR2799 [hs#41/ location 58/2. Xqfg]
NR899 [hs#16/ location 14b/2. Xqfg/AFTD#3/7]	SR2699 [hs#42/ location 57/2. Xqfg]
NR999 [hs#17/ location 15/2. Xqfg]	SR2599 [hs#43/ location 56/3a. Xfh: Xa]
NR1099 [hs#18/ ts#8/ location 19/2. Xqfg]	SR2499 [hs#44/ ts#19/location 55/3c. Xfh: Xfa]
NR1199 [hs#19/ location 24/3a. Xfh: Xa]	SR2399 [hs#45/ location 53/3b. Xfh: Xqf]
NR1299 [hs#20/ ts#9/ location 25/3d. Xfh: Xhb (amphibolite hb blobs1/2)]	SR2299 [hs#46/ location 53/3a. Xfh: Xa]
NR1399 [hs#21/ts#10/location 26/3d. Xfh: Xhb (amphibolite hb blobs2/2)]	SR2199 [hs#47/ location 50/3a. Xfh: Xa]
NR13*99 [hs#22/ts#11/ location 26a/3e.Xfh:Xqms (quartz mica schist "whiteschist")]	SR2099 [hs#48/ ts#20/location 49/3b. Xfh: Xqf]
NR1499 [hs#23/ ts#12/location 27/3c. Xfh: Xfa]	SR1999 [hs#49/ location 48/3a. Xfh: Xa]
NR2099 [hs#24/ location 34/3a. Xfh: Xa]	SR1899 [hs#50/ location 47/3a. Xfh: Xa]
NR1999 [hs#25/ ts#13/location 33/3c. Xfh: Xfa]	SR1799 [hs#51/ ts#21/location 46/6. intrusive (i)]
NR1899 [hs#27/ location 31/3a. Xfh: Xa/AFTD#5/7]	SR1699 [hs#52/ ts#22/location 45/3a. Xfh: Xa]
NR17*99 [hs#26/ location 32/6. intrusive (i))/AFTD#4/7]	SR1599 [hs#53/ location 44/3c. Xfh: Xfa]
NR1799 [hs#28/ location 30/3b. Xfh: Xqf/AFTD#6/7]	SR1499 [hs#54/ location 44/3c. Xfh: Xfa]
NR1699 [hs#29/ location 29/3a. Xfh: Xa]	SR1399 [hs#55/ location 43/3a. Xfh: Xa]

NR1599 [hs#30/ location 28(WMOST NR) /3c. Xfh: Xfa]	SR1299 [hs#56/ ts#23/ location 42/6. intrusive (i)]
	SR1099 [hs#57/ location 40/3a. Xfh: Xa]
	SR999 [hs#58/ts#24/ location 39/3b. Xfh: Xqf]
	SR899 [hs#59/ location 38/3b. Xfh: Xqf]
	SR799 [hs#60/ location 37/3b. Xfh: Xqf]
	SR699 [hs#61/ts#25/location 36/3c. Xfh: Xfa]
	SR499 [hs#63/ location 23/3b. Xfh: Xqf]
	SR399 [hs#64/ location 22/3b. Xfh: Xqf/AFTD#7/7]]
	SR599 [hs#62/location 35 (WMOST SR)/3a. Xfh: Xa]
IS (INTERRIDGE SADDLE) HAND SPECIMENS	
IS199 [hs#67/ location 80(IS)/3a. Xfh: Xa (black a.g)]	

APPENDIX C: HAND SPECIMENS

HAND SPECIMEN PETROLOGIC SAMPLE ID Petrologic Lithologic Unit (rock name) [hand specimen #/thinsection#(if applicable)/location #]	DESCRIPTION	ELSE/COMMENTS (photo#){thin section #/25 w/ %KSPAR} [color: weathered & fresh; F.G./C.G. {fine grained or coarse grained?; UPPER CASE=grain size, lower case = not grain size}]{AKA}
[1] NR2699 1a. Xag:Xh (black a.g.) EMOST NR [hs#1/ts#1/location 78]	black! fine-grained, huge amphibolite exposure blocky banded; highly weathered and dissolution occurred; quartz veins parallel to foliation and weathering along planes of foliation; dense!!! Black gneissic amphibolite with massive rhomb-like blocks; glittery & micaceous w/ biotite.	(Figures 34b, 34c & 66) {thin section #1/25 w/ ~5% KSPAR(veins)} [F.G./c.g.] [fresh=black & white{gray} (vs. weathered=gray to black)] {AKA: BGA; Hb feldspathic gneiss; Xhb: hornblende gneiss}
[2] NR2599 1a. Xag:Xh (black a.g.) [hs#2/location 77]	black! fine grained tabular black amphibolite breaks fissily and not as blocky as NR2699; quartz veins scattered and mostly along planes of	[F.G./c.g.] [weathered=brown to gray & fresh = black with greenish cast (chlorite?biotite?hornblende?) {formerly BGA; black amphibolite gneiss}

	foliation, hb stretching lineation resembles slicks (slickenslideish); micaceous & glittery platy fissile shard.	
[3] NR2499 1a. Xag:Xh (black a.g.) [hs#3/location 76]	black! similar to NR2699 blocky rhomb w/ hb grains resembling slicks; coarse-grained hornblende(hb)!	[f.g./C.G.] [weathered=black(glittery) to brown & fresh = black!! (hb rich!!)] {formerly BGA}
[4] NR2399 1b. Xag:Xf (gray c-b a.g.) [hs#4/ts#2/location 75]	fine-grained platy (not blocky!) gray [f=felsic/feldspathic] compositionally-banded (comp-banded) amphibolite gneiss; broken along contact between banding along a vein and plane of foliation; f.g. amphibolite gneiss; quartzite-like feel!!	(Figures 35a, 35b & 35c) (thin section #2/25 w/ ~30% KSPAR...KSPAR-rich!!!) [F.G./c.g.] [weathered=gray & fresh = black & white (gray)] {formerly Xqfa}
[5] NR2299 1b. Xag:Xf (gray c-b a.g.) [hs#5/location 73]	gray-tan glittery thin platy tabular slightly fissile felsic ~porphyroblastic qf amphibolite gneiss ~Xag:Xfs; ~SR3699; transitional unit from Xh into Xqfg micaceous w/ quartzite-like feel.	[f.g./C.G.] [color: weathered = dark brown to tan to gray & fresh = pinkish-orangeish-tan]
[6] NR2199 1a. Xag:Xh (black a.g.) (out of place? Another stripe? Float?) [hs#6/location 72]	thick stacked stair-stepped shard and not rhomb-like block; an amphibolite!!! Hornblende-rich and hb grains resembles slicks; quartz veins crosscut foliation.	(Figure 34a) [f.g./C.G.] [color: weathered = orangeish brown & fresh = black]
[7] NR499 1c. Xag: Xfs (qfschist) [hs#7/ts#3/location 11]	tan schistose brittle glittery micaceous qf amphibolite (not gneissic but rather schistose); with ~50% kspar + 20% quartz, 15% plagioclase & 10% muscovite&biotite (micaceous schistose matrix; ~SR3499 & SR3399.	(Figure 36b) {thin section #3/25 w/ ~50% KSPAR...k-spar richer!} [f.g./C.G.] [color: weathered = orangeish light brown & fresh = yellowish white]
[8] NR4*99 5b. Pfs(1c.Xag:Xfs) (Pqfschist: PXfs) [hs#8/ts#4/location 11:upridge]	fine-grained matrix (groundmass)!!! Pinkish-tan-gray quartzofeldspathic pod/porphyroblastic (elongate @ 2.75cm length x 1.25 cm diameter) rock with pods of dark gray sillimanite in the core mantled by a finer grained white ribbon quartz; similar to photo 61 while in dippold's field area by willow creek; micas expressed on the surface and throughout the fine-grained micaceous groundmass; maroon kspar veins throughout.	(Figures 41a, 41b & 41c) {thin section #4/25 w/ ~10% KSPAR} [F.G./c.g.] [color: weathered = pinkish-light_brown & fresh = pinkish-tan-gray] {AKA NR4a99/NR4'99; "lumpy goobers"; "good 'n plenty"; "elk poop gneiss"; Pqf}
[9] NR599 2. Xqfg (quartzofeldspathic gneiss) [hs#9/ts#5/location	quartzofeldspathic gneiss with muscovite & biotite	{thin section #5/25 w/ ~10% KSPAR; ORIENTED!!!} [F.G./c.g.] [color: weathered=maroon-orange-pink & fresh=pinkish-brown] AFTD#1/7; rock pulverized, destroyed and separated into

12/AFTD#1/7{separated & age-dated}}		mineral separates to be age-dated by the apatite fission-track dating method and found to be ~20Ma in age therefore exhumed with extension of the Rio Grande rifting episode. [the only specimen thin sectioned, age dated & oriented (EMOST on NR of age date)!!!!!!]
[10] NR199 2. Xqfg (quartzofeldspathic gneiss) [hs#10/location 05]	quartzofeldspathic gneiss.	[F.G./c.g.] [color: weathered = pinkish-brown & fresh = brownish gray]
[11] NR1*99 2. Xqfg (quartzofeldspathic gneiss) [hs#11/location 06/AFT#2/7{separated & age-dated}]	a dark amphibolite (quartzofeldspathic?) gneiss with kspar pods weathered maroon and quartz pods within an arcuate shard w/ biotite, hornblende, quartz and plagioclase feldspar.	[f.g./C.G.] [color: weathered = maroon & fresh = black!!!] AFTD#2/7; rock pulverized, destroyed and separated into mineral separates to be age-dated by the apatite fission-track dating method and found to be ~20Ma in age therefore exhumed with Cenozoic extension of the Rio Grande rifting episode.
[12] NR299 2. Xqfg (quartzofeldspathic gneiss) [hs#12/location 06]	mica hb kspar ~like NR1*99 with pods; micaceous and schistose; an arcuate chunk with flat-topped bowl-like shape; ~Xfs; stair-stepped and not too gneissic (more schistose).	[f.g./C.G.] [color: weathered = pinkish tan to maroon & fresh = gold tan brown to black]
[13] NR399 2. Xqfg (quartzofeldspathic gneiss) [hs#13/ts#6/location 07]	thin platy and fissile gray amphibolite; ~SR3599 & SR3699 feldspathic/felsic pods; radiating cluster of muscovite on top surface ~ufo-pod; gneissic with ½ way notable band and above is k-spar rich!!! And below is no k-spar (~25%kspar entire slab).	(Figure 37c) {thin section #6/25 w/ ~25%KSPAR; ORIENTED!!!} [F.G./c.g.] [color: weathered = orangeish-brown to pinkish-tan(light brown) & fresh = light gray]
[14] NR699 4.Xcs (calc-silicate) [hs#14/ts#7/location 14]	weird vuggy calc-silicate (AKA lime-silicate) amphibolite?? gneiss with a weathered dolomitic appearance & slickensides within prospect mine hole; protolith dirty quartzite?	(Figures 39a, 39b & 39c) [thin section #7/25 w/ ~2.5 %KSPAR] [f.g./C.G.] [color: weathered = grayish green & fresh = green matrix with red calcite rhombs within, AKA “Christmas/watermelon rock”]
[15] NR799 2. Xqfg (quartzofeldspathic gneiss) [hs#15/location 14a]	qfg blocky and not tabular with an arcuate face break; ~SR3299.	[F.G./c.g.] [color: weathered = yellowish tan to dark brown to pinkish orangeish gray & fresh = black & white therefore fine-grained gray-black!!]
[16] NR899 2. Xqfg (quartzofeldspathic gneiss) [hs#16/location 14b/AFTD#3/7{separated & age-dated}]	quartzofeldspathic gneiss	[F.G./c.g.] [color: weathered = pinkish-light_brown & fresh = brownish-gray] AFTD#3/7; rock pulverized, destroyed and separated into mineral separates to be age-dated by the apatite fission-track dating method and found to be ~80-40Ma in age, therefore exhumed with the compression and shortening of the

		Laramide Orogeny).
[17] NR999 2. Xqfg (quartzofeldspathic gneiss) [hs#17/location 15]	blocky qfg.	[F.G./c.g.] [color: weathered = maroon to orangeish tan & fresh = gray (black & white)]
[18] NR1099 2. Xqfg (quartzofeldspathic gneiss) [hs#18/ts#8/location 19]	quartz blobs parallel to, stretched out (36 N21W) and elongated along the plane of foliation (N45E 35SE) of metamorphic fabric.	(Figures 43c, 67a & 67b) {thin section #8/25 w/ ~<1%KSPAR} [f.g./C.G.] [color: weathered = light pink to gray to black {gray lenticular quartz blobs} & fresh = gray {fine-grained quartz matrix}]
[19] NR1199 3a. Xfh: Xa (amphibolite gneiss) [hs#19/location 24]	fine-grained blocky amphibolite!!	[F.G./c.g.] [color: weathered = brownish black & fresh = black with green epidote veins]
[20] NR1299 3d.Xfh:Xhb (amphibolite (3a. Xfh:Xa) hb blobs 1/2) [hs#20/ts#9/location 25]	hornblende blobs 1/2 like NR1399: foliated (no foliations/lineations/fabric visible?) hornblende grains in fine grained matrix; thin elongate rectangular hornblende grains.	{thin section #9/25 w/ ~1%KSPAR} [F.G./c.g.] [color: weathered = brown & fresh = black!!!]
[21] NR1399 3d.Xfh:Xhb (amphibolite (3a. Xfh:Xa) hb blobs 2/2) [hs#21/ts#10/location 26]	hornblende blobs 2/2 like NR1299: fine grained amphibolite with hornblende blobs like NR1299 downridge and adjacent; dense massive and rhomb-like blocks with quartz veins perpendicular to the plane of foliation of the hornblende blob plane & diagonal to also.	(Figures 43a & 43b) [hand specimen photo#?]) {thin section #10/25 w/~1.5%KSPAR} [F.G./c.g.] [color: weathered = brown gray & fresh = gray (black fine-grained)]
[22] NR13*99 3e. Xfh:Xqms (quartz mica schist "whiteschist") [hs#22/ts#11/location 26a] (a.k.a. NR13a99)	micaceous glittery layered schistose white intrusive with 30% quartz, 30%, plagioclase, 25% muscovite, 10% microcline, & 5% sillimanite (therefore a metamorphosed pegmatite and not a pegmatite due to schistosity!!). a mere sliver/lens with the Xfh unit. Koutner's quartz mica schist (PCqms)?	(Figures 44f & 44g) {thin section #11/25 w/~10%KSPAR (along veins on top and bottom of specimen)} [F.G./c.g.] [color: weathered = gold pink brown & fresh = white to pinkish white] [AKA NR13a99 & NR13*99] (AKA "whitie" & "whiteschist")
[23] NR1499 3c. Xfh: Xfa (feather amphibolite) [hs#23/ts#12/location 27]	feather amphibolite(f.a.)!!!; ~like NR1999; ~rhomb-like block of fine-grained groundmass/matrix and coarse grains of hornblende; faulted veins indicate normal movement	(Figure 65) {thin section #12/25 w/ ~5%KSPAR} [f.g./C.G.] [color: weathered = greenish black w/ blue & fresh = black]
[24] NR2099 3a. Xfh: Xa (amphibolite gneiss) [hs#24/location 34]	black amphibolite!! quartz and epidote blobs and veins and an arcuate fracture on small chunk/block/~cube	(Figure 19) [F.G./c.g.] [color: weathered = brownish black & fresh = black (fine-grained)]
[25] NR1999 3c. Xfh: Xfa (feather amphibolite) [hs#25/ts#13/location 27]	gray (black and white) feather amphibolite with huge crystals of hornblende and biotite (more than feather amphibolite NR1499); stair-stepped stacked thin tabular piece	(Figure 38g & 38h) {thin section #13/25 w/ ~5-10%KSPAR} [f.g./C.G.] [color: weathered = gray & fresh = black!!!]

n 33]	slightly foliated with radiating crystal clusters; big blob within sample; ~SR1599 & ~SR699	
[26] NR17*99 6. intrusive (i) [hs#26/location 32/ AFTD#4/7{separated & age-dated}]	pegmatitic igneous intrusive/intrusion	(Figure 23) [f.g./C.G.] [color: weathered = pink & fresh = pinkish white] AFTD#4/7; rock pulverized, destroyed and separated into mineral separates to be age-dated by the apatite fission-track dating method and found to be ~46-299Ma in age therefore cooled through low temperatures during the compressional late cretaceous Laramide Orogeny. (pxs [cps&opx] diposide & augite separated out)
[27] NR1899 3a. Xfh: Xa (amphibolite gneiss) [hs#27/location 31/ AFTD#5/7{separated & age-dated}]	micaceous (biotite & muscovite) amphibolite	(Figure 23) [F.G./c.g.] [color: weathered = gray & fresh = black]; AFTD#5/7; rock pulverized, destroyed and separated into mineral separates to be age-dated by the apatite fission-track dating method and found to be ~46-299Ma in age therefore cooled through low temperatures during the Ancestral Rockies Orogeny. (pxs [cps&opx] diposide & augite separated out)
[28] NR1799 3b. Xfh: Xqf (quartzofeldspathic gneiss) [hs#28/location 30/ AFTD#6/7{separated & age-dated}]	quartzofeldspathic amphibolite gneiss	(Figures 23 & 24) [F.G./c.g.] [color: weathered = pinkish-brown-orange & fresh = gray] ; AFTD#6/7; rock pulverized, destroyed and separated into mineral separates to be age-dated by the apatite fission-track dating method and found to be ~46-299Ma in age therefore cooled through low temperatures during the compressional late cretaceous Laramide Orogeny. (pxs [cps&opx] diposide & augite separated out)
[29] NR1699 3a. Xfh: Xa (amphibolite gneiss) [hs#29/location 29]	black amphibolite!! black and dense with no prominent foliation and gneissic texture; random quartz veins looks marble-like in veiny texture.	(Figure 23) [F.G./c.g.] [color: weathered = dark black (lichenated) & fresh = black!!]
[30] NR1599 3c. Xfh: Xfa (feather amphibolite) WMOST NR [hs#30/location 28]	Appeared to be a Xqf in field; dense black amphibolite with hornblende, biotite and plagioclase; ~looks like NR1699	(Figure 23) [N43W 62SW]) [f.g./C.G.] [color: weathered = brownish black (with gneissic bands) & fresh = black (with feathers)]
[31] SR3699 1b. Xag:Xf (gray c-b a.g.) [hs#31/ts#14/location 71]	thin platy tabular fissile gray compositionally-banded amphibolite gneiss (amphibolite!!).	{thin section #14/25 w/~10%KSPAR} [F.G./c.g.] [color: weathered = tannish-gray to greenish-gray & fresh = light tan]
[32] SR3599 5a. Pf(1b.Xag:Xf) PXf/Pgray c-b a.g. [hs#32/ts#15/location	amphibolite gneiss gray compositionally-banded amphibolite gneiss pod/porphyroblastic rock (AKA	(Figures 40a & 40b) {thin section #15/25 w/ ~1%KSPAR} [F.G./c.g.] [color: weathered = gray & fresh = gray with white pods within]

n 69]	fpods, ufo pods in glitterball schist) Huge (5 cm diameter x 1.82 cm height) porphyroblasts of muscovite (Dippold; does not scratch glass) with quartz (thought plagioclase initially) within and mantling; micaceous (biotite and muscovite) matrix (with hornblende) with fine grained muscovite mantling to cause weakness in matrix & cause to be easily weathered; zonation of mantling minerals quartz and muscovite; no NR specimen found.	
[33] SR3499 1c. Xag:Xfs (qfschist) [hs#33/location 66]	brittle tan glittery micaceous crumbly schistose (not gneissic) qfamph with ~75% KSPAR; ~NR499; identical to SR3399 collected at same location.	(Figure 36a) [hand specimen photo: fig 36a)] [f.g./C.G.] [color: weathered = orangeish-light brown & fresh = yellowish-white-light brown]
[34] SR3399 1c. Xag:Xfs (qfschist) [hs#34/location 66]	brittle tan glittery micaceous crumbly schistose (not gneissic) qfamph with ~75% KSPAR; ~NR499; identical to SR3499 collected at same location.	[f.g./C.G.] [color: weathered = orangeish-light brown & fresh = yellowish-white-light brown]
[35] SR3799 5b. Pfs(1c.Xag:Xfs) PXfs (Pqfschist) [hs#35/location 65]	~NR4*99 {SR1*99 [hs#65/location 01] AND SR299 [hs#66/location 02 (located between hs#35 [SR3799] & hs#36[SR3299])]; Elongate (2.75 cm length x 1.25 cm diameter) porphyroblasts	(Figure 41a) [f.g./C.G.] [color: weathered = pinkish-tan & fresh = pinkish-gray]
[36] SR3299 2. Xqfg (quartzofeldspathic gneiss) [hs#36/location 64]	blocky (compared to platy SR3199 & SR3099 upslope) & dense with cubic/block jointing/fracturing {SR1*99 [hs#65/location 01] AND SR299 [hs#66/location 02 (located between hs#35 [SR3799] & hs#36[SR3299])]; ~NR799	[F.G./c.g.] [color: weathered = pinkish-tan to whitish-pink (2 faces differ in color) & fresh = light gray]
[37] SR3199 2. Xqfg (quartzofeldspathic gneiss) [hs#37/ts#16/location 63]	a thin platy triangular chunk/shard w/ the top surface weathered along and veins paralleling foliation; ~50% quartz, 15% plagioclase & 20% microcline.	{thin section #16/25 w/ ~20%KSPAR} [F.G./c.g.] [color: weathered = maroon to pinkish-tan & fresh = light pinkish gray]
[38] SR3099 2. Xqfg (quartzofeldspathic gneiss) [hs#38/ts#17/location 61]	pink qfg [thought an intrusive pegmatite prior but grains are locked and migration along boundaries has occurred; protolith may have been an intrusive of identical mineralogy...happens to get it's name cpf by being in a trough of a possible fault]; "c.p.f." = "conspicuous ("attracting attention") pink fill" triangular flat thin platy shard that feels like a sandstone and looks like a quartzite.	(Figure 32) {thin section #17/25 w/ ~5%KSPAR throughout} [F.G./c.g.] [color: weathered = light pink to whiteish pink & fresh = light pink to whiteish pink] "cpf"="conspicuous pink fill"
[39] SR2999	dark black amphibolite!!	[F.G./c.g.] [color: weathered = brownish

2. Xqfg (quartzofeldspathic gneiss) (Xh?...float? out of place? Another stripe?) [hs#39/location 60]		black & fresh = black!!!]
[40] SR2899 2. Xqfg (quartzofeldspathic gneiss) [hs#40/ts#18/location 59]	qfg “blocks with pods” massive blocky pods; quartz mantles the kspar pod, with plagioclase, kspar and epidote also present; resemble stretched out and pinched off veins; fractures like SR3299	(Figures 42a, 42b & 42c) {thin section #18/25 w/ ~10-15%KSPAR(in both pod & matrix)} [F.G./c.g. (C.G. pods in a f.g. matrix)] [color: weathered = pinkish gray & fresh = gray to white]
[41] SR2799 2. Xqfg (quartzofeldspathic gneiss) [hs#41/location 58]	pink qfg weathers out along planes of foliation to result in a stair-stepped schistose/gneissic appearance; REPRESENTATIVE QFG SAMPLE!!!!	(Figure 37b) [F.G./c.g.] [color: weathered = orangeish pinkish tan to maroon & fresh = gray (black & white)]
[42] SR2699 2. Xqfg (quartzofeldspathic gneiss) [hs#42/location 57]	pink qfg ~identical to SR2799; last qfg of type along traverse before transitioning over to Xfh:Xqf.	[F.G./c.g.] [color: weathered = orangeish pinkish tan & fresh = whiteish pink to gray (black & white)]
[43] SR2599 3a. Xfh: Xa (amphibolite gneiss) [hs#43/location 56]	black amphibolite with epidote and quartz veins parallel to and weathered out along (on one face) the plane of foliation.	[f.g./C.G.] [color: weathered = brownish black & fresh = black & white]
[44] SR2499 3c. Xfh:Xfa (feather amphibolite) (NOT 3a.Xfh: Xa!!) [hs#44/ts#19/location 55]	feather black & green amphibolite with feathery artwork of hornblende grains; massive large hornblende and biotite grains; black amphibolite with epidote and diopside giving a greenish cast and quartz veins stretched out; ~75% hornblende & 15% plagioclase.	(Figure 33) {thin section #19/25 w/ ~0-1%KSPAR} [f.g./C.G.] [color: weathered = brownish black & fresh = black!!]
[45] SR2399 3b. Xfh: Xqf (quartzofeldspathic gneiss) [hs#45/location 53]	a weird thin platy shard of brittle micaceous crumbly quartzofeldspathic gneiss.	(Figure 33) [F.G./c.g.] [color: weathered = orangeish tan & fresh = gray (black & white) tan]
[46] SR2299 3a. Xfh: Xa (amphibolite gneiss) [hs#46/location 53]	black amphibolite!!!! with abundant white quartz veins randomly oriented in various directions and not as gneissic...just a black amphibolite.	(Figure 33) [f.g./C.G.] [color: weathered = brownish-black & fresh = black (with white isolated in veins throughout)]
[47] SR2199 3a. Xfh: Xa (amphibolite gneiss) [hs#47/location 50]	black amphibolite!!! blackamph more schistose than gneissic and brittle along stacked and stair-stepped planes of foliation; hornblende resembles slicks and stretching penetrative mineral lineation.	[f.g./C.G.] [color: weathered = brownish-black (for the most part) & fresh = black & white (~equal amounts and random grain orientation)]
[48] SR2099 3b. Xfh: Xqf (quartzofeldspathic	a thin triangular chunk of qfg with veins perpendicular to foliation {located between SR2099 & SR199	{thin section #20/25 w/ ~15%KSPAR} [F.G./c.g.] [color: weathered = orangeish-pinkish-tan & fresh = gray]

gneiss) [hs#48/ts#20/location 49]	is a light igneous intrusion }.	
[49] SR1999 3a. Xfh: Xa (amphibolite gneiss) [hs#49/location 48]	dense & ~platy black amphibolite resembles ~SR2599 {located between SR2099 & SR199 is a light igneous intrusion }.	[f.g./C.G.] [color: weathered = black w/ lichenation! & fresh = black!]
[50] SR1899 3a. Xfh: Xa (~qf-ish amphibolite gneiss) [hs#50/location 47]	black amphibolite!!! black amph;; *a weird specimen where the top surface resembles a qfg and the two layers/beds are sharply defined orangeish hue and the rest of the specimen is black-brown.	[F.G./c.g.] [color: weathered = brownish-black to orangeish tan (like a qfg!) & fresh = dark gray (shimmery with needles randomly arranged...reflects light)]
[51] SR1799 6. Xfh:i (igneous intrusive (i)) [hs#51/ts#21/location 46]	a light (leuco/silicic/felsic) granitic (aplitic?) igneous intrusion with apatite grains and quartz, plagioclase, microcline, biotie, & muscovite.	(Figures 44d & 44e) {thin section #21/25 w/ ~33.33%KSPAR} [f.g./C.G.] [color: weathered = brown & fresh = white to pinkish white]
[52] SR1699 3a. Xfh: Xa (amphibolite gneiss) [hs#52/ts#22/location 45]	black amphibolite!! blackamph! Located @ 12446' with minimal microcline and the rest hornblende, plagioclase & biotite; resembles NR1999 in the shape of the shard being an elongate rod; AND resembles SR2499 just downslope in coarse-grained black & white randomly arranged grains in roughly equal amounts to each other; tabular like SR2299 & SR2199 downslope.	(Figures 38d & 33) {thin section #22/25 w/ ~1-5%KSPAR} [f.g./C.G.] [color: weathered = grayish-black & fresh = black!(w/white)]
[53] SR1599 3c. Xfh:Xfa (feather amphibolite) [hs#53/location 44]	a black mafic!! feather amphibolite with slicks?/hornblende grains? Exposed on the top face of the rock and not weathered, so pretty recent freshly exposed; splotchy random black and white coarse grains and quartz veins parallel to foliation/slicks; ~like SR1499.	[f.g./C.G.] [color: weathered = yellow-brown & fresh = black! (w/white veins)]
[54] SR1499 3c. Xfh:Xfa (feather amphibolite) [hs#54/location 44]	black mafic amphibolite (feather amphibolite) with slicks and/or hornblende grains in alignment; wedge-shaped shard; coarse-grained ~like SR1599.	(Figure 55)[f.g./C.G.] [color: weathered = brownish-yellow & fresh = black!]
[55] SR1399 3a. Xfh: Xa (amphibolite gneiss) [hs#55/location 43]	black amphibolite that weathers like a bif and has hematite (feo/iron oxide) on the weathered surface; oxidation produces orange oxide.	[F.G./c.g.] [color: weathered = orange maroon black (weathers like a bif!) & fresh = black]
[56] SR1299 6. Xfh:i (igneous intrusive (i)) [hs#56/ts#23/location 42]	pegmatitic graphic felsic! intrusion with muscovite books and parallel graphic quartz	(Figures 38a, 44b & 44c) {thin section #23/25 w/ ~50-60%KSPAR} [f.g./C.G.] [color: weathered = light pink to light brown & fresh = light pink]
[57] SR1099 3a. Xfh: Xa	a black amphibolite!! blackamph in a massive blocky rhomb-like chunk;	(Figure 38c) [f.g./C.G.] [color: weathered = brownish-black & fresh = black]

(amphibolite gneiss) [hs#57/location 40]	dense and heavy; coarse grains of hornblende and veins perpendicular to one another.	
[58] SR999 3b. Xfh: Xqf (quartzofeldspathic gneiss) [hs#58/ts#24/location 39]	fine grained gray amphibolite (qfg-ish) expressed in small chunks; exhibits gneissic black and white banding.	(Figure 38f) {thin section #24/25 w/ ~2.5%KSPAR} [F.G./c.g.] [color: weathered = gray & fresh = light gray {black & white bands}]
[59] SR899 3b. Xfh: Xqf (quartzofeldspathic gneiss) [hs#59/location 38]	light brown qfg w/ face weathers to resemble the Dakota FM being maroon to brown w/ quartzite layer.	(Figure 38e) [F.G./c.g.] [color: weathered = maroon to brown w/ quartzite layer (Dakota-like weathered face) & fresh = gray]
[60] SR799 3b. Xfh: Xqf (quartzofeldspathic gneiss) [hs#60/location 37]	quartzofeldspathic gneiss.	(Figure 54) [F.G./c.g.] [color: weathered = splotchy brownish-tan to black & fresh = gray]
[61] SR699 3c. Xfh: Xfa (feather amphibolite) [hs#61/ts#25/location 36]	a small chunk of very dark black amphibolite specimen (blackamph) located between SR499 (location 23) and SR799 (location 37) with a large prominent fine grained kspar vein in the middle ~1/3 thick as the length of slide and light in color; epidote veins also. ~NR1999.	{thin section #25/25 w/ ~10%KSPAR} [f.g./C.G.] [color: weathered = black with brown vein & fresh = dark gray with white vein]
[62] SR599 3a. Xfh: Xa (amphibolite gneiss) WMOST SR [hs#62/location 35]	black amphibolite gneissic black & white banded fine-grained foliated (& @ top of the weathered surface the spars have altered to clay minerals).	(Figures 38a & 38b) [F.G./c.g.] [color: weathered = black to pinkish-light_brown (lichenated ☺) & fresh = gray w/ light brown veins crosscutting]
[63] SR499 3b. Xfh: Xqf (quartzofeldspathic gneiss) [hs#63/location 23]	an arcuate weird shard of micaceous quartzofeldspathic gneiss ~SR2399.	(Figure 38a) [F.G./c.g.] [color: weathered = light pinkish-orange to light brown & fresh = dark gray]
[64] SR399 3b. Xfh: Xqf (quartzofeldspathic gneiss) [hs#64/location 22/ AFTD#7/7 {separated & age-dated}] located at the apex of the summit of 13472'	Quartzofeldspathic gneiss	(Figure 21) [f.g./C.G.] [color: weathered = pinkish-brown & fresh = gray]; AFTD#7/7; rock pulverized, destroyed and separated into mineral separates to be age-dated by the apatite fission-track dating method [and found to be ?? (~46-299Ma in age therefore cooled through low temperatures during the compressional late cretaceous Laramide Orogeny?).
[65] SR1*99 1c. Xag: Xfs (qfschist) [hs#65/location 01]	brittle tan glittery micaceous crumbly schistose (not gneissic) qfamph (hbfeldspathic) with ~50-75% kspar, quartz, plagioclase & muscovite/biotite (micaceous schistose matrix/groundmass); biotite flakes random & muscovite stretching penetrative mineral	[f.g./C.G.] [color: weathered = orangeish-tan & fresh = yellowish-white]

	lineation bears n25e and plunges 32; strike and dip of metamorphic foliation of fabric = N60W 28NE; ~NR499, SR3499 & SR3399.	
[66] SR299 4.Xcs (calc-silicate) [hs#66/location 02]	calc-silicate amphibolite gneiss amphibolite exposure on way up the SR with epidote and quartz veins along coarse-grained foliation; ~NR699 & photo 04.	[f.g./C.G.] [color: weathered = grayish green & fresh = green and red]
[67] IS199 3a. Xfh: Xa (amphibolite gneiss) [hs#67/location 80 (in IS; AKA NR2799)]	black amphibolite! fine-grained foliated dense black amphibolite with gneissic black & white banding; hornblende, biotite and plagioclase.	[F.G./c.g.] [color: weathered = brownish-black & fresh = black]
[68] SR3899 1a. Xag:Xh (black a.g.) [hs#68/location 81]	black! dense fine grained tabular black amphibolite gneiss with quartz veins parallel to and weathering along planes of foliation	[F.G./c.g.] [color: weathered = brown to gray to black & fresh = black]
[69] SR3999 1a. Xag:Xh (black a.g.) EMOST SR. [hs#69/location 82]	thick blocky massive black amphibolite gneiss w/ coarse grained hornblende grains resembling slicks and thick quartz veins crosscutting, oriented randomly, but mostly along planes of foliation.	[f.g./C.G.] [color: weathered = grayish-black & fresh = black!!]

APPENDIX D: THIN SECTIONS

SPECIMEN/ SAMPLE ID [THIN SECTION #/HAND SPECIMEN #/LOCATIO N#]	ROCK (LITHOLOG IC) UNIT NAME	MEGASCOPI C/MACROSC OPIC COLOR	AVERA GE GRAIN SIZE	TEXTURE	COMPOSITI ON % TOTAL MASS [Q/Q+SPAR S] {PLAG/PLA G+KSPAR} <%HB> HQPM (increase or decrease in Hornblende(H), Quartz(Q), Plagioclase Feldspar(P), & Microcline Potassium Feldspar (M) relative to previous thin section quantities; if = then no change; does	COMMENTS/R EMARKS/FEAT URES: E.G. PROSPECT MINE ID#; SIMILARITIES ACROSS RIDGELINE & ALONG RIDGELINE (FIGURE #)

					not apply to igneous intrusions)	
NR2699 EMOST NR [ts#1/hs#1/location 78]	1a. Xag:Xh (Black a.g.)	Black	Fine grained; Hornblende ~1-3 mm (relatively coarse grained to entire rock) Plagioclase ~0.3-0.6 mm; Microcline ~0.2-0.5mm; Quartz ~0.2-0.5mm; Biotite ~0.2-0.5mm	Gneissic Layering; Overall = granolepidoblastic Hornblende(brown)= Idioblastic Nematoblastic, elongation aligned with plane of foliation; Plagioclase = retrogranular sericitized Microcline = tartan twinning only in veins Quartz = polygonal granoblastic Biotite = lepidoblastic	Hornblende ~75% Plagioclase ~10% Microcline ~5% (veins) Quartz ~5% (veins & matrix) Biotite ~5% Sphene <1% Apatite <1% Feoxides <1% Calcite (veins) <1% Epidote <1% [0.25] {0.67} <75> (75H, 5Q, 10P, & 5M)	@9879-9880' elevation; 38 29.672' & 106 11.756'; Fine-grained black amphibolite gneiss with quartz veins predominantly parallel to foliation but perpendicular brittle deformation w/calcite-filled & sericitized cross-cutting foliation; plagioclase zoned; hornblende altered to epidote; glittery & micaceous w/ biotite; Kouther epidotized; hornblende concentrated & medium grain size w/ quartz uncommon (vs. NR2399 hornblende less common & smaller grain size w/more common quartz) (Figures 34b, 34c & 66).
NR2399 [ts#2/hs#4/location 75]	1b. Xag:Xf (Gray comp-banded a.g.)	Black and white, therefore gray	Very fine grained; Hornblende ~ 0.2-0.5 mm Microcline ~ 0.1-0.8 mm Quartz ~0.1-0.8 mm Plag 0.1-	Gneissic; Hornblende = nematoblastic Microcline = xenoblastic Quartz = granonematoblastic Plagioclase = xenoblastic	Hornblende ~40% Microcline ~30% (pre-60) Quartz ~15% Plagioclase ~10% Biotite ~1.5% Muscovite ~1.5%	Hornblende very fine grained; Plagioclase excessively sericitized, platy & fissile, hornblende and quartz layers with quartz veins parallel to and cross-cutting foliation, with

			0.8 mm Biotite ~0.3-0.7 mm		Apatite <1% Feoxides <1% Epidote Zircon Sphene Calcite [0.27] {0.14} <40> ↓H ↑Q =P ↑M (40H, 15Q, 10P & 30M)]	weathering out along veins; supposedly located in Kouther's PCSZ shear zone; hornblende slightly altered with retrograde alteration to epidote producing greenish cast; hornblende less common & smaller grain size w/more common quartz (vs. NR2699 hornblende concentrated & medium grain size w/ quartz uncommon) (Figures 35a, 35b & 35c)
NR499 [ts#3/hs#7/lo cation 11]	1c. Xag:Xfs (QfSchist)	Yellowish- light brown	Overall: coarse grained; equigran ular; Microcli ne~ 0.2- 0.4mm; Quartz ~ 0.1-0.2 mm(fine- grained); Plag ~0.3-0.5 mm; Biotite ~0.5mm	Not as gneissic but rather schistose (schistosity corresponds with bedding of parent rock [p.554 WT&G]); Overall = granolepidoblasti c Microcline = Xenoblastic granoblastic & poikiloblastic Quartz = granoblastic & poikiloblastic with inclusions; Micas (Muscovite, Biotite & Chlorite) = lepidoblastic	Microcline ~50% (pre- 75) Quartz ~20% Plagioclase ~15% Muscovite ~5% Biotite ~5% Chlorite <1% Feoxides <1% Apatite <1% Calcite <1% Sphene <1% Zircon <1% Epidote <1% [0.24] {0.23} <0> ↓H ↑Q ↑P ↑M (0H, 20Q, 15P & 50M)]	Coarse-grained qfschist (qfamph with an increase in micas & increase in feldspars) w/ Hornblende altered to epidote (not chlorite) and micas altering to clay minerals; Microcline with quartz inclusions; micaceous and schistose with increase in biotite and muscovite; ~SR3499 & SR3399 (Figure 36b).
NR4*99 [ts#4/hs#8/lo cation 11a]	5b.Pfs (1c. Xag:Xfs (PqfSchist/Qf gporphyrobla stic/Pqf)	Pinkish- orange-brown	Fine grained; MATRI X: (Microcli	Overall: granolepidoblasti c Quartz = Polygonal	Quartz ~ 60% Sillimanite ~ 10% Microcline	Elongate Porphyroblasts (2.75 cm length x 1.25 cm diameter) of

			ne, Quartz, Hornblende, & Muscovite @ 0.1-0.4 mm; PODS: ~1.0mm; Quartz ~0.2-0.4 mm Sillimanite ~0.5 mm Microcline ~0.1-0.2 mm Muscovite ~0.5mm Biotite ~0.2-0.4 mm ;Hornblende ~0.2-0.4 mm	granoblastic Sillimanite = fibrolitic Microcline = granoblastic Muscovite = lepidoblastic	~10% (between blasts/pods & in matrix) Muscovite ~ 5% Biotite ~ 5% Hornblende ~5% Plagioclase <1% Sericite <1% Apatite <1% Feoxides <1% [0.86] {0.01} <0> =H ↑Q ↓P ↓M (0H, 60Q, <1P & 10M)]	coarser quartz being replaced by muscovite from the outside in, and mantled by muscovite and finer grained polygonal ribbon quartz; Dark gray sillimanite core replaced inside & out by muscovite; Contained in ksp and micaceous matrix weathered out easily along schistose fabric; Quartz with rutile needles; Feldspars altering to sericite; Plagioclase almost fully altered to sericite; Kspar Microcline veins parallel in schistose fabric (Figures 41a, 41b & 41c).
NR599 [ts#5/hs#9/location 12/AFTD#1/7 {separated&age-dated}]	2.Xqfg (quartzofeldspathic gneiss)	Pinkish-brown	Overall: fine-grained Quartz ~ 0.1-0.4 mm (fine grained!!) Epidote = 0.5-1.0mm	Overall: granolepidoblastic w/ gneissic Quartz = polygonal granoblastic (migrated grain boundaries due to pressure solutions) Hornblende = nematoblastic Muscovite = idioblastic lepidoblastic Biotite = idioblastic lepidoblastic	Quartz ~ 60% Microcline ~ 10-15% Hornblende ~ 10% Plagioclase ~ 5% Biotite ~ 2.5% Muscovite ~ 2.5% Feoxides ~ 1% Chlorite <1% Apatite <1% Zircon <1% [0.75] {0.33} <10> ↑H =Q ↑P ↑M (10H, 60Q,	ORIENTED & AGE DATED; the only specimen to have a hand specimen, thin section and be a f-t dated {~20Ma}; fine grained matrix; veins subtle and not pronounced; fine-grained quartz mantles coarser grained quartz; porphyroblasticity minimized; feldspars slightly altered to sericite & micas altered to clay minerals;

					5P & 15M)	hornblende short linear parallel stubs; dextral (right lateral) sense of movement; Qfg with hornblende and epidote indicate transition into amphibolites (p.554 WT&G).
NR399 [ts#6/hs#13/[location 07]	2.Xqfg (quartzofeldspathic gneiss)	Pinkish-brown	Fine-grained; Quartz ~ 0.1-0.4mm (med grained compared to smaller E) Microcline ~0.2-0.4mm; Plagioclase ~0.2-0.4 mm; Hornblende ~ 0.1-0.2 mm; Biotite ~0.1-0.2 mm; Muscovite ~0.1-0.2 mm	Overall: granolepidoblastic Quartz = polygonal granoblastic (layering of quartz) Hornblende = nematoblastic Biotite = lepidoblastic; Muscovite = lepidoblastic	Quartz ~ 40% Microcline ~ 25% Plagioclase ~ 25% Hornblende ~ 5% Biotite ~ 5% Muscovite ~ 1% Apatite ~ 1% [0.44] {0.50} <5> ↓H ↓Q ↑P ↑M (5H, 40Q, 25P & 25M)	ORIENTED; Mine ID=#23/03/70; top half of thin section and hand specimen (weathered surface) is ksparrich and bottom half sericitized plagioclase (Figure 37c).
NR699 [ts#7/hs#14/[location 14]	4.Xcs (2a.Xqfg:Xcs (calc -silicate gneiss))	Brownish-green weathered (green & pink fresh)	Coarse grained; Calcite = large coarse grains ~2.0-5.0 mm; Quartz ~0.2-0.8 mm; Hornblende ~0.8-1.0 mm; Epidote ~0.2-0.3	Calcite idioblastic rhombohedrons Quartz = polygonal granoblastic Hornblende = nematoblastic Sericite = xenoblastic	Calcite ~ 30% Quartz ~ 30% Hornblende ~ 25% Sericite ~ 5% Feoxides ~ 5% Plagioclase ~ 1% (laths) Microcline ~ 3% Orthoclase(untwinned) ~	Stretched strained quartz; greenish-blue to blackish-blue hand specimen with orange rusted iron oxide lining the dissolutional cavities in the calcite; hornblende (green) & calcite (red) "Watermelon/Christmas rock";

			mm; Sericite ~1.0-2.0 mm (large); else ~0.3mm		1% Epidote <1% Diopside <1% Sphene <1% Zircon <1% Apatite <1% [0.88] {0.25} <25> ↑H ↓Q ↓P ↓M (25H, 30Q, 1P & 3M)	sericitized feldspars; hornblende altering to epidote (biotite and chlorite); fractures pass through the grains and not around them as in a sandstone; Untwinned plag; microcline bxa- & orthoclase bxa+; (Figures 39a, 39b & 39c)
NR1099 [ts#8/hs#18/ ocation 19]	2.Xqfg (quartzofelds pathic gneiss)	Pinkish- brown-orange	Coarse grained; Plagiocla se ~0.5mm Quartz ~0.7- 1.0mm; Muscovit e ~0.5- 0.9 mm; Microcli ne ~0.2- 0.3 mm	Overall: granolepidoblasti c Plagioclase = xenoblastic Quartz = polygonal poikiloblastic! Muscovite = lepidoblastic Microcline = xenoblastic	Plagioclase ~ 60% Quartz ~ 25% (blobs & matrix) Muscovite ~ 15% Microcline ~ 1% Apatite <1% [0.29] {0.98} <0> ↓H ↓Q ↑P ↓M (0H, 25Q, 60P & 1M)	ORIENTED; Large Quartz blobs (coarse grains mantled by fine grains) oriented diagonal crosscutting slide and parallel to each other; Plagioclase sericitized matrix; veins filled and crosscut looks granitic; no hornblende (Figures 43c, 67a & 67b).
NR1299 [ts#9/hs#20/ ocation 25]	3d.Xfh:Xhb (amphibolite (3a. Xfh:XA) hb blobs1/2)	Gray (black & white)	Fine grained; Hornblen de ~0.3- 0.6 mm; Plagiocla se ~0.2- 0.4 mm; Quartz ~0.1-0.2 mm; Biotite ~0.1-0.2 mm; Microcli ne ~0.1- 0.2 mm	Overall: granolepidoblasti c Hornblende = idioblastic nematoblastic Plagioclase = xenoblastic Quartz = polygonal granoblastic Biotite = lepidoblastic Microcline = granoblastic	Hornblende ~ 65% Plagioclase ~ 15% Quartz ~ 15% Biotite ~ 5% Microcline ~ 1% Feoxides ~ 1% Apatite ~ 1% [0.48] {0.94} <65> ↑H ↓Q ↓P =M (65H, 15Q, 15P & 1M)	Hornblende and biotite (resemble mica fish) porphyroblasts within finer grained quartz and plagioclase matrix.
NR1399 [ts#10/hs#21/ ocation 26]	3d.Xfh:Xhb (amphibolite (3a. Xfh:XA)	Gray (black & white)	Fine grained; Quartz	Overall: grano lepidoblastic Hornblende =	Quartz ~ 50% Hornblende ~	Hornblende porphyroblasts mantled by

	hb blobs2/2)		~0.1-0.2 mm; Hornblende ~0.3-0.6 mm; Biotite ~0.1-0.2 mm; Plagioclase ~0.2-0.4 mm; Microcline ~0.1-0.2 mm; Else ~0.1-0.2 mm	idioblastic nematoblastic Plagioclase = xenoblastic Quartz = polygonal granoblastic Biotite = lepidoblastic Microcline = granoblastic	40% Biotite ~ 5% Plagioclase ~ 2.5% Microcline ~ 1.5 % Apatite ~ 1% FeOxides ~ 1% [0.93] {0.63} <40> ↓H ↑Q ↓P ~M (40H, 50Q, 2.5P & 1.5M)	biotite within finer grained quartz and plagioclase matrix oriented along subtle foliation; thick quartz veins crosscut foliation both diagonally and perpendicularly (more quartz veins than neighboring identical specimen); ~12 grains sparsely oriented diagonally & parallel across slide (Figures 43a & 43b).
NR13a99 (AKA NR13*99) [ts#11/hs#22/location 26a]	3e. Xfh:Xqms (quartz mica schist "whiteschist")	White	Fine grained; Quartz = coarse grains (0.4-0.8mm) and fine grains (0.1-0.2mm) matrix; Plagioclase ~0.2-0.3 mm; Muscovite = 0.1-0.2 mm small flakes; Sillimanite ~0.2-0.3 mm	Overall: granolepidoblastic Quartz = hypidioblastic; Plagioclase = hypidioblastic; Muscovite = lepidoblastic Microcline = xenoblastic Grain migration boundaries	Quartz ~ 30% Plagioclase ~ 30% Muscovite ~ 25% Microcline ~ 10% Sillimanite ~ 5% Apatite ~ 1% [0.43] {0.75} <0> ↓H ↓Q ↑P ↑M (0H, 30Q, 30P & 10M)	Coarse grains of quartz pitted out with muscovite flakes within and on the edges, and smaller quartz grains in matrix with elongate and stretched out tabular minerals of muscovite and sillimanite; quartz & microcline veins line the outer edges; fine-grained metamorphosed quartzofeldspathic coarse-grained pegmatite containing sillimanite; "Whiteschist" (Sidman) (Figures 44f & 44g)
NR1499 [ts#12/hs#23/location 27]		Gray (black & white)	Overall Coarse grained; Hornblende ~1.0-	Overall: granoblastic; Hornblende = idioblastic perfect grains	Hornblende ~ 75% Biotite ~ 10%	microcline and quartz veins parallel to foliation appear offset and

			2.0 mm (feathers) & 0.1-0.2 (matrix) mm; Biotite ~0.2-0.4 mm; Quartz ~0.2-0.6 mm; Microcline ~0.2-0.4 mm; Plagioclase ~ 0.2-0.4 mm	nematoblastic Biotite = lepidoblastic Quartz = polygonal granoblastic Microcline = granoblastic Plagioclase = granoblastic	Quartz ~ 10% Microcline ~ 5% Plagioclase (untwinned) ~ 1% Apatite ~ 1% [0.63] {0.17} <75> ↑H ↓Q ↓P ↓M (75H, 10Q, 1P & 5M)	faulted/extended and subjected to brittle deformation and indicate normal movement; veins also diagonal and crosscutting foliation; . heterogranular with both coarse-grained fan shape (like NR1999) and fine-grained matrix hornblende grains (Figure 65).
NR1999 [ts#13/hs#25/location 33] WMOST NR	3c.Xfh:Xfa (feather amphibolite)	Gray (black & white)	Coarse grained; Hornblende = coarse grained ~2.0-4.0 mm "feathers"; Microcline ~0.2-1.0 mm; Plagioclase ~0.2-1.0 mm; Quartz ~0.2-0.5 mm; Biotite ~ 0.8-1.0 mm; else ~0.1-0.2 mm	Overall: granoblastic Hornblende = hypidioblastic nematoblastic Microcline = hypidioblastic Plagioclase = xenoblastic Quartz = polygonal granoblastic Biotite = hypidioblastic	Hornblende ~ 70% Microcline ~ 10% Plagioclase ~ 10% Quartz ~ 5% Biotite ~ 2.5% Epidote ~ 1.5% Diopside ~ 1% Apatite ~ 1% [0.20] {0.50} <70> ↓H ↓Q ↑P ↑M (70H, 5Q, 10P & 10M)	Coarse grains of hornblende with some biotite; Sericitization of spars; Hornblende radiating crystal clusters; slight foliation with radiating grains fan shape like NR1499; ~SR1699. (Figures 38g & 38h)
SR3699 [ts#14/hs#31/location 71] EMOST SR	1b. Xag:Xf (gray comp-banded a.g.)	Gray (black & white)	Fine-grained; Quartz ~ 0.5-1.0mm Microcline ~0.1-1.0 mm; Hornblende ~0.2-	Quartz = polygonal granoblastic (w/ 120° triple junctions); Microcline = xenoblastic; Hornblende = nematoblastic Muscovite	Quartz ~ 60% Microcline ~ 10% Hornblende ~ 10% Muscovite ~ 10% Plagioclase ~ 5%	A very fine-grained gray comp-banded qf amphibolite gneiss resembles a quartzite (quartz too high and hornblende too low, otherwise an

			0.5 mm Muscovite ~0.2-0.3 mm; Plagioclase ~0.2-0.5 mm; Biotite ~0.5-0.8mm	Plagioclase Biotite	Biotite ~ 5% Apatite < 1% [0.80] {0.33} <10> (10H, 60Q, 5P & 10M)	Xfs); two porphyroblasts with quartz intergrown within; cross-cutting quartz veins form slight lineaments across slight metamorphic fabric; brittle deformation with veins crosscut/offset.
SR3599 [ts#15/hs#32/ location 69]	5a. Pf (1b.Xag:Xf {PXf/Pgray c-b a.g.})	Gray (black & white)	Fine-grained; Hornblende(matrix) ~0.1-0.2 mm; Biotite(matrix) ~0.1-0.2 mm; Muscovite(matrix) ~0.1-0.2 mm; Plagioclase(matrix) ~0.1-0.2 mm; Microcline(matrix) ~0.1-0.2mm; Blasts >5.0mm: Muscovite & Quartz	Overall: granonematolepidoblastic Quartz = polygonal granoblastic; Hornblende = nematoblastic; Muscovite = lepidoblastic; Biotite = lepidoblastic;	Quartz ~ 40% Hornblende ~ 20% Muscovite ~ 20% (15% pods & 5% matrix) Biotite ~ 10% Plagioclase ~ 10% Microcline ~ 1% Apatite ~ 1% [0.78] {0.91} <20> ↑H ↓Q ↑P ↓M (20H, 40Q, 10P & 1M)	Large/huge (5 cm diameter x 1.82 cm length) porphyroblasts of muscovite with quartz both within and mantling; aluminous schistose micaceous matrix with fine grained muscovite mantling to cause weakness in matrix & cause to be easily weathered; zonation of mantling minerals; with hornblende and plagioclase increasing (relative to quartz and microcline) grades into an amphibolite
SR3199 [ts#16/hs#37/ location 63]	2.Xqfg (quartzofeldspathic gneiss)	Pinkish-orange-brown	Fine-grained; Quartz = Large ~1.0-2.0 mm crystals; Microcline ~0.8-1.0 mm;	Overall: granolepidoblastic Quartz = polygonal granoblastic poikiloblastic Microcline = xenoblastic Plagioclase =	Quartz ~ 50% Microcline ~ 20% Plagioclase ~ 15% Hornblende ~ 5% Biotite ~ 5% Muscovite ~	Upper portion weathered and relatively Microcline rich!!; sericitized and weathered excessively with iron oxides; a few porphyroblasts

			Plagioclase ~0.8-1.0 mm;	xenoblastic Hornblende = nematoblastic Muscovite = lepidoblastic Biotite = lepidoblastic	2.5% Apatite ~ 1.5% FeOxides ~ 1% [0.59] {0.43} <0> ↓H ↑Q ↑P ↑M (0H, 50Q, 15P & 20M)	and large quartz crystals; located immediately E of suspected fault; minimal hornblende
SR3099 [ts#17/hs#38/ location 61]	2.Xqfg (quartzofelds pathic gneiss)	Pink	Fine- grained; Quartz ~0.1-0.2 mm; Plagioclase ~0.1- 0.2 mm ; Microcline ~0.1- 0.2 mm; Biotite ~0.1-0.2 mm; Muscovite ~0.1- 0.2 mm	Overall: granoblastic; Quartz = polygonal granoblastic; Plagioclase = xenoblastic Microcline = xenoblastic Biotite = lepidoblastic Muscovite = lepidoblastic	Quartz ~75% (veins and matrix) Plagioclase ~ 10% Microcline ~ 5% Biotite ~ 5% Muscovite ~ 2.5% FeOxides ~ 1% Apatite ~ 1% [0.83] {0.67} <0> =H ↑Q ↓P ↓M (0H, 75Q, 10P & 5M)	Microcline sericitized and weathered with iron oxides; a few quartz porphyroblasts lined along foliation plane with reddish quartz veins; photo 41 “c.p.f” = “conspicuous pink fill” quartzofeldspathic gneiss may have been an intrusive initially but since been metamorphosed (Figure 32).
SR2899 [ts#18/hs#40/ location 59]	2.Xqfg (quartzofelds pathic gneiss)	Pinkish-gray	Fine- grained; MATRIX: Quartz ~0.1-0.2 mm; Microcline ~0.1- 0.2 mm; Plagioclase ~0.2- 0.4 mm; Hornblende ~0.2- 0.3 mm; Biotite ~0.2-0.4 mm; Muscovite ~0.1- 0.2 mm ~>5.0 mm PODS:	Overall: granolepidonema toblastic	Quartz ~ 60% Microcline ~ 15% Plagioclase ~ 10% Hornblende ~ 5% Biotite ~ 5% Muscovite ~ 1.5% Apatite ~ 1% Epidote ~ 1% FeOxides ~ 1% [0.71] {0.40} <5> ↑H ↓Q =P ↑M (5H, 60Q, 10P & 15M)	Microcline predominantly within porphyroblast and mantled by fine-grained ribbon quartz; some microcline in matrix; Plagioclase sericitized; Microcline and FeOxide veins cut across foliation; porphyroblasticit y increases at this location to football-sized porphyroblasts; AKA “qfg bw/p {qfg blocks with pods}”; (Figures 42a, 42b & 42c).

			Quartz ~4.0mm (~0.1-0.2 mm ribbon quartz mantles) Microcli ne (~1.0- 2.0 mm core)			
SR2499 [ts#19/hs#44/ location 55]	3c.Xfh:Xfa (feather amphibolite)	Gray (black & white)	Coarse- grained; Hornblen de ~0.3- 0.4 mm; Plagiocla se ~0.1- 0.2 mm; Biotite ~ 0.2-0.3 mm; Quartz ~ 0.1-0.2 mm; Microcli ne ~0.1- 0.2 mm Muscovit e ~0.2- 0.3 mm	Overall = granoblastic Hornblende = nematoblastic Plagioclase = xenoblastic Biotite= lepidoblastic Quartz = polygonal granoblastic Microcline = xenoblastic Muscovite = lepidoblastic	Hornblende ~ 75% Plagioclase ~ 15% Biotite ~ 5% Quartz ~ 2.5% Microcline ~ 1% Muscovite ~ 0.5% Diopside ~ 0.5% Epidote <1% Apatite <1% [0.14] {0.94} <75> ↑H ↓Q ↑P ↓M (75H, 2.5Q, 15P & 1M)	Massive large feather grains of hornblende not in fan shape like NR1999 & NR1499; biotite and diopside large grains also; “feathery artwork” texture; random grains with foliation & epidote veins; Microcline depleted; transitions into an amphibolite from a quartzofeldspathi c gneiss by increasing hornblende and plagioclase and decreasing quartz and microcline; (Figure 33).
SR2099 [ts#20/hs#48/ location 49]	3b. Xfh:Xqf (quartzofelds pathic gneiss)	Pinkish-brown	Fine- grained; Quartz ~0.1-0.3 mm; Hornblen de ~0.3- 0.6 mm; Microcli ne ~0.2- 0.4 mm; Biotite ~0.4-0.8 mm; Plagiocla se ~0.1- 0.3 mm;	Overall: granonematolepi doblastic Quartz = pitted and poikiloblastic Hornblende = nematoblastic; Microcline = xenoblastic granoblastic; Plagioclase = xenoblastic granoblastic; Biotite = lepidoblastic Muscovite =	Quartz ~ 50% Hornblende ~ 15% Microcline ~ 15% Plagioclase ~ 15% Biotite ~ 10% Plagioclase ~ 5% Muscovite ~ 5% FeOxides ~ 1% (veins)	Adjacent to intrusion; quartz veins (iron oxide filled too) both parallel and perpedicular to foliation, and crosscutting fabric; quartzite in appearance ; transitions from an amphibolite back into a quartzofeldspathi c gneiss by increasing quartz and microcline

			Muscovite ~0.1-0.3 mm	lepidoblastic	Apatite ~ 1% [0.71] {0.25} <15> ↓H ↑Q ↓P ↑M (15H, 50Q, 5P & 15M)	relative to decreasing hornblende and plagioclase.
SR1799 [ts#21/hs#51/ location 46]	6. intrusive (i) pegmatitic	Pink	Coarse-grained; Quartz ~1.0-2.0 mm; Microcline ~ 0.8-1.0 mm; Plagioclase ~ 0.8-1.0 mm; else ~ 0.1-0.2 mm		Quartz ~ 32% Microcline ~ 32% Plagioclase ~ 32% Apatite ~ <1% Muscovite ~ <1% Biotite <1% Hornblende <1% [0.33] {0.50} <1> (1H, 33Q, 33P & 33M)	Radiating myrmekitic quartz; quartz replacing microcline and plagioclase in a plagioclase-rich matrix; granitic intrusive with small reddish apatites; from SR3099: ↑H ↓Q ↑P ↓M (Figures 44d & 44e)
SR1699 [ts#22/hs#52/ location 45]	3a. Xfh: Xa (amphibolite gneiss)	Black	Coarse-grained; Hornblende ~0.4-0.8 mm; Plagioclase ~0.3-0.6 mm; Microcline ~0.2-0.4 mm; Biotite ~0.2-0.4 mm;	Overall: granonematoblastic; foliated gneissic; Hornblende = nematoblastic, a crystal pitted and filled with quartz; Plagioclase = xenoblastic; Microcline = xenoblastic; Biotite & Muscovite = lepidoblastic; Quartz = granoblastic;	Hornblende ~ 75% Plagioclase ~ 10% Microcline ~ 5% Biotite ~ 5% Quartz ~ 2.5% Epidote ~ 1% Diopside ~ 1% Apatite ~ 1% Muscovite ~ 1% [0.14] {0.66} <75> (75H, 2.5Q, 10P & 5M)	Dark black foliated feathery amphibolite; minimal Microcline & Plagioclase sericitized. Coarse-grained black & white randomly arranged mineral grains of equal amounts to each other with green epidote veins Located at 12446' on SR.
SR1299 [ts#23/hs#56/ location 42]	6. i (intrusive)	Pink	Coarse-grained; Microcline ~5.0-10.0 mm; Orthoclase ~2.0-5.0 mm; Muscovite ~0.8-1.0 mm; Quartz ~	Overall: graphic; Microcline = euhedral; Orthoclase = euhedral; Quartz = euhedral;	Microcline ~ 50% Orthoclase ~15% Muscovite ~ 15% Quartz ~ 15% Plagioclase ~ 5% Apatite < 1% [0.18] {0.07} <0> (0H,	Large crystal grains fused together; graphic and not myrmekitic quartz intergrowth in feldspar; perthitic intergrowth within microcline (potassium-rich

			2.0-5.0 mm; Plagioclase ~0.4-0.8 mm		15Q, 5P & 50M)	host of exsolved sodium-rich phase [albite]); untwinned orthoclase; Microcline and quartz micrographic (<0.1mm)
SR999 [ts#24/hs#58/ location 39]	3b. Xfh:Xqf (quartzofeldspathic gneiss)	Pinkish-brown	Fine-grained; Hornblende ~0.1-0.2 mm; Plagioclase ~0.2-0.3 mm; Quartz ~0.2-0.3 mm; Biotite ~0.1-0.2 mm; Muscovite ~ 0.1-0.2 mm; Microcline ~0.1-0.2 mm	Overall: granonematoblastic Hornblende = nematoblastic Plagioclase = xenoblastic Quartz = polygonal granoblastic Biotite = lepidoblastic Muscovite = lepidoblastic Microcline = xenoblastic	Hornblende ~ 70% Plagioclase ~ 10% Quartz ~ 10% Biotite ~ 5% Muscovite ~ 2.5% Microcline ~ 2.5% Apatite <1% FeOxides <1% [0.44] {0.80} <70> (70H, 10Q, 10P & 2.5M)	Fine-grained wavy quartzofeldspathic amphibolite gneiss with black and white gneissic banding.
SR699 [ts#25/hs#61/ location 36] WMOST SR	3c.Xfh:Xfa (feather amphibolite)	Black	Coarse-grained; Hornblende ~2.0-3.0 mm; Plagioclase ~1.0 mm; Microcline ~1.0mm; Quartz ~ 0.1-0.2 mm; Diopside ~ 2.0-3.0 mm; Epidote ~2.0-3.0 mm	Overall: granoblastic; Hornblende = nematoblastic Plagioclase = xenoblastic Microcline = xenoblastic Quartz = xenoblastic	Hornblende ~ 70% Plagioclase ~ 10% Microcline ~ 10% Quartz ~ 5% Diopside ~ 1.5% Epidote ~ 1% Apatite ~ 1% [0.20] {0.50} <70> =H ↓Q =P ↑M (70H, 5Q, 10P & 10M)	ORIENTED; Very dark black feather amphibolite located between two qfg exposures with large quartz, kspars, epidote & diopside veins crosscutting fabric; surrounded by predominantly sericitized plagioclase; random grains not as foliated.

APPENDIX E: FIELD MEASUREMENTS

LOCATION # [NR/SR]	ATTITUDE	AZIMUTH & (STRIKE)	DIP	PLUNGE	BEARING (AKA TREND)	RAKE	ROCK (LITHOLOGIC) UNIT NAME	ELSE: FEATURE (fracture/lineation) & LITHOLOGY; [PETROLOGIC SAMPLE #, e.g. NR#99 & SR#99] {hand specimen # [1-69]} {petrologic sample: not oriented}
01 [SR]	N60W 28NE	300 (N60W)	28 NE	28	n27e	87 from nw	1c. Xag: Xfs (qfschist)	Stretching lineation of muscovite [SR1*99] {hs#65} (L1[down dip]) (F1)
02 [SR]	N05W 20NE	355 (N05W)	20NE				4. Xcs (calc-silicate)	Metamorphic foliation/ Fabric; epidote and quartz veins oriented along the foliation; [SR299] {hs#66} (F2)
03 [SR]	N20W 30SW	340 (N20W)	30SW					Metamorphic foliation/ Fabric; on

							2. Xqfg (quartzofeldspathic gneiss)	the SW side of the SR (F3)
03 [SR]	N45E	045 (N45E)	83 NW				2. Xqfg (quartzofeldspathic gneiss)	Fracture/Joint (J1)
03 [SR]	N45W	315 (N45W)	74 SW				2. Xqfg (quartzofeldspathic gneiss)	Fracture/Joint (J2)
03' [SR]	~ N to NW (NNW)	335 (N25W)					2. Xqfg (quartzofeldspathic gneiss)	Lineament/linear trend in vegetation (T1)
04 [SR]	N23W 34NE	337 (N23W)	34NE				2. Xqfg (quartzofeldspathic gneiss)	Metamorphic foliation & NW lineament trend (F4) (T2)
05 [NR]	N25W 25NE	335 (N25W)	25NE				2. Xqfg (quartzofeldspathic gneiss)	Metamorphic foliation/fabric which coincides with NW lineament [NR199] {hs#10} (F5) (T3)
05 [NR]	N23W 20NE	337 (N23W)	20NE				2. Xqfg (quartzofeldspathic gneiss)	Metamorphic foliation/fabric [NR199] {hs#10} (F6)
06 [NR]	N65W 15NE	295 (N65W)	15NE				2. Xqfg (quartzofeldspathic gneiss)	Metamorphic foliation/fabric; foliation coincides with lineament; deserted prospect mine site (ID#23/02/69) [NR1*99] {hs#11} (F7) (T4)

06 [NR]	N63W 23NE	297 (N63W)	23NE				2. Xqfg (quartzofeldspathic gneiss)	Metamorphic foliation/fabric with quartz veins subparallel to foliation; [NR299] {hs#12} (F8)
07 [NR]	N25W 25NE	335 (N25W)	25NE				2. Xqfg (quartzofeldspathic gneiss)	Metamorphic foliation/fabric prospect mine (ID# 23/03/70) [NR399] {ts#6/hs#13} (F9)
07 [NR]	N25E 65SE	025 (N25E)	65SE				2. Xqfg (quartzofeldspathic gneiss)	Fracture (J3)
07 [NR]	N25E 25SE	025 (N25E)	25SE	59	n15e	37 from ne	2. Xqfg (quartzofeldspathic gneiss)	Stretching lineation; [NR399] {hs#13} (F10) (L2[down strike])
08 [NR]	N35W 28NE	325 (N35W)	28NE				4. Xcs (calc-silicate) [within 2.Xqfg (quartzofeldspathic gneiss)]	Metamorphic foliation/fabric of (F11)
09 [NR]	N35W 70NE	325 (N35W)	70NE					Metamorphic foliation/fabric on top of ridge at 11100' with Kspar veins and joints/frac

								tures oriented NW; very similar to gneiss NR399 at location 7 (F12)
09 [NR]	N37W 69NE	323 (N37W)	69NE				2. Xqfg (quartzofeldspathic gneiss)	Metamorphic foliation with kspars veins coinciding with fractures (F13) (J4)
10 [NR]	N42W 63NE	318 (N42W)	63NE				2. Xqfg (quartzofeldspathic gneiss)	Metamorphic foliation (F14)
11 [NR]	N30W 40NE	330 (N30W)	40NE	59	n07e	44 from nw	1c. Xag: Xfs (qfschist)	Stretching lineation of and a rough contact with the amphibolite to the east; [NR499] {hs#7/ts#3} (F15) (L3[down dip])
11 [NR]	N27W 37NE	333 (N27W)	37NE				1c. Xag: Xfs (qfschist)	Fracture/Joint of quartzofeldspathic schist (amphibolite to the east [NR499] {hs#7/ts#3} (J5)
11 [NR]	N27W	333 (N27W)						Trend/rough lineament of contact of quartzofeldspathic schist to west &

								1c. Xag: Xfs (qfschist)	amphibolite to the east [NR499] {hs#7/ts#3} (T5)
11a [NR]	N32W 51NE	328 (N32W)	51NE	40	n11e	56 from ne		1c. Xag: Xfs (qfschist)	Stretching lineation; foliation parallels contact) [NR4*99] {hs#7/ts#3} (F16) (L4[down dip]) (T?)
12 [NR]	N10W 24NE	350 (N10W)	24NE	14	n23e	35 from nw		2.Xqfg (quartzofeldspathic gneiss)	Stretching lineation of biotite & hornblende [NR599] (F17) (L5[down dip]) {hs#9/ts#5}
13 [NR]	N35W 19NE	325 (N35W)	19NE					2.Xqfg (quartzofeldspathic gneiss)	Metamorphic foliation/fabric (F18)
13 [NR]	N37W 89NE	323 (N37W)	89NE					2.Xqfg (quartzofeldspathic gneiss)	Metamorphic foliation with elongated quartz porphyroblasts which indicate a right lateral (dextral) sense of movement (F19) (T6)
13 [NR]	N44E 88NW	044 (N44E)	88NW					2.Xqfg (quartzofeldspathic gneiss)	Fracture (J6)
14 [NR]	N35W 28NE	325 (N35W)	53NE	42	n07w				Slicks [NR699] {hs#14/ts#

						56 from nw	4. Xcs (calc-silicate) [within 2.Xqfg (quartzofeldspathic gneiss)]	#7} (F20) (L6[down strike])
14 [NR]	N23W 47NE	337 (N23W)	47NE				4. Xcs (calc-silicate) [within 2.Xqfg (quartzofeldspathic gneiss)]	Metamorphic foliation [[NR699] {hs#14/ts #7} (F21)
14 [NR]	N18W 53NE	342 (N18W)	53NE				4. Xcs (calc-silicate) [within 2.Xqfg (quartzofeldspathic gneiss)]	Metamorphic foliation/ fabric [NR699] {hs#14/ts #7} (F22)
14b [NR]	N02W 81SW	358 (N02W)	81SW	34	n08w	34 from nw	2.Xqfg (quartzofeldspathic gneiss)	Slicks (F23) (L7[down strike]) [NR799] {hs#15} Location 14b = [NR899] {hs#16 AFTD#3/ 7(separate & age- dated)}
15 [NR]	N54W 71NE	306 (N54W)	71NE					Metamorphic foliation/ Fabric & rough contact between) amphibolite to the SW and qfg to NE; fabric parallels lineations thought to be faults

							2.Xqfg (quartzofeldspathic gneiss)	noted in the aerial photos; on top of 11100' hilltop; [NR999] {hs#17} (F24)
15 [NR]	N46W 73NE	314 (N46W)	73NE				2.Xqfg (quartzofeldspathic gneiss)	Fracture (NW) & rough contact between amph to SW & gfg to NE (J7) (T7)
16 [NR]	N70W 85NE	290 (N70W)	85NE	85	n42e	92 from nw	2.Xqfg (quartzofeldspathic gneiss)	Slicks; inferred fault steps down to the N (F25) (L8[down dip: steps down to N])
16 [NR]	N69W 28NE	291 (N69W)	28NE				2.Xqfg (quartzofeldspathic gneiss)	Trend of Plane lineament (T8)
17 [NR]	N20W 76SW	340 (N20W) [axial plane]	76SW [fold axis]	11	s20e	8 from sw	2.Xqfg (quartzofeldspathic gneiss)	Axial plane (NW) and folds axis (SW) (F26) (L9 [upstrike])
17 [NR]	N20W 76SW	340 (N20W)	76SW				2. Xqfg (quartzofeldspathic gneiss)	Fracture plane parallels NW axial plane (J8)
18 [NR]	N06W 62NE	354 (N06W)	62NE				2. Xqfg (quartzofeldspathic gneiss)	Metamorphic foliation/fabric (F27)
19 [NR]	N35E 35SE	035 (N35E)	35SE	21	n68e		2. Xqfg (quartzofeldspathic gneiss)	Stretching lineation [NR1099] {hs#18/ts#8} (F28) (L10[down

							38 from ne	thic gneiss)	nstrike])
19 [NR]	N15E 42SE	015 (N15E)	42SE					2. Xqfg (quartzofeldspathic gneiss)	Fracture/Joint [NR1099] {hs#18/ts#8} (J9)
20 [NR]	N45E 60NW	045 (N45E)	60NW	60	n43w		89 from nw	2. Xqfg (quartzofeldspathic gneiss)	Slicks (F29) (L11[downdip])
21 [NR]	N55W 42NE	305 (N55W)	42NE	42	n31e		87 from ne	2. Xqfg (quartzofeldspathic gneiss)	Slicks suspected fault area (F30) (L12 [downdip])
21 [NR]	N17E 55SE	017 (N17E)	55SE	55	s08e		85 from nw	2. Xqfg (quartzofeldspathic gneiss)	Slicks (F31) (L13[downdip])
21 [NR]	N40E 86SE	040 (N40E)	86SE	10	n40e		10 from sw	2. Xqfg (quartzofeldspathic gneiss)	Slicks (F32) (L14[downstrike])
21 [NR]	N45W 26NE	315 (N45W)	26NE	17	n6w		42 from nw	2.Xqfg (quartzofeldspathic gneiss)	Slicks; steps down to the N; suspected fault area (F33) (L15[downstrike])
22 [SR]	N30E 25NW	030 (N30E)	25NW					3b. Xfh: Xqf (quartzofeldspathic gneiss)	Metamorphic foliation/fabric atop 13472'; [SR399] {hs#64} (F34)
23 [SR]	N85E 28SE	085 (N85E)	28SE					3b. Xfh: Xqf (quartzofeldspathic gneiss)	Metamorphic foliation top of 13472' in photo 15); [SR499] {hs#63} (F35)
24 [NR]	N05E 65SE	005 (N05E)	65SE						Metamorphic foliation/

								3a. Xfh: Xa (amphibolite gneiss)	fabric [NR1199] {hs#19} (F36)
24 [NR]	N10W 76SW	350 (N10W)	76SW					3a. Xfh: Xa (amphibolite gneiss)	Metamorp hic foliation/ fabric [NR1199] {hs#19} (F37)
25 [NR]	N25W 40NE	335 (N25W)	40NE					3d. Xfh: Xhb (amphibolite hb blobs 1/2)	Metamorp hic foliation/ fabric [NR1299] {hs#20/ts #9} (F38)
25 [NR]	N25W 40NE	335 (N25W)	40NE					3d. Xfh: Xhb (amphibolite hb blobs 1/2)	Fracture plane [NR1299] {hs#20/ts #9} (J10)
26 [NR]	N19E 63SE	019 (N19E)	63SE					3d. Xfh: Xhb (amphibolite hb blobs 2/2)	Metamorp hic foliation [NR1399] {hs#21/ts #10} (F39)
26a [NR]	N23E 54SE	023 (N23E)	54SE					3e. Xfh:Xqms (quartz mica schist)	Metamorp hic foliation/f abric [NR13*99] {hs#22/ts #11} (F40)
27 [NR]	N05W 34NE	355 (N05W)	34NE	23	n35e	45 from ne		3c. Xfh: Xfa (feather amphibolite)	Slicks [NR1499] {hs#23/ts #14} (F41) (L16 [downdip])
27 [NR]	N37W 87NE	323 (N37W)	87 NE					3c. Xfh: Xfa (feather amphibolite)	Fracture/J oint [NR1499] {hs#23/ts #14} (J11)
27 [NR]	N56E 67NW	056 (N56E)	67 NW					3c. Xfh: Xfa	Fracture/J oint [NR1499]

							(feather amphibolite)	{hs#23/ts #14} (J12)
28 [NR]	N43W62SW	317 (N43W)	62SW				3a. Xfh: Xa (amphibolite gneiss)	Metamorphic foliation/fabric; just under 12660'; [NR1599] {hs#30/photo 22} (F42)
29 [NR]	N45W 53NE	315(N45W)	53NE				3a. Xfh: Xa (amphibolite gneiss)	Metamorphic foliation/fabric [NR1699] {hs#29} (F43)
30 [NR]	N45W 47SW	315(N45W)	47SW				3b. Xfh: Xqf (quartzofeldspathic gneiss)	Metamorphic foliation/fabric [NR1799] {hs#28/A FTD#6/7} (F44)
31 [NR]	N57W 60SW	303 (N57W)	60SW				3a. Xfh: Xa (amphibolite gneiss)	Metamorphic foliation/fabric [NR1899] {hs#27/A FTD#5/7} (F45)
32 [NR]	N70W 64SW	290 (N70W)	64SW				6.i (intrusive)	Trend of contact of metamorphic fabric with pegmatitic igneous body [NR17*99] {hs#26/A FTD#4/7} (T9)
33 [NR]	N37W 64NE	323 (N37W)	64NE					Metamorphic foliation/fabric; on top of the flat saddle between

							3a. Xfh: Xa (amphibolite gneiss)	12106' and 12075'; [NR1999] {hs#25} (F46)
34 [NR]	N42W 71SW	318(N42W)	71 SW				3a. Xfh: Xa (amphibolite gneiss)	Metamorp hic foliation/ fabric [NR2099] {hs#24} (F47)
35 [SR]	N55E 70SE	055(N55E)	70SE				3a. Xfh: Xa (amphibolite gneiss)	Metamorp hic foliation/ Fabric; [SR599] {hs#62} (F48)
35 [SR]	N75E 63SE	075(N75E)	63SE				3a. Xfh: Xa (amphibolite gneiss)	Metamorp hic foliation/ fabric of an amphiboli tic exposure; [SR599] {hs#62} (F49)
36 [SR]	N12W 65NE	348 (N12W)	65 NE				3a. Xfh: Xa (amphibolite gneiss)	Fracture/J oint [SR699] {hs#61/ts #25} (J13)
36 [SR]	N17W 77NE	343 (N17W)	77 NE				3a. Xfh: Xa (amphibolite gneiss)	Fracture/J oint [SR699] {hs#61/ts #25} (J14)
36 [SR]	N65E 73NW	065 (N65E)	73NW				3a. Xfh: Xa (amphibolite gneiss)	Fracture/J oint [SR699] {hs#61/ts #25} (J15)
37 [SR]	N45E 30SE	045 (N45E)	30SE				3b. Xfh: Xqf (quartzofeldspa thic gneiss)	Metamorp hic foliation/ fabric. [SR799] {hs#60} (F50)

								Brittle Fracture Plane/Joint face towards the lakes [SR799] {hs#60} (J16)
37 [SR]	N30W69SW	330 (N30W)	69SW					3b. Xfh: Xqf (quartzofeldspathic gneiss)
37 [SR]	N87E	087 (N87E)						Trend ~E/W. [SR799] {hs#60} (T10)
37 [SR]	N27E	027 (N27E)						Trend ~N/S [SR799] {hs#60} (T11)
38 [SR]	N27E 50NW	027 (N27E)	50NW					Metamorphic foliation/fabric; [SR899] {hs#59} (F51)
38 [SR]	N05W 87NE	355 (N05W)	87NE					Fracture/Joint face resembles a shear face; trends ~N/S; [SR899] {hs#59} (J17)
39 [SR]	N80E 40NW	080 (N80E)	40NW					Metamorphic foliation/fabric [SR999] {hs#58/ts#24} (F52)
39 [SR]	N60E 38NW	060 (N60E)	38NW					Metamorphic foliation/fabric [SR999] {[hs#58/ts#24} (F53)
40 [SR]	N07W 77NE	353 (N07W)	77NE					Lineament contact [SR1099]

							(amphibolite gneiss)	{hs#57} (T12)
41 [SR]	N80E 70NW	080 (N80E)	70NW				3a. Xfh: Xa (amphibolite gneiss)	Metamorphic foliation/fabric [SR1199] (F54)
41 [SR]	N76E 68NW	076 (N76E)	68NW				3a. Xfh: Xa (amphibolite gneiss)	Fracture/Joint face ~E/W [SR1199] (J18)
41 [SR]	N05W 79NE	355 (N05W)	79 NE				3a. Xfh: Xa (amphibolite gneiss)	Fracture/Joint face due ~N/S [SR1199] (J19)
42 [SR]	N35E 74NW	035 (N35E)	74NW				6. i (intrusive)	Fracture/Joint [SR1299] {hs#56/ts #23} (J20)
42 [SR]	N10W 60SW	350 (N10W)	60SW				6. i (intrusive)	Fracture/Joint [SR1299] {hs#56/ts #23} (J21)
43 [SR]	N54E 76SE	054 (N54E)	76SE				3a. Xfh: Xa (amphibolite gneiss)	Fracture/Joint [SR1399] {hs#55} (J22)
43 [SR]	N69W 87SW	291 (N69W)	87SW				3a. Xfh: Xa (amphibolite gneiss)	Fracture/Joint [SR1399] {hs#55} (J23)
44 [SR]	N10W 79NE	350 (N10W)	79NE	17	n07w	17 from ne	3c. Xfh:Xfa (feather amphibolite)	Metamorphic foliation with slicks of hornblende stretching mineral [SR1599] {hs#53} (F55) (L17[downstrike])
44 [SR]	N72W 75SW	288 (N72W)	75SW				3c. Xfh:Xfa	Fracture/Joint [SR1599]

							(feather amphibolite)	{hs#53} (J24)
44 [SR]	N30E 30SE	030 (N30E)	30SE				3c. Xfh:Xfa (feather amphibolite)	Fracture/Joint [SR1499] {hs#54} (J25)
45 [SR]	N57E 54SE	057 (N57E)	54SE				3a. Xfh: Xa (amphibolite gneiss)	Metamorphic foliation/fabric [SR1699] {hs#52/ts#22} (F56)
45 [SR]	N25W 46NE	335 (N25W)	46NE				3a. Xfh: Xa (amphibolite gneiss)	Fracture/Joint [SR1699] {hs#52/ts#22} (J26)
47 [SR]	N30W 50SW	330 (N30W)	50SW				3a. Xfh: Xa (amphibolite gneiss)	Metamorphic foliation/fabric joint faces [SR1899] {hs#50} (F57)
47 [SR]	N90E 58S	090 (N90E)	58 S				3a. Xfh: Xa (amphibolite gneiss)	Fracture/Joint face E/W [SR1899] {hs#50} (J27)
47 [SR]	N27W 84SW	333 (N27W)	84 SW				3a. Xfh: Xa (amphibolite gneiss)	Fracture/Joint face [SR1899] {hs#50} (J28)
49 [SR]	N47E 60NW	047 (N47E)	60 NW				3b. Xfh: Xqf (quartzofeldspathic gneiss)	Metamorphic foliation/fabric [SR2099] {hs#48/ts#20} (F58)
51 [SR]	N65W 57SW	295 (N65W)	57SW	48	n21e		3a. Xfh: Xa (amphibolite	Metamorphic foliation/fabric with slicks (F59) (L18)

						62 from nw	gneiss)	[updip])
51 [SR]	N05E 67SE	005 (N05E)	67SE				3a. Xfh: Xa (amphibolite gneiss)	Fracture/ Joint oriented ~N/S (J29)
51 [SR]	N63W 71SW	297 (N63W)	71 SW				3a. Xfh: Xa (amphibolite gneiss)	Fracture/ Joint ~E/W (J30)
52 [SR]	N25E 70SE	025 (N25E)	70SE				3b. Xfh: Xqf (quartzofeldspa thic gneiss)	Fracture/ Joint @ 12120' (J31)
53 [SR]	N07W 63SW	353 (N07W)	63SW				3a. Xfh: Xa (amphibolite gneiss)	Fracture/ Joint [SR2299] {hs#46} (J32)
53 [SR]	N10E 79SE	010 (N10E)	79 SE				3b. Xfh: Xqf (quartzofeldspa thic gneiss)	Fracture/ Joint [SR2399] {hs#45} (J33)
54 [SR]	N75E 63NW	075 (N75E)	63 NW				3b. Xfh: Xqf (quartzofeldspa thic gneiss)	Metamorp hic foliation/ fabric (F60)
56 [SR]	N60E 65NW	060 (N60E)	65 NW				3a. Xfh: Xa (amphibolite gneiss)	Metamorp hic foliation/f abric [SR2599] {hs#43} (F61)
56 [SR]	N90E 64NW	090 (N90E)	64NW				3a. Xfh: Xa (amphibolite gneiss)	Fracture/ Joint ~due E/W [SR2599] {hs#43} (J34)
56 [SR]	N04W 83SW	356 (N04W)	83SW				3a. Xfh: Xa (amphibolite gneiss)	Fracture/ Joint ~due N/S [SR2599] {hs#43} (J35)
58 [SR]	N90E 89SE	090 (N90E)	89SE				2. Xqfg (quartzofeldspa	Metamorp hic foliation/f abric; [SR2799] {hs#41}

							thic gneiss)	(F62)
59 [SR]	N89W 90NE	271 (N89W)	90NE				2. Xqfg (quartzofeldspathic gneiss)	Fracture/ Joint [SR2899] {hs#40} (J36)
60 [SR]	N70W 47NE	290 (N70W)	47NE				1a. Xag:Xh (black a.g.)	Metamorphic foliation/f abric [SR2999] {hs#39} (F63)
61 [SR]	N43W 84NE	317 (N43W)	84 NE				2. Xqfg (quartzofeldspathic gneiss)	Fracture/J oint [SR3099] {hs#38/ts #17} (J37)
61 [SR]	N43W	317 N43W)					2. Xqfg (quartzofeldspathic gneiss)	Trend of ~NW contact [SR3099] {hs#38/ts #17} (T13)
62 [SR]	N70W 54NE	290 (N70W)	54NE				2. Xqfg (quartzofeldspathic gneiss)	Fracture/ Joint (J38)
64 [SR]	N15E 73SE	015 (N15E)	73SE				2. Xqfg (quartzofeldspathic gneiss)	Fracture/ Joint [SR3299] {hs#36} (J39)
64 [SR]	N73W 84SW	287 (N73W)	84SW				2. Xqfg (quartzofeldspathic gneiss)	Fracture/ Joint [SR3299] {hs#36} (J40)
66 [SR]	N15E 86NW	015 (N15E)	86NW				1c. Xag: Xfs (qfschist)	Metamorphic foliation/f abric [SR3399] {hs#34} (F64)
66 [SR]	N27E 79NW	027 (N27E)	79NW				1c. Xag: Xfs (qfschist)	Metamorphic foliation/f abric [SR3499] {hs#33} (F65)
66 [SR]	N10E 78SE	010 (N10E)	78SE				1c. Xag: Xfs (qfschist)	Fracture/ Joint on

								top of 10840'- 10880' just SW of 10787' [SR3399] {hs#34} [SR3499] {hs#33} (J41)
66 [SR]	N80W 65SW	280 (N80W)	65SW				1c. Xag: Xfs (qfschist)	Fracture/ Joint on top of 10840'- 10880' just SW of 10787' [SR3399] {hs#34} [SR3499] {hs#33} (J42)
67 [SR]	N45W 47NE	315 (N45W)	47NE				1b. Xag: Xf (gray c-b a.g.)	Metamorp hic foliation/ fabric in a prospect hole at 10787' (F66)
68 [SR]	N55W 68NE	305 (N55W)	68NE				1b. Xag: Xf (Gray comp- banded a.g.)	Metamorp hic foliation/ fabric (F67)
69 [SR]	N32W 89NE	328 (N32W)	89NE				5a. Pf (1b.Xag:Xf) PXf/Pgray c-b a.g.	Metamorp hic foliation/ fabric [SR3599] {hs#32/ts #15} (F68)
70 [SR]	N20W 29NE	340 (N20W)	29NE				1b. Xag: Xf (gray c-b a.g.)	Metamorp hic foliation/ Fabric (F69)
72 [NR]	N20W 45NE	340 (N20W)	45NE				1a. Xag:Xh (black a.g.)	Metamorp hic foliation/ fabric; [NR2199] {hs#6} (F70)

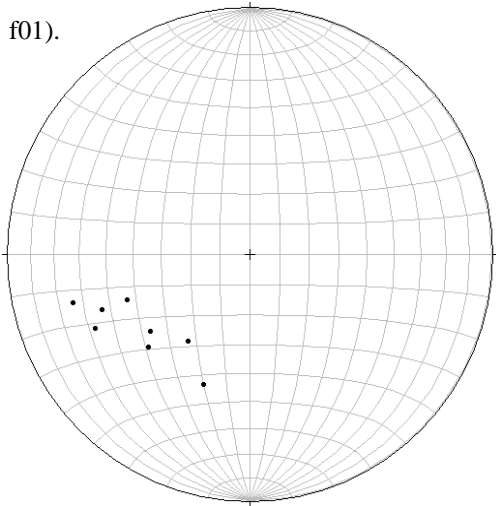
							1b. Xag:Xf (gray c-b a.g.)	Metamorphic foliation/ fabric [NR2299] {hs#5} (F71)
73 [NR]	N55W 64NE	305 (N55W)	64NE					
74 [NR]	N80E 84NW	080 (N80E)	84NW				1a. Xag:Xh (black a.g.)	Fracture/ Joint (J43)
74 [NR]	N26W 55SW	334 (N26W)	55 SW				1a. Xag:Xh (black a.g.)	Fracture/ Joint (J44)
74 [NR]	N13W	347 (N13W)					1a. Xag:Xh (black a.g.)	Trend NW of quartz veins across NE plane (T14)
75 [NR]	N06W 59NE	324 (N06W)	59NE				1b. Xag:Xf (gray c-b a.g.)	Metamorphic foliation/ fabric; Figure 35a looking S at exposure. [NR2399] {hs#4/ts# 12} (F72)
75 [NR]	N12W 67NE	348 (N12W)	67NE				1b. Xag:Xf (gray c-b a.g.)	Fracture/ Joint [NR2399] {hs#4/ts# 12} (J45)
75 [NR]	N16W 65NE	344 (N16W)	65NE				1b. Xag:Xf (gray c-b a.g.)	Fracture/ Joint [NR2399] {hs#4/ts# 12} (J46)
75 [NR]	N16W 79NE	344 (N16W)	79NE				1b. Xag:Xf (gray c-b a.g.)	Trend [NR2399] {hs#4/ts# 12} (T15)
76 [NR]	N15W 65NE	345 (N15W)	65NE				1a. Xag:Xh (black a.g.)	Metamorphic foliation/ fabric [NR2499] {hs#3} (F73)
77 [NR]	N20W 55NE	340 (N20W)	55NE	30	n03e			Metamorphic foliation/ fabric

								with hornblende stretching mineral lineation [NR2599] {hs#2} (F74) (L19 [downdip])
						37 from ne	1a. Xag:Xh (black a.g.)	
78 [NR]	N25W 60NE	335 (N25W)	60NE				1a. Xag:Xh (black a.g.)	Metamorphic foliation/fabric @ 38.29.672 & 106.11.756 and ~9879/9880'; [NR2699] {hs#1/ts#1} (F75)
79 [NR]	N54W 36NE	306 (N54W)	36NE				1a. Xag:Xh (black a.g.)	Metamorphic foliation/fabric @ 38.29.82 & 106.11.72 looking over to a prominent qfg amphibolite exposure on a roadcut of CR221 (F76)
80 [NR]	N87W 23SW	273 (N87W)	23 SW				3a. Xfh: Xa (amphibolite gneiss)	Metamorphic foliation/fabric [IS199] {hs#67} (F77)
81 [SR]	N37W 43NE	323 (N37W)	43 NE				1a. Xag:Xh (black a.g.)	Metamorphic foliation/fabric [SR3899]

								{hs#68} (F78)
82 [SR]	N42W 47NE	318 (N42W)	47 NE				1a. Xag:Xh (black a.g.)	Metamorphic foliation/ fabric [SR3999] {hs#69} (F79)

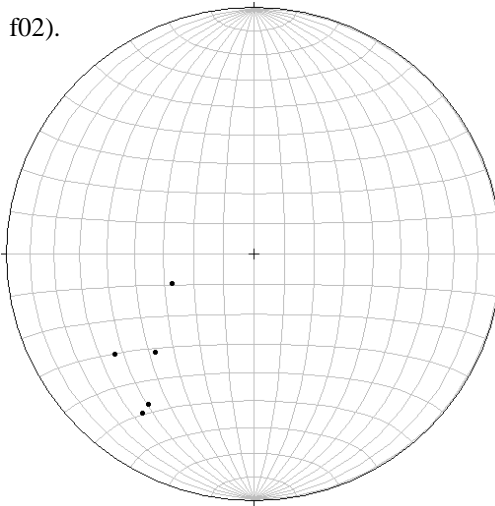
APPENDIX F: STEREAONETS

f01).



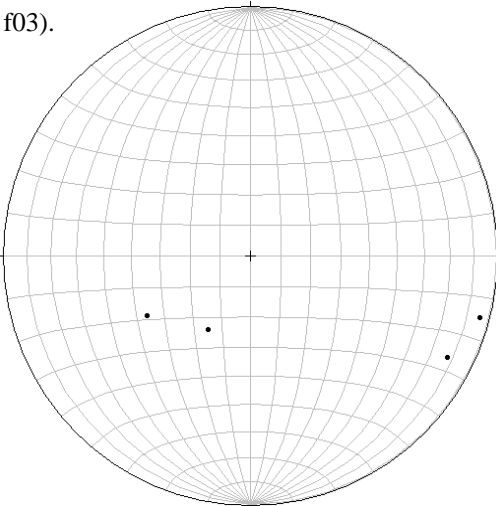
foliations NRSR 1a Xag Xh f01 [8]

f02).



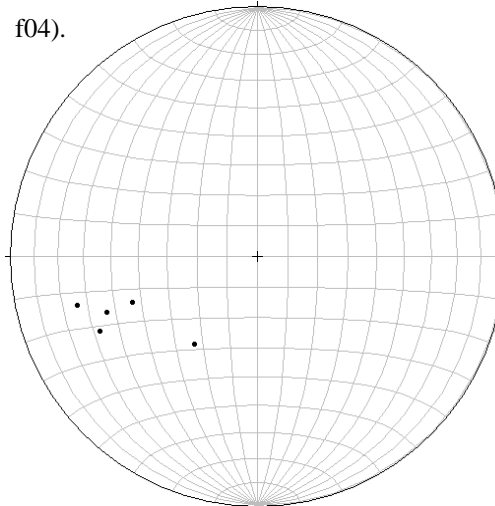
foliations NRSR 1b Xag Xf wo5aPf f02 [5]

f03).



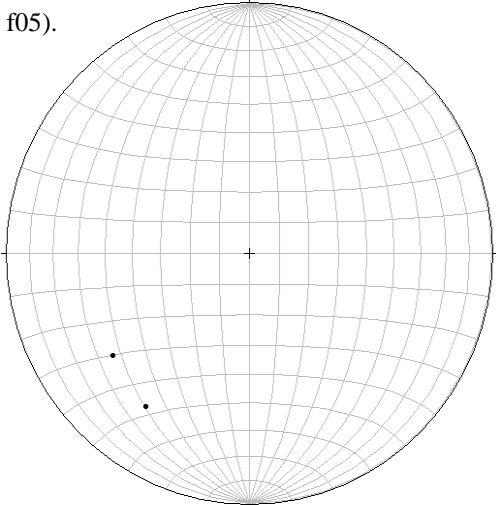
foliations NRSR 1c Xag Xfs wo5bPfs f03 [4]

f04).



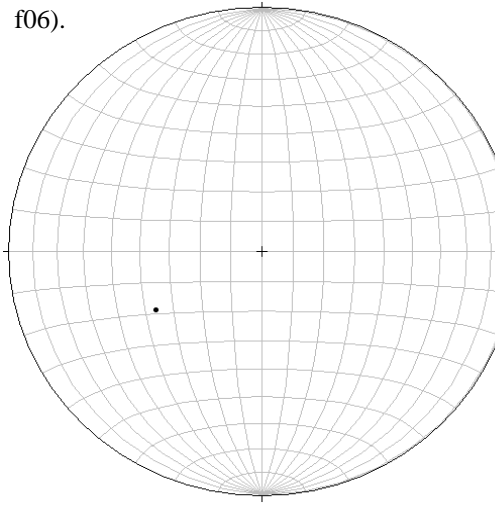
foliations NR 1a Xag Xh f04 [5]

f05).



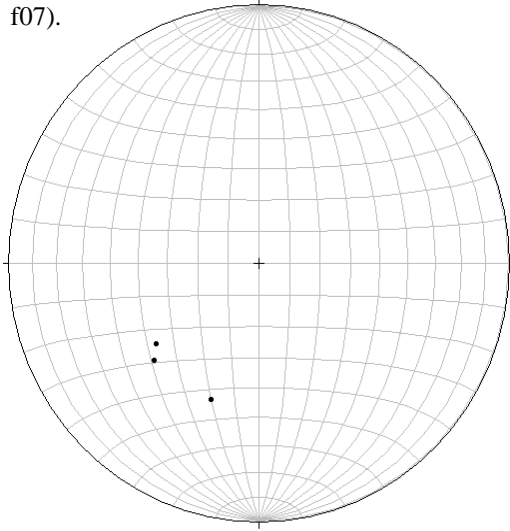
foliations NR 1b Xag Xf f05 [2]

f06).



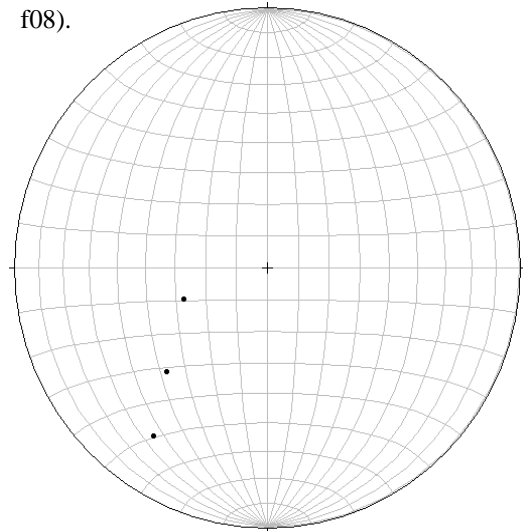
foliations NR 1c Xag Xfs wo5bPfs f06 [1]

f07).



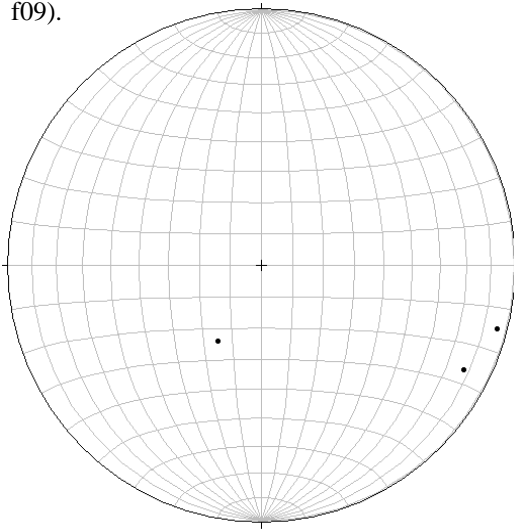
foliations SR 1a Xag Xh f07 [3]

f08).



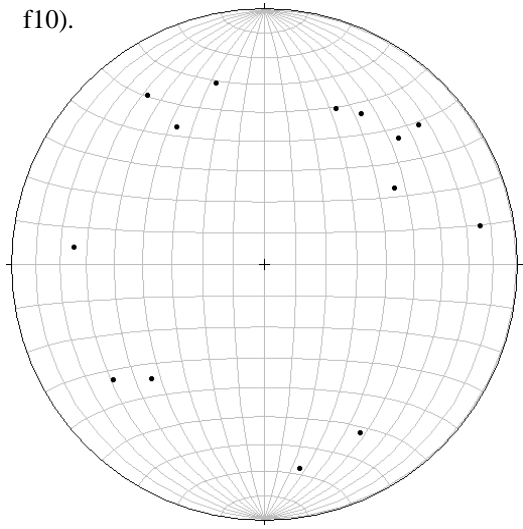
foliations SR 1b Xag Xf wo5aPf f08 [3]

f09).



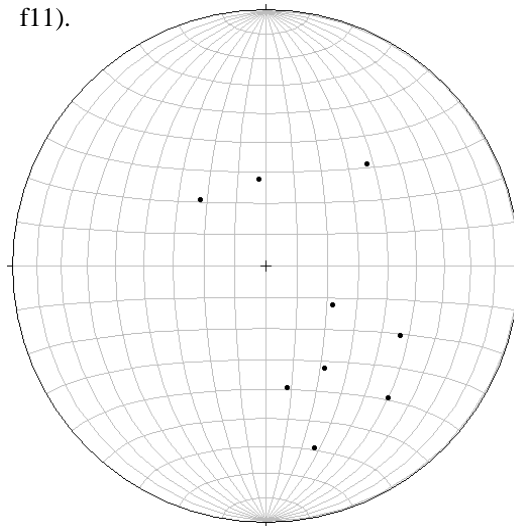
foliations SR 1c Xag Xfs f09 [3]

f10).



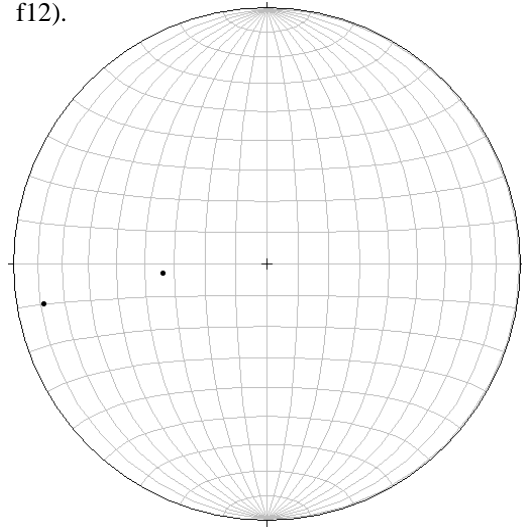
foliations NRSR 3a f10 [14]

f11).



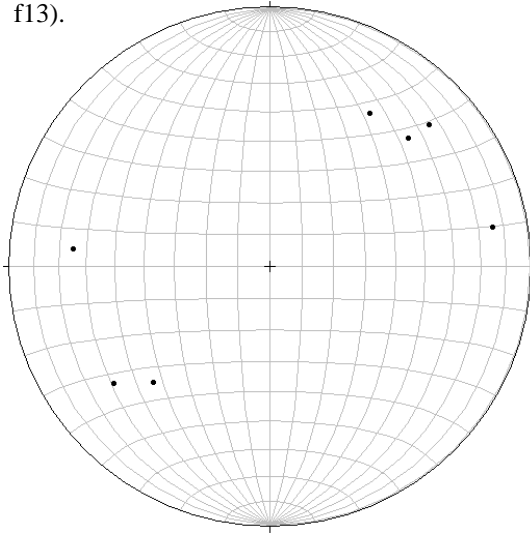
foliations NRSR 3b f11 [9]

f12).



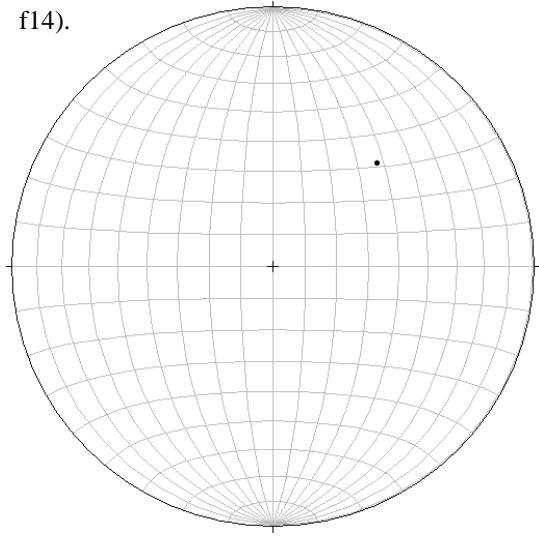
foliations NRSR 3c f12 [2]

f13).



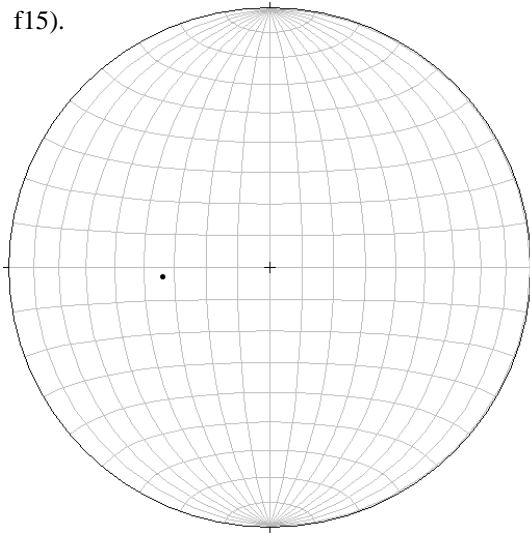
foliations NR 3a f13 [7]

f14).



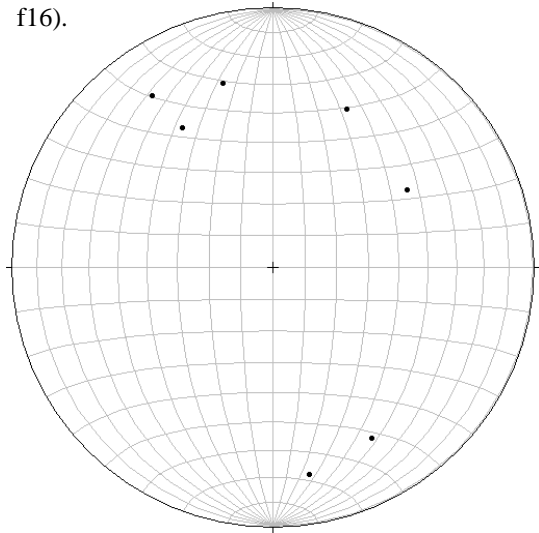
foliations NR 3b f14 [1]

f15).



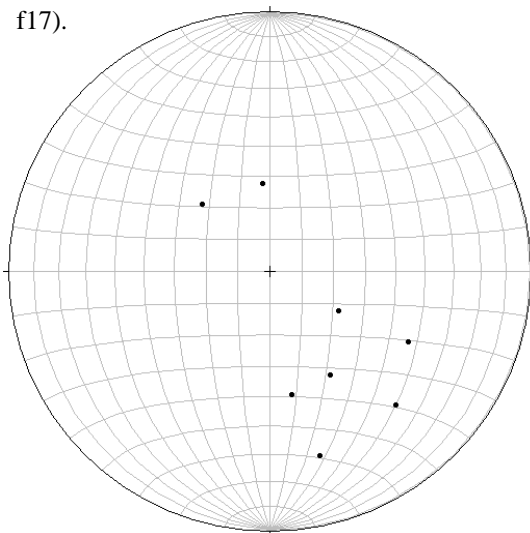
foliations NR 3c f15 [1]

f16).



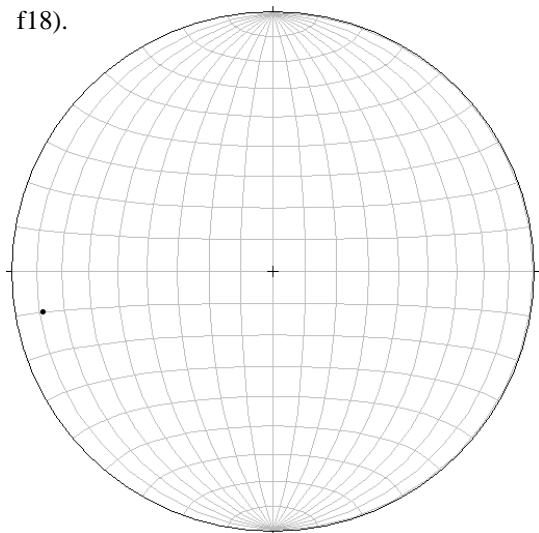
foliations SR 3a f16 [7]

f17).



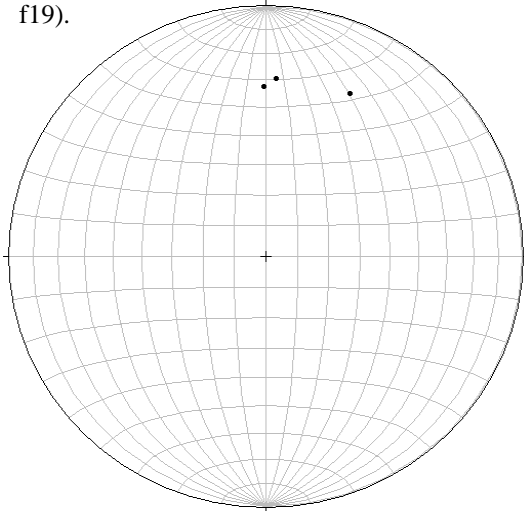
foliations SR 3b f17 [8]

f18).



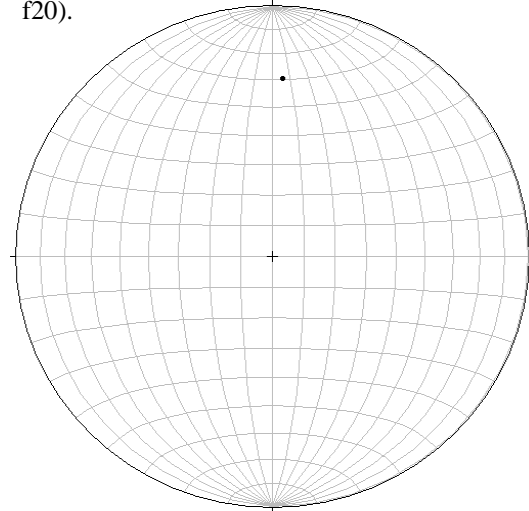
foliations SR 3c f18 [1]

f19).



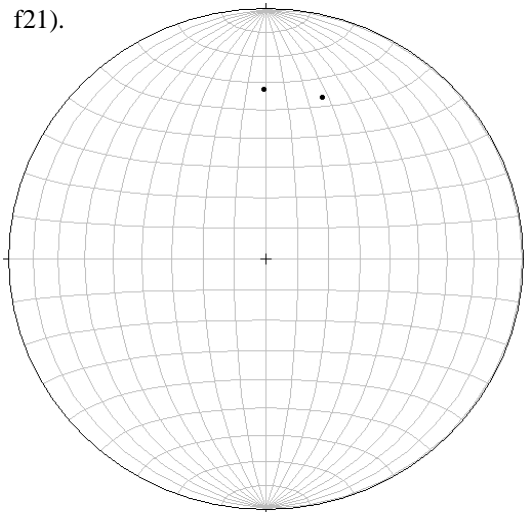
lineations NR 1 Xag f19 [3]

f20).



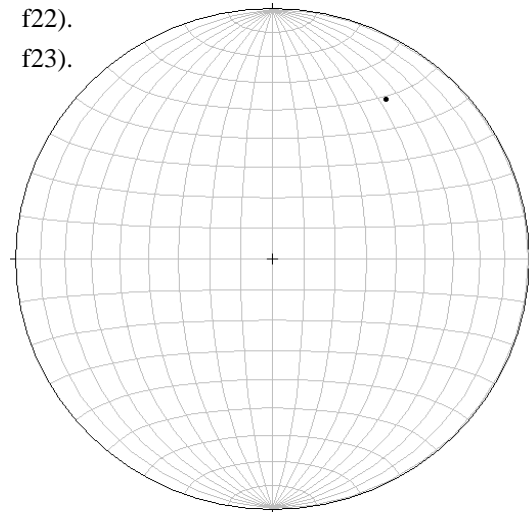
lineations NR 1a Xag Xh f20 [1]

f21).



lineations NR 1c Xag Xfs f21 [2]

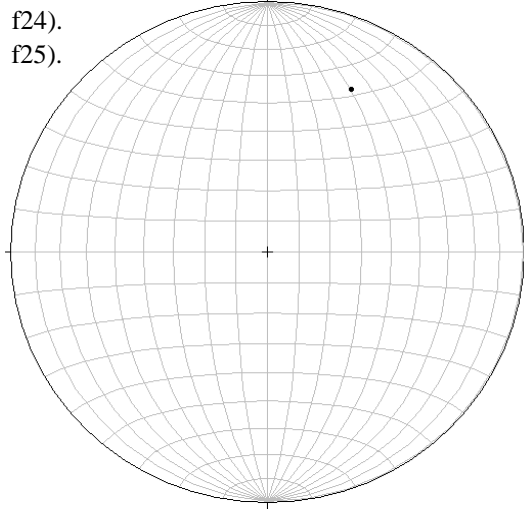
f22).



f23).

lineations NR 3 Xfh f22 f23 [1]

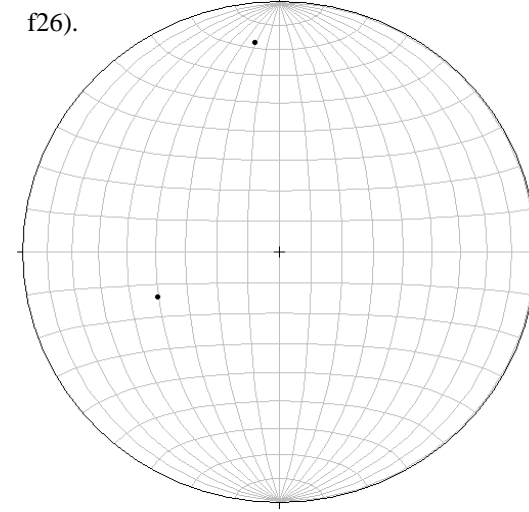
f24).



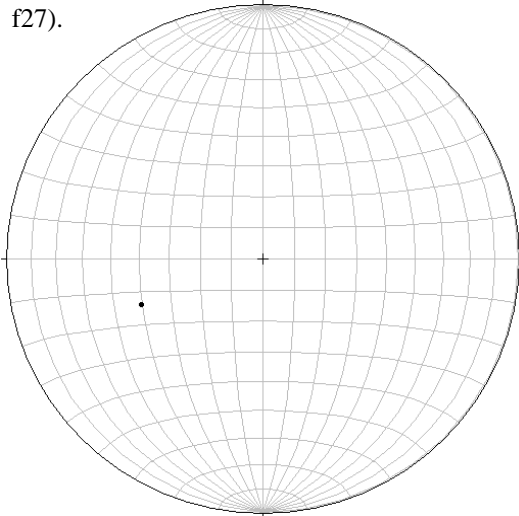
f25).

lineations SR 1 Xag f24 f25 [1]

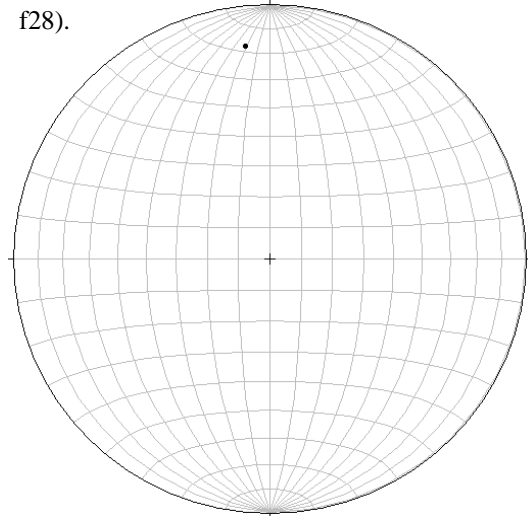
f26).



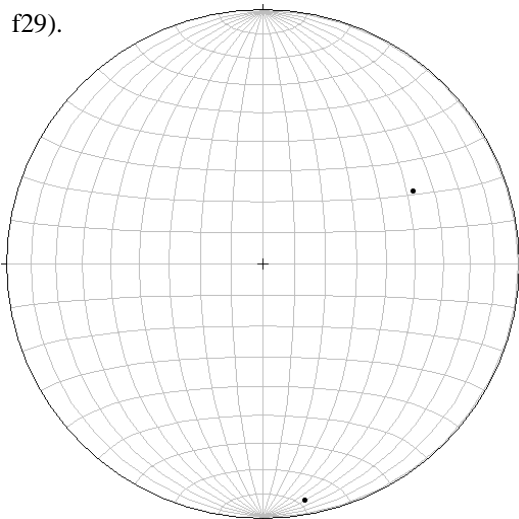
lineations SR 3 Xfh f26 [2]



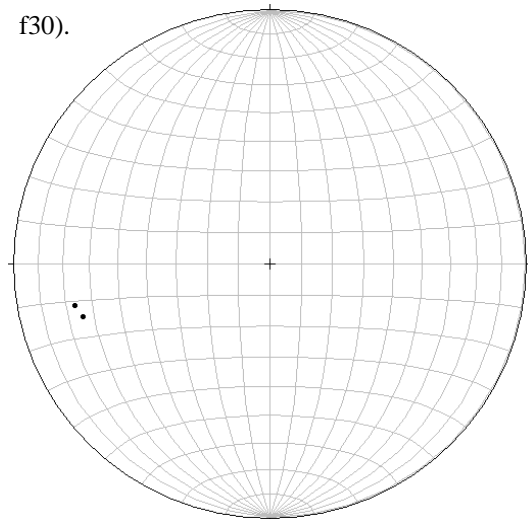
lineations SR 3a Xfh Xa f27 [1]



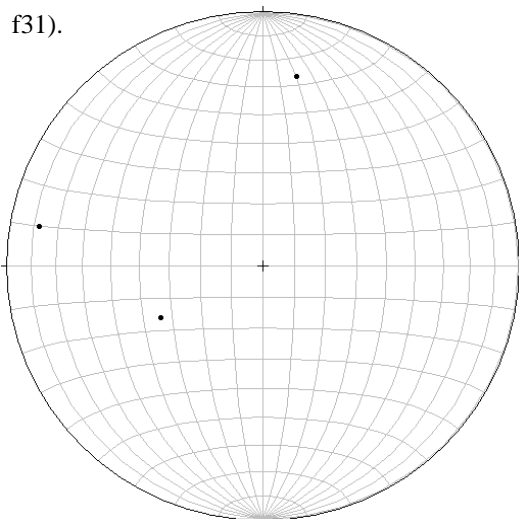
lineations SR 3c Xfh Xfa f28 [1]



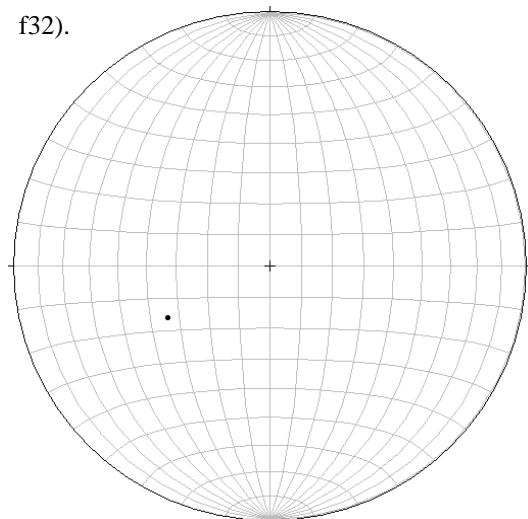
fractures NR 1a Xag Xh f29 [2]



fractures NR 1b Xag Xf f30 [2]

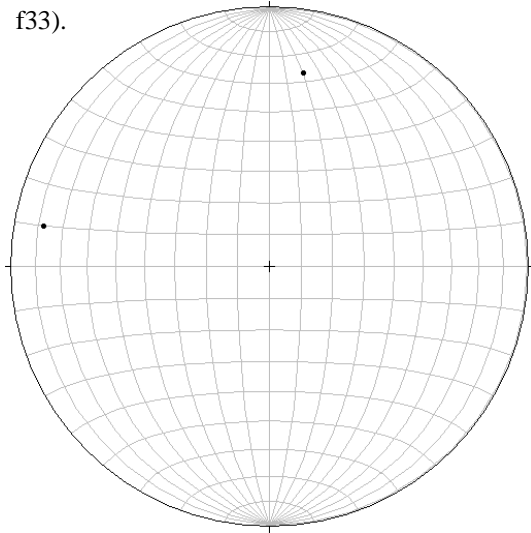


fractures NRSR 1c Xag Xfs f31 [3]



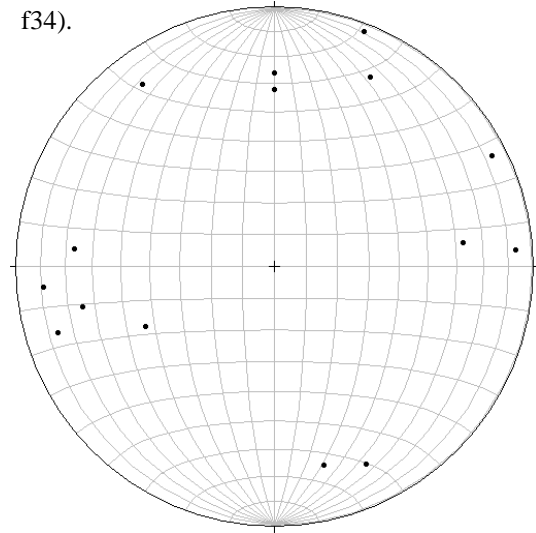
fractures NR 1c Xag Xfs f32 [1]

f33).



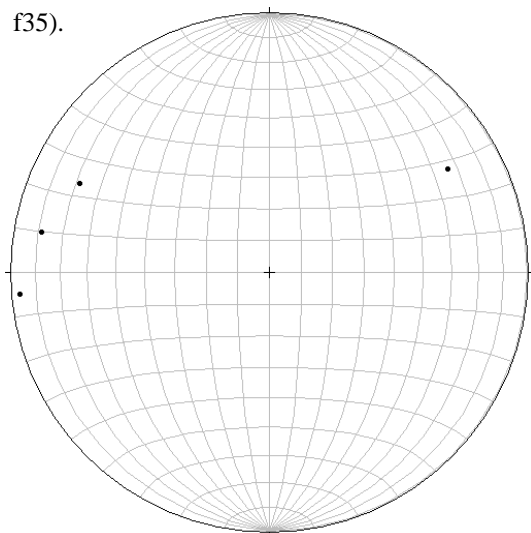
fractures SR 1c Xag Xfs f33 [2]

f34).



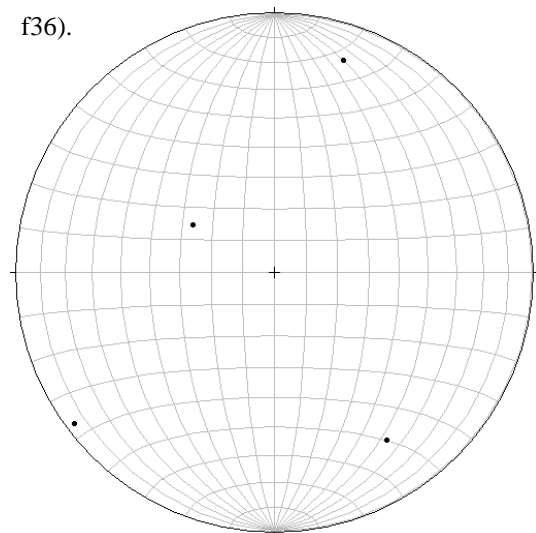
fractures SR 3a Xfh Xa f34 [15]

f35).



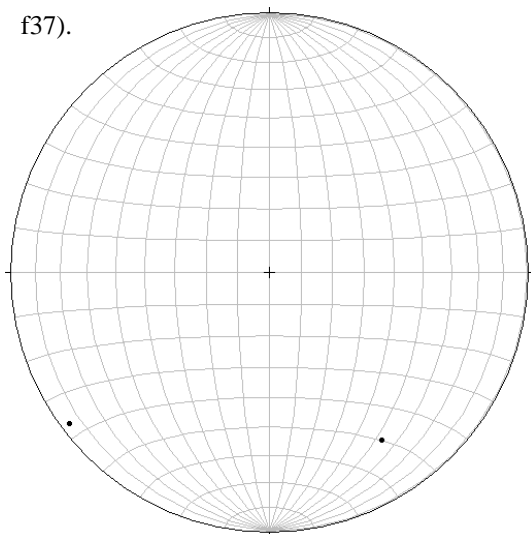
fractures SR 3b Xfh Xqf f35 [4]

f36).



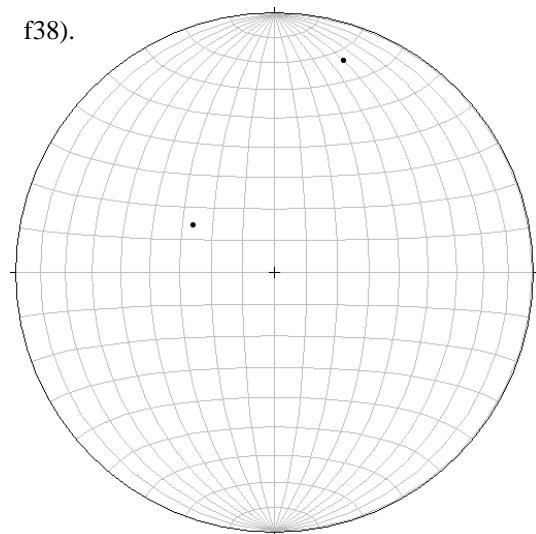
fractures NRSR 3c Xfh Xfa f36 [4]

f37).



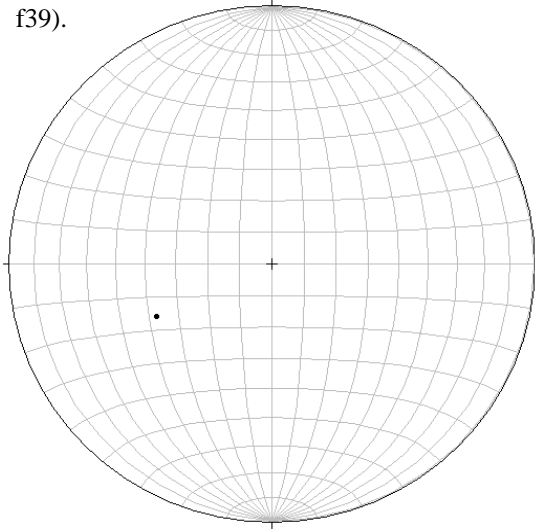
fractures NR 3c Xfh Xfa f37 [2]

f38).



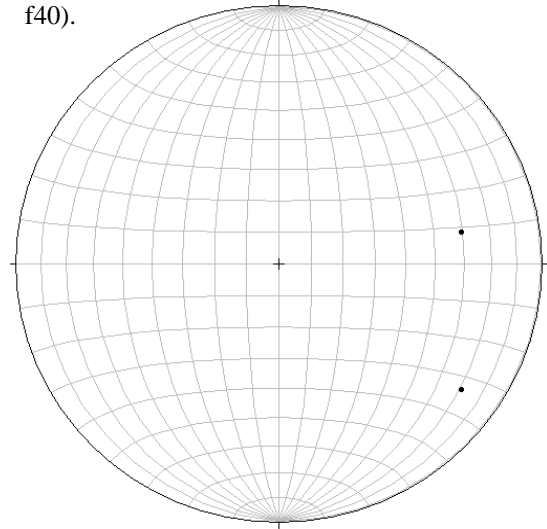
fractures SR 3c Xfh Xfa f38 [2]

f39).



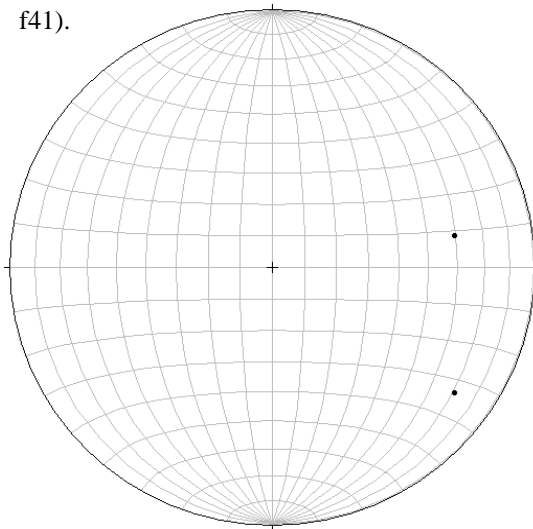
fractures NRSR 3d Xfh Xhb f39 [1]

f40).



fractures NRSR 6 i f40 [2]

f41).



fractures SR 6 i f41 [2]

APPENDIX G: PLATES:

PLATE I: Structural Map

PLATE II: Petrologic Map

PLATE III: Cross-section

PETROLOGIC SPECIMENS/SAMPLES BY UNIT & RIDGELINE:

QUANTITY HAND SPECIMENS = ()
 QUANTITY THIN SECTIONS = []
 QUANTITY AFT SAMPLE SITES/MINERAL SEPARATIONS = { }
 { 6 NR } = NR599, NR1*99, NR899, NR17*99, NR1899 & NR1799
 { 1 SR } = SR399

BY UNIT:	BY RIDGELINE:
Xag (16) [6] (0)	NR (30) [13] (6)
Xqfg (18) [7] (3)	SR (38) [12] (1)
Xfh (35) [12] (4)	IS (01) [00] (0)
TOTAL (69) [25] (7)	TOTAL (69) [25] (7)

BY UNIT & RIDGELINE:

NR (30) = 8(1.Xag) + 10(2.Xqfg) + 12(3.Xfh)
 SR (38) = 8(1.Xag) + 8(2.Xqfg) + 22(3.Xfh)
 IS (01) = 0(1.Xag) + 0(2.Xqfg) + 1(3.Xfh)

EQUIVALENCES ACROSS RIDGELINES:

NR2299 ~ SR3699 (1b.Xag:Xf)
 NR499 ~ SR1*99, SR3499 & SR3399 (1c.Xag:Xfs)
 NR799 ~ SR3299 (2.Xqfg)
 NR1999 ~ SR699 (3c.Xfh:Xfa)
 NR699 ~ SR299 (4.Xcs)
 NR4*99 ~ SR3799 (5b.Pfs)

Xfh
 NR (12) [5] (3)
 SR (22) [7] (1)
 IS (01) [0] (0)
 TOTAL (35) [12] (4)
 NR (12) = 4A's, 2Q's, 3F's 1hb, 1qms & 1i
 SR (22) = 9A's, 7Q's, 4F's & 2i's

Xqfg
 NR (10) [4] (3)
 SR (8) [3] (0)
 TOTAL (18) [7] (3)

NR Xag
 NR Xag:Xh (3) [1] (0)
 NR Xag:Xf (3) [1] (0)
 NR Xag:Xfs (2) [2] (0)
 TOTAL NR Xag (8) [4] (0)

Xag
 NR (8) [4] (0)
 SR (8) [2] (0)
 TOTAL (16) [6] (0)

SR Xag
 SR Xag:Xh (2) [0] (0)
 SR Xag:Xf (2) [2] (0)
 SR Xag:Xfs (4) [0] (0)
 TOTAL SR Xag (8) [2] (0)

LEGEND:

- LOCATION
- Ⓢ LOCATION IDENTIFICATION NUMBER (see APPENDIX F)
- FAULT (DASHED WHERE INFERRED; BAR AND BALL ON DOWNTHROWN SIDE)
- GEOLOGIC CONTACT (DASHED WHERE INFERRED)
- NR NORTH RIDGELINE
- SR SOUTH RIDGELINE
- PCSZ PASS CREEK SHEAR ZONE (PCSZ)
- FOLD
- X PROSPECT MINE
- A-A' LINE OF CROSS-SECTION
- NR#99 HAND SPECIMEN IDENTIFICATION (ALSO SR#99 & IS#99)
- THIN SECTIONS (25)
- AFT SAMPLES (7)
- BOTH THIN SECTION & AFT SAMPLE (1)
- REPRESENTATIVE SAMPLE

LITHOLOGIC UNITS:

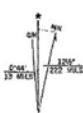
- 1. PRECAMBRIAN AMPHIBOLITE GNEISS (Xag)
- 1. PRECAMBRIAN AMPHIBOLITE GNEISS (Xag)
- 1a. PRECAMBRIAN AMPHIBOLITE GNEISS: BLACK AMPHIBOLITE GNEISS (Xag:Xh)
- 1b. PRECAMBRIAN AMPHIBOLITE GNEISS: GRAY COMPOSITIONALLY-BANDED AMPHIBOLITE GNEISS (Xag:Xf)
- 1c. PRECAMBRIAN AMPHIBOLITE GNEISS: QUARTZOFELDSPATHIC SCHIST (Xag:Xfs)
- 2. PRECAMBRIAN QUARTZOFELDSPATHIC GNEISS (Xqfg)
- 3. PRECAMBRIAN FELSIC HORNBLENDIC GNEISS (Xfh)
- 3. PRECAMBRIAN FELSIC HORNBLENDIC GNEISS (Xfh)
- 3a. PRECAMBRIAN FELSIC HORNBLENDIC GNEISS: HORNBLENDIC AMPHIBOLITE GNEISS (Xfh:Xa)
- 3b. PRECAMBRIAN FELSIC HORNBLENDIC GNEISS: FELSIC QUARTZOFELDSPATHIC GNEISS (Xfh:Xqf)
- 3c. PRECAMBRIAN FELSIC HORNBLENDIC GNEISS: FEATHER AMPHIBOLITE (Xfh:Xfa)
- 3d. PRECAMBRIAN FELSIC HORNBLENDIC GNEISS: HORNBLende PORPHYROBLASTS (Xfh:Xhb)
- 3d. PRECAMBRIAN FELSIC HORNBLENDIC GNEISS: QUARTZ MICA SCHIST (Xfh:Xqms)
- 4. CALC-SILICATE GNEISS (Xcs; 2a.Xqfg:Xcs)
- 5a. PORPHYROBLASTIC GRAY COMPOSITIONALLY-BANDED AMPHIBOLITE GNEISS "POD" ROCK (Pf)
- 5b. PORPHYROBLASTIC QUARTZOFELDSPATHIC SCHIST "POD" ROCK (Pfs)
- 6. IGNEOUS INTRUSIONS (I)

FAULTS:

- PCF PASS CREEK FAULT (1)
- HJ1 HUMP JUT FAULT SPLAY 1 (2)
- HJ2 HUMP JUT FAULT SPLAY 2 (2)
- WCTF WILLOW CREEK TRANSFER FAULT (3)
- DD DRAINAGE DIVIDE FAULT (5)
- SZ PASS CREEK SHEAR ZONE FAULT (6)

Mapped, edited, and published by the Geological Survey

Control by USGS and NGS/NOAA
 Topography by photogrammetric methods from aerial photographs taken 1975. Field checked 1976. Map edited 1980
 Projection: Colorado coordinate system, central zone (Lambert conformal conic)
 10,000-foot grid ticks based on Colorado coordinate system, central and south zones
 1000-meter Universal Transverse Mercator grid, zone 13
 1927 North American Datum
 To place on the predicted North American Datum 1983 move the projection lines 4 meters north and 51 meters east as shown by dashed corner ticks
 Fine red dashed lines indicate selected fence lines
 Certain land lines are omitted because of insufficient data



0 1000 2000 3000 4000 5000 6000 7000 8000 9000 10000 FEET
 0 1 2 3 4 5 6 7 8 9 10 KILOMETER

CONTOUR INTERVAL 40 FEET
 NATIONAL GEODETIC VERTICAL DATUM OF 1929

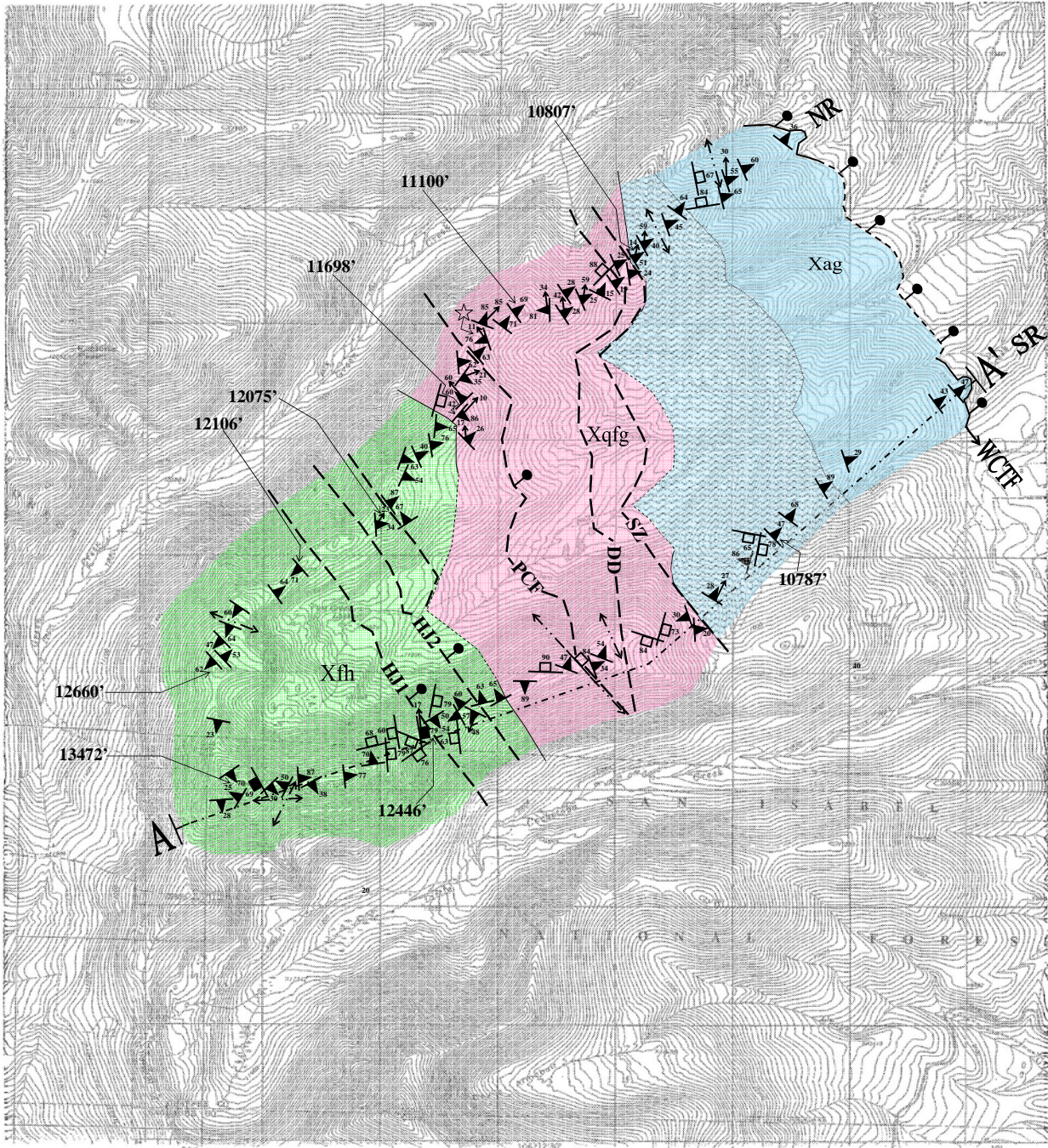


ROAD CLASSIFICATION:
 Light duty road, hard or improved surface
 Unimproved road

PLATE I: PETROLOGIC MAP

REBECCA "BECKY" ROBBINS





LEGEND:

- FAULT (DASHED WHERE INFERRED; BAR AND BALL ON DOWNTROWN SIDE; ARROWS INDICATE APPARENT RELATIVE MOVEMENT)
- GEOLOGIC CONTACT (DASHED WHERE INFERRED)
- NR** NORTH RIDGELINE
- SR** SOUTH RIDGELINE
- STRIKE AND DIP OF METAMORPHIC FOLIATION
- STRIKE AND DIP OF METAMORPHIC FOLIATION WITH BEARING AND PLUNGE OF LINEATION
- STRIKE AND DIP OF JOINT/FRACTURE/BFP
- STRIKE AND DIP OF FACE
- TREND
- PASS CREEK SHEAR ZONE (PCSZ)
- FOLD
- PROSPECT MINE
- LINE OF CROSS-SECTION

LITHOLOGIC UNITS:

- 1. PRECAMBRIAN AMPHIBOLITE GNEISS (Xag)
- 2. PRECAMBRIAN QUARTZOFELDSPATHIC GNEISS (Xqfg)
- 3. PRECAMBRIAN FELSIC HORNBLENDIC GNEISS (Xfh)

FAULTS:

- PCF** PASS CREEK FAULT (1)
- HJ1** HUMP JUT FAULT SPLAY 1 (2)
- HJ2** HUMP JUT FAULT SPLAY 2 (2)
- WCTF** WILLOW CREEK TRANSFER FAULT (3)
- DD** DRAINAGE DIVIDE FAULT (5)
- SZ** PASS CREEK SHEAR ZONE FAULT (6)

Mapped, edited, and published by the Geological Survey

Control by USGS and NGS/NOAA

Topography by photogrammetric methods from aerial photographs taken 1975. Field checked 1975. Map edited 1980

Projection: Colorado coordinate system, central zone (Lambert conformal conic)

10,000-foot grid ticks based on Colorado coordinate system, central and south zones

1000-meter Universal Transverse Mercator grid, zone 13

1927 North American Datum

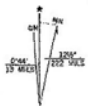
To place on the predicted North American Datum 1983

move the projection lines 4 meters north and

51 meters east as shown by dashed corner ticks

Fine red dashed lines indicate selected fence lines

Certain land lines are omitted because of insufficient data



CONTOUR INTERVAL 40 FEET
NATIONAL GEODEIC VERTICAL DATUM OF 1929



QUADRANGLE LOCATION

ROAD CLASSIFICATION

Light duty road, hard or improved surface

Unimproved road

PLATE II: STRUCTURAL MAP

REBECCA "BECKY" ROBBINS



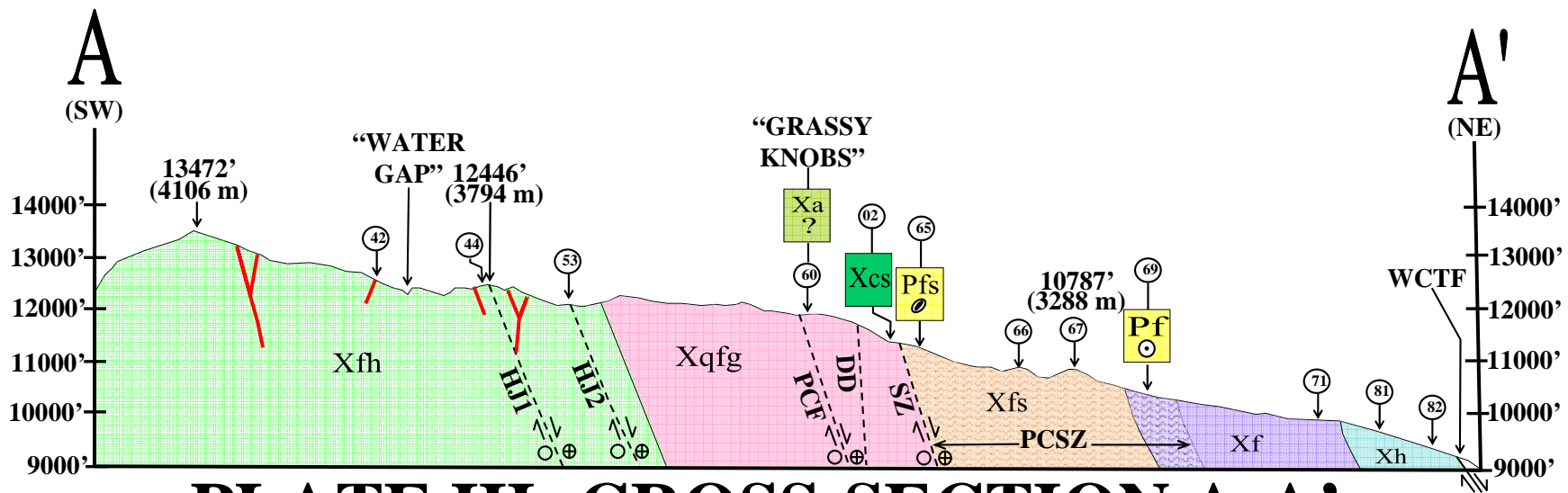


PLATE III: CROSS-SECTION A-A'

LOOKING NORTHWEST AT PROFILE OF SOUTH RIDGELINE (SR)

SCALE: 1" = 2000' (610 m)



LEGEND:

- ⊕ LOCATION IDENTIFICATION NUMBER (see APPENDIX F)
- ↔ FAULT (DASHED WHERE INFERRED; ARROWS INDICATE APPARENT RELATIVE MOVEMENT)
- - - GEOLOGIC CONTACT (DASHED WHERE INFERRED)
- HORIZONTAL MOVEMENT (AWAY FROM VIEWER)
- ⊕ HORIZONTAL MOVEMENT (TOWARDS VIEWER)
- ▨ PASS CREEK SHEAR ZONE (PCSZ)

FAULTS:

- PCF** PASS CREEK FAULT (1)
- HJ1** HUMP JUT FAULT SPLAY 1 (2)
- HJ2** HUMP JUT FAULT SPLAY 2 (2)
- WCTF** WILLOW CREEK TRANSFER FAULT (3)
- DD** DRAINAGE DIVIDE FAULT (5)
- SZ** PASS CREEK SHEAR ZONE FAULT (6)

LITHOLOGIC UNITS:

- 1. PRECAMBRIAN AMPHIBOLITE GNEISS (Xag)
 - 1a. PRECAMBRIAN AMPHIBOLITE GNEISS: BLACK AMPHIBOLITE GNEISS (Xag:Xh)
 - 1b. PRECAMBRIAN AMPHIBOLITE GNEISS: GRAY COMPOSITIONALLY-BANDED AMPHIBOLITE GNEISS (Xag:Xf)
 - 1c. PRECAMBRIAN AMPHIBOLITE GNEISS: QUARTZOFELDSPATHIC SCHIST (Xag:Xfs)
- 2. PRECAMBRIAN QUARTZOFELDSPATHIC GNEISS (Xqfg)
- 3. PRECAMBRIAN FELSIC HORNBLENDIC GNEISS (Xfh)
- 4. CALC-SILICATE GNEISS (Xcs; 2a.Xqfg:Xcs)
- 5a. PORPHYROBLASTIC GRAY COMPOSITIONALLY-BANDED AMPHIBOLITE GNEISS "POD" ROCK (Pf)
- 5b. PORPHYROBLASTIC QUARTZOFELDSPATHIC SCHIST "POD" ROCK (Pfs)
- 6. IGNEOUS INTRUSIONS (i)

